Alma Mater Studiorum - Università di Bologna

DOTTORATO DI RICERCA IN

IL FUTURO DELLA TERRA, CAMBIAMENTI CLIMATICI E SFIDE SOCIALI

Ciclo 35

Settore Concorsuale: 04/A4 - GEOFISICA

Settore Scientifico Disciplinare: GEO/12 - OCEANOGRAFIA E FISICA DELL'ATMOSFERA

ADVANCED REPRESENTATION OF THE OCEAN/SEA ICE DYNAMICS AT HIGH LATITUDES

Presentata da: Iuliia Selivanova

Coordinatore Dottorato

Silvana Di Sabatino

Supervisore

Doroteaciro Iovino

Co-supervisore

Nadia Pinardi

Esame finale anno 2023

Abstract

Sea ice is a fundamental element of global climate system, with numerous impacts on the polar environment. The ongoing drastic changes in the Earth's sea ice cover highlight the necessity of monitoring the polar regions and systematically evaluating the quality of different numerical products. The main objective of this thesis is to improve our knowledge of the representation of Arctic and Antarctic sea ice using comprehensive global ocean reanalyses and coupled climate models. The dissertation will explore (i) the Antarctic marginal ice zone (MIZ) and pack ice area in the ensemble mean of four global ocean reanalyses called GREP; (ii) historical representation of the Arctic and Antarctic sea ice state in HighResMIP models; (iii) the future evolution of Arctic sea ice in HighResMIP models. Global ocean reanalyses and GREP are found to adequately capture interannual and seasonal variability in both pack ice and MIZ areas at hemispheric and regional scales. The advantage of the ensemble-mean approach is proved as GREP smooths the strengths and weaknesses of single systems and provides the most consistent and reliable estimates. This work is intended to encourage the use of GREP in a wide range of applications. The analysis of sea ice representation in the coupled climate models shows no systematic impact of the increased horizontal resolution. We argue that a few minor improvements in sea ice representation with the enhanced horizontal resolution are presumably not worth the major effort of costly computations. The thesis highlights the critical importance to distinguish the MIZ from consolidated pack ice both for investigating changes in sea ice distribution and evaluating the product's performance. Considering that the MIZ is predicted to dominate the Arctic sea ice cover, the model physics parameterizations and sea ice rheology might require modifications. The results of the work can be useful for modelling community.

Acknowledgements

This thesis could not have been possible without certain people I would like to thank.

First and foremost, I am sincerely grateful to my research supervisor, Dr. Doroteaciro Iovino, for her guidance, patience, and faith in me. Her immense knowledge of physical oceanography and scientific enthusiasm have motivated me to keep up working through the stages of PhD research.

I would like to thank the coordinator of the PhD program "Future Earth, climate change, and societal challenges", Prof. Nadia Pinardi, for making this journey possible and for the inspirational insights she gave us during the classes and seminars.

I am thankful to the head of the ocean modeling and data assimilation division, Dr. Simona Masina, for her expertise and valuable recommendations during the preparation of the first publication.

I am also grateful to the CMCC staff and other PhD students for answering all my questions, being willing to help, and sharing good moments together.

I would like to express my gratitude to Prof. Marcello Vichi, the director of the Marine and Antarctic Research center for Innovation and Sustainability (MARIS) at the University of Cape Town, for his kindness and warm welcome during my stay as a guest student. I appreciate his advice, interest, punctuality and willingness to discuss the results of the work.

I am very grateful to the Institute of Advanced Studies of the University of Bologna which provided me with accommodation during the years of PhD research. I was extremely lucky to receive this scholarship.

I would also like to give special thanks to my therapist for helping me to handle anxiety during the PhD journey.

Last and not least, I owe a big thanks to my friends and mom, whose support and love I felt across the distance.

"All models are wrong, but some are useful."

George Box

List of Figures

Contents

Chapter 1
Introduction

1.1 The role of sea ice in climate

Sea ice is frozen seawater floating on the top of the ocean. It grows and melts on a seasonal basis both in the Arctic and the Antarctic regions. Even though it forms mainly in the polar regions, its profound effects are not limited to the regional climate but are spreading farther beyond. Changes in sea ice properties have implications on ocean circulation, large-scale atmospheric dynamics, and weather patterns across the globe (Jaiser et al., 2012).

Sea ice is a crucial component in the Earth's climate system. Due to its insulating and reflective properties, it regulates the exchanges between the ocean and the atmosphere and considerably modifies the ocean/atmosphere interplay at seasonal and interannual time scales. Along with playing the role of physical barrier to the air-sea exchanges, sea ice acts as a natural sunscreen reflecting major of the incoming solar radiation. With its much higher albedo compared to the dark ocean surface, sea ice and snow on it largely alter the radiation budget in polar regions. Consistently interacting with ocean, atmosphere, snow, and land ice, sea ice is involved in multiple feedbacks, which are responsible for the amplification or damping of initial perturbation in the climate system. Thus, sea ice significantly contributes to the high sensitivity of polar regions to climate forcing. A subtle change in the sea ice can trigger complex feedbacks and bring dramatic shifts in the Earth's climate system (Goosse et al., 2018).

Sea ice plays a critical role in ocean dynamics by changing buoyancy and water stratification. During its formation and growth in autumn, sea ice releases salt into the underlying ocean increasing its density and promoting vertical convection, and deep water formation (Cavalieri and Martin, 1994) and eventually affecting the global ocean thermo-haline circulation (Dickson et al., 1988). Likewise, when the ice melts it releases fresh water into the upper ocean which leads to the stabilization of the surface layer and suppression of deep water convection (Haine et al., 2015).

Sea ice-covered regions represent a large unique ecosystem supporting biodiversity at different scales ranging from bacteria and algae to birds and marine mammals. Individual species rely on sea ice as a habitat for feeding, breeding, and hunting (Stern and Laidre, 2016; Watanabe et al., 2020). Sea ice supports relevant biological and chemical processes such as primary marine production, and delivery of nutrients to the deep and trophic interactions (Randelhoff et al., 2020; Gorman et al., 2021). Any variation in sea ice-

dependent biota at the bottom of the food chain affects the organisms at higher trophic levels (Massom and Stammerjohn, 2010).

The extent to which sea ice influences the global climate system depends on its properties, e.g. area, thickness, and volume. At the same time, sea ice acts as a sensitive indicator of ongoing climate change itself. All of this underscores the importance of understanding and monitoring ongoing changes in the polar regions as well as evaluating the realism of sea ice representation in the climate models which produce the projections of the future evolution of the Earth's climate system.

1.2 Polar regions

1.2.1 Geography

At first sight, going to the polar regions takes us to seemingly identical remote, cold, hostile environments: both the ice caps surround the geographic North and the South poles. Despite the two places being located in high-latitudes and receiving similar annual insolation, there are fundamental differences in their sea ice characteristics and variability attributed to the contrast in geography and leading physical processes (Fig. 1.1).

The Arctic Ocean is peculiar in terms of seafloor topography including both the deep ocean basin reaching a depth of over 5000 m and vast shallow continental shelves (Holmes et al., 2012). The land-locked ocean, the Arctic Ocean can be considered as Atlantic's estuary: despite the connection with the Pacific Ocean through the narrow and shallow Bering Strait, the Arctic Ocean receives the major inflow of warm and saline water from the North Atlantic, through the Barents Sea and Fram Strait, the only pathway where deep water exchange takes place (yearly average Atlantic heat inflow is $\sim$ 73 TW; Smedsrud et al., 2010). Because the Arctic is almost entirely encircled by land, the sea ice expansion is constrained toward the lower latitudes where it can be easily melted: the export of sea ice outside the region is relatively limited in movement which increases the chance of ice floes to converge and pile up. This geographic feature allows the ice to grow thicker (up to 4 m), together with strong ocean stratification acting as a barrier for the heat transfer from the relatively warm Atlantic layer to the ice bottom (Carmack et al., 2015). The Arctic sea ice can persist throughout the melting season and survive for years. The large-scale atmospheric circulation dominated by the Beaufort High drives the clockwise rotation of the Beaufort Gyre and the Transpolar Drift. The drift of sea ice driven by the Beaufort Gyre affects the spatial distribution of the Arctic sea ice thickness and favours the ice to remain during summer (Maksym et al., 2012). The Transpolar Drift promotes the ice to move from the Siberian Shelf towards Fram Strait, the main gate for sea ice export in the Arctic (Serreze and Meier, 2019). Freshwater transport through

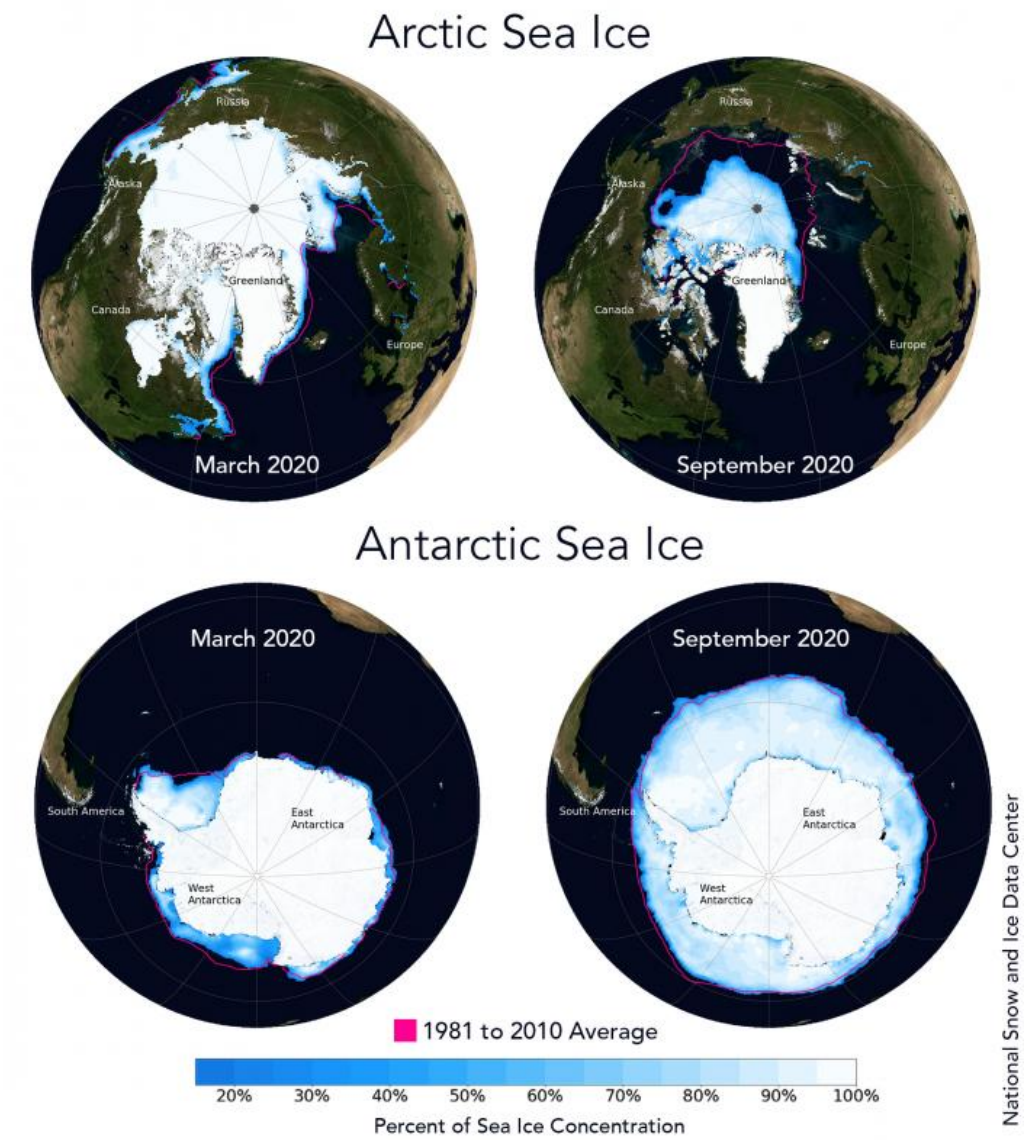

Figure 1.1: Average minimum and maximum sea ice during March and September 2020 for the Arctic and Antarctic as compared to the 1981 to 2010 average. Source: National Snow and Ice Data Center.

the Fram Strait plays a crucial role in the deep water convection in the Labrador Sea since the enhanced sea ice export decreases the density of upper ocean saline waters and hence leads to disruption of water mass transformation (Koenigk et al., 2007). The major atmospheric mode at the inter-annual and decadal scales over the Northern Pole is the Arctic Oscillation (AO) which represents the variation in the atmospheric pressure and wind pattern in middle and high northern latitudes (Thompson and Wallace, 1998). The atmospheric circulation driven by changes in the AO strength affects the sea ice motion and distribution of sea ice concentration and thickness (Rigor et al., 2002).

In the Southern Hemisphere, in contrast, the highest latitudes are occupied by the Antarctic continent, surrounded by open ocean. The sea ice creates a fringe around the continent's coastline whose principal feature is the presence of a thick ice sheet that in-

teracts with the local ocean-atmosphere-sea ice system. Driven by strong and persistent winds, known as katabatic winds (gravity winds blowing down the slope; Parish and Cassano, 2003), sea ice can freely move and expand northward not constrained by solid barriers (Gordon, 1981). At its maximum extent, Antarctic sea ice reaches lower latitudes at about 55°S where it encounters the Antarctic Circumpolar Current (Eayrs et al., 2019) which isolates the polar fresh and cold waters from the warmer mid-latitude waters (Martinson, 2012). Despite the large sea ice cover and substantial advancement of ice edge towards the equator in winter, the Antarctic ice is very thin - less than 1-meter thick on average: the thicker ice forms only through ridging and rafting (Worby et al., 2008). The Antarctic sea ice primarily consists of small pancake ice floes which form in wave conditions, a great part of which constitutes the marginal ice zone (highly dynamic transitional zone between the open sea and inner pack ice), which in certain months can make up more than a half of the total ice extent (Stroeve et al., 2016). In the weakly stratified ocean with strong heat exchange from warm deep waters to the surface, thin ice can be easily melted away so only little amount of ice persists in summer. The sea ice edge expansion and contraction are controlled by the large-scale atmospheric circulation dominated by the Antarctic Circumpolar Trough, the low-pressure belt around the continent (Enomoto and Ohmura, 1990). As a result, the waxing and waning of the Antarctic sea ice represent the greatest seasonal ice area changes on Earth with a sixfold increase from the annual minimum of nearly $3 \cdot 10^6\ km^2$ to maximum of $18 \cdot 10^6\ km^2$ (Eayrs et al., 2019). Changes in the position of the westerly jet are governed by the Southern Annual Mode - the dominant atmospheric mode in the Antarctic which refers to the difference in the zonal mean sea level pressure between the mid-latitudes and the pole. The main circumpolar flow is deviated by permanent low-pressure systems around Antarctica, the deepest of which is the Amundsen Sea Low, the driver of sea ice variability in the South Pacific (Raphael et al., 2016). The hallmark of the Antarctic sea ice is the strong asymmetry of its seasonal variability with 7 months of expansion and 5 months of contraction whilst the Arctic ice cover takes equal time for advance and retreat. Different length of growth and melt periods in Antarctica is tied to wind-driven Ekman forcing (Enomoto and Ohmura, 1990; Eayrs et al., 2019). Although, a recent study argued that the primary reason driving the asymmetry of the sea ice extent is the distribution of the insolation at the top of the atmosphere (Roach et al., 2022).

The contrasting nature of sea ice in two polar regions determines its different response to climate change as well as its impact on other components of the climate system.

1.2.2 Arctic sea ice variability

sea ice extent is the most common variable to describe the past and recent sea ice cover in the polar regions and it is generally defined as areal coverage with at least 15%

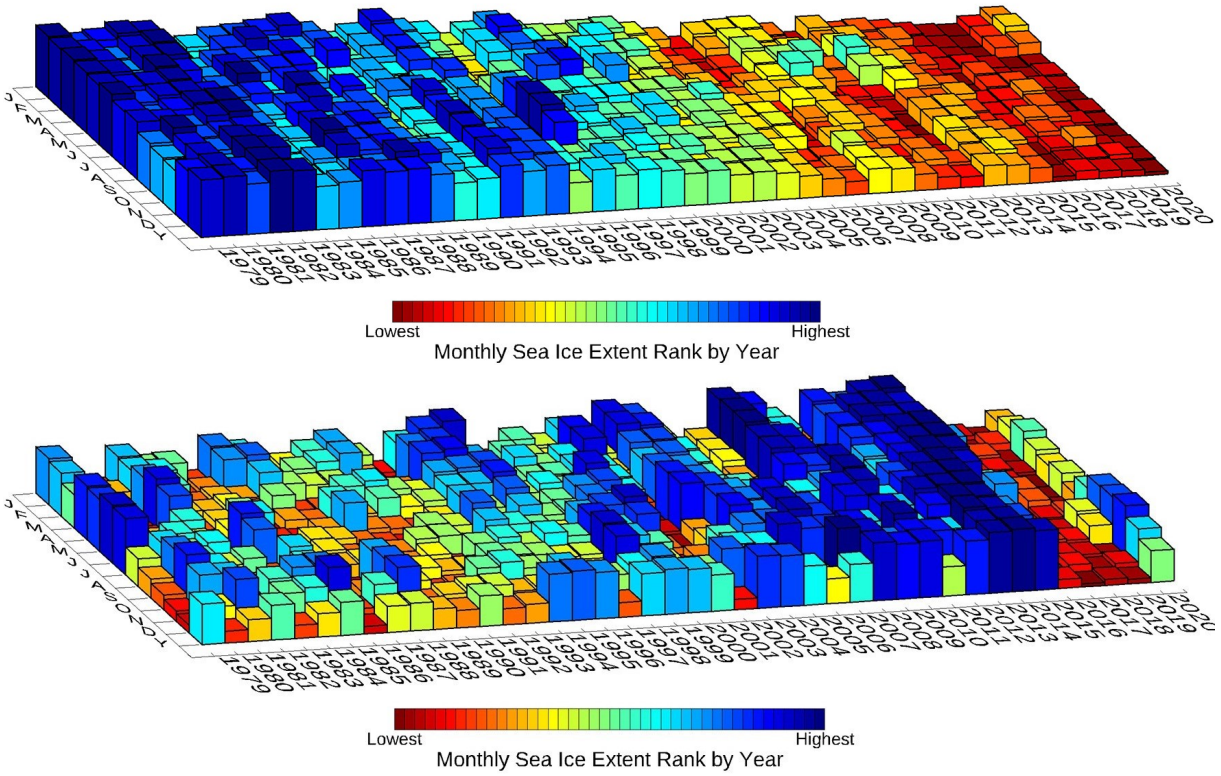

Figure 1.2: Arctic (upper panel) and Antarctic (lower panel) sea ice extent rankings by year, for each calendar month and the yearly average, over the 42-year period 1979-2020 (Parkinson et al., 2021)

ice coverage. sea ice area is a different way of estimating sea ice cover which refers to the integral sum of the product of ice concentration and area of all grid cells with at least 15% ice concentration. From satellite-based passive microwave observations it is possible to determine the sea ice extent and sea ice area for Arctic and Antarctic sea ice since late 1970s. In the last 4 decades, trends of the sea ice extent and sea ice area have been observed, which evolves differently in the northern and southern polar regions.

Since the beginning of the satellite era, the Arctic has shown an unprecedented loss of sea ice extent (Onarheim et al., 2018) - glaring evidence of climate change. The substantial recession is observable in all months: since 1986 the Arctic has not experienced monthly record highs in sea ice extent while 93 record lows have been reached (Fig. 1.2; Parkinson and DiGirolamo, 2021). The most pronounced decline occurs at the minimum extent in September whose linear trend is about -81200 km^2 (12.7%) per year from 1979 to 2021 compared to -43800 km^2 (2.9%) per year at the annual maximum in March (https://nsidc.org/). The summer decrease is not equal over the period of satellite observations: the rate of sea ice loss doubled over 1993-2006 and slightly slowed over 2007-2020 compared to 1979-1992 (Perovich et al., 2020). The severe reduction in September sea ice extent is better illustrated by the absolute decrease of $3.49 \cdot 10^6$ km^2 since 1979

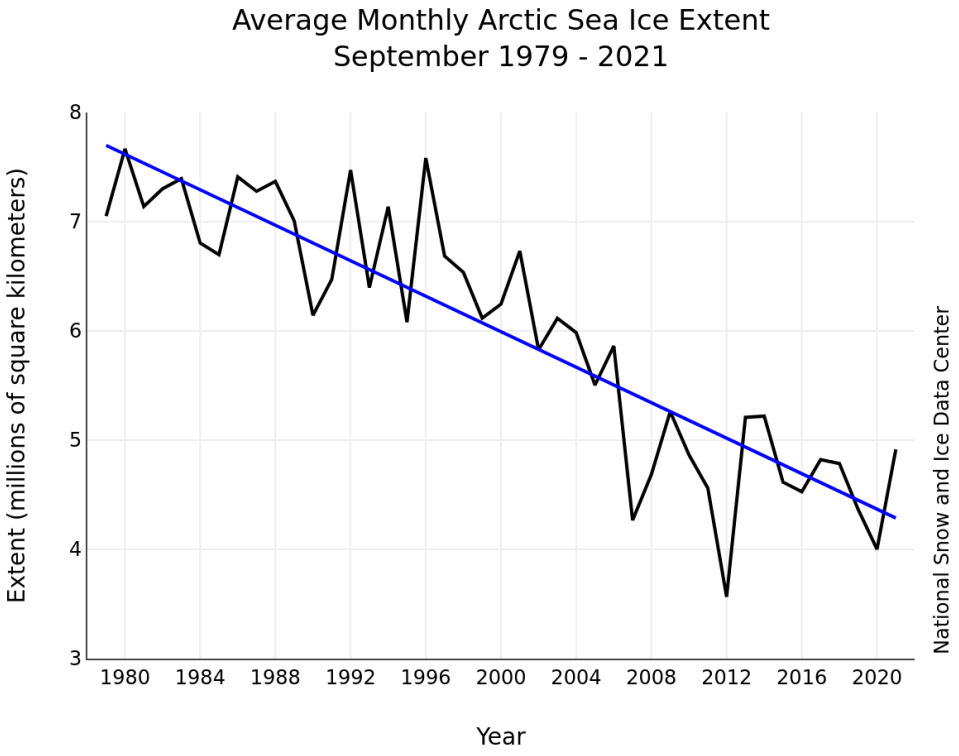

Figure 1.3: Monthly September ice extent for 1979 to 2021. Source: National Snow and Ice Data Center.

(Fig. 1.3). Because of the different intensity of monthly trends, the seasonal cycle of the sea ice extent becomes more pronounced resembling that of the Antarctic (Serreze and Meier, 2019). Despite the downward trends observed in all sub-regions, there is a large regional variability (Fig. 1.4). Summer sea ice decline is dominated by the Eurasian Shelf Seas with the greatest contribution of the East Siberian Sea (Watts et al., 2021), while the winter hotspot is located in the Barents Sea (Árthun et al., 2021). Moreover, the Barents Sea has experienced the most prominent lengthening of ice-free season (40 days per decade) compared to the rest of the Arctic with 9 days per decade due to earlier ice retreat and later advance (Notz and Stroeve, 2016).

Along with the reduction in its coverage, sea ice is changing its thickness and age. The retrieval of an overall trend in sea ice thickness is difficult since detailed measurements of sea ice thickness are still lacking compared to the well-documented change in sea ice extent: the available satellite-based estimates cover short periods and in-situ measurements are limited to the spatial and temporal coverage. Available measurements from submarine sonars, satellite altimeters (ICESat and CryoSat-2), and satellite scatterometers show that the Arctic-wide ice thickness decreased by 34% between 2000 and 2012, which corresponds to a decline of about 0.58 ± 0.07 m per decade (Lindsay and Schweiger, 2015), with a winter decline of approximately 2 m since the 1980s (Kwok, 2018). As the

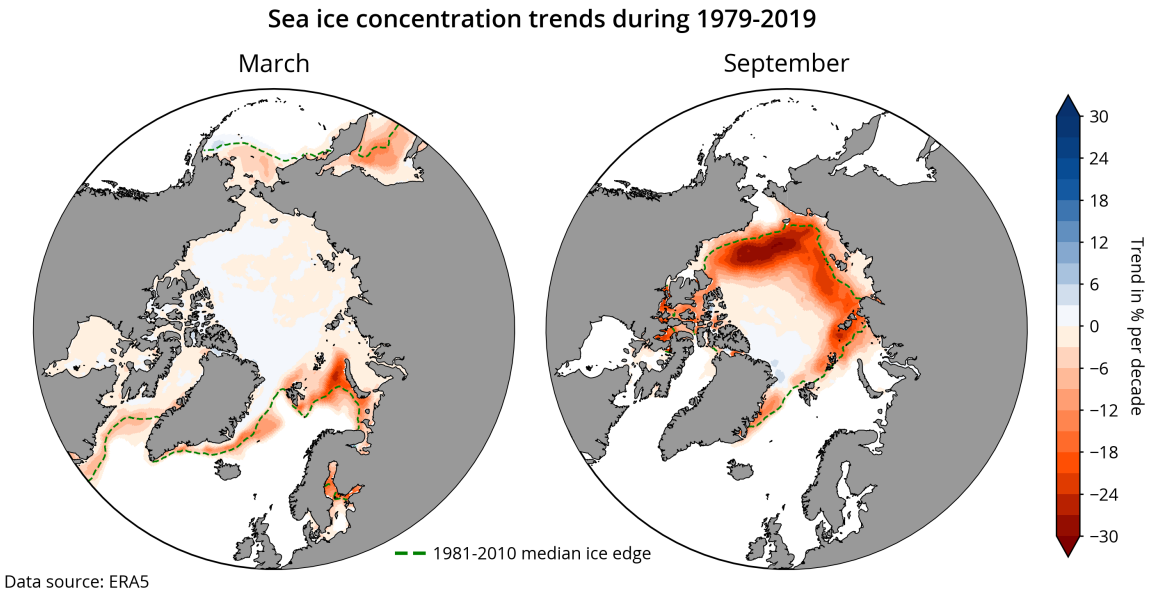

Figure 1.4: Linear trends in sea ice concentration during 1979-2019 per decade for March (left) and September (right). The dashed green line shows the position of the median ice edge during 1981-2010. Source: Copernicus Climate Change Service (C3S)/ECMWF.

ice thins, it becomes more vulnerable to the external dynamic and thermodynamic forcing, leading to increased importance of ice-albedo feedback, a strong positive feedback in the climate system due to the albedo contrast between water and ice (Goosse et al., 2018). The ice-albedo feedback promotes further hastening of the melt (Stroeve et al., 2012b). Thinner ice is more mobile and thus more responsive to winds, ocean waves and currents. The diminishing and thinning sea ice reduces the ice strength, which contributes to the redistribution of sea ice and results in increased sea ice motion (Rampal et al., 2011; Kwok et al., 2013) and higher sea ice export from the Arctic (Döscher et al., 2014). As a combination of sea ice area and thickness, sea ice volume is disappearing at more alarming rate resulting in nearly 70% reduction in summer over 1979-2021 (https://psc.apl.uw.edu/) driven mainly by the multi-year ice. The real sea ice shrinking might be even more dramatic since the estimates of the ice thickness are found to be overestimated according to new observations of snow depth (Kacimi and Kwok, 2022). The multi-year ice which used to be a key feature of the Arctic ice cover constituting for over 30%, now makes up nearly 4.4% of the winter ice pack (Fig. 1.5; Perovich et al., 2020). This marks a transition to the first-year ice regime that moves toward a seasonally ice-free Arctic which is predicted to happen by the middle of the century (Notz and Stroeve, 2016; Notz and Community, 2020).

Sea ice shrinking in the Northern Hemisphere is largely related to the Arctic Amplification (Previdi et al., 2021), an iconic feature of global warming, when the increase of the surface air temperature in the Arctic is much more prominent (up to 4 times) relative to the globe (Rantanen et al., 2022). The mechanisms driving the enhanced warming in high

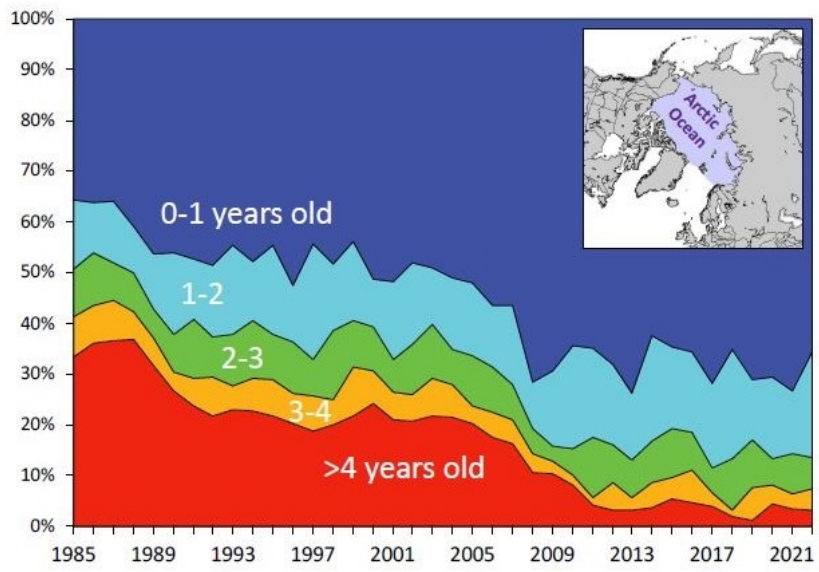

Figure 1.5: The time series from 1985 through 2022 of percent cover of the Arctic Ocean by different sea ice ages during the March 12 to 18 period. Source: NASA NSIDC.

latitudes, which is not observable in the Southern hemisphere, are complex, interrelated, and not completely understood (Henderson et al., 2021) resulting in high uncertainty in Arctic climate projections (Taylor et al., 2022). Among multiple physical processes contributing to Arctic Amplification (e.g. Bintanja et al., 2018; Graversen and Burtu, 2016; Yoshimori et al., 2017), the ocean-atmosphere energy exchanges in autumn and winter are considered to play a major role (Screen and Simmonds, 2010; Boeke and Taylor, 2018; Chung et al., 2021). There are also numerous positive feedbacks which favour further warming (Goosse et al., 2018), of which ice/snow-related have a considerable contribution to Polar Amplification due to reflective properties (Previdi et al., 2021). Apart from unprecedented warming in the atmosphere, there is also growing evidence of changes occurring to the Arctic Ocean, known as Atlantification - the transition to a state resembling the Atlantic Ocean (Polyakov et al., 2017). Atlantification is associated with the strengthening and warming of Atlantic inflow (Ingvaldsen et al., 2021) and the weakening of halocline (Ivanov et al., 2016) which favours heat transfer from relatively warm Atlantic water layer to the surface waters and bottom of sea ice cover.

1.2.3 Antarctic sea ice variability

In sharp contrast to the Arctic, the Antarctic sea ice has not experienced a continuous downward trend but rather has expanded on average since 1979 (Fig. 1.6). Satellite records reveal a graduated long-term overall increase in sea ice cover at a rate of nearly 1.5% per decade for the period 1979-2015 (Simmonds, 2015; Stammerjohn and Maksym, 2017; Parkinson, 2019). The overall increase in the annual sea ice cover was uneven with a fivefold faster expansion over 2000-2014 compared to 1979-1999 (Eayrs et al., 2021).

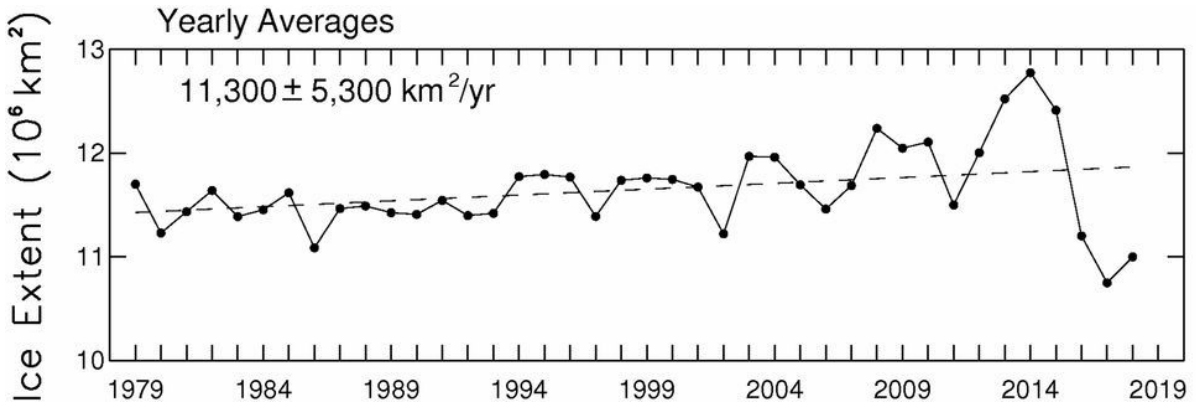

Figure 1.6: Yearly average sea ice extents and their line of linear least squares fit (Parkinson, 2019)

The unexpected response of the Antarctic sea ice cover to global warming, known as the Antarctic paradox (Simmonds, 2015), puzzled the scientific community and gave rise to multiple attempted explanations attributed to large-scale atmospheric circulation (Stammerjohn et al., 2008; Turner et al., 2015; Meehl et al., 2016), regional wind patterns (Holland and Kwok, 2012; Blanchard-Wrigglesworth et al., 2021), ice-ocean feedbacks (Goosse and Zunz, 2014), massive loss of Antarctic ice sheets (Bintanja et al., 2013; Haid et al., 2017), ozone depletion (Polvani et al., 2011), delayed response of the Southern Ocean to the anthropogenic forcing (Armour et al., 2016). The annual-mean Antarctic sea ice extent reached a record high of $12.8 \cdot 10^6\ km^2$ in 2014, followed by an unexpected decline that led to an unprecedented and abrupt drop in November of 2016 (Fig. 1.2; Parkinson, 2019), with the lowest annual mean value in 2017 ($10.7 \cdot 10^6\ km^2$). The area of reduced ice cover around Antarctica between 2014 and 2017 is comparable to the total ice loss in the Arctic over 20 years. The sudden sea ice retreat in late 2016 has been tied to wind pattern in the precedent seasons (Stuecker et al., 2017; Wang et al., 2019), zonal wave number three index associated with strong southward heat advection (Schlosser et al., 2018), large-scale atmospheric circulation (Turner et al., 2017).

Since the variability of Antarctic sea ice cover is highly heterogeneous in space, it is necessary to consider the evolution of sea ice extent and its seasonality on a regional basis (e.g. Parkinson, 2019; Turner et al., 2015). The circumpolar positive trend in Antarctic sea ice extent is composed of regionally opposing sea ice changes, particularly in the (western) Ross Sea and the adjacent Bellingshausen and Amundsen Seas (Turner et al., 2015) (Fig. 1.7). Thus, the sea ice extent increases, except for the sector of the Bellingshausen and Amundsen Seas with a decrease of -2.5 $\pm$ 1.2% per decade in the period 1979-2018 (Parkinson, 2019). In contrast, the strongest increase in sea ice extent has been observed in the western pacific sector with a rate of 2.3 $\pm$ 1.2% per decade in the same period (Parkinson, 2019). Trends in the remaining sectors are comparable or slightly higher than the Antarctic-wide positive overall circumpolar trend. Thus, the

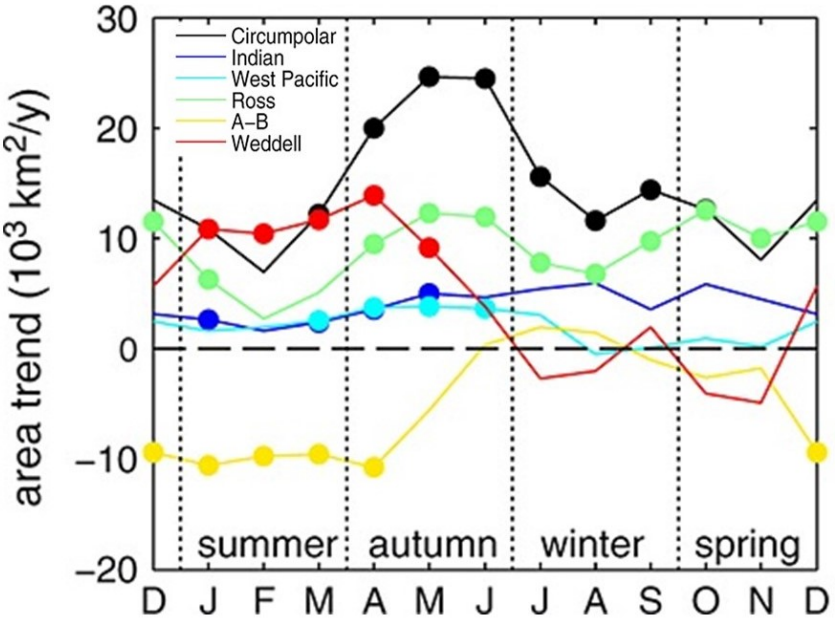

Figure 1.7: Interannual trends in monthly total ice area (Holland, 2014)

overall increase in Antarctic sea ice extent is a slight imbalance between the positive trend in East Antarctica and the contrasting trends in the western part. As a result of sea ice-upper ocean feedbacks (Holland, 2014), changes in the timing of sea ice advance and retreat impact the length of ice-free season. Similarly to the ice extent trends, there is a regional pattern of trends in the duration of sea ice-free season with prolongation in the Bellingshausen Sea and a decrease in the western Ross Sea (Hobbs et al., 2016). The spatio-temporal variability of trends suggests that a combination of oceanic and atmospheric processes amplified by complex feedbacks and interactions with ice shelves contribute differently to various parts of the Southern Ocean.

However, the unified description of the mechanisms behind changes in sea ice cover around Antarctica is still missing. Unlike sea ice cover, the knowledge of changes in characteristics of Antarctic sea ice thickness and volume is limited due to the critical scarcity of in-situ observations and large uncertainties in retrievals from radar altimeters. The estimates using models reveal the thickening in the Ross and the Weddell Seas and the thinning in the Bellingshausen Sea which corresponds to trends in wind-driven sea ice motion (Holland, 2014).

1.3 Climate modelling

The alarming rate of warming highlights the importance of projecting future climate in order to evaluate its response under different emission scenarios, assess implications and possible risks, and mitigate its effects. Together with observations, climate modelling provides a backbone of our understanding of the changing climate. The general circulation

models (GCMs) are comprehensive tool to gain insights into the physical processes and interactions in the Earth's system in the past and present as well as project the future evolution of various climate phenomena.

GCMs represent a system of differential equations of large-scale fluid motion and thermodynamics. The equations are solved in discrete grid cells individually for elements of the climate system at fixed-time intervals and integrated over time. At the beginning of the climate model development, the models were designed only for one aspect of the climate system (standalone atmospheric or ocean models). Since the Earth is inherently coupled, the interactions among the components are crucial for reasonable simulation of climate dynamics. In this regard, the approach allowing model components to interact simultaneously, referred to as coupling, became a key element of comprehensive climate models. The first coupled models linked the ocean and the atmosphere permitting the exchange of heat and momentum fluxes at the boundary between components. From the beginning of the 1990s, the coupled ocean-atmosphere models began to incorporate also other physical components - the land surface, the cryosphere and lately biogeochemistry.

With an increasing number of institutions developing coupled GCMs starting from the end of the last century, an issue arose concerning the comparability of the outputs produced by those models. Since then, following the growing need to systematically evaluate the performance of the coupled GCMs, the World Climate Research Programme's (WCRP) established the climate model intercomparison project (CMIP; Meehl et al., 2000). Started over 25 years ago, CMIP gathered the collaborative efforts of modelling groups around the world to systematically investigate the changing climate associated both with natural variability and radiative forcing. To address this, a common protocol was developed including standards in the model setup, design of experiments, output format, and naming convention. This facilitated multi-model intercomparison and assessment of the strengths and weaknesses of different models. Since 1995, CMIP went through 6 phases with sophistication at each stage allowing examination of the improvements across the CMIP phases.

Significant efforts of modelling groups around the world contributed to considerable advancement in computational efficiency, the complexity of the models, and increases in the spatial resolution which together aim to improve the realism of the simulated features in the climate system. For example, increased horizontal resolution in CMIP6 models led to better representation of tropical and Arctic cyclones (Li et al., 2021; Song et al., 2021), western boundary currents (Gupta et al., 2021), Atlantic Meridional Overturning Circulation (Roberts et al., 2020), ocean heat content in the Northern Atlantic (Docquier et al., 2019). However, there are still many errors in model simulations and large uncertainties in projections of future climate, which are broadly attributed to model defi-

ciencies (Tebaldi et al., 2021; Meehl et al., 2020). There is evidence of systematic biases associated with the representation of mixed-phase clouds (Tan et al., 2016; Zelinka et al., 2020), lack of coupled ice sheet interactions (Bronselaer et al., 2018), surface ocean warm bias (Beadling et al., 2019) and equatorward shift of the westerly jet stream (Ceppi et al., 2012). Moreover, fully coupled models are influenced by biases through coupling between the components so the errors in the exchanged fields amplify with time. Even small errors grow rapidly owing to the involvement of the chaotic dynamics of the atmosphere (Alizadeh, 2022). Sea ice is highly sensitive to atmospheric and ocean forcing so biases in temperature and salinity of the ocean, wind patterns, radiative fluxes, and ocean circulation might translate into errors in sea ice in the model simulations. On the other hand, not accurate sea ice representation in the models influences vice versa the aspects of the atmosphere and the ocean.

The widely recognized way to improve the GCM's ability and credibility to simulate observed climate records and to reduce the model uncertainties is to increase the spatial grid resolution. The limited resolution (typically 1°) of current climate models is a critical source of uncertainty in all applications of climate and Earth System modelling, including to predictions, projections and risk assessments. However, the requirement for a multitude of multi-centennial simulations, including poorly constrained Earth System processes and feedbacks, has meant that model resolution within CMIP has progressed very slowly. The benefits of higher resolution ($\sim$ 25 km) in all model components have been abundantly demonstrated (e.g. (Grist et al., 2018; Roberts et al., 2020; Meccia et al., 2021). The High-Resolution Model Intercomparison Project (HighResMIP, Haarsma et al., 2016) endorsed by CMIP6, applies, for the first time, a multi-model approach to the systematic investigation of the impact of horizontal resolution. HighResMIP has enabled standardization of experimental design for high-resolution simulations ($\sim 0.25°$), and has galvanized the international community towards a more systematic exploration of the role of resolution. HighResMIP exercise concentrates on delivering the best representation, at the highest horizontal resolutions possible, of the processes that are important for the evolution of climate on decadal timescales, with a specific focus on the period 1950-2050, with a major emphasis on assessing the benefits of substantial increases in the atmosphere and ocean-sea ice resolutions. On the other hand, high computational cost raises the debates on the feasibility of enhanced resolution since the beneficial effect might be controversial (e.g. Haarsma et al., 2020; Docquier et al., 2020; Koenigk et al., 2021). Another caveat is that the horizontal resolution up to $\sim 0.25°$ is still not sufficient to resolve mesoscale eddies, particularly in the high latitudes where the baroclinic Rossby radius is on the order of kilometers (Khosravi et al., 2022). This leads to underrepresented local processes such as air-sea fluxes, mixing, temperature, and salinity transport (Huot et al., 2022), which eventually might affect the simulation of ocean dynamics and thermodynamics.

In light of unsuccessful attempts of the modern models to describe the Antarctic paradox and reproduce sea ice expansion trends (Roach et al., 2018; Holmes et al., 2019), increased spatial resolution is found to improve the representation of the long-term variability in the Antarctic: model simulations using locally eddy-resolving configurations are able to reproduce upward sea ice trends (Rackow et al., 2022). This finding marks a promising stage on the way to reliable projections in this region. Another important source of uncertainty is the amount of greenhouse emissions, which strongly depend on human decisions. Insufficient understanding of the multiple feedbacks involved in the physical processes in combination with unknown radiative forcing imposes additional challenges to get plausible predictions of future climate.

1.3.1 Arctic sea ice in climate model simulations

Over the historic period, the CMIP climate models tend to reasonably simulate seasonal variability of the Arctic sea ice extent, capturing maximum in March and minimum in September. Following the progress from CMIP Phase 3 to Phase 5 (e. g. Stroeve et al., 2012a; Shu et al., 2015), the models participating in CMIP6 exhibit some improvement in the representation of sea ice area and volume revealing closer agreement between the ensemble-mean and data-based estimates (Davy and Outten, 2020). However, CMIP6 models still produce a wide spread of mean Arctic sea ice area, capturing the observational record within the multi-model ensemble spread (Notz and Community, 2020). The advancement in narrowing the inter-model uncertainty in sea ice extent since the last phase does depend on the season: while in summer the inter-model spread among CMIP6 models is reduced, in winter the large ensemble spread remains (Shu et al., 2020). The spatial distribution of sea ice is poorly reproduced in individual models in certain regions, which is most likely attributed to ocean forcing. For example, the misrepresentation of the currents in the North Atlantic leads to the inaccurate distribution of heat fluxes at the Arctic gateway which affects the position of the ice edge (Watts et al., 2021). Another source of the regional biases can be attributed to the complexity of the sea ice model: the models with the Sea Ice Simulator have more sea ice in the Barents and East Greenland Seas (Long et al., 2021). There is a higher model spread in the simulation of sea ice volume (Davy and Outten, 2020) since sea ice thickness is the key source of uncertainty in sea ice state simulation (Zygmuntowska et al., 2014). Only half of CMIP6 models can adequately simulate March and September sea ice thickness (Watts et al., 2021). While CMIP5 multi-model mean consistently overestimates sea ice volume in all months, CMIP6 ensemble-mean has a small bias, yet it produces an overestimated seasonal cycle (Davy and Outten, 2020). The proper representation of sea ice thickness distribution still remains a fundamental problem for climate numerical modelling. Although clear improvements since the previous generation of CMIP, the biases in the spatial distribu-

tion and mean quantities of sea ice thickness persist in CMIP6 models. Despite many models being able to locate the thickest ice north of Greenland and the Canadian Arctic Archipelago as well as thin ice in the marginal seas, there are large compensation biases: compared to reanalysis data (PIOMAS), the models tend to overestimate thick ice and underestimate thin ice. Considering the long-term variability, the CMIP6 multi-model mean has a closer agreement with the reanalysis estimates for sea ice area trends, than their CMIP5 counterparts, yet the seasonal cycle of the trends is usually underrepresented and the inter-model spread remains large. In contrast, for the monthly trends in sea ice volume, no improvements are observable with the new phase of experiments (Davy and Outten, 2020). However, the time series of September sea ice area and volume show a better fit to reanalysis data in CMIP6 ensemble mean compared to that from CMIP5 (Davy and Outten, 2020). CMIP6 models better capture the sensitivity of Arctic sea ice to changes in the forcing compared to CMIP3 and CMIP5 models, but there is still an underestimation of the response of Arctic sea ice area to warming (Notz and Community, 2020). Although all global climate models agree on the further decline in sea ice extent, they exhibit considerable inter-model spread generally underestimating the rate of ice shrinking and thinning (Shen et al., 2021). The model simulations predict that the Arctic becomes "ice-free" (September sea ice extent below $1 \cdot 10^6\ km^2$) before the middle of the twenty-first century (Notz and Community, 2020), yet the timing of the event largely depends on the combination of RCPs and SSPs (Davy and Outten, 2020). The reduction of the uncertainties in the projected Arctic sea ice conditions remains challenging for the modelling community. Apart from the model imperfections, the great obstacle to narrowing the uncertainty is a critical paucity of observations, particularly thickness, that can be used to constrain the model simulations (Massonnet et al., 2018).

1.3.2 Antarctic sea ice in climate model simulations

In the Antarctic, compared to the Arctic, climate models present lower confidence in simulating historical variability of sea ice area which has been a consistent challenge throughout CMIP generations. Poor representation of the historical mean state undermines the credibility of future projections of the Antarctic sea ice evolution as well as future changes in the westerly jet stream, water mass transformation, heat, and carbon storage. Furthermore, the improvements in the simulation of sea ice cover from previous CMIP to CMIP6 are not sufficiently evident and consistent biases are still present. The models are able to plausibly simulate the seasonal cycle of sea ice area, accurately capturing the asymmetry with longer growth and shorter melt periods. However, the CMIP6 ensemble mean is consistently lower than observations in all months with the strongest discrepancy in May (Roach et al., 2020). The inter-model spread in sea ice area climatology remains high, particularly in summer (Shu et al., 2020), and exceeds twice that

in the Arctic. Global climate models fail to realistically simulate the observed Antarctic sea ice variability (Roach et al., 2020). While in the real world, the Antarctic sea ice area experienced a long-term increase (Parkinson, 2019), the models produce decreasing trends in response to the warming. Only 11% of CMIP6 models captured an expansion increase in the Antarctic sea ice extent over 1979-2005 (Shu et al., 2020) compared to 15% during the fifth phase of CMIP (Shu et al., 2015). Even though some models were able to simulate a slight upward trend, none of them could capture the spatial pattern of sea ice concentration trends (Shu et al., 2020). CMIP6 models also lose Antarctic sea ice at a higher pace in comparison to their predecessors, which is owing to the higher sensitivity of the sea ice area to increasing air temperature (Holmes et al., 2022).

1.4 Scope of the thesis

The purpose of this dissertation is to improve our knowledge of the temporal and spatial variability of sea ice properties in the Arctic and Antarctic regions. To this end, we analyze the ability of state-of-the-art global ocean reanalyses and last generation of coupled climate models to reproduce observed sea ice records and simulate future sea ice change and its link to climate change. First, we have studied the sea ice representation in reanalyses systems where the ocean and sea ice components are combined with atmospheric forcing and observations. Then we continued with more complex pictures where the whole climate system is represented within the last generation of the coupled models at high resolution.

The thesis presents the main features in the model treatment of sea ice at both poles and highlights the systematic biases and shortcomings of the individual models by comparing their estimates to satellite records and data-based products. I address the following scientific questions in this dissertation:

- How robust are representations of sea ice state in the recent past?
- How trustworthy are projections of sea ice in the near future?
- Can we rely on current simulations and projections to understand the future of sea ice?

Consistent assessment of the model performance in reproducing sea ice mean-state, spatial heterogeneity, temporal variability, and trends is beneficial for identifying shortcomings due to missing/poor parameterizations in state-of-the-art models, improving model descriptions of sea ice (thermos)dynamics properties and the key atmospheric-sea ice-ocean physical processes, and obtaining more robust projections of future sea ice evolution. The results of this dissertation aim to provide key knowledge on current shortcomings in representing polar processes at the atmosphere-ice-ocean inter-phase in existing

models and suggest recommendations for required model improvements. This study also aims to understand whether the focus on the net circumpolar changes in sea ice cover is sufficient to investigate the changes in sea ice distribution or whether the knowledge of sea ice distribution within different sea ice classes can enhance our understanding of how the sea ice cover is changing and will change. Given the key role that the marginal ice zone (MIZ) plays in the responses of Arctic and Antarctic ice covers to climate change, while many studies focus on the total sea ice, we give particular attention to the seasonal and interannual variability of the marginal ice against consolidated pack ice. To highlight the importance of identifying different sea ice classes in order to assess the model skill in simulating sea ice cover, this study addresses the following questions:

- How accurate is the representation of sea ice classes in ocean reanalysis and coupled climate models?
- Can the marginal ice zone be a better indicator of climate change compared to total sea ice and shed light on hemispheric and regional ice variability on seasonal and interannual time scales?
- Can the proper simulation of the marginal ice zone improve climate projections?

Our results might draw the attention of the modelling community to the necessity to adapt model physics to the current ice regimes and develop new metrics and reduce uncertainties.

1.5 Outline of the thesis

This thesis consists of 5 Chapters. The Introduction (Chapter 1) provides an overview of the role of sea ice in the climate system, the past and present temporal and spatial changes in the Arctic and Antarctic sea ice properties, and models performance in simulating sea ice mean state and variability at both poles. Chapter 2 presents the model systems and experimental design used in the thesis, the observational estimates used for validations and the applied metrics. Chapter 3 collects two published manuscripts in which the variability of the Antarctic sea ice area is analyzed in time/space using an ensemble of global ocean/sea ice reanalyses (available through Copernicus Marine Service). The focus is to investigate how ocean reanalysis can distinguish between marginal ice zone and consolidated pack ice, and reproduce their observed seasonal and interannual variability at hemispheric and regional scales against a set of observation-based products. This analysis helps highlighting the different response of sea ice classes to external forcing in the recent past and sheds light on the mechanisms behind the baffling behaviour of Antarctic sea ice cover. The second important goal of the study is to investigate the benefits of a multi-system ensemble approach which works to smooth the errors from the individual ensemble members and to encourage the use of GREP in a wide range of applications.

The manuscripts have been published in 2022:

Iovino D*, **Selivanova J***, Masina S and Cipollone A (2022) The Antarctic Marginal Ice Zone and Pack Ice Area in CMEMS GREP Ensemble Reanalysis Product. Front. Earth Sci. 10:745274. doi: 10.3389/feart.2022.745274.

* *co-first authorship*

Iovino D, **Selivanova J**, Lavergne T, Cipollone A, Masina S, and Garric G. Changes in the Antarctic Marginal Ice Zone in von Schuckmann K et al. 2022 Copernicus marine service ocean state report, Issue 6. J. Oper. Oceanogr. 13, S1-S220. doi: https://doi.org/10.1080/1755876X.2022.2095169.

Chapter 4 continues to analyse the changes in the Antarctic sea ice. The focus is on the historical period 1979-2014 as simulated in a set of European coupled climate models in the framework of the HighResMIP. The aim of this study is to assess the accuracy of coupled models to simulate seasonal and long-term variability of the Antarctic sea ice area and volume and investigate the impact of mesh grid resolutions on the model performances. The sea ice interplay with ocean and atmosphere is investigated to find a link of systematic biases in the sea ice representation to the other components biases. This chapter constitutes the basis of a manuscript to be submitted in the next months to a peer-review journal.

In Chapter 5, I analyze the past and future of the Arctic sea ice using again the HighResMIP model outputs from the coupled historical ("hist-1950") and future ("highres-future") runs. In this study, the realism of the models to reproduce mean state and historical sea ice variability on hemispheric and regional scales is analysed. Assessed the multi-model, multi-resolution representation of the Arctic ice and the systematic differences (if any), we evaluate the future projections of the Arctic sea ice state, and investigate the impact of the ocean/atmosphere horizontal resolution in reproducing the first Arctic ice-free summer and the ice concentration and volume loss in at regional scales.

Summary of the dissertation and a list of references for Chapters 1, 2, 4, and 5 can be found at the end of the dissertation.

Chapter 2
Methods

This Chapter presents a synthesis of the set of global ocean reanalyses and coupled climate models considered in the dissertation. The Chapter provides an overview of remote sensing instruments to monitor sea ice properties and gives a description of the observation-based products used here for assessing the realism of numerical systems. We present the metrics to evaluate amount of sea ice cover and its temporal/spatial variability. We focus on the necessity to distinguish sea ice classes - the MIZ and consolidated pack ice. The Chapter provides a comparison between two different methodologies to identify the MIZ: the conventional approach defining the MIZ through SIC thresholds and the statistical one based on day-to-day SIC variability. Using satellite estimates, ocean reanalyses, and coupled climate models we examine seasonal and long-term variability and spatial patterns of the MIZ extent in two approaches.

2.1 Tools

2.1.1 Global Ocean Reanalyses from CMEMS

Global ocean-sea ice reanalyses (ORAs) are an essential tool for assessing the variability and trends of ocean and sea ice properties in the recent past. In comparison to coupled climate models, they integrate ocean and sea ice observations through data assimilation schemes and indirectly integrate meteorological observations through fixed atmospheric forcing generally from atmospheric reanalyses (Dee et al., 2014; Storto et al., 2019). Compared with in-situ or satellite observations, ORAs are not only continuous in time and space, but also show inherent ocean model physics (Storto et al., 2019). ORAs represent a useful tool for in-depth investigation of the major climate phenomena, particularly those which are not directly observed. In this regard, the ORAs are of special significance in studying and monitoring the ice and ocean conditions in polar regions. In view of the above advantages, ORAs are widely used to study sea ice trends and sea ice interactions with the atmosphere and ocean (e.g. Chevallier et al., 2017; Ponsoni et al., 2019; Uotila et al., 2019; Spreen et al., 2011), or as initial and boundary conditions for sea ice in seasonal forecasting systems (e.g. Day et al., 2014; Guemas et al., 2016).

Even though the reanalyses are able to provide robust estimates of the mean state and variability of essential climate variables (Storto et al., 2019), they are not flawless: the fidelity of the ORAs depends on the reliability of ocean and sea-ice models and assimilation methods, and the accuracy of observational datasets. The model- and observations-related

deficiencies both contribute to the systematic errors in the reanalyses. The average of the values of individual reanalyses, i.e. the ensemble-mean reanalysis, can be considered as one single system. A multi-model ensemble approach might offer the best possible quality of the estimates of studied metrics since the ensemble operator smooths the strengths and weaknesses of individual ORAs. Furthermore, it is practically difficult to deduce which of the individual ORAs performs the best: the performance depends on the diagnostic and season, which highlights the feasibility of the multi-model approach. In this dissertation, we use the monthly outputs from the ensemble-mean reanalysis GREP produced by the Copernicus Marine Environment Monitoring Service (CMEMS) of the European Union, covering the period 1993-2019 (product reference GLOBAL REANALYSIS PHY 001 031). The GREP product is made up of four comprehensive ORAs (C-GLORSv7, Storto et al., 2016; FOAM-GloSea5, MacLachlan et al., 2015; GLORYS2v4, Lellouche et al., 2013; ORAS5, Zuo et al., 2019). All ensemble members are based on NEMO ocean model (Nucleus for European Modelling of the Ocean model, e.g. Madec et al., 2022). NEMO is a hydrostatic, finite-difference, primitive-equation general circulation model. All ensemble members are driven by common atmospheric forcing from the European Centre for Medium Range Weather Forecasts (ECMWF) ERA-Interim (Dee et al., 2011) but with different bulk formulas. The ORAs employ a tripolar mesh at the eddy-permitting resolution, ORCA025 grid (0.25°). This global configuration allows to explicitly represent mesoscale dynamics at middle-latitude, not in subpolar and polar ocean sectors (poleward of $\sim 50^{\circ}$ in each hemisphere). Three out of four ORAs employ thermodynamic-dynamic the Louvain-la-Neuve Sea-Ice Model (LIM2; Fichefet and Maqueda, 1997), among which two use elasto-visco-plastic rheology and one (ORAS5) implements visco-plastic rheology. The fourth reanalysis (FOAM) includes version 4.1 of the Los Alamos sea-ice model (CICE; Hunke, 2010). CICE is dynamic-thermodynamic sea-ice model, which employs five thickness categories and the elastic-viscous-plastic rheology and has more sophisticated physical formulations compared to LIM2. ORAs assimilate different observational products. SIC forcing is derived from OSISAF (Lavergne et al., 2019) in C- GLORSv7 and FOAM, Ifremer/CERSAT in GLORYS2v4 and OSTIA product (Good et al., 2020) in ORAS5. All reanalyses are available on monthly scale but C-GLORSv7 also provides data on a daily scale. Besides the aforementioned differences, there are many other differences among the single ORAs including data assimilation schemes, bias correction schemes, bulk formulations, and error definitions. All those differences among individual members contribute to the ensemble spread.

2.1.2 CMIP simulations

The coupled model intercomparison project (CMIP) is one of the fundamental elements of climate science at present and defines a collaborative framework designed to

improve knowledge of the past, present, and future climate change arising from natural and forced variability in a multi-model context. The CMIP collects and archives multiple model outputs in a standardized format to facilitate each-other comparison and make them freely available to a wide research community all over the world. The CMIP phase 6, recently released, differs from the previous phases by the experimental design and organization with more than twenty individually-designed MIPs (Eyring et al., 2016) addressing specific scientific topics as in Fig. 2.1. Following the efforts to improve the representation of many aspects of sea ice during previous phases of CMIP, a specific diagnostic project was launched in CMIP6, the Sea-Ice Model Intercomparison Project (SIMIP; Notz et al., 2016) with the overall objective to analyse the role of sea ice for the changing climate using coupled climate systems. Specifically, SIMIP provided a better understanding of the behavior of sea ice in the models, and of the degree to which models can reflect the real world. To assess the realism of sea-ice simulations, a new protocol for the climate-model output was designed with five groups of sea-ice related variables, each describing a key aspect of sea-ice evolution: sea-ice state variables, tendencies of sea-ice mass, heat and freshwater fluxes, sea-ice dynamics, and integrated quantities (Notz et al., 2016).

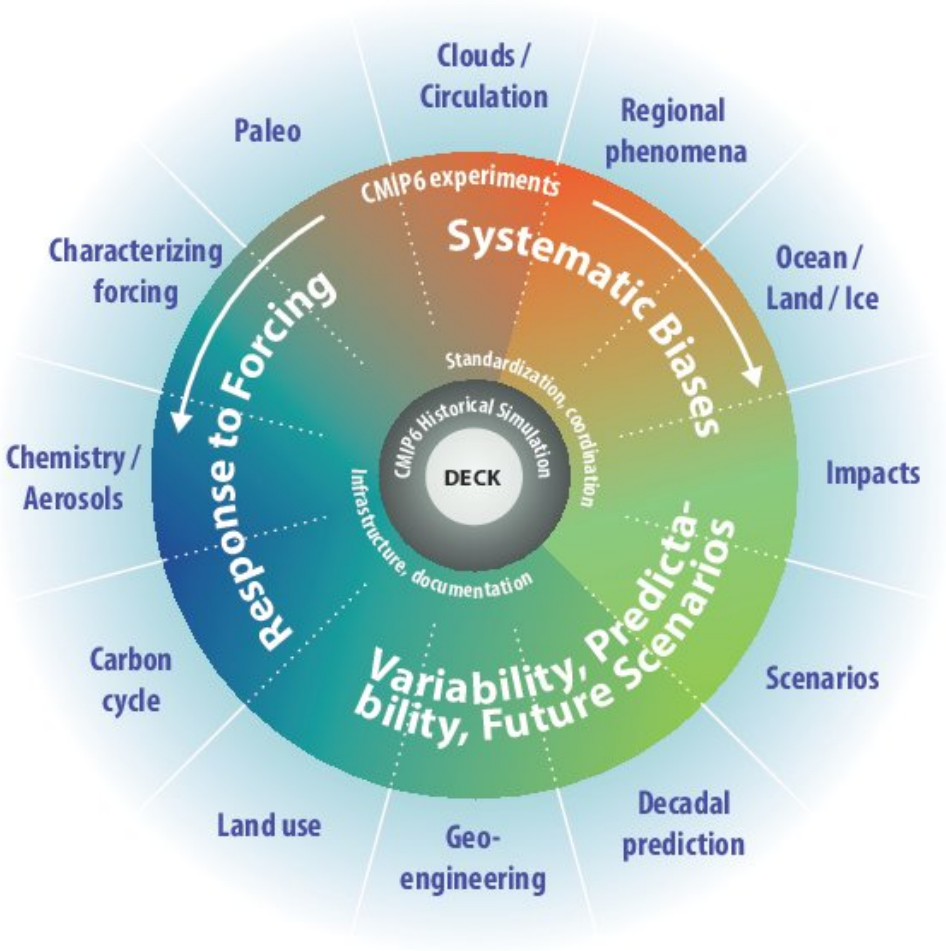

Figure 2.1: Schematic of the CMIP/CMIP6 experiment design; (Eyring et al., 2016)

CMIP6 climate models have been extensively assessed against their ability to capture a broad range of large-scale and regional climate processes (e.g. Robson et al., 2020; Watterson et al., 2021; Zanowski et al., 2021). In some cases, they show significant improvements compared to CMIP5 GCMs with reduced biases against observations. However, not all GCMs are equally skillful in capturing the climate processes that drive climate variability and change. Key biases and large uncertainties in climate projections generally remain. Reducing model biases remains one of the priorities of modelling groups worldwide. Robust projections of climate variability and change, particularly at regional scales, rely on the driving processes being represented with fidelity in model simulations. The role of enhanced spatial grid resolution is widely recognized as the way to better represent processes in all components of the climate system, tackle biases, and improve the realism of the model simulations. Progresses in high-performance computing resources and big data management have enabled climate models to simulate more processes in detail and on smaller scales.

The High Resolution Model Intercomparison Project (HighResMIP; Haarsma et al., 2016) is one of the CMIP6-endorsed projects, which applied a multi-model approach to the systematic investigation of the impact of enhanced horizontal grid resolution in the ocean and atmosphere on the representation of various climate phenomena. HighResMIP thereby focuses on one of the CMIP6 broad questions, "what are the origins and consequences of systematic model biases?". A coordinated set of experiments has been designed into three tiers (Fig. 2.2; Haarsma et al., 2016):

- Tier 1 consisting of atmosphere-only runs using observed SST forcing for the period 1950-2014 (highresSST-present)
- Tier 2 consists of couple runs including simulations with fixed 1950-forcing (control-1950), historical forcing until 2014 (hist-1950) and future projected forcing based on CMIP6-SS5 until 2050 (*highres-future*)
- Tier 3 as an extension of Tier 1 starting from 2015 (*highresSST-future*). These experiments use CMIP6 SSP5-8.5 scenario forcing.

In this thesis, the model outputs of coupled historical and future runs (*hist-1950* and *highres-future*) are used. Six different GCMs are considered with a combination of fourteen model configurations (based on resolution changes). A brief description of each of the models is given below.

The first model is the ECMWF Integrated Forecast System (ECMWF-IFS) cycle 43r1 (Roberts et al., 2018). The ocean and sea ice components are based on version 3.4 of the Nucleus for European Modelling of the Ocean (NEMO; Madec et al., 2022) and LIM2 with the viscous-plastic rheology. The atmospheric component is a hydrostatic, semi-Lagrangian, semi-implicit dynamical-core model the Integrated Forecasting System (IFS).

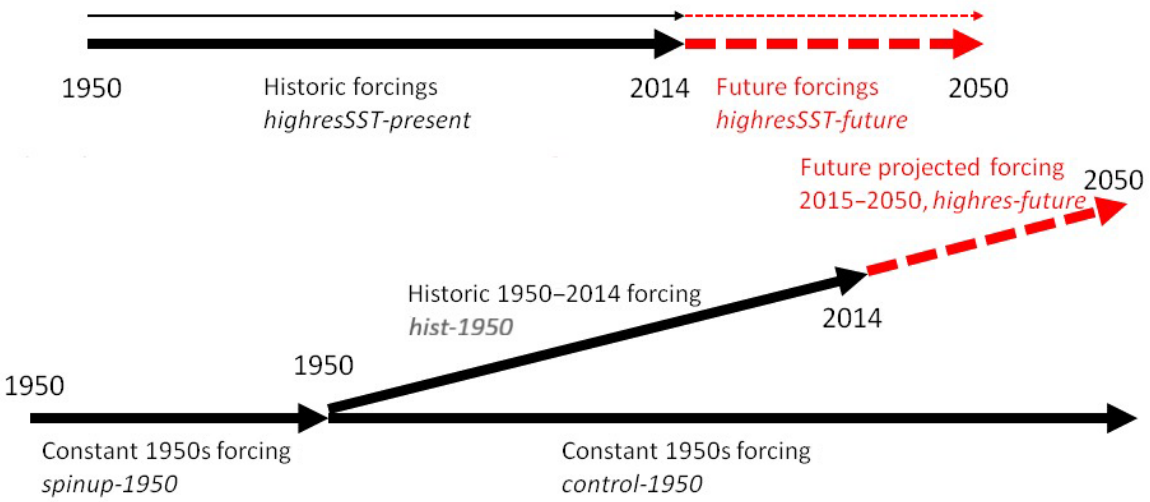

Figure 2.2: Short outline of HighResMIP design (Haarsma et al., 2016).

The land surface component is the Hydrology Tiled ECMWF Scheme of Surface Exchanges over Land (H-TESSEL; Balsamo et al., 2009). There are three configurations with varying ocean and atmosphere resolution. The low-resolution configuration (ECMWF-IFR-LR) is based on the ORCA1 tripolar ocean grid (resolution of 1°) and the Tco199 atmosphere grid (nominal resolution of 50km). The high-resolution configuration (ECMWF-IFR-HR) uses the ORCA025 eddy-permitting grid and Tco399 atmosphere grid (nominal resolution of 25 km). The intermediate resolution configuration (ECMWF-IFR MR) shares the atmospheric resolution with ECMWF-IFR-LR and the ocean resolution with ECMWF-IFR-HR.

HadGEM3-GC3.1, hereafter referred to as HadGEM3, is the Global Coupled 3.1 configuration of the Hadley Centre Global Environmental Model 3 (Williams et al., 2018). The model is composed of NEMO3.6 for the ocean and CICE5.1 for sea ice. The atmosphere (the Unified Model; Cullen, 1993) and land (the Joint UK Land Environment Simulator; Best et al., 2011). components run on the same grid. The model provides three different configurations. The coarse configuration, HadGEM3-LL, runs with the ORCA1 ocean grid and the N96 atmosphere grid (nominal resolution of 250 km). The intermediate configuration, HadGEM3-MM, uses the ORCA025 ocean grid and the N216 atmosphere (nominal resolution of 100 km). The finest configuration, HadGEM3-HM, uses the ORCA025 ocean grid and the N512 atmosphere grid (nominal resolution of 50 km).

The third model, EC-Earth3P, is a part of the EC-Earth3 family developed by the EC-Earth Consortium (Haarsma et al., 2020). It comprises version 3.6 of the NEMO ocean model and version 3 of the Louvain-la-Neuve sea-Ice Model (LIM3; Rousset et al., 2015), which is a dynamic-thermodynamic sea-ice model using five ice thickness categories and elastic viscous plastic rheology. The atmosphere and land use IFR model and H-TESSEL

of the ECMWF, respectively. The two versions of the model participate in HighResMIP: the first one is EC-Earth-LR with the TI255 atmosphere grid (nominal resolution of 100 km) and ORCA1 ocean grid; and the second one is EC-Earth3P-HR, which employs the ORCA025 grid for the ocean and the TI511 grid for the atmosphere.

CNRM-CM6-1 is the result of collaboration between the Centre National de Recherches Météorologiques (CNRM) and Cerfacs (Voldoire et al., 2019). The ocean component, NEMO3.6, is coupled to version 6 of the sea ice model GELATO. Gelato includes five thickness categories and uses elastic-viscous-plastic rheology. The CNRM-CM6 comprises version 6.3 of the global atmospheric model ARPEGE-Climat coupled to the surface component SURFEX (Masson et al., 2013), which simulates fluxes of heat, energy, and momentum. There are two configurations. The low-resolution configuration, CNRM-LR, is based on the eORCA1 ocean grid and the TI127 atmosphere grid (nominal resolution of 250 km). The fine-resolution configuration, CNRM-HR, runs on the eORCA025 ocean grid and the TI359 atmosphere grid (nominal resolution is of 100 km). The eORCA grid is the extension of ORCA, which permits a more realistic representation of the ice shelves edges in Antarctica ((Mathiot et al., 2017).

The fifth model, CMCC-CM2, is the contribution of Euro-Mediterranean Center on Climate Change to HighResMIP (Cherchi et al., 2019). The ocean component based on NEMO3.6 is coupled to CICE4.0 for sea ice. The atmosphere and land use version 4 of the Community Atmosphere Model (CAM, Neale et al., 2013 and version 4.5 of the Community Land Model (CLM, Oleson et al., 2013), respectively. Two configurations are distributed on the same ORCA025 grid. The only difference between the configurations is the atmosphere resolution: the coarser configuration, CMCC-CM-HR, has a resolution of 1° while the finer configuration, CMCC-CM2-VHR, runs with a resolution of 0.25°.

The sixth model is version 1.2 of Max-Planck Institute Earth System Model (MPI-ESM, Müller et al., 2018). It is made up of version 1.6.3 of the Max Planck Institute Ocean model (MPIOM, Jungclaus et al., 2013) and version 6.3 of the European Centre/Hamburg atmospheric model (ECHAM6.3) which includes the land surface model JSBACH (Stevens et al., 2013). MPIOM is a free-surface ocean-sea ice model using hydrostatic and Boussinesq approximations. The two model configurations use the same tripolar ocean grid TP04 at 0.4° resolution but the atmosphere grids are different: the first configuration, MPI-HR, runs on T127 with a nominal resolution of 100 km while the second configuration, MPI-VHR, uses T255 grid (the nominal resolution of 50 km).

2.1.3 Observation-based products

Before the satellite era, remote polar environments made ground- or ship-based research difficult, and sea ice was one of the least known features of the global climate

system. The sea ice mean state and changes were inferred from a number of sources of in-situ measurements such as buoys, submarines, aircraft, and ships (Smith et al., 2019). However, in-situ measurements are sparse in time and space, particularly in the Antarctic region. On October 1978, the Scanning Multichannel Microwave Radiometer (SMMR) began its mission aboard the Nimbus-7 satellite, launching the modern sea ice satellite record. SMMR used multiple microwave frequencies to accurately observe ice concentration, or the percentage of sea ice covering a given area. In addition, SMMR was capable of distinguishing younger, thinner ice from older, thicker, and more resilient sea ice. Starting from 1979, the set of satellites has provided a continuous record of sea ice coverage for both hemispheres, data archived and distributed by NSIDC (National Snow and Ice Data Center, https://nsidc.org/). Passive microwave radiometers enable sea ice monitoring by detecting microwaves naturally emitted by sea ice surface. Passive microwave data are the keystone of the satellite sea ice record and marked an essential step in observing seasonal and long-term variability of sea ice concentration. However, information on sea ice thickness is also needed to monitor ice changes. Because sea ice thickness is an essential parameter to quantify the real 3D structure of the sea ice volume, a comprehensive picture of sea ice evolution has been absent until quite recently. Satellite-based altimetry has increased our knowledge of spatial and temporal coverage of sea ice thickness. The Environmental satellite (EnviSat) was launched in March 2002 by the European Space Agency (ESA) and has operated until April 2012. EnviSat carried onboard 10 instruments and monitored a wide range of environmental characteristics including sea ice thickness at both poles (Tilling et al., 2019; Wang et al., 2022). In 2003, the Ice, Cloud, and land Elevation Satellite (ICESat) mission was launched by NASA to track sea ice thickness (SIT), as well as ice sheet heights, clouds, and land cover (Kwok and Cunningham, 2008). Shortly before ICESat was decommissioned in 2009, Nasa operated the IceBridge mission to fly similar instruments over the poles aboard aircraft to continue the record until a follow-on mission, ICESat-2, could be launched in September 2018. In the same decade, ESA launched the CryoSat-2 mission dedicated to measuring polar sea ice thickness and monitoring changes in ice sheets (Laxon et al., 2013). SIT remote sensing with radar altimetry is an indirect method that relies on retrievals of sea ice freeboard. This method is based on certain assumptions and parametrizations that introduce several uncertainty factors, some arise from the radar measurements themselves, and others are induced during the ensuing processing. Uncertainties are related to the distortion of the signal over different surface types and the lack of reliable estimates of snow thickness covering the ice (Alexandrov et al., 2010; Tilling et al., 2015). In the Antarctic, the large uncertainties are also attributed to the relatively small freeboard (Maksym and Markus, 2008).

Many algorithms have been developed to retrieve ice properties (mainly SIC) from

satellite-based (e.g. Svendsen et al., 1987; Cavalieri et al., 1984; Tikhonov et al., 2016), and hence many sea ice products. Among those, for this study four well-known and validated records are considered: NOAA/NSIDC Climate Data Record (CDR) version 3 (Meier et al., 2017) and version 4 (Meier et al., 2021), EUMETSAT OSISAF Climate Data Record and Interim Climate Data Record (release 2, products OSI-450 and OSI-430-b, (Lavergne et al., 2019), and IFREMER/CERSAT (Ezraty et al., 2007). They all cover the period from 1979 onward and are available at monthly and daily (since 1987) time resolution. CDR algorithm leverages two well-established sea ice concentration algorithms: the NASA Team (NT) algorithm (Cavalieri et al., 1984) and the Bootstrap (BT) algorithm (Comiso, 1986). The combination of the strengths of two algorithms has a beneficial effect on the accuracy of the output (Meier et al., 2021) CDR uses gridded brightness temperatures in low frequencies from the Nimbus-7 SMMR (18, 37 GHz) and the DMSP series of SSM/I and SSMIS passive microwave radiometers (19.4, 22.2, 37 GHz). Different ratios of frequencies are used to filter weather effects. The output data is distributed on a 25 km x 25 km polar stereographic grid. The CDR version 4, released in June 2021, includes a number of updates including altered weather filter thresholds in the Southern hemisphere and filled Arctic pole hole (Meier et al., 2021). The second passive microwave data record comes from the EUMETSAT Ocean-Sea Ice Satellite Application Facilities (OSISAF). OSI-450 is the second major version of the OSISAF Global Sea Ice Concentration Climate Data Record covering the period from 1979 to 2015. The Interim OSI-430-b complements OSI-450 starting from 2016 onwards. OSI-450 SIC is based on the SMMR (1979-1987), SSM/I (1987-2008), SSMIS (2006-2015) instruments using 19.35 and 37 GHz frequency, and ERA Interim reanalysis data (**?**), gridded to a 25 km x 25 km grid. OSI-430-b uses SSMIS data from NOAA CLASS, and operational analysis and forecast from ECMWF. The third SIC dataset we present here is developed at IFREMER/Centre d'Exploitation et de Recherche SATellitaire (CERSAT), using the Artist Sea Ice (ASI) algorithm developed at the University of Bremen. The ASI algorithm blends the Svendsen algorithm (Svendsen et al., 1987) and the NASA team algorithm (Cavalieri et al., 1999); it is based on the 85.5 GHz channel brightness temperature data. The SIC field from IFREMER/CERSAT product is distributed at 12.5 km. Although the higher frequency channels have a higher spatial resolution, they are more sensitive to weather effects (water vapor and clouds) that reduce the accuracy of SIC retrievals (Pang et al., 2018).

Understanding the large-scale characteristics of SIT is a tough challenge due to the sparse distribution of in-situ observations (Worby et al., 2008). A set of different approaches are also available and applied to retrieve SIT from satellite measurements. It is well known that satellite observations have wider spatiotemporal coverage than in-situ observations. However, previous studies indicate that there is large uncertainty in SIT data retrieval from satellite altimeters owing to the relatively small freeboard mainly in

the Antarctic sea ice (Maksym and Markus, 2008) and the lack of knowledge about snow depth, as well as sea-ice and snow density (Alexandrov et al., 2010). There are still large differences among satellite-based SIT estimates; even though the SIT spatial distribution can be similarly reproduced, uncertainties on thickness values are large and regionally dependent. Since no observational data set of sea ice thickness is available until now that spans a long time period and is spatially continuous, this thesis relies on reanalysis data from the Pan-Arctic Ice Ocean Modeling and Assimilation System (PIOMAS, Zhang and Rothrock, 2003) and the Global Ice-Ocean Modeling and Assimilation System (GIOMAS, Zhang and Rothrock, 2003) to represent observed sea ice thickness. PIOMAS is a numerical model with sea ice and ocean components, and the capabilities of assimilating satellite sea ice concentration and sea surface temperature. The ice thickness is derived from the internal sea ice (thermo)dynamics, creating a continuous time series. It has been extensively evaluated against satellite, submarine, and in situ observations (e.g. Stroeve et al., 2014; Wang et al., 2016; Labe et al., 2018; Lang et al., 2017; Laxon et al., 2013; Wang et al., 2016). Despite some spatial bias in the ice thickness distribution, where the reanalysis tends to overestimate (underestimate) thin (thick) ice thickness, the estimates were found to agree well with observations. GIOMAS is the global configuration of the model reanalysis and assimilates the same ice and ocean variables. It is extensively used as reference in climate and model assessment studies in the Antarctic region (Uotila et al., 2017; DuVivier et al., 2020; Liao et al., 2022; Shu et al., 2015) and predictions (Ordoñez et al., 2018; Morioka et al., 2021). However, GIOMAS has been less widely evaluated in part because there are far fewer observations of Antarctic SIT against which evaluation is possible (DuVivier et al., 2020). Besides thickness and volume, the outputs provided by GIOMAS include monthly mean sea ice concentration, sea ice velocity, snow depth, sea ice growth and melt rate, for both Arctic and Antarctic regions, from 1970 to present. The data comprises also some of the ocean variables, such as sea surface temperature and salinity, and ocean velocities. Some technical aspects of the systems follow. PIOMAS and GIOMAS are composed of global Parallel Ocean and sea Ice Model (POIM) coupled to a data assimilation scheme. The models ingest SIC from the NSIDC near-real time product (Brodzik and Stewart, 2016) and SST from NCEP/NCAR reanalysis (Kalnay et al., 1996). POIM couples the Parallel Ocean Program (POP) with an eight-category thickness and enthalpy distribution (TED) sea-ice model. The average horizontal spatial resolution of the global mesh is 0.8° x 0.8° (about 60 km x 60 km). In the Northern hemisphere, the model is distributed on a stretched GOCC grid with the northern grid pole located in Greenland; the horizontal resolution in the Arctic is up to 22 km. In the Southern hemisphere, the model grid is based on a spherical coordinate system.

2.2 Methodologies

The area of the ocean covered by sea ice is usually described in terms of sea-ice extent (SIE) and sea-ice area (SIA), which are highly correlated but have different value. Both are computed from the percentage of each grid cell covered by ice (SIC). SIE is defined as the integral sea-ice area of grid cells with a SIC higher than a certain threshold value, conventionally 15%; this value stems from the uncertainty in the methodology to retrieve SIC using passive microwave sensors. SIA is calculated as the sum of sea-ice areas of all grid cells, i.e. $\sum_{i=1}^{N} SIC_i$ x A_i, where A_i is the area the given grid cell and index i runs over the grid cell of the domain. Overall, SIA excludes open water areas between the ice floes, while SIE marks all grid cells with at least 15% SIC as 100%. Because the uncertainties from passive microwave retrievals have less effect on SIE, it is often used to describe sea-ice coverage.

To calculate the inconsistency between reanalyses and satellite products we employ the integrated ice area error (IIAE) approach (Roach et al., 2018, 2020) adapted from the extent-based integrated ice-edge error metric (IIEE, Goessling et al., 2016). The IIAE identifies the area on which ORAs and observations which are considered as a "true state" disagree. The IIAE represents a sum of overestimated (O) and underestimated (U) sea-ice area.

$$IIAE = O + U$$

with

$$O = \int_A max(c_m - c_o, 0) dA$$

and

$$U = \int_A max(c_o - c_m, 0) dA,$$

where A is the area of interest, c_m is the simulated sea ice concentration, and c_o is the observed sea ice concentration.

In our study, to examine the spatial and temporal variability of the sea ice in the very sensitive marginal ice zone, particular interest is given to the representation of sea ice classes in addition to the total sea ice area. We divide sea ice in marginal ice zone (MIZ) and consolidated pack ice.

The MIZ is qualitatively defined as the area where sea ice properties are impacted by open-ocean processes, especially ocean surface gravity waves (Wadhams, 1986). Considered as a transition region, the MIZ separates the open ocean conditions from the consolidated pack ice. The plausible estimates of the MIZ and time/space variability of its area/extent are essential for understanding atmosphere-ice-ocean interactions and biological processes. However, it is challenging to accurately determine the boundaries between the sea ice classes. In addition, the physical processes that identify the MIZ,

cannot be obtained at high frequency and large scales. As viewed by remote sensors, the MIZ is historically identified as the area capped by 15% and 80% SIC boundaries using satellite passive microwave SIC (Strong and Rigor, 2013; Aksenov et al., 2017; Rolph et al., 2020). Following the studies in the Arctic, where the threshold-based definition adequately distinguishes the MIZ from the pack ice, the method was directly applied to the Antarctic. Given that sea ice in the Antarctic is dominated by seasonal pancake ice, the air-sea interactions might not strongly depend on sea-ice coverage and the fully ice-covered ocean does not necessarily correspond to pack ice conditions (Alberello et al., 2019; Vichi et al., 2019; Brouwer et al., 2021). An alternative statistical approach to detect the MIZ conditions is proposed by Vichi (2022). The method is based on the temporal and spatial variability of SIC and considers the highly dynamic nature of the MIZ. For each grid cell, the daily SIC anomaly is computed as a difference between daily SIC and yearly averaged SIC for the respective month. Then, the standard deviation of the daily anomaly is calculated for each month:

$$\sigma^m_{SIC}=\sqrt{\frac{1}{N}\sum_{i=1}^{N}(\sigma^m_i)^2},$$

where (σ^m_i) is the daily SIC anomaly, m is the month and N is the total number of days in the month.

The climatological monthly standard deviation of the anomalies (σ_{SIC}), referred to as the indicator, is calculated by merging all the daily anomalies from the same month in different years:

$$\sigma_{SIC}=\sqrt{\frac{1}{N}\sum_{j=1}^{N*Y}(\sigma_i)^2},$$

with Y being the number of years and the index j running over the number of days of each month.

Hence, the open-ocean or pack ice conditions are more likely to experience small perturbation relative to the long-term mean SIC. To differentiate the MIZ from more consolidated ice, the threshold of 10% is chosen from the median distribution of σ_{SIC}. The grid cells with σ_{SIC} exceeding 10% are identified as MIZ. Apart from being physically explained, this method is perspective as it might overcome the disparity among the algorithms that can provide contrasting estimates of total and marginal sea-ice extents (Stroeve et al., 2016).

To compare two methods in detecting the MIZ we show climatological values of σ_{SIC} in different months together with the mean position of 15% and 80% sea ice edges (Fig. 2.3). It is evident that Vichi's approach suggests an extended area with MIZ-like properties: despite high sea ice fractions, the region can still exhibit high day-to-day variability which is characteristic of the MIZ.

The annual seasonal cycle of the MIZ extent over 1993-2019 period for C-GLORSv7 and CDR estimated using two approaches is shown in Fig. 2.4. The MIZ extent in CDR

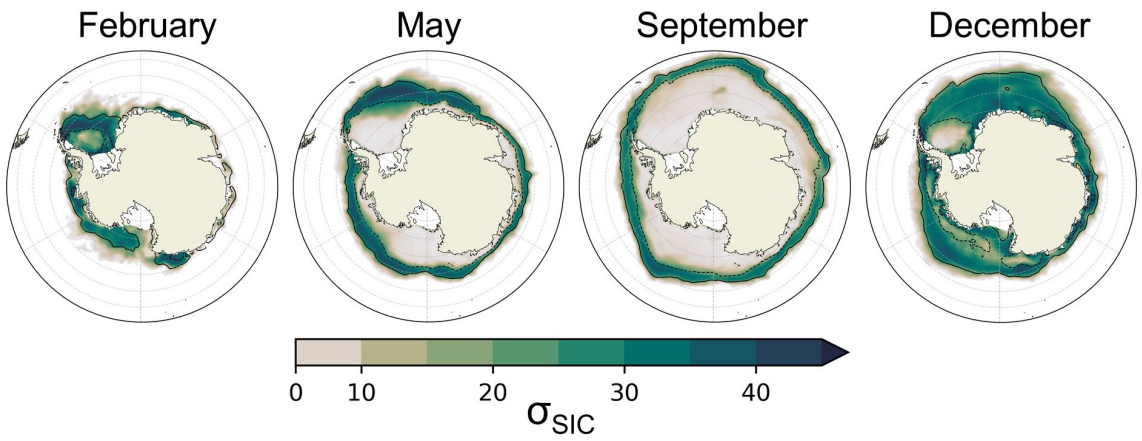

Figure 2.3: Climatological values of the indicator (σ_{SIC}) in the Antarctic in C-GLORSv7 for the years 1993-2019. Contours indicate the mean position of 15% (solid) and 80% (dashed) ice concentration.

has the annual minimum in February and the maximum in December with both methods, but σ_{SIC}-based approach reproduces a larger MIZ. When comparing the two methods, it is clear that the major difference is in the advance season for both datasets: the threshold-based MIZ extent grows continuously from February to October, while σ_{SIC})-based approach indicates that the MIZ expands from February to May and then remains constant until October. Using the conventional approach, the two products are consistent in the shape of the mean seasonal cycle with slightly higher values in C-GLORSv7 in all months, the alternative method exhibits stronger bias from May to October while in the rest of the year there is close agreement between two datasets.

To assess the differences between the two approaches for the MIZ definition on a long-term scale, we evaluate monthly trends (as a function of longitude and month) in the MIZ extent calculated for CDR for the years 1993-2019 (Fig. 2.5). The spatial pattern is reproduced in a similar way, however, there are a number of discrepancies, the most pronounced of which occur in the Weddell Sea: the σ_{SIC}-based approach reveals more negative trends in different seasons. The differences might also be attributed to the fact that the SIC-based definition is limited by the temporal resolution: the monthly fields of SIC are not able to capture the highly dynamic nature of the MIZ. he examination of seasonal and long-term variability of the MIZ extent using C-GLORSv7 and CDR reveal that the choice of approach for the MIZ definition does not significantly modify the result.

The comparison between two MIZ definitions is also carried out for HighResMIP model outputs (Figure 2.6). For both methods, the models simulate seasonal minimum in February and maximum in December and generally underestimate the MIZ extent in comparison to CDR. There is no significant difference between the two methods, however, the σ_{SIC}-approach suggests a slightly higher MIZ extent in the advance season from April to September. Using a conventional approach, two models (HadGEM3 and CMCC-CM2)

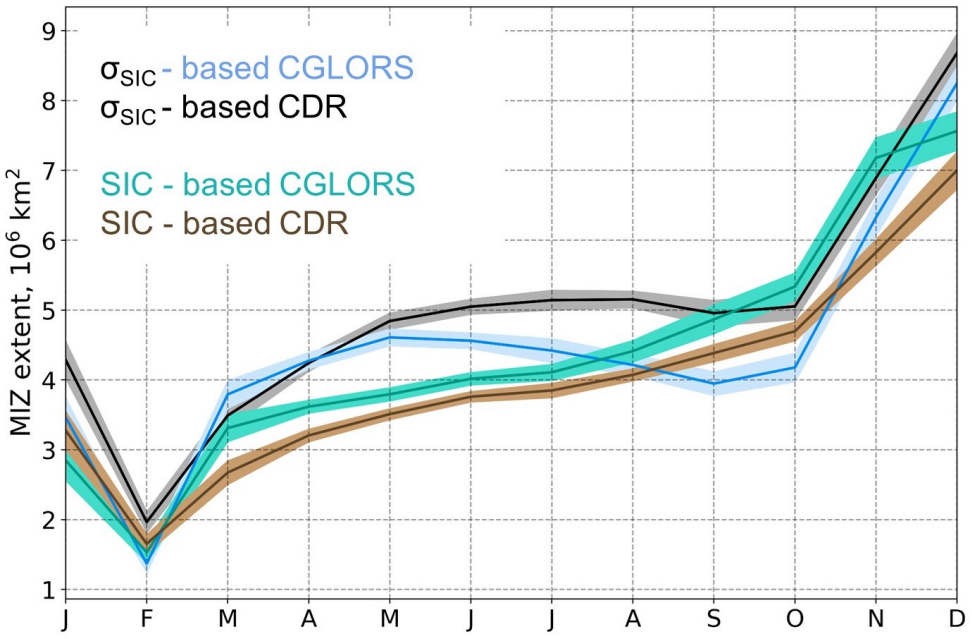

Figure 2.4: Seasonal cycle of the Antarctic MIZ extent estimated from concentration criterion (15% < SIC < 80%) and σ_{SIC} criterion (σ_{SIC} > 10%) for CGlORSv7 and NSIDC CDRv3 for the years 1993-2019

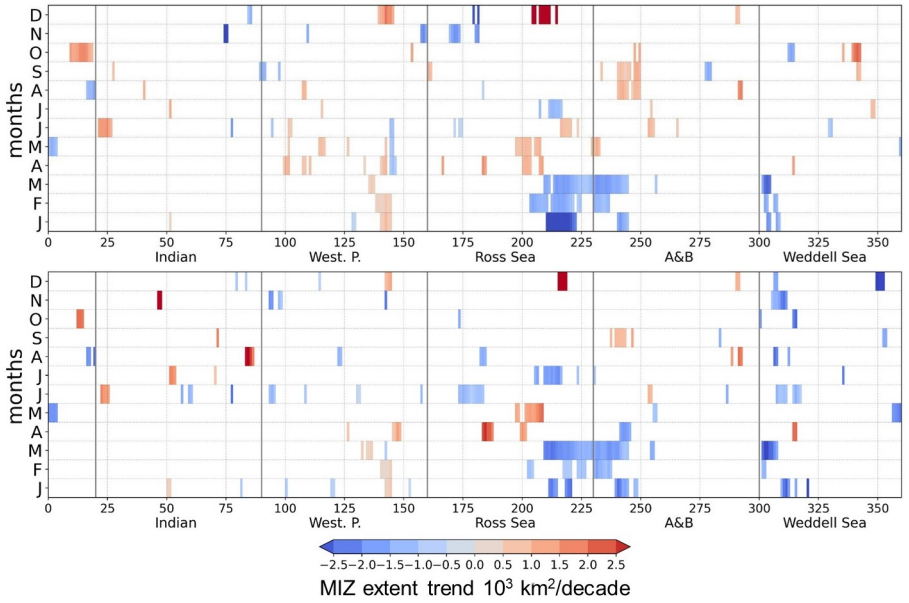

Figure 2.5: Monthly trends (1993-2019) in MIZ extent, as a function of longitude estimated from concentration criterion (15% < SIC < 80%; upper panel) and σ_{SIC} criterion (σ_{SIC} > 10%; lower panel) for CDR. Only significance higher than 95% are shown.

largely overestimate the MIZ extent in December and January which reflects the rapid spring sea ice retreat in these models while with the σ_{SIC}-approach they simulate a higher extent relative to satellite estimates only in January. Additionally, HadGEM3 and CMCC-CM2 do not exhibit pronounced growth of the MIZ extent in the advance season which is seen in the other models: the values are constant from March to October. EC-Earth3

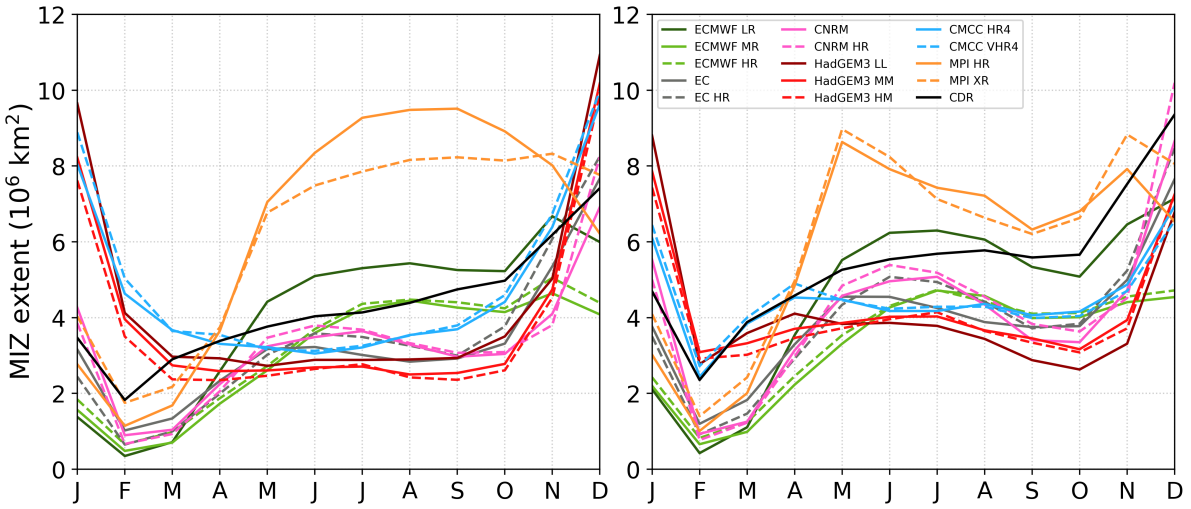

Figure 2.6: Seasonal cycle of the Antarctic MIZ extent estimated from concentration criterion ($15\% < \text{SIC} < 80\%$; left) and σ_{SIC} criterion ($\sigma_{SIC} > 10\%$; right) for HighresMIP models and NSIDC CDRv4 for the years 1993-2019.

and CNRM simulate a slight decrease of the MIZ extent from July to October when the total sea-ice cover expands to its largest seasonal extent which results in a second MIZ extent maximum in June. MPI-ESM produces distinct from the other models seasonal cycle in the MIZ extent: with the threshold approach, the model shows similar to the total sea-ice extent seasonality with considerable spring expansion and the maximum peak in September while using the σ_{SIC}-definition leads to sharp growth from February to May followed by a decrease until September and a second maximum in November.

The climatological maps of the indicator for February and December, months of the MIZ minimum and maximum extent, are shown in Figure 2.7. Apart from different amount of sea ice, the models differ on the intensity of the MIZ conditions and the area of high intensity. In February, the models generally underestimate the intensity compared to CDR. Even the models with similar to CDR February MIZ extent (HadGEM3 and CMCC-CM2) demonstrate the lower intensity of temporal SIC variability. In December, during the rapid sea ice retreat, the region presenting the MIZ features expands. The models exhibit high SIC variability and some of them are close to the estimates from CDR.

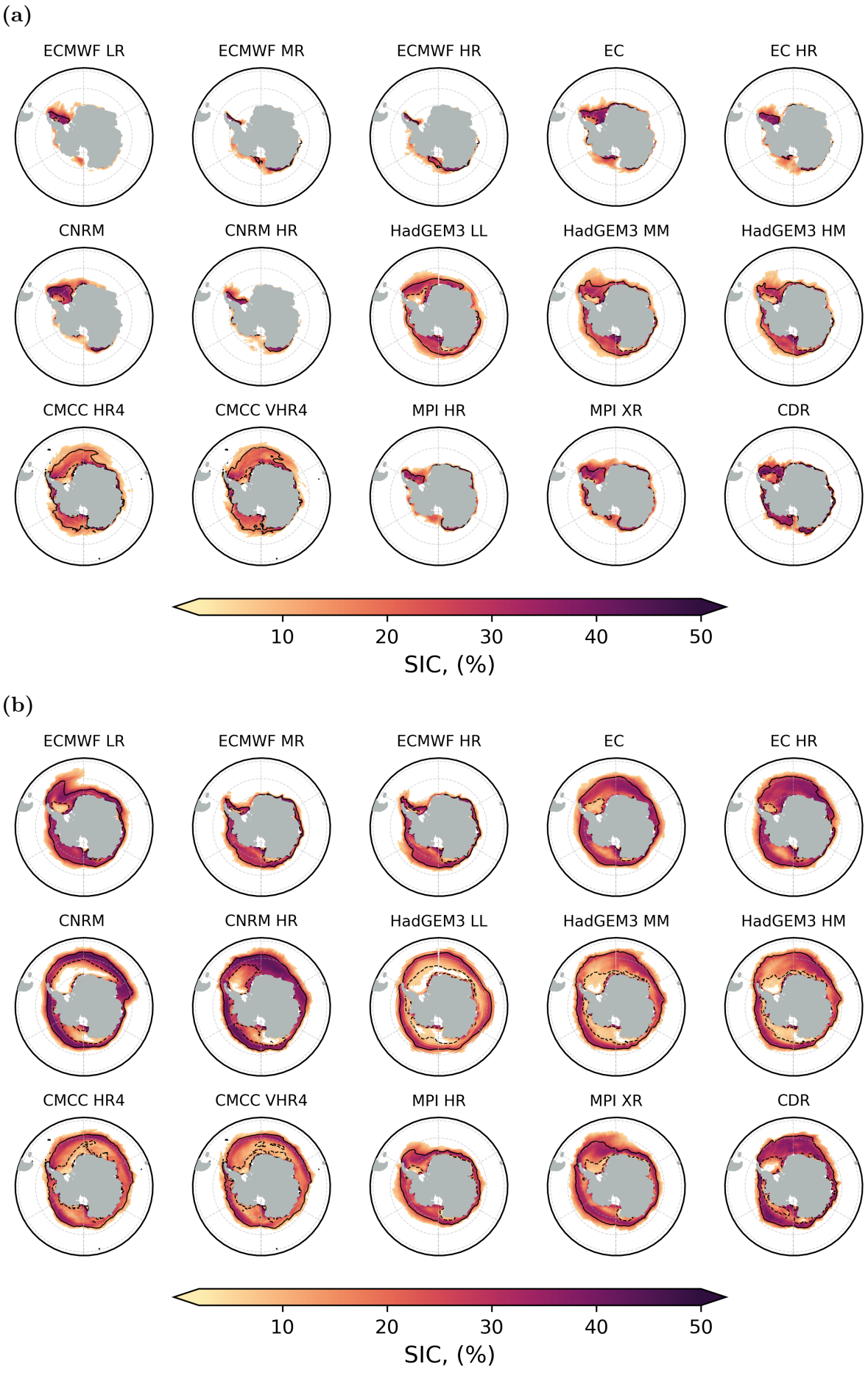

Figure 2.7: Climatological values of the indicator (σ_{SIC}) for HighresMIP models and NSIDC CDRv4, computed as the standard deviation of the daily anomalies for February (a) and December (b), averaged over 1993-2014.

Chapter 3

Sea ice in Global Ocean reanalyses

Global ocean reanalyses represent an essential tool for investigating temporal and spatial variability of the ocean and sea-ice properties in the recent past and present. The current Chapter describes how sea ice is treated in the ensemble-mean of four global ocean reanalyses GREP produced within the European Copernicus Programme. We start to investigate sea-ice changes and examine the realism of sea-ice representation from the Northern Hemisphere. (Figure 3.1). We find that GREP is in close agreement with

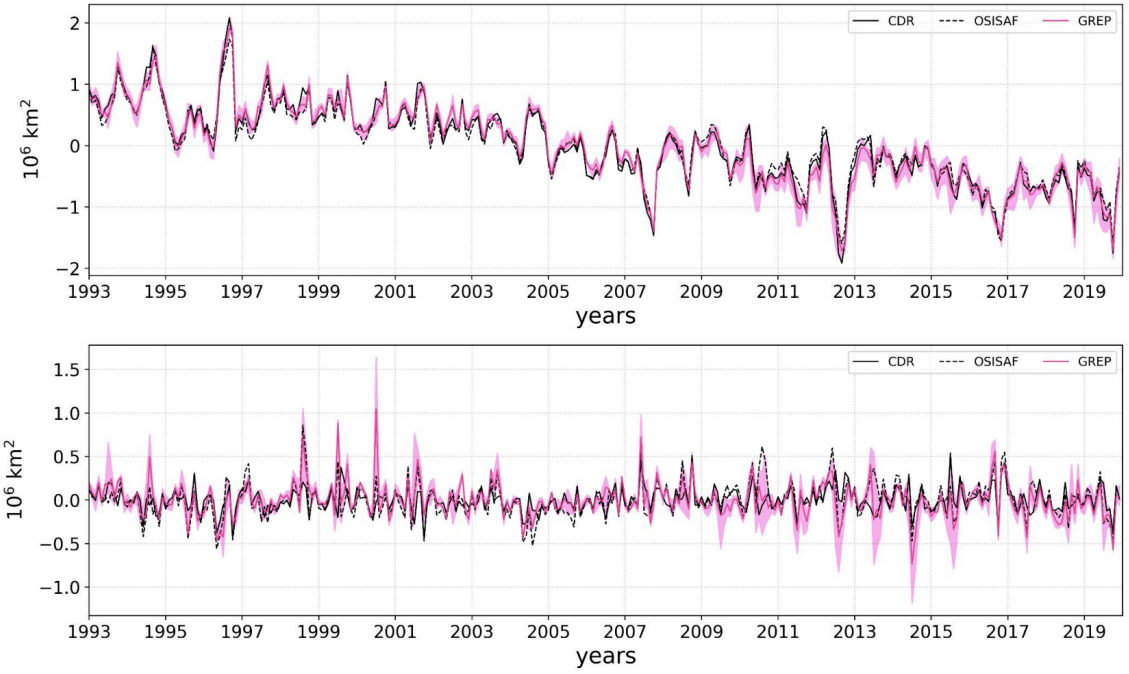

Figure 3.1: Time series of (upper panel) monthly averages and (lower panel) monthly anomalies of Antarctic sea ice area in GREP (magenta) and CDR (black) from January 1993 to December 2019, for GREP (magenta), CDR (black solid) and OSISAF (black dashed). Pink shading denotes the envelope of GREP members.

satellite estimates for SIA: GREP properly reproduces interannual variability, decreasing trend, as well as record summer lows of 2007 and 2012. GREP and satellite products are consistent for the yearly average SIA trend which is -0.07 million km^2/year for GREP, -0.07 million km^2/year for CDR, and -0.06 million km^2/year for OSISAF. The ensemble spread is relatively narrow nearly until the end of the 2000s and slightly increases at the end of the time series when the pace of sea-ice loss has accelerated. For the MIZ area, CDR and OSISAF are not always consistent throughout the time series which reflects uncertainties of the SIC retrievals due to varying surface properties within the MIZ re-

gion. GREP generally agrees well with CDR and presents similar pattern of interannual variability. The trends for the annual average MIZ are close to zero and not significant for all datasets. The ensemble spread is larger compared to SIA and increases starting from the 2010s.

Considering a poor understanding of sea-ice area changes in the Southern Hemisphere, we dedicate a particular focus on the Antarctic region. The Chapter examines the realism of global ocean reanalyses in the representation of the Antarctic sea-ice area from 1993 to 2019. The Chapter explores time/space changes in sea ice distribution within the marginal ice zone and consolidated pack ice highlighting their different response to climate change. The results of the analysis are contributed to two publications presented below.

frontiers in Earth Science

ORIGINAL RESEARCH
published: 10 February 2022
doi: 10.3389/feart.2022.745274

The Antarctic Marginal Ice Zone and Pack Ice Area in CMEMS GREP Ensemble Reanalysis Product

Doroteaciro Iovino[1*†], *Julia Selivanova*[1,2*†], *Simona Masina*[1] *and Andrea Cipollone*[1]

[1]*Ocean Modeling and Data Assimilation Division, Centro Euro-Mediterraneo Sui Cambiamenti Climatici, Bologna, Italy,*
[2]*Department of Physics and Astronomy, University of Bologna, Bologna, Italy*

Global ocean reanalyses provide consistent and comprehensive records of ocean and sea ice variables and are therefore of pivotal significance for climate studies, particularly in data-sparse regions such as Antarctica. Here, for the first time, we present the temporal and spatial variability of sea ice area in the ensemble of global ocean reanalyses produced by the Copernicus Marine Environment Monitoring Service (CMEMS) for the period 1993–2019. The reanalysis ensemble robustly reproduces observed interannual and seasonal variability, linear trend, as well as record highs and lows. While no consensus has been reached yet on the physical source of Antarctic-wide ice changes, our study also emphasizes the importance of understanding the different responses of ice classes, marginal ice zone (MIZ) and pack ice, to climate changes. Modifications of the distribution of MIZ and pack ice have implications for the level of air/sea exchanges and for the marine ecosystem. Analysis of the spatial and temporal variability of ice classes can provide further insights on long-term trends and help to improve predictions of future changes in Antarctic sea ice. We assess the ability of the reanalysis ensemble to adequately capture variability in space and time of the MIZ and pack ice area, and conclude that it can provide consistent estimates of recent changes in the Antarctic sea ice area. Our results show that the Antarctic sea ice area agrees well with satellite estimates, and the hemispheric and regional sea ice area variability are properly reproduced on seasonal and interannual time scales. Although the ensemble reanalysis product tends to slightly overestimate MIZ in summer, results show that it properly represents the variability of MIZ minima and maxima as well as its interannual variability during the growing and melting seasons. Our results confirm that Global Reanalysis Ensemble Product is able to reproduce the observed substantial regional variability, in regions covered by marginal ice.

Keywords: Antarctic sea ice, marginal ice zone, pack ice, ocean reanalyses, GREP

OPEN ACCESS

Edited by:
Stefanie Arndt,
Alfred Wegener Institute Helmholtz Centre for Polar and Marine Research (AWI), Germany

Reviewed by:
Alexander Fraser,
University of Tasmania, Australia
Lu Zhou,
University of Gothenburg, Sweden

***Correspondence:**
Doroteaciro Iovino
dorotea.iovino@cmcc.it
Julia Selivanova
iuliia.selivanova@unibo.it

[†]These authors share first authorship

Specialty section:
This article was submitted to Cryospheric Sciences, a section of the journal Frontiers in Earth Science

Received: *21 July 2021*
Accepted: *17 January 2022*
Published: *10 February 2022*

Citation:
Iovino D, Selivanova J, Masina S and Cipollone A (2022) The Antarctic Marginal Ice Zone and Pack Ice Area in CMEMS GREP Ensemble Reanalysis Product. Front. Earth Sci. 10:745274. doi: 10.3389/feart.2022.745274

INTRODUCTION

Antarctic sea ice plays a critical role in the polar and global climate and ecosystems, modulating the exchanges of momentum, gases and heat between the ocean and the atmosphere. A deep knowledge of sea ice variability is necessary for adequately simulating these fluxes and thus for climate modelling. In stark contrast to the Arctic, where sea ice has declined significantly in all areas and seasons (e.g., Parkinson and Cavalieri, 2012; Serreze and Stroeve 2015; Onarheim et al., 2018), Antarctic sea ice has not experienced a drastic and continuous decline during recent decades. Satellite

records show a slight increasing trend in total annual-mean Antarctic sea ice extent (SIE) at a rate of ~1.5% per decade for the 1979–2015 period, with modest increases in the maxima and minima (Turner et al., 2015; Comiso et al., 2017), albeit individual regions experienced much larger gains and losses that almost offset each other overall (Parkinson, 2019). After record maxima successively occurred in 2012, 2013, and 2014, Antarctic sea ice decreased below the long-term average in 2015, with unprecedented record low minima in 2016, 2017 and 2018 (Parkinson, 2019). However, the recent decrease does not signify a change in the sign of the long-term trend, which remains positive over the period 1979–2019, though with lower magnitude compared to the 1979–2015 trend (Wachter et al., 2021).

Understanding this quasi-stable situation in Antarctic sea ice and its link to climate change is still a significant scientific challenge (Kennicutt et al., 2015). Rather than by a single mechanism, the long-term sea ice variability is driven by a combination of processes, such as local changes in the atmospheric dynamics and wind patterns (e.g., Holland and Kwok, 2012; Meehl et al., 2016; Vichi et al., 2019; Blanchard-Wrigglesworth et al., 2021), shifts in the dominant modes of large-scale atmospheric circulation in the southern hemisphere (Stammerjohn et al., 2008), changes in the vertical structure of the near-surface water column (Goosse and Zunz, 2014; Venables and Meredith, 2014), changes in ice albedo feedback (Riihelä et al., 2021), ice-ocean feedbacks (Goosse and Zunz, 2014; Frew et al., 2019), and variability of the ice sheet water discharge (Bintanja et al., 2013; Haid et al., 2017; Pauling et al., 2017). These processes combine in different ways at regional scales. Significant regional contrasts and variability are nested within the Antarctic-wide changes: while the Ross and Weddell Seas dominate the overall upward trend, the Amundsen-Bellingshausen Seas have undergone a considerable decrease (Massom and Stammerjohn, 2010; Parkinson, 2019). High-magnitude seasonal variability is also disguised in long-term expansion of total sea ice cover: a complex seasonal pattern of trends emerges across the regions, with positive expansion trend in one season and negative in another (Holland, 2014; Hobbs et al., 2016; Parkinson, 2019). Considering the spatial and seasonal heterogeneity of trends, the Antarctic-wide changes could not aid in the attribution of those trends. The focus instead should be on the regional and seasonal variability which may give a better understanding of the long-term changes in Antarctic sea ice area.

While changes in total sea ice at different spatial/temporal scales remain puzzling, it is likely that these changes also affect the distribution and variability of ice classes in different ways (Stroeve et al., 2016; Iovino et al., 2022). Here, we define ice classes to distinguish between consolidated pack ice and the marginal ice zone (MIZ). Understanding how the spatial patterns of different ice classes change may help to elucidate the mechanisms contributing to the expansion of Antarctic ice in some regions and contraction in others (Maksym et al., 2012). In spite of the large winter cover, sea ice around Antarctica forms a vast field of small broken ice floes, with compact and consolidated ice remaining all year around only in a few coastal regions (e.g., Holland et al., 2014). The MIZ is highly dynamic and its response to climate variability differs from the inner pack ice: it undergoes faster melting due to a larger lateral melt rate (Tsamados et al., 2015), responds more easily to winds and current forcing (Manucharyan and Thompson, 2017; Alberello et al., 2020), and is highly vulnerable to waves and swell (Kohout et al., 2014). The MIZ is fundamental for climate dynamics and polar ecosystems, given its roles as a region of intense atmosphere-sea ice interactions and as a physical buffer between the consolidated pack ice zone and the effects of open ocean dynamics (e.g., Squire 2007). Monitoring changes of the MIZ environment can help us understand the associated changes in the climate system. An accurate assessment of Antarctic MIZ variability is still missing, as well as a deep insight into how ice conditions correlate with atmospheric fields and surface oceanic waves (Meylan et al., 2014, Sutherland and Balmforth 2019). The MIZ can be operationally defined through sea ice concentration (SIC) thresholds as the transitional region between open water and consolidated pack ice, where the ocean is covered by SIC between 15 and 80% (e.g., Pauling et al., 2017).

There is growing demand for comprehensive records of the historical ocean state. Ocean Reanalyses (ORAs) represent an essential tool to monitor long-term variability of various climate indices, especially in areas with sparse data such as the Antarctic Ocean. Observations alone can not reasonably reproduce consistent and homogeneous time series of three-dimensional gridded fields of ocean and ice parameters. Model simulations, on other hand, can provide somewhat accurate information regarding the ocean and ice mean states and variability, despite being prone to errors related to model formulation, initialization and forcing. A number of experiments with global ocean-sea ice models were carried out in the framework of the Coordinated Ocean-ice Reference Experiments (CORE-II) and the Ocean Model Intercomparison Project (OMIP), albeit with little focus on sea ice performance in polar regions (e.g., Downes et al., 2015; Farneti et al., 2015; Tsujino et al., 2020). Most CORE-II models are found to underestimate Antarctic SIC in summer and reproduce the sea ice edge further south compared to observations (Downes et al., 2015). The OMIP simulations reproduce a very wide range of models spread in sea ice concentration and volume, with ratios of the maximum to the minimum reaching a factor of two to three (Tsujino et al., 2020). Inaccurate representation of sea ice and a large spread across model output is due to the fact that these model systems are not constrained by observations through data assimilation schemes. The advantage of ORAs with respect to observation-only products and ocean models, is the combination of ocean/sea ice models and observational data sets driven by atmospheric forcing. The errors from models and forcing datasets are reduced through assimilation of observations. Ocean reanalyses are a fundamental tool for climate investigation, as indicated by the large number of studies that make use of them. Within the Ocean Reanalyses Intercomparison Project (Balmaseda et al., 2015), several exercises were undertaken to study the variability of many well-constrained ocean fields, such as steric sea level (Storto et al., 2017), air-sea heat fluxes (Valdivieso et al., 2017), ocean heat content (Palmer et al., 2017). ORAs are also a key tool for evaluating key climate diagnostics that are not

directly observed, such as deep ocean warming (Balmaseda et al., 2013), the reconstruction of the overturning circulation (Jackson et al., 2016). Few ORAs studies so far have focused on their performance in polar regions. Chevallier et al. (2017) used 14 global ORAs to analyze the seasonal variability of the sea ice area and sea ice edge position in the Arctic region. They showed that the ensemble-mean SIC agrees quite well with the observations but there is significant disagreement among systems in simulated sea ice thickness (which is not directly assimilated in any of the ORAs). However, they also revealed a large spread in the representation of pack ice and the MIZ extent. Using a set of 10 ORAs, Uotila et al. (2019) found an overall agreement with observations in the location of both Arctic and Antarctic sea ice edges, and showed that ORAs are able to capture seasonal variability of sea ice area (SIA). The large differences in the 10 reanalysis systems resulted in a poor representation of the seasonal variability of the MIZ and pack ice area. Nevertheless, Uotila et al. (2019) discussed the fidelity of ensemble mean estimates and proved that the multi-system concept provides the most robust results owing to the cancellation of the individual errors.

In this study, we investigate the interannual and seasonal changes of Antarctic SIA on hemispheric and regional scales with the purpose of identifying the differences between MIZ and total/consolidated pack ice. We use an ensemble-mean of four global ocean-sea ice reanalyses (ORAs) together with long-term passive microwave sea ice estimates. We examine the quality of the Global ocean Reanalysis Ensemble Product (version 2, hereafter called GREP) provided by the Copernicus Marine Environment Monitoring Service (CMEMS) of the European Union. GREP is an ensemble of four global ocean-sea ice reanalyses produced at eddy-permitting resolution for the period from 1993 to present. GREP has already been successfully validated with respect to a range of ocean variables (Masina et al., 2015; Storto et al., 2019) and have been largely adopted for evaluating key climate diagnostics that are not easily observed. In this study, we evaluate the capability of GREP in reproducing the Antarctic sea ice area in the marginal ice and pack ice regions, in the 1993–2019 period. We analyse the interannual and seasonal variability in five sectors of the Antarctic Ocean. The main objectives of this work are to validate GREP Antarctic SIA against satellite estimates and to investigate the benefits of a multi-system ensemble approach. Since the multi-model mean can offset systematic errors of individual systems, we expect GREP to perform generally better than single reanalysis and provide the most consistent estimates of sea ice state and variability. We also intend to encourage the use of GREP in a wide range of applications.

DATA AND METHODS

The Global Reanalysis Ensemble Product (GREP version 2) consists of four global ocean-sea ice reanalyses (C-GLORSv7, Storto et al., 2016; FOAM-GloSea5, MacLachlan et al., 2015; GLORYS2v4, Lellouche et al., 2013; ORAS5, Zuo et al., 2019), all constrained by satellite and *in-situ* observations, and driven by the ECMWF ERA-Interim atmospheric reanalysis (Dee et al., 2011). Monthly means of ocean and sea ice variables, for individual reanalysis as well as the ensemble mean and spread, are produced and freely disseminated by CMEMS through the CMEMS catalogue (product reference GLOBAL_REANALYSIS_PHY_001_031).

The four reanalyses share the ocean components of the state-of-the-art NEMO model, and are produced on the same tripolar ORCA025 grid at an eddy-permitting resolution (approximately ¼ degree of horizontal resolution and 75 depth levels). Three reanalyses use the LIM2 thermodynamic-dynamic sea-ice model, while the other (FOAM-GloSea5) employs CICE4.1 which includes more complex physics parameterizations compared to LIM2. Although many physical and numerical schemes are similar in the four reanalyses, there are a number of significant changes including the ocean model version and some parameterizations, thus introducing differences in the four ocean model configurations. There are also differences in the data assimilation methods used by the single products, in terms of data assimilation scheme, code, frequency of analysis and assimilation time-windows, input observational data-sets, error definitions and bias correction schemes, which introduce a large number of uncertainties as ensemble spread. The main characteristics of the GREP members are summarized in **Table 1** – a detailed description of model setup and data assimilation methods is outside of the scope of this study. GREP and its constituent reanalyses cover the altimetric period from 1993. Our analysis extends to 2019.

We consider a set of sea ice satellite products in order to evaluate the GREP performance. We use SIC fields from NOAA/NSIDC Climate Data Record (version 3, Meier et al., 2017, hereafter CDR), EUMETSAT OSISAF Climate Data Record and Interim Climate Data Record (release 2, products OSI-450 and OSI-430-b, Lavergne et al., 2019), and IFREMER/CERSAT (Ezraty et al., 2007). Firstly, the CDR algorithm output is a combination of SIC estimates from two well-established algorithms: the NASA Team (NT) algorithm (Cavalieri et al., 1984) and the Bootstrap (BT) algorithm (Comiso 1986). CDR SIC is based on gridded brightness temperatures (TBs) from the Nimbus-7 SMMR and the DMSP series of SSM/I and SSMIS passive microwave radiometers; the final product is provided at daily and monthly frequency on a 25 km × 25 km grid.

Secondly, the EUMETSAT OSI-450 is a level 4 product that covers the period from 1979 to 2015. The sea ice concentration is computed from the SMMR (1979–1987), SSM/I (1987–2008), and SSMIS (2006–2015) instruments, as well as ECMWF ERA-Interim data. The Interim OSI-430-b extends OSI-450 from 2016 onwards; it is an off-line product based on the same algorithms as OSI-450, and uses SSMIS data available through the NOAA CLASS, as well as operational analysis and forecast from ECMWF. The data processing introduced an open-water filter aimed at removing weather-induced false ice over open water, which unfortunately may remove some true low-concentration ice in the MIZ (Lavergne et al., 2019). OSISAF products are delivered at daily frequency on a 25 × 25 km grid. Lastly, the IFREMER/CERSAT product used here is derived from high

TABLE 1 | The central characteristics of ocean reanalyses.

Name	CGLORSv7	GLORYS2v4 (hereafter GLORYS2)	ORAS5	FOAM-GLOSEA5v13
Institution	CMCC	Mercator Ocean	ECMWF	United Kingdom Met Office
Ocean-ice model	NEMO3.6-LIM2 (EVP rheology)	NEMO3.1-LIM2 (EVP rheology)	NEMO3.4-LIM2 (VP rheology)	NEMO3.2-CICE4.1 (EVP rheology)
Time period	1986–2019	1993–2019	1979–2019	1993–2019
Sea ice data assimilation method	Linear nudging	Reduced order KF (SEEK)	3DVAR-FGAT	3DVAR
Ocean data assimilation method	3DVAR (7 days)	SAM2 (SEEK) (7 days)	3DVAR-FGAT (5 days)	3DVAR (1 day)
DA sea ice data	OSI-SAF	IFREMER/CERSAT	OSTIA (reprocessed before 2008, analysis from 2008)	OSI-SAF
Thickness categories	1	1	1	5

frequency channels of SSM/I that yield a spatial resolution of 12.5 × 12.5 km. SIC is provided at daily and monthly frequency.

It is worth mentioning that OSISAF and IFREMER/CERSAT sea ice concentration are ingested by the data assimilation systems employed in the ORAs constituting GREP, while CDR is not assimilated in any ORA. The use of CDR is, hence, considered an advantage for the robustness of the GREP validation; OSISAF and IFREMER/CERSAT datasets are anyway used in our analysis. It has been shown that NT generally underestimates SIC (Andersen et al., 2007; Meier et al., 2014), and overestimates MIZ and underestimates pack ice by a factor of two compared to BT (Stroeve et al., 2016). On the other hand, BT produces too low SIC under extremely cold conditions (Comiso et al., 1997). The CDR algorithm blends NT and BT output concentration by selecting, for each grid cell, the higher concentration value, taking advantage of the strengths of each algorithm to produce concentration fields more accurate than those from either algorithm alone. Since passive microwave instruments tend to underestimate SIC, the aforementioned approach is considered to be more accurate (Meier et al., 2014). Given that observational datasets and ORAs use different horizontal grids, we interpolated the former onto the ORCA025 grid for the grid-point diagnostics.

In this paper, sea ice variability is described in terms of sea ice area (SIA) rather than sea ice extent (SIE). Sea ice extent is defined as the integral sum of the areas of all grid cells with at least 15% ice concentration, whereas sea ice area is the sum of the product of each grid cell area with at least 15% ice concentration and the respective ice concentration. Hence, sea ice area excludes open water areas between ice floes. Although these two metrics are highly correlated, uncertainties in SIC retrievals from passive microwave sensors have a larger impact on SIA that results in a weaker agreement across data records.

In addition to the total sea ice area, we consider two sea ice classes defined through SIC thresholds. The MIZ is here identified as the region extending from the outer sea ice–open-ocean boundary (defined by SIC equal to or higher than 15%) to the boundary of the consolidated pack ice (defined by 80% SIC). This definition has been previously used by Stroeve et al. (2016) to assess observed MIZ changes in Antarctica. The consolidated pack ice is then defined as the area with ice concentrations higher than 80%.

The seasonal variability of SIA is analysed for total, pack and MIZ sea ice on the hemispheric domain and in selected regions where satellite records have highlighted large differences in the ice response to climate. As in previous studies (e.g., Parkison and Cavalieri, 2012), the Antarctic domain is divided in the following five sectors (**Figure 1**): Weddell Sea (60° W–20° E, plus the small ocean area between the east coast of the Antarctic Peninsula and 60° W), Indian Ocean (20–90° E), western Pacific Ocean (90–160° E), Ross Sea (160° E–130° W), and the combined Amundsen-Bellingshausen Seas (130–60° W).

RESULTS

We begin with the assessment of the interannual variability of total SIA reproduced by GREP and derived from satellite data sets. The GREP and observational products monthly-mean SIA is presented for the Southern Ocean as a whole, from January 1993 to December 2019, in **Figure 2A**. GREP SIA ranges from the summer minima occurring in February to winter maxima occurring generally in September, with a huge amount of sea ice growing and melting each year in very good agreement with observations. While the reanalysis ensemble slightly underestimates minima and maxima SIA, it correctly reproduces the large interannual variability, and properly depicts the record high in September 2014 (16.73×10^6 km^2 in GREP and 17.42×10^6 km^2 in CDR) and the marked decreases in the subsequent 3 years, with the record low in February 2017 (1.16×10^6 km^2 in GREP and 1.57×10^6 km^2 in CDR). GREP and CDR monthly anomalies of SIA show similar patterns and trends are basically consistent (**Figure 2B**), with an upward trend in yearly average SIA of 0.32×10^6 km^2/decade in GREP and 0.31×10^6 km^2/decade in CDR for 1993–2014, and trend close to zero (-0.04×10^6 km^2/decade in GREP and -0.036×10^6 km^2/decade in CDR) for the entire period 1993–2019. The good agreement between the three observational products (gray shading) and the four ORAs (pink shading) is notable; differences are greatest at the winter maxima.

To quantify the inconsistency between GREP and satellite estimates, we use the integrated ice area error (IIAE) approach of Roach et al. (2018, 2020). The IIAE identifies the area of sea ice on which ORAs and observations disagree; it is computed as the sum

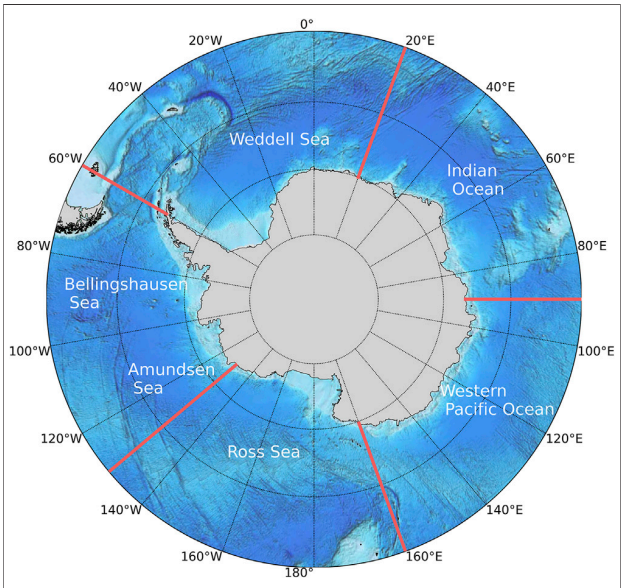

FIGURE 1 | Map of the five Antarctic sectors used in the regional analysis.

of overestimated (O) and underestimated (U) sea ice area. These two O and U components are calculated as the sum of the product of the area and the SIC of each grid cell where GREP has a higher or lower concentration compared to observations. We apply the same metric also to pack ice and MIZ to determine how each sea ice class contributes to the overall error. The location of sea ice classes in CDR estimates is taken as the "true state". The time series of IIAE O and U components for total ice, pack ice and the MIZ area computed relative to CDR are shown for the period 1993–2019 (**Figure 3**).

For every month, errors are very low relative to the mean SIA values, even for February and September. In general, GREP tends to underestimate total SIA area with the error ranging from 0.1 × 10^6 km^2 in March-April to 0.7 × 10^6 km^2 in October-December. Reanalyses generally tend to reproduce lower SIC than CDR, within the pack ice region: while IIAE O component in pack ice is relatively small (~0.05 × 10^6 km^2 all year round) and similar among the individual ORAs, IIAE U component grows up to 0.6 × 10^6 km in August-November and doubles for two reanalysis products. The MIZ also contributes to the total overestimated and underestimated area, but the error does not generally exceed 0.2 × 10^6 km^2. There is one ORA outlier (GLORYS2) that generally contributes to overestimating SIA, and one (CGLORS) to underestimating it. The former (the latter) reproduces too high (low) SIC in the MIZ. Overall, GREP performs well owing to minimization of systematic errors in individual products. Additionally, the error in the ensemble mean is consistent throughout the years, which is not the case for single ensemble members.

The accuracy of GREP and individual ORAs in reproducing the spatial distribution of SIC is shown in **Figure 4**, where maps of the SIC root mean square errors (RMSE) for GREP and individual ORAs against CDR are presented for September

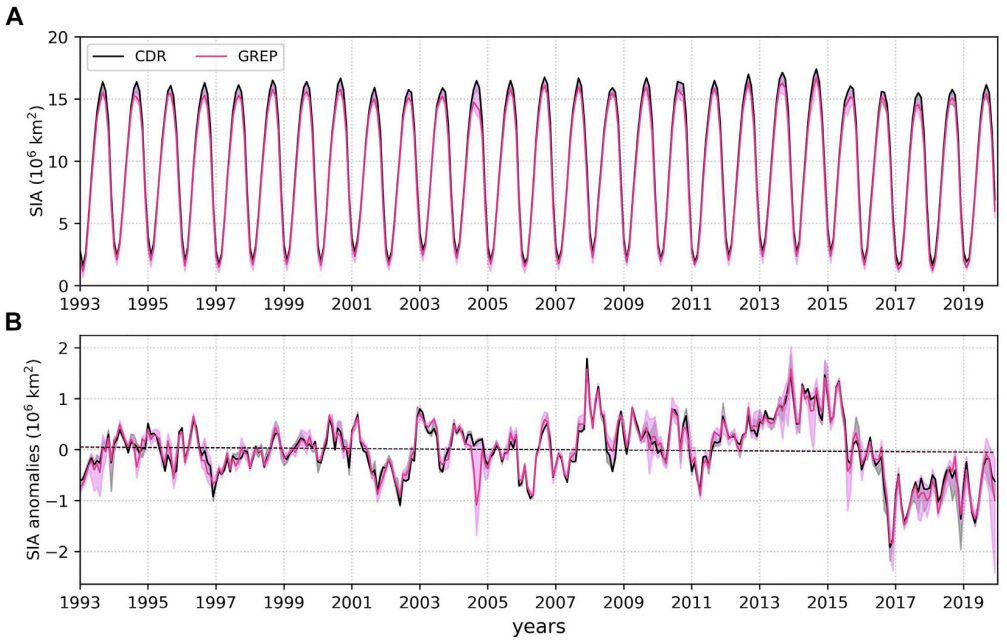

FIGURE 2 | Time series of **(A)** monthly averages and **(B)** monthly anomalies of Antarctic sea ice area in GREP (magenta) and CDR (black) from January 1993 to December 2019, for GREP (magenta) and CDR (black). Pink (gray) shading denotes the envelope of GREP members (CDR, OSISAF, Ifremer CERSAT satellite records).

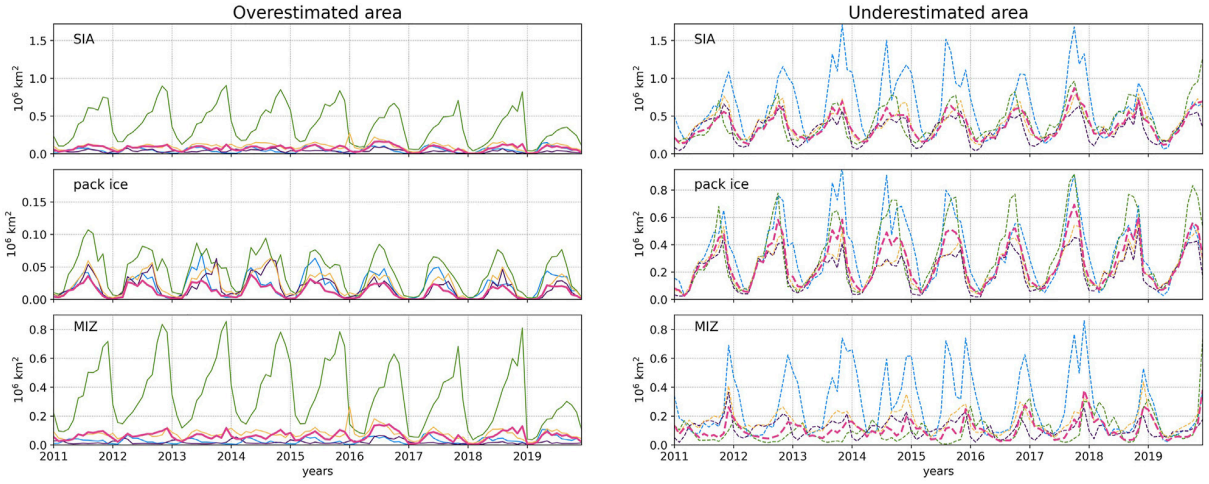

FIGURE 3 | Time series of the GREP integrated ice area error components (in magenta) calculated with respect to CDR for total SIA (top panel), pack ice (middle panel) and the MIZ (bottom panel). Area of sea ice where GREP simulates higher (lower) SIC is on the left (right) column. The *y*-axis scales for pack ice are different. Thin lines represent the individual ORAs: CGLORS in light blue, FOAM-GloSea5 in violet, GLORYS2 in green, and ORAS5 in yellow–the same colors will be used in the following figures for single ORAs.

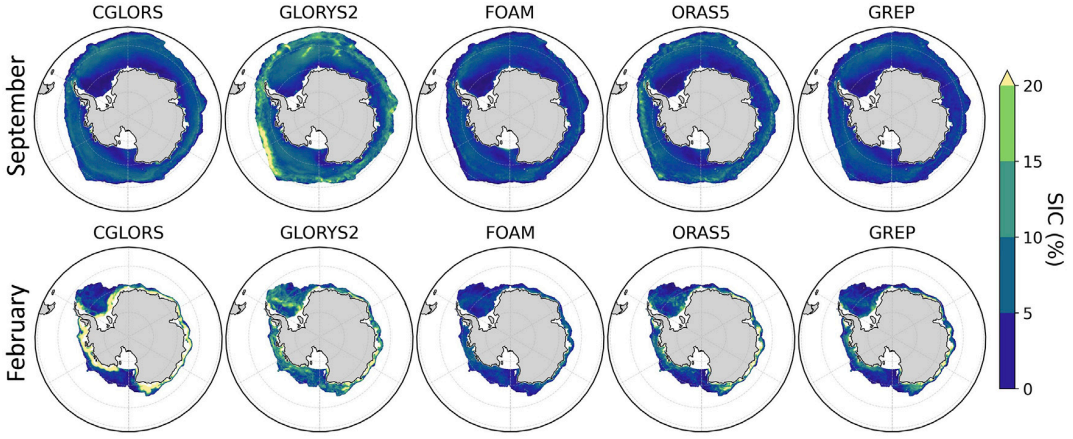

FIGURE 4 | Mean root mean square error for SIC at every grid cell for the single ORAs and GREP against CDR in September (upper row) and February (lower row).

and February, which are typically the months of maximum and minimum ice coverage respectively. The monthly climatologies are computed over the years 1993–2019. The sign of the errors has also been analyzed through the spatial distribution of the average bias (not shown). In September, RMSEs are lower than 5% along the Antarctic coast for all ORAs and tend to grow towards the ice edge, with the highest values generally smaller than 15% except for one single product, GLORYS2, which overestimates SIC by up to 20% in the Ross Sea and the Bellingshausen and Amundsen Seas. In February, the largest disagreement with CDR is located near the Antarctic coast, in particular in the Indian Ocean and the Western Pacific Ocean sectors, where three of the four ORAs underestimate the observed concentration. This error may be primarily linked to the reanalyses representation of sea ice drift and the Antarctic coastal current in the eastern Antarctica (not shown). One product (CGLORS) exhibits an unique behavior with the RMSE for SIC exceeding 30% along the entire Antarctic coastline - this indicates a lower concentration compared to CDR that may be related to a large warm bias in sea surface temperature along the coast, in particular in the Indian and the Western Pacific Oceans (not shown). GREP compares well with satellite estimates considering that the RMSEs are of the same order as the uncertainties from SIC retrievals using passive microwave radiometry (Ivanova et al., 2015). Time evolution of the mean over area RMSE (not shown) indicates that the

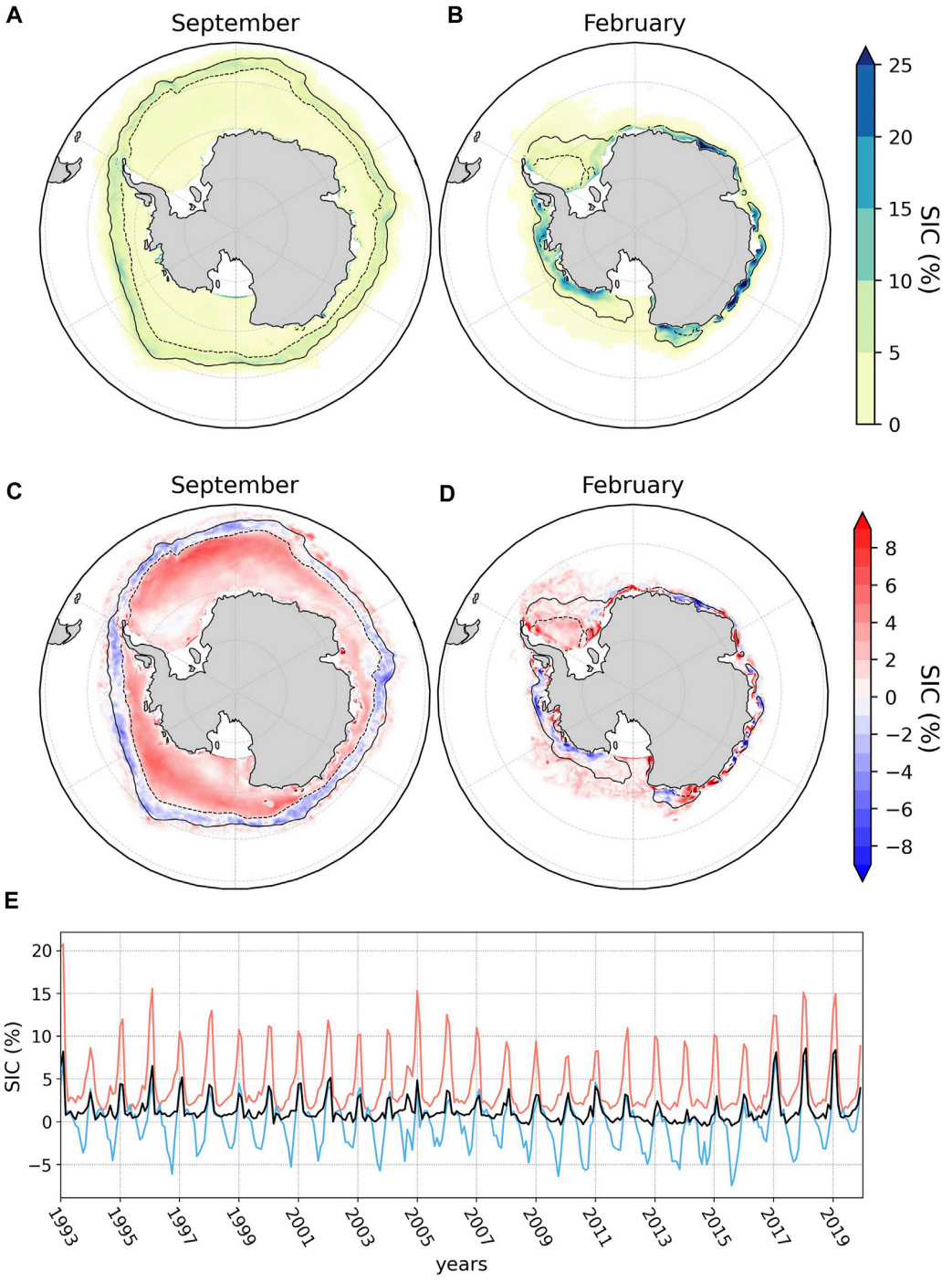

FIGURE 5 | Spatial distribution of **(A,B)** ensemble spread (ES) and **(C,D)** difference (in %) between GREP RMSE and ES for SIC in September and February. Contours indicate the mean position of 15% (solid) and 80% (dashed) ice concentration over the period 1993–2019 from CDR. **(E)** Time series of the difference (in %) between GREP RMSE and ES spread of SIC for total area (black), pack ice (red), the MIZ (blue).

RMSE for GREP concentration is up to ~10% in summer months (January-February) and does not exceed 7% in other months.

We also analyze the ensemble spread (ES) in order to assess the overall consistency across ORAs (**Figures 5A,B**). The largest ES in SIC (~35% in February) is found during the melting season

everywhere along the Antarctic coast, except in the Weddell and the Ross Seas. Increased ES is consistent with uncertainties coming from the assimilated satellite data - SIC retrievals present larger uncertainties within the melting season due to surface wetness and a broad variety of sea ice forms that affect sea ice emissivity (Ivanova et al., 2015; Meier and Stewart, 2019). In September, there is high consistency among ORAs due to the larger portion of stable and compact pack ice. Larger ES is located in the MIZ and does not exceed 10%. Finally, we compare RMSE of GREP SIC calculated against CDR, with the SIC ES to evaluate whether the ensemble is over-dispersive or under-dispersive. The spatial distribution of the metric (GREP RMSE minus ES) is shown for September and February in **Figures 5C,D**. GREP is over-dispersive when RMSE < ES (blue/negative) and under-dispersive when RMSE > ES (red/positive). In September, it appears that ensemble dispersion depends on sea ice class: GREP is over-dispersive in the MIZ (represented by the region between contour lines), whereas GREP is under-dispersive within the pack ice. This means that ORAs agree better on the representation of high concentration in the region of stable pack ice, where the ORAs performances are less challenging compared to the MIZ. In February, there does not seem to be a direct relationship between ensemble dispersion and sea ice class. The pattern of the difference is heterogeneous, particularly along the coast of the eastern Antarctic. In the Weddell and Ross Seas, the GREP remains over-dispersive. Time series of the difference between GREP RMSE and ES better presents the opposite behavior of sea ice classes and the contribution to total sea ice changes (**Figure 5E**). The compensation between sea ice classes in all seasons, except in summer, translates into close-to-zero values for the total ice concentration. From December to February, GREP RMSE exceeds ES in both pack ice and the MIZ, leading to an increased difference for the total ice area.

Seasonal Variability

We proceed with an assessment of the consistency of the seasonal sea ice variability between the reanalysis ensemble and satellite estimates. The climatological mean seasonal cycle of the circumpolar SIA as represented by GREP, single ORAs and observational estimates, is shown for total sea ice, pack ice, and MIZ, in **Figure 6A**. The seasonal cycle of Antarctic sea ice is consistent among ORAs and in phase with observations. All systems have a maximum in total SIA in September, and a minimum in February; it takes about 7 months to expand sixfold from summer minimum of ~2.5 $\times$ 10^6 km^2 to winter maximum of ~15 $\times$ 10^6 km^2, and about 5 months to melt again. It is worth noting that the ensemble spread of ORA SIA is limited throughout the year, and is comparable to the estimated observational uncertainty. The seasonal cycle of Antarctic-wide total SIA is dominated by the variability of pack ice, whose area evolves at the same rate as total ice. GREP slightly underestimates the area of pack ice from August for the melting season (only one reanalysis, GLORYS2, is larger than observational products), but all ORAs align well with observations during refreezing in autumn.

The seasonal changes in the MIZ are quite different from those in total ice and pack ice. On average, the MIZ advance needs about 10 months to progress from near the coast (in February) to its most equatorward maximum (in November or December) and about only 2 months to revert to a minimum. After summer, the MIZ area grows simultaneously with pack ice, in part transforming into it, and continues to expand in spring after the total (and pack) SIA peaks. The further increase in the MIZ area after the consolidated ice pack begins to melt implies that, as it starts to retreat, the pack ice converts in part to MIZ over a wider area. We note the Antarctic MIZ/pack-ice ratio is close to 1 from December to March. GREP is always in the observed envelope; the ensemble spread of ORA SIA is generally smaller or comparable to the estimated observational uncertainty. Here, the larger spread among the observed MIZ area (found also between NT and BT algorithms by Stroeve et al., 2016) reflects the different ability of high and low frequency channels used in the different data algorithms to retrieve low fraction sea ice. However, GLORYS2 underestimates the MIZ area from July to December, and this can be attributed to faster sea ice consolidation in the growing season. This is consistent with the IIAE analysis (**Figure 3**), which indicates that this system simulates higher SIC in those grid cells that are considered to belong to the MIZ in observations, and with the RMSE of SIC (**Figure 4**) with larger errors in the outer ice region where MIZ is located. CGLORS underestimates the MIZ area in summer from December to February, causing a large impact on the minimum of total SIA (as seen in **Figures 3**, **4**).

For all sea ice classes, the highest consistency among datasets is observed throughout autumn freezing, from March to June. Overall, due to the realistic performance of all single members and the cancellation of systematic errors, GREP reproduces robust estimates of the seasonal cycle of Antarctic total ice area and the two sea ice classes.

The different seasonality of sea ice classes is a notable result that confirms a different interplay of ice classes with the ocean and the atmosphere. Seasonal variability of Antarctic sea ice is governed by the position of the circumpolar trough relative to the ice edge and associated wind field and Ekman transport (Enomoto and Ohmura, 1990; Eayrs et al., 2019). In spring, when the circumpolar trough is north of the ice edge, hastened conversion of pack ice to the MIZ is supported by divergence which results in opening of pack ice. This consequently facilitates solar absorption in the upper ocean and accelerates lateral melting of ice floes (e.g., Perovich and Jones, 2014) which contributes to the MIZ growth. From December to February, the MIZ area rapidly retreats together with pack ice, driven by southward Ekman forcing and sea ice convergence. However, the MIZ represents a significant part of the overall ice cover from December to March (the proportion between the MIZ and pack ice area is in the range between 0.8 and 1.2).

Analysis in the Sub-regions

Since Antarctic sea ice variability and trends are spatially heterogeneous (e.g., Parkinson and Cavalieri, 2012; Parkinson 2019), the analysis of the Antarctic circumpolar sea ice is rather limited. In this section, we investigate the accuracy of GREP

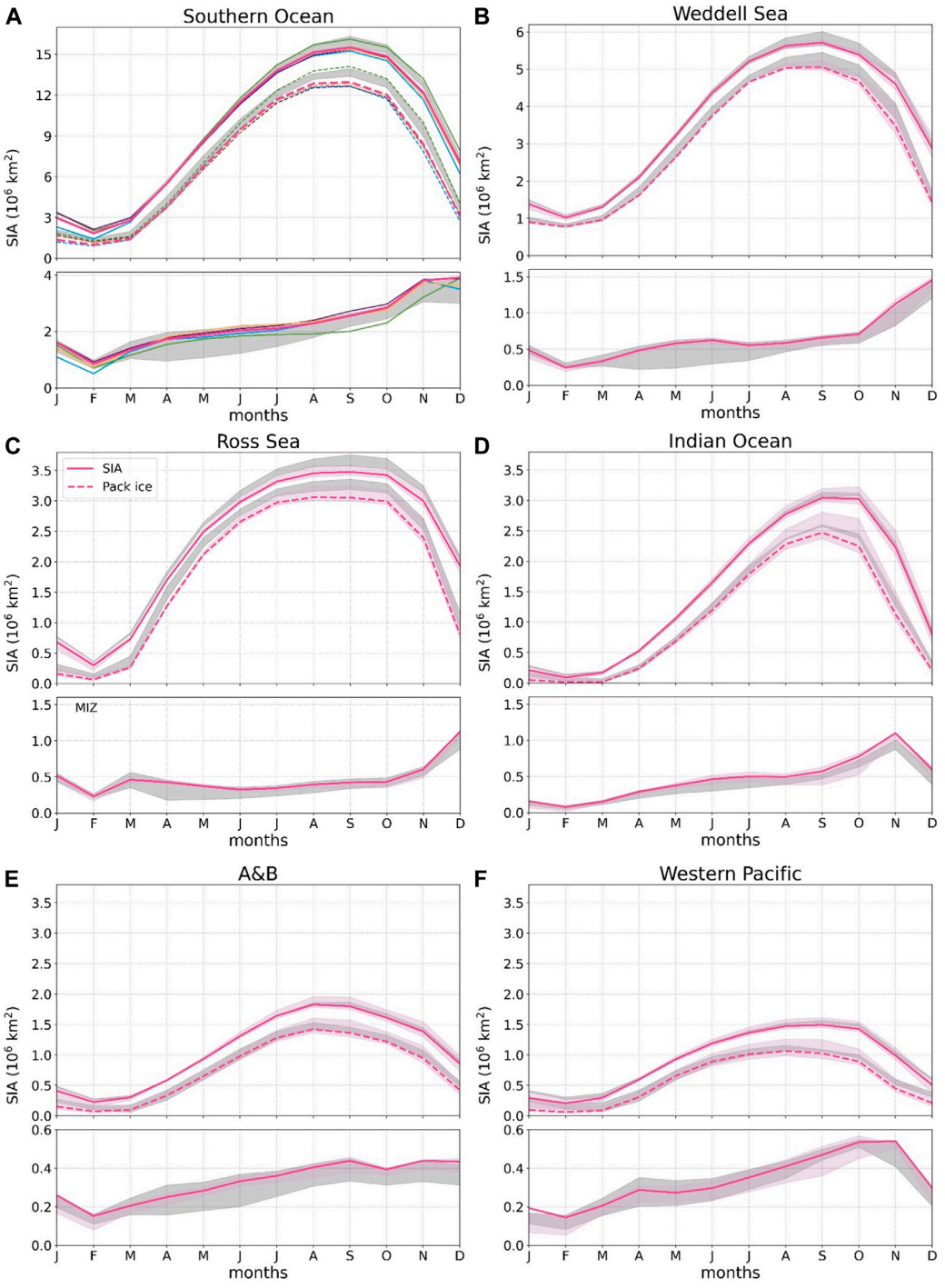

FIGURE 6 | Mean seasonal cycle (1993–2019) in the total SIA (solid), pack ice (dashed) (upper subplots), and the area covered by Marginal Ice Zone (MIZ) (lower subplots) computed for GREP (in magenta) and the individual ORA (thin colored lines) in the Antarctic-wide region **(A)**, for GREP in the five sub-sectors **(B-F)**. Pink shading denotes the envelope of GREP members. Gray shading denotes the envelope of observational estimates (CDR, OSISAF, Ifremer CERSAT). Please note the different y-axis scales for the Southern Ocean and Weddell Sea.

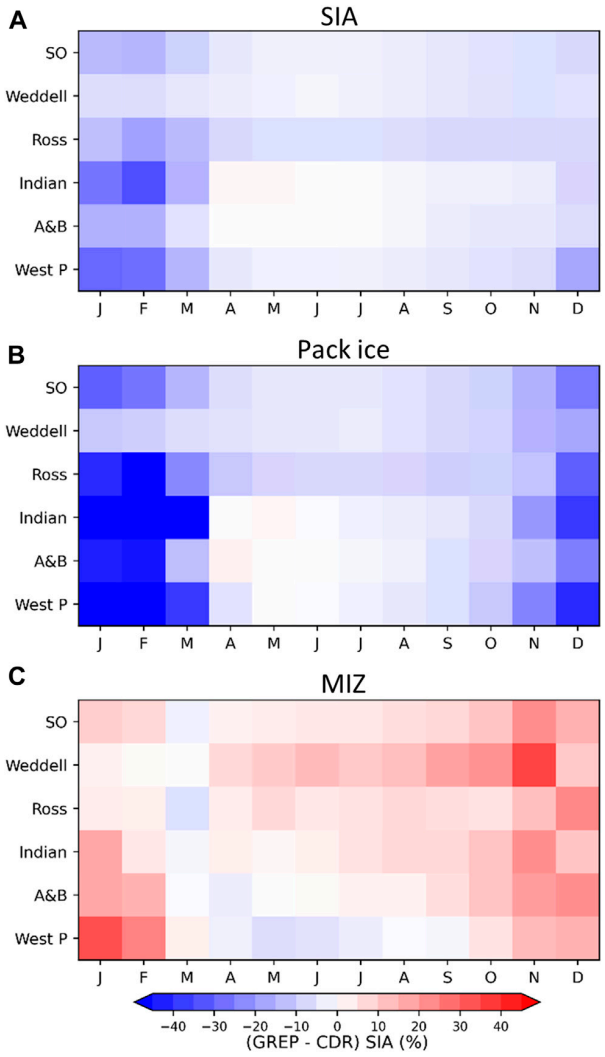

FIGURE 7 | Seasonal cycle of (GREP minus CDR, in %) monthly climatology of **(A)** total ice (upper panel), **(B)** pack ice (middle) and **(C)** MIZ area in the Southern Ocean and its five sectors. Differences are shown as a percentage of CDR values computed for the years 1993–2019. Red (blue) indicates that GREP reproduces higher (lower) SIA compared to CDR.

performance on regional scales by analysing the seasonal variability of total ice, pack ice and MIZ area for each of the five Antarctic sectors (shown in **Figure 1**), and by comparing GREP output with the CDR product.

As expected, there are significant differences among the five sectors in the amount of ice classes, the timing of maxima and minima, the rate of sea ice expansion and the retreat phase (**Figures 6B–F**). This contrast in the regional patterns of sea ice growth and melt is associated with geographic differences and interplay of leading climate processes (Maksym et al., 2012).

There is a very good agreement between GREP and CDR variability in all regions (**Figures 6B–F**, **Figure 7**). It is worth noting that the spread in observational products (and in the reanalyses) varies not only among sea ice classes, but also among regions. The spread of observational estimates of MIZ area is generally larger than the spread of the reanalysis ensemble, in particular in the Weddell Sea and Ross Sea in autumn months and in the Amundsen-Bellingshausen (A-B) Seas from March to December.

As in the Southern Ocean as a whole, all sectors exhibit a large annual cycle of monthly total SIA (**Figure 6**), with asymmetric growth and melt seasons. However, there are large differences in the timing and magnitude of the sub-region seasonality, given that the rate of waxing and waning of sea ice and the interplay with air-sea components vary across the sectors. Minima of total SIA always occur in February and maxima occur frequently in September (**Figure 6**), although with much greater interannual variability than in the Southern Ocean as a whole (not shown). The pattern and ratio of pack and marginal ice widely varies among the regions.

The regional variability as reproduced by the GREP ensemble-mean is described for individual sectors. In the Weddell Sea (**Figure 6B**), the SIA is much higher than other regions and has the largest distribution of pack ice. Its seasonality is consistent with the Southern Ocean as a whole. From the February minima ($\sim 1 \times 10^6$ km^2), total and pack ice areas begin to expand in March and peak (at $\sim 5.7 \times 10^6$ km^2 and $\sim 5 \times 10^6$ km^2 respectively) on average in September, but maximum timing varies frequently from August to October (not shown). The Weddell Sea provides the greatest contribution (~55%) to the summer sea ice area in the Southern Ocean, due to the presence of consolidated pack ice all year around. In agreement with CDR, the ensemble-mean shows that the Weddell Sea holds the largest percentage (~75%) of February pack ice. The MIZ area also starts to advance in March and continues to increase until December ($\sim 1.45 \times 10^6$ km^2), as the pack ice quickly retreats. In this region, the sea ice cover expands northwards until it reaches a region with strong air-sea dynamics. North of the consolidated pack ice region, ice continues to advance, thanks to further freezing or breaking by the winds and currents.

The second largest contribution to the Antarctic-wide ice area comes from the Ross Sea (**Figure 6C**). In this sector, the total ice and pack ice areas present a large asymmetric seasonal cycle, with, approximately, a 9-months growth period and a 3-months melting period. With almost no pack ice, the total sea ice and MIZ areas have a marked minimum always occurring in February. There is a large variability in the timing of total and consolidated pack ice maxima occurring generally from August to October and reaching $\sim 3.5 \times 10^6$ km^2 and $\sim 3 \times 10^6$ km^2 respectively. In February, the minimum SIA mainly consists of MIZ that covers ~ 0.25 10^6 km^2; the MIZ fraction is then nearly constant throughout the expansion and retreat of the pack ice, with a maximum in December (1.13×10^6 km^2) as the pack ice rapidly decays. The Ross Sea, like the Western Pacific (**Figure 6F**), exhibits a second peak in the MIZ area in March, in the freezing season, when the area of MIZ and pack ice starts to expand and the increasing sea ice consolidation is accompanied by MIZ-to-pack ice transformation.

In the Indian Ocean, the total SIA maximum (3×10^6 km^2) is reached in October rather than September (**Figure 6D**), about

1 month later the pack ice peak (2.4×10^6 km^2) is reached. The pack ice tends to disappear completely in summer and when MIZ comprises the largest portion of the overall ice cover. The MIZ advances from March until November when its area (~1.1×10^6 km^2) is comparable to that of pack ice.

At their largest, the A-B Seas and Western Pacific Ocean together account for less than 20% of the Antarctic-wide SIA, with the lowest winter maxima (1.83 and 1.5×10^6 km^2, respectively); they can weakly affect the Antarctic sea ice seasonal cycle. In both sectors, the areas of consolidated pack ice and MIZ are generally comparable in the winter months. The A-B Seas are in major contrast with the rest of the Southern Ocean (Parkinson, 2019), and are characterized by an overall downward sea ice trend (not shown) related to the upper ocean warming at the west of the Antarctic Peninsula (e.g., Ducklow et al., 2012). Seasonality of ice expansion and retreat are almost symmetric for total ice and pack ice areas (**Figure 6D**) that both peak in August (the maximum timing varies from July to October from year to year) and are minimum between February and March. The MIZ area increases during most of the year, from February to December. There is a large interannual variability in the timing of the maximum that results in the double peaks in September and November (approximately 0.42×10^6 km^2). Here, the MIZ area does not further increase when pack ice starts to retreat, in contrast to other regions. The MIZ gives the largest contribution to total area from January to April. In this sector the spread of observational estimates of MIZ is very large compared to the ORAs spread- GREP is always located within the observed envelope. In the Western Pacific Ocean, the total SIA reaches the highest value from August to October (**Figure 6F**), with the maximum generally occurring in September (~1.5×10^6 km^2). While pack ice area exhibits very low values and stays nearly constant throughout the summer period, MIZ area presents a prominent minimum in February and then begins to quickly expand until November when it exceeds pack ice area. The MIZ area remains larger until autumn.

Figure 7 shows how GREP representation of the seasonal variability of total ice, pack ice and the MIZ area differs from CDR estimates; due to the large regional contrasts in the amount of sea ice, the differences are expressed as a percentage of the average of CDR values. For total SIA, the difference between GREP and CDR is almost everywhere within 15% from April to December (**Figure 7A**). Thus, GREP seasonal variability is consistent in time and space with the observed sea ice changes over the period 1993–2019. The largest differences are generally found in summer, in particular in the Indian Ocean and the Western Pacific where GREP area is about 25% lower than CDR. The accuracy of GREP stands out in the Weddell Sea where total sea ice area differs from CDR data by -7% at the most. The high quality of total sea ice in the reanalysis ensemble results from the contrasting behaviour of pack and MIZ area. Differences have a similar pattern for pack ice areas, but with different magnitudes. The highest values are found from December to March when GREP tends to generally underestimate the area of consolidated ice in all sectors. Due to the very low amount of pack ice area in both GREP and CDR in spring and summer, this metric typically detects small differences with respect to CDR. For example, GREP pack ice area differs by ~70% from CDR in the Indian Ocean in February, when pack ice area has almost disappeared in the region, with values lower than 0.1×10^6 km^2. As for the total ice, it is in the Weddell Sea sector that GREP better reproduces the seasonal variability of the pack sea ice area. Overall, the ensemble-mean reproduces a larger area of the MIZ almost everywhere. As for pack ice, GREP and CDR differences are the smallest in the growing season when GREP MIZ extends 10% more than CDR at most - differences stay small but reverse in the Western Pacific Ocean during autumn-winter months. The GREP MIZ area is 20–30% larger than observed estimates generally in November-December, when it approaches its maximum values. The largest departures from CDR are found in the Western Pacific sector in January and the Weddell Sea in November. It is worth noting that the MIZ area reproduced by GREP has generally the largest differences from the observational estimates when they present large spread (**Figure 6**).

DISCUSSION

Understanding the mechanisms and rates of Antarctic sea ice change is crucial from a climate-change perspective. Sea ice concentration retrieved from satellite microwave radiometers has been available on a daily basis since the late 1980s at a horizontal resolution finer than 25 km. However, these observational estimates are highly dependent on which passive microwave methods and sea ice algorithms are used (Ivanova et al., 2014; 2015). There are dozens of such algorithms available. Although these products agree quite well on area trends, absolute values of total SIC and SIA are not necessarily consistent with each other. There are also large differences among observed products in the regional ice distribution and trends, as well as in the contribution of consolidated ice or MIZ in the total ice cover (Stroeve et al., 2016). This is of particular importance for accurate assessment of processes contributing to climate change and assimilation of sea-ice in models. Reliable estimates of sea ice concentration and relative parameters are necessary to constrain also other ice parameters in modelling studies of past, present and future variability.

Simulation of Antarctic sea ice remains a fundamental challenge for state-of-the-art climate models (e.g., Holmes et al., 2019; Roach et al., 2020). Despite advances in climate modeling capabilities, the CMIP5 and CMIP6 intermodel spread in Antarctic sea ice extent is large, especially in summer, and the observed weak upward trend of the Antarctic ice extent is not captured yet (Turner et al., 2013; Roach et al., 2020; Shu et al., 2020; Shu et al., 2020). The poor accuracy of Antarctic sea ice changes in the CMIP exercises limits our understanding on what drives regional and seasonal Antarctic sea ice changes, including feedback and competing processes.

Our analysis confirms that ocean reanalyses are a fundamental tool for investigating climate variability and for evaluating key climate diagnostics that are not directly observed (e.g., Masina and Storto, 2017). Given the robustness of its mean and the implicit quantification of uncertainty by means of the spread, the multi-model ensemble provides a

robust representation of the spatial and temporal variability of Antarctic sea ice. Although sea ice concentration is the most well-constrained sea ice parameter, the ensemble spread mainly comes from differences in implemented data assimilation schemes but also from other sources of uncertainty such as differences in models, observational datasets and air-sea flux formulations.

We found strong consistency between the reanalysis ensemble and the satellite products, and GREP generally outperforms or at least equals individual reanalyses in approaching observation-based estimates of sea ice area. The advantage of the multi-model approach is highlighted by the fact that it is practically impossible to determine which one of four performs the best for all metrics and seasons. GREP smooths the strengths and weaknesses of single systems and provides the most consistent and reliable estimates of the mean state and variability of sea ice area. Nevertheless, advancement in model formulations and data assimilation schemes in single members could reduce the impact of ORAs shortcomings on the realism and accuracy of the ensemble-mean solution.

Although the main objective of the study is the evaluation of the GREP ability to reproduce the observed sea ice area on interannual and seasonal scales, our results also confirm the importance of regional variability and the distinction in sea ice classes. They should be considered when assessing how Antarctic sea ice varies in model simulations and when investigating the different processes that are likely contributing to ice interannual and seasonal.

We focus on how consolidated pack ice and the marginal ice change in relation to their different characteristics and therefore their different sensitivities to the external forcing. Differences in the seasonality of ice classes suggest that their variability is driven by changes in wind and ocean conditions in a different way. While the description of processes controlling the distribution of the MIZ and pack ice is out of scope of this study, we emphasize that a better knowledge of temporal and spatial variability in the MIZ and pack ice can provide a deeper insight of possible driving mechanisms behind these changes. We show that both GREP (and individual ORAs) and satellite products present considerable differences in the climatological mean seasonal cycle in the area of ice classes. The net circumpolar changes in sea ice area is the result of the interplay of MIZ and pack ice, and their different response to changing wind and ocean conditions. The annual waxing and waning of sea ice cover implies redistribution of ice floes between the MIZ and pack ice from month to month as well as spatial expansion and contraction of sea ice edge. When pack ice starts to melt and its area to retreat in spring, the breaking of ice floes contributes to the MIZ expansion that continues for 2–3 months. That results in a strong asymmetry in the MIZ seasonal cycle in all Antarctic regions, with approximately 9–10 months of advance and 2–3 months of retreat. Contractions and expansions of pack ice and the MIZ do not necessarily follow the changes in the location of the outer sea ice edge: ice classes can contribute to changes in sea ice coverage in different ways or even exhibit an opposite behavior (Stroeve et al., 2016). GREP reproduces regional differences in the proportion between pack and MIZ, the timing and duration of freezing and melting seasons, in close agreement with observation-based results (e.g., Stroeve et al., 2016; Parkinson, 2019; Wang et al., 2021).

The reanalysis ensemble agrees well with the CDR product on the different contributions of MIZ and pack ice to changes in the Antarctic-wide total ice. Monthly trends (computed as function of longitude and month) in the total, pack and marginal ice area (**Figure 8**) indicate a large degree of seasonal and regional variability around Antarctica. In all sectors and for all months, the spatial patterns and magnitude of statistically significant positive and negative trends in total ice area are highly consistent between GREP and CDR in all sectors. Results highlight the necessity to distinguish between sea ice classes in order to assess the quality of numerical systems. Although GREP and CDR are similar in SIA trends, there are some inconsistencies when looking at sea ice classes: GREP barely reproduces the correct magnitude of trends in the Eastern Antarctic and does not simulate the MIZ area expansion in December in the Ross Sea. Generally, in both GREP and CDR, significant trends in the MIZ are less pronounced but more heterogeneous in space, and they tend to offset the significant trends in pack ice. This is for example evident in the Ross Sea, where no trend is found in the observed total sea ice area in December, due to compensation between the opposite trends in the MIZ and pack ice. Positive trends in total SIA are generally dominated by statistically significant positive trends in the consolidated pack ice as in the western Weddell Sea from January to March. Both ice classes contribute to the statistically significant negative trends in the eastern Ross Sea and eastern A-B Seas in summer. The regional variability of the MIZ area trends during spring and autumn is consistent with a complex pattern of changes in timing of sea ice advance, retreat and duration (e.g., Eayrs et al., 2019).

Differences between GREP and CDR can be also explained by some limitations in our analysis. The first caveat concerns the methodology: we distinguish sea ice classes through sea ice concentration thresholds. Although the SIC-based definition is the one most often used (e.g., Strong and Rigor, 2013; Stroeve et al., 2016; Rolph et al., 2020), Vichi (2021) showed that it is not able to adequately capture the features of the Antarctic MIZ, in which ice dynamics is determined by oceanic and atmospheric processes. Indeed, this definition of the MIZ is not physically or dynamically explained; the lower boundary is linked to uncertainty from SIC retrievals (Comiso & Zwally, 1984) while the upper boundary corresponds to the WMO definition of "close ice" (WMO, 2009). In fact, the properties of Antarctic ice cover do not directly depend on the degree of coverage. *In-situ* measurements carried out in the Southern Ocean showed that close pack ice with SIC up to 100% do have the dynamical properties of the MIZ (Alberello et al., 2019; Vichi et al., 2019; Brouwer et al., 2021), which discredits the reliability of threshold-based definition. Vichi (2021) proposed an alternative MIZ definition that is based on statistical properties of the SIC and its spatial and temporal variability. The new method indicates the measure of variability, which is a key feature of the marginal ice. It also overcomes the disparity among the algorithms that could considerably differ in their representations of sea ice concentration, area and extent.

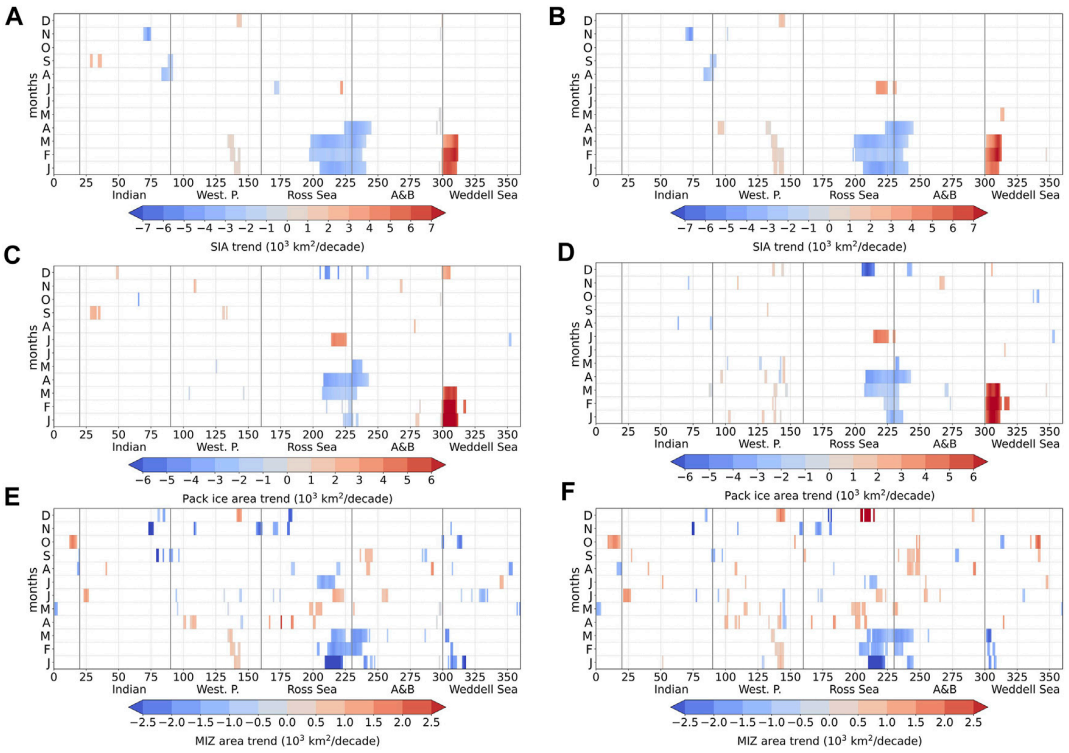

FIGURE 8 | Monthly trends (1993–2019) in regional areas of total ice **(A,B)**, pack ice **(C,D)**, and MIZ **(E,F)**, as a function of longitude. Left (right) columns correspond to GREP (CDR). Only significance higher than 95% are shown. Note that colorbar scales are different for ice classes.

Given the highly dynamic nature of the MIZ, another limitation of this study is the temporal resolution of GREP and ORAs output provided by CMEMS. Our analysis is constrained by monthly means of SIC from reanalyses. The use of daily fields might be more appropriate to investigate the MIZ variability and its linkage to regional interactions with ocean and atmosphere.

CONCLUSION

We assessed the accuracy of the CMEMS Global Reanalysis Ensemble Product (GREP) in reproducing the evolution in time and space of Antarctic total sea ice and discriminating the consolidated pack ice from the MIZ. Antarctic sea ice area from GREP is compared to a set of sea ice satellite products. GREP properly reproduces interannual and seasonal variability of total sea ice area both on hemispheric and regional scales. GREP is shown to properly represent the interannual and seasonal variability of pack and MIZ areas during the growing and melting seasons, as well as their minima and maxima. More evident discrepancies between GREP and satellite products occur during summer, when the spread among individual ORA increases; one product tends to underestimate MIZ area and another to overestimate pack ice area. Nonetheless, due to minimization of the single errors, the ensemble mean provides the most consistent and reliable estimates. The spatial distribution of RMSE in SIC also indicates that GREP smooths out strengths and weaknesses of individual systems.

For all ice classes, the ensemble spread is comparable to the spread among the observational estimates. The quality of GREP is generally comparable to that of satellite data sets and the differences between GREP and CDR are comparable or even smaller than differences between different algorithms (Stroeve et al., 2016). The seasonal cycle of the total sea ice area is within the observational uncertainty almost all year round, while the pack ice area is generally underestimated and the MIZ area is in the upper end of the observational range. This compensation between sea ice classes partly reflects misplacement of sea ice across the basin compared to the "true state".

Dispersion of GREP in sea ice concentration also appears to depend on sea ice classes. Due to the compensation between the opposite behavior in pack ice (GREP is under-dispersive) and the MIZ (GREP is over-dispersive), the difference between GREP RMSE and GREP ES is close to zero for the total ice area.

On a regional scale, the Weddell Sea is the region where GREP provides the most accurate representation of sea ice area, while the largest and most persistent discrepancies occur in the Indian and the Western Pacific sectors. This spatial distinction in GREP performance is attributed to the proportion of pack ice and the MIZ in the regions. Given its highly dynamic nature, the MIZ is more challenging to simulate compared to pack ice.

Considering that ocean reanalyses are widely used as boundary and initial conditions in forecasting systems, sub-optimal representation of the SIC distribution and variability can affect the quality of the output. The results of the current work proved the quality of the GREP product with regard to sea ice concentration and associated metrics. GREP agrees well with satellite products, and can be used to get a robust estimate of current sea ice state and recent trends in sea ice area and extent. However, improvement in data assimilation techniques, space-time data coverage in the ice-covered Southern Ocean regions, and availability of other ice properties (such as thickness and drift) from satellite measurements will most probably enhance the quality of ORAs and GREP in polar regions.

DATA AVAILABILITY STATEMENT

ORAs data and satellite datasets analyzed in this study are all freely available online. GREP output (product identifier GLOBAL_REANALYSIS_PHY_001_031) and its full documentation are provided by the Copernicus Marine Environment Monitoring Service, and are available to download through CMEMS webpage https://resources.marine.copernicus.eu/products Sea Ice Concentration data sets can be downloaded at the following links:

- NOAA/NSIDC Climate Data Record data set: https://nsidc.org/data/g02202/versions/3/
- EUMETSAT OSISAF: https://osi-saf.eumetsat.int/products/sea-ice-products
- Ifremer/CERSAT: ftp://ftp.ifremer.fr/ifremer/cersat/products/gridded/psi-concentration/

AUTHOR CONTRIBUTIONS

DI conceived and designed this study, and wrote the manuscript. JS analyzed, simulated and observed datasets, and contributed to the interpretation of results and editing. SM and AC reviewed the manuscript.

FUNDING

DI was funded by the European Union's Horizon 2020 research and innovation program under Grant agreement No 101003826 via the project CRiceS (Climate Relevant interactions and feedbacks: the key role of sea ice and Snow in the polar and global climate system). JS was supported by the Italian National Program for Research in Antarctica (PNRA) via the project INVASI (Interannual Variability of the Antarctic Sea Ice/ocean system from ocean reanalyses, Reference Number PNRA18-00244). AC and SM were supported by Copernicus Marine Service "Global Ocean Reanalysis for the GLO MFC" (Reference number: 114-R&DGLO-RAN-CMEMS).

REFERENCES

Alberello, A., Bennetts, L., Heil, P., Eayrs, C., Vichi, M., MacHutchon, K., et al. (2020). Drift of Pancake Ice Floes in the winter Antarctic Marginal Ice Zone during Polar Cyclones. *J. Geophys. Res. Oceans* 125 (3), e2019JC015418. doi:10.1029/2019jc015418

Alberello, A., Onorato, M., Bennetts, L., Vichi, M., Eayrs, C., MacHutchon, K., et al. (2019). Brief Communication: Pancake Ice Floe Size Distribution during the winter Expansion of the Antarctic Marginal Ice Zone. *The Cryosphere* 13 (1), 41–48. doi:10.5194/tc-13-41-2019

Andersen, S., Tonboe, R., Kaleschke, L., Heygster, G., and Pedersen, L. T. (2007). Intercomparison of Passive Microwave Sea Ice Concentration Retrievals over the High-concentration Arctic Sea Ice. *J. Geophys. Res. Oceans* 112 (C8), 1. doi:10.1029/2006jc003543

Balmaseda, M. A., Hernandez, F., Storto, A., Palmer, M. D., Alves, O., Shi, L., et al. (2015). The Ocean Reanalyses Intercomparison Project (ORA-IP). *J. Oper. Oceanography* 8 (Suppl. 1), s80–s97. doi:10.1080/1755876x.2015.1022329

Balmaseda, M. A., Trenberth, K. E., and Källén, E. (2013). Distinctive Climate Signals in Reanalysis of Global Ocean Heat Content. *Geophys. Res. Lett.* 40 (9), 1754–1759. doi:10.1002/grl.50382

Bintanja, R., van Oldenborgh, G. J., Drijfhout, S. S., Wouters, B., and Katsman, C. A. (2013). Important Role for Ocean Warming and Increased Ice-Shelf Melt in Antarctic Sea-Ice Expansion. *Nat. Geosci* 6 (5), 376–379. doi:10.1038/ngeo1767

Blanchard-Wrigglesworth, E., Roach, L. A., Donohoe, A., and Ding, Q. (2021). Impact of Winds and Southern Ocean SSTs on Antarctic Sea Ice Trends and Variability. *J. Clim.* 34 (3), 949–965. doi:10.1175/jcli-d-20-0386.1

Brouwer, J., Fraser, A. D., Murphy, D. J., Wongpan, P., Alberello, A., Kohout, A., et al. (2021). *Altimetric Observation of Wave Attenuation through the Antarctic Marginal Ice Zone Using ICESat-2*. The Cryosphere Discuss. [preprint], in review. doi:10.5194/tc-2021-367

Cavalieri, D. J., Gloersen, P., and Campbell, W. J. (1984). Determination of Sea Ice Parameters with the Nimbus 7 SMMR. *J. Geophys. Res.* 89 (D4), 5355–5369. doi:10.1029/jd089id04p05355

Chevallier, M., Smith, G. C., Dupont, F., Lemieux, J.-F., Forget, G., Fujii, Y., et al. (2017). Intercomparison of the Arctic Sea Ice Cover in Global Ocean-Sea Ice Reanalyses from the ORA-IP Project. *Clim. Dyn.* 49 (3), 1107–1136. doi:10.1007/s00382-016-2985-y

Comiso, J. C., Cavalieri, D. J., Parkinson, C. L., and Gloersen, P. (1997). Passive Microwave Algorithms for Sea Ice Concentration: A Comparison of Two Techniques. *Remote sensing Environ.* 60 (3), 357–384. doi:10.1016/s0034-4257(96)00220-9

Comiso, J. C. (1986). Characteristics of Arctic winter Sea Ice from Satellite Multispectral Microwave Observations. *J. Geophys. Res.* 91 (C1), 975–994. doi:10.1029/jc091ic01p00975

Comiso, J. C., Gersten, R. A., Stock, L. V., Turner, J., Perez, G. J., and Cho, K. (2017). Positive Trend in the Antarctic Sea Ice Cover and Associated Changes in Surface Temperature. *J. Clim.* 30 (6), 2251–2267. doi:10.1175/jcli-d-16-0408.1

Comiso, J. C., and Zwally, H. J. (1984). Concentration Gradients and Growth/decay Characteristics of the Seasonal Sea Ice Cover. *J. Geophys. Res.* 89 (C5), 8081–8103. doi:10.1029/jc089ic05p08081

Dee, D. P., Uppala, S. M., Simmons, A. J., Berrisford, P., Poli, P., Kobayashi, S., et al. (2011). The ERA-Interim Reanalysis: Configuration and Performance of the Data Assimilation System. *Q.J.R. Meteorol. Soc.* 137 (656), 553–597. doi:10.1002/qj.828

Downes, S. M., Farneti, R., Uotila, P., Griffies, S. M., Marsland, S. J., Bailey, D., et al. (2015). An Assessment of Southern Ocean Water Masses and Sea Ice during 1988-2007 in a Suite of Interannual CORE-II Simulations. *Ocean Model.* 94, 67–94. doi:10.1016/j.ocemod.2015.07.022

Ducklow, H., Clarke, A., Dickhut, R., Doney, S. C., Geisz, H., Huang, K., et al. (2012). "The marine Ecosystem of the Western Antarctic Peninsula," in *Antarctica: An Extreme Environment in a Changing World*. Editors

A. Rogers, N. Johnston, A. Clarke, and E. Murphy. First Edn. (Oxford: Blackwell Publishing Ltd).

Eayrs, C., Holland, D., Francis, D., Wagner, T., Kumar, R., and Li, X. (2019). Understanding the Seasonal Cycle of Antarctic Sea Ice Extent in the Context of Longer-Term Variability. *Rev. Geophys.* 57 (3), 1037–1064. doi:10.1029/2018rg000631

Enomoto, H., and Ohmura, A. (1990). The Influences of Atmospheric Half-Yearly Cycle on the Sea Ice Extent in the Antarctic. *J. Geophys. Res.* 95 (C6), 9497–9511. doi:10.1029/JC095iC06p09497

Ezraty, R., Girard-Ardhuin, F., Piollé, J. F., Kaleschke, L., and Heygster, G. (2007). "Arctic and Antarctic Sea Ice Concentration and Arctic Sea Ice Drift Estimated from Special Sensor Microwave Data," in *Département d'Océanographie Physique et Spatiale, IFREMER, Brest, France and University of Bremen Germany* (IFREMER), 2.

Farneti, R., Downes, S. M., Griffies, S. M., Marsland, S. J., Behrens, E., Bentsen, M., et al. (2015). An Assessment of Antarctic Circumpolar Current and Southern Ocean Meridional Overturning Circulation during 1958-2007 in a Suite of Interannual CORE-II Simulations. *Ocean Model.* 93, 84–120. doi:10.1016/j.ocemod.2015.07.009

Frew, R. C., Feltham, D. L., Holland, P. R., and Petty, A. A. (2019). Sea Ice-Ocean Feedbacks in the Antarctic Shelf Seas. *J. Phys. Oceanography* 49 (9), 2423–2446. doi:10.1175/jpo-d-18-0229.1

Goosse, H., and Zunz, V. (2014). Decadal Trends in the Antarctic Sea Ice Extent Ultimately Controlled by Ice-Ocean Feedback. *The Cryosphere* 8 (2), 453–470. doi:10.5194/tc-8-453-2014

Haid, V., Iovino, D., and Masina, S. (2017). Impacts of Freshwater Changes on Antarctic Sea Ice in an Eddy-Permitting Sea-Ice-Ocean Model. *The Cryosphere* 11 (3), 1387–1402. doi:10.5194/tc-11-1387-2017

Hobbs, W. R., Massom, R., Stammerjohn, S., Reid, P., Williams, G., and Meier, W. (2016). A Review of Recent Changes in Southern Ocean Sea Ice, Their Drivers and Forcings. *Glob. Planet. Change* 143, 228–250. doi:10.1016/j.gloplacha.2016.06.008

Holland, P. R., Bruneau, N., Enright, C., Losch, M., Kurtz, N. T., and Kwok, R. (2014). Modeled Trends in Antarctic Sea Ice Thickness. *J. Clim.* 27 (10), 378. doi:10.1175/jcli-d-13-00301.1

Holland, P. R., and Kwok, R. (2012). Wind-driven Trends in Antarctic Sea-Ice Drift. *Nat. Geosci* 5 (12), 872–875. doi:10.1038/ngeo1627

Holland, P. R. (2014). The Seasonality of Antarctic Sea Ice Trends. *Geophys. Res. Lett.* 41 (12), 4230–4237. doi:10.1002/2014gl060172

Holmes, C. R., Holland, P. R., and Bracegirdle, T. J. (2019). Compensating Biases and a Noteworthy Success in the CMIP5 Representation of Antarctic Sea Ice Processes. *Geophys. Res. Lett.* 46 (8), 4299–4307.

Iovino, D., Selivanova, J., Lavergne, T., Cipollone, A., Masina, S., and Garric, G. (2022). Changes in the Antarctic Marginal Ice Zone, in Copernicus Marine Service Ocean State Report, Issue 6. *J. Oper. Oceanography* 1, 1. accepted.

Ivanova, N., Johannessen, O. M., Pedersen, L. T., and Tonboe, R. T. (2014). Retrieval of Arctic Sea Ice Parameters by Satellite Passive Microwave Sensors: A Comparison of Eleven Sea Ice Concentration Algorithms. *IEEE Trans. Geosci. Remote Sensing* 52 (11), 7233–7246. doi:10.1109/tgrs.2014.2310136

Ivanova, N., Pedersen, L. T., Tonboe, R. T., Kern, S., Heygster, G., Lavergne, T., et al. (2015). Inter-comparison and Evaluation of Sea Ice Algorithms: towards Further Identification of Challenges and Optimal Approach Using Passive Microwave Observations. *The Cryosphere* 9 (5), 1797–1817. doi:10.5194/tc-9-1797-2015

Jackson, L. C., Peterson, K. A., Roberts, C. D., and Wood, R. A. (2016). Recent Slowing of Atlantic Overturning Circulation as a Recovery from Earlier Strengthening. *Nat. Geosci* 9 (7), 518–522. doi:10.1038/ngeo2715

Kennicutt, M. C., Chown, S. L., Cassano, J. J., Liggett, D., Peck, L. S., Massom, R., et al. (2015). A Roadmap for Antarctic and Southern Ocean Science for the Next Two Decades and beyond. *Antartic Sci.* 27 (1), 3–18. doi:10.1017/s0954102014000674

Kohout, A. L., Williams, M. J. M., Dean, S. M., and Meylan, M. H. (2014). Storm-induced Sea-Ice Breakup and the Implications for Ice Extent. *Nature* 509 (7502), 604–607. doi:10.1038/nature13262

Lavergne, T., Sørensen, A. M., Kern, S., Tonboe, R., Notz, D., Aaboe, S., et al. (2019). Version 2 of the EUMETSAT OSI SAF and ESA CCI Sea-Ice Concentration Climate Data Records. *The Cryosphere* 13 (1), 49–78. doi:10.5194/tc-13-49-2019

Lellouche, J.-M., Le Galloudec, O., Drévillon, M., Régnier, C., Greiner, E., Garric, G., et al. (2013). Evaluation of Global Monitoring and Forecasting Systems at Mercator Océan. *Ocean Sci.* 9 (1), 57–81. doi:10.5194/os-9-57-2013

MacLachlan, C., Arribas, A., Peterson, K. A., Maidens, A., Fereday, D., Scaife, A. A., et al. (2015). Global Seasonal Forecast System Version 5 (GloSea5): a High-Resolution Seasonal Forecast System. *Q.J.R. Meteorol. Soc.* 141, 1072–1084. doi:10.1002/qj.2396

Maksym, T., Stammerjohn, S., Ackley, S., and Massom, R. (2012). Antarctic Sea Ice-A Polar Opposite? *oceanog* 25 (3), 140–151. doi:10.5670/oceanog.2012.88

Manucharyan, G. E., and Thompson, A. F. (2017). Submesoscale Sea Ice-Ocean Interactions in Marginal Ice Zones. *J. Geophys. Res. Oceans* 122, 9455–9475. doi:10.1002/2017JC012895

Masina, S., Storto, A., Ferry, N., Valdivieso, M., Haines, K., Balmaseda, M., et al. (2015). An Ensemble of Eddy-Permitting Global Ocean Reanalyses from the MyOcean Project. *Clim. Dyn.* 49, 813–841. doi:10.1007/s00382-015-2728-5

Masina, S., and Storto, A. (2017). Reconstructing the Recent Past Ocean Variability: Status and Perspective. *J Mar. Res.* 75 (6), 727–764. doi:10.1357/002224017823523973

Massom, R. A., and Stammerjohn, S. E. (2010). Antarctic Sea Ice Change and Variability - Physical and Ecological Implications. *Polar Sci.* 4 (2), 149–186. doi:10.1016/j.polar.2010.05.001

Meehl, G. A., Arblaster, J. M., Bitz, C. M., Chung, C. T. Y., and Teng, H. (2016). Antarctic Sea-Ice Expansion between 2000 and 2014 Driven by Tropical Pacific Decadal Climate Variability. *Nat. Geosci* 9 (8), 590–595. doi:10.1038/ngeo2751

Meier, W. N., Fetterer, F., Savoie, M., Mallory, S., Duerr, R., and Stroeve, J. (2017). *NOAA/NSIDC Climate Data Record of Passive Microwave Sea Ice Concentration*. version 3. Boulder, Colorado USA: NSIDC: National Snow and Ice Data Center.

Meier, W. N., Peng, G., Scott, D. J., and Savoie, M. H. (2014). Verification of a New NOAA/NSIDC Passive Microwave Sea-Ice Concentration Climate Record. *Polar Res.* 33 (1), 21004. doi:10.3402/polar.v33.21004

Meier, W. N., and Stewart, J. S. (2019). Assessing Uncertainties in Sea Ice Extent Climate Indicators. *Environ. Res. Lett.* 14 (3), 035005. doi:10.1088/1748-9326/aaf52c

Meylan, M. H., Bennetts, L. G., and Kohout, A. L. (2014). *In Situ* measurements and Analysis of Ocean Waves in the Antarctic Marginal Ice Zone. *Geophys. Res. Lett.* 41, 5046–5051. doi:10.1002/2014GL060809

Onarheim, I. H., Eldevik, T., Smedsrud, L. H., and Stroeve, J. C. (2018). Seasonal and Regional Manifestation of Arctic Sea Ice Loss. *J. Clim.* 31 (12), 4917–4932. doi:10.1175/jcli-d-17-0427.1

Palmer, M. D., Roberts, C. D., Balmaseda, M., Chang, Y.-S., Chepurin, G., Ferry, N., et al. (2017). Ocean Heat Content Variability and Change in an Ensemble of Ocean Reanalyses. *Clim. Dyn.* 49 (3), 909–930. doi:10.1007/s00382-015-2801-0

Parkinson, C. L., and Cavalieri, D. J. (2012). Arctic Sea Ice Variability and Trends, 1979–2010. *The Cryosphere* 6 (4), 881–889. doi:10.5194/tc-6-871-2012

Parkinson, C. L. (2019). A 40-y Record Reveals Gradual Antarctic Sea Ice Increases Followed by Decreases at Rates Far Exceeding the Rates Seen in the Arctic. *Proc. Natl. Acad. Sci. USA* 116 (29), 14414–14423. doi:10.1073/pnas.1906556116

Pauling, A. G., Smith, I. J., Langhorne, P. J., and Bitz, C. M. (2017). Time-dependent Freshwater Input from Ice Shelves: Impacts on Antarctic Sea Ice and the Southern Ocean in an Earth System Model. *Geophys. Res. Lett.* 44 (20), 10–454. doi:10.1002/2017gl075017

Perovich, D. K., and Jones, K. F. (2014). The Seasonal Evolution of Sea Ice Floe Size Distribution. *J. Geophys. Res. Oceans* 119, 8767–8777. doi:10.1002/2014JC010136

Riihelä, A., Bright, R. M., and Anttila, K. (2021). Recent Strengthening of Snow and Ice Albedo Feedback Driven by Antarctic Sea-Ice Loss. *Nat. Geosci.* 14, 832–836. doi:10.1038/s41561-021-00841-x

Roach, L. A., Dean, S. M., and Renwick, J. A. (2018). Consistent Biases in Antarctic Sea Ice Concentration Simulated by Climate Models. *The Cryosphere* 12 (1), 365–383. doi:10.5194/tc-12-365-2018

Roach, L. A., Dörr, J., Holmes, C. R., Massonnet, F., Blockley, E. W., Notz, D., et al. (2020). Antarctic Sea Ice Area in CMIP6. *Geophys. Res. Lett.* 47, e2019GL086729. doi:10.1029/2019GL086729

Rolph, R. J., Feltham, D. L., and Schröder, D. (2020). Changes of the Arctic Marginal Ice Zone during the Satellite Era. *The Cryosphere* 14 (6), 1971–1984. doi:10.5194/tc-14-1971-2020

Serreze, M. C., and Stroeve, J. (2015). Arctic Sea Ice Trends, Variability and Implications for Seasonal Ice Forecasting. *Phil. Trans. R. Soc. A.* 373 (2045), 20140159. doi:10.1098/rsta.2014.0159

Shu, Q., Wang, Q., Song, Z., Qiao, F., Zhao, J., Chu, M., et al. (2020). Assessment of Sea Ice Extent in CMIP6 with Comparison to Observations and CMIP5. *Geophys. Res. Lett.* 47 (9), e2020GL087965. doi:10.1029/2020gl087965

Stammerjohn, S. E., Martinson, D. G., Smith, R. C., Yuan, X., and Rind, D. (2008). Trends in Antarctic Annual Sea Ice Retreat and advance and Their Relation to El Niño–Southern Oscillation and Southern Annular Mode Variability. *J. Geophys. Res. Oceans* 113 (C3), 1. doi:10.1029/2007jc004269

Storto, A., Masina, S., Balmaseda, M., Guinehut, S., Xue, Y., Szekely, F., et al. (2017). Steric Sea Level Variability (1993-2010) in an Ensemble of Ocean Reanalyses and Objective Analyses. *Clim. Dyn.* 49 (3), 709–729. doi:10.1007/s00382-015-2554-9

Storto, A., Masina, S., and Navarra, A. (2016). Evaluation of the CMCC Eddy-permitting Global Ocean Physical Reanalysis System (C-GLORS, 1982-2012) and its Assimilation Components. *Q.J.R. Meteorol. Soc.* 142, 738–758. doi:10.1002/qj.2673

Storto, A., Masina, S., Simoncelli, S., Iovino, D., Cipollone, A., Drevillon, M., et al. (2019). The Added Value of the Multi-System Spread Information for Ocean Heat Content and Steric Sea Level Investigations in the CMEMS GREP Ensemble Reanalysis Product. *Clim. Dyn.* 53 (1), 287–312. doi:10.1007/s00382-018-4585-5

Stroeve, J. C., Jenouvrier, S., Campbell, G. G., Barbraud, C., and Delord, K. (2016). Mapping and Assessing Variability in the Antarctic Marginal Ice Zone, Pack Ice and Coastal Polynyas in Two Sea Ice Algorithms with Implications on Breeding success of Snow Petrels. *The Cryosphere* 10 (4), 1823–1843. doi:10.5194/tc-10-1823-2016

Strong, C., and Rigor, I. G. (2013). Arctic Marginal Ice Zone Trending Wider in Summer and Narrower in winter. *Geophys. Res. Lett.* 40 (18), 4864–4868. doi:10.1002/grl.50928

Sutherland, B. R., and Balmforth, N. J. (2019). Damping of surface waves by floating particles. *Physical Review Fluids* 4 (1), 014804.

Tsamados, M., Feltham, D., Petty, A., Schroeder, D., and Flocco, D. (2015). Processes Controlling Surface, Bottom and Lateral Melt of Arctic Sea Ice in a State of the Art Sea Ice Model. *Phil. Trans. R. Soc. A.* 373, 20140167. doi:10.1098/rsta.2014.0167

Tsujino, H., Urakawa, L. S., Griffies, S. M., Danabasoglu, G., Adcroft, A. J., Amaral, A. E., et al. (2020). Evaluation of Global Ocean-Sea-Ice Model Simulations Based on the Experimental Protocols of the Ocean Model Intercomparison Project Phase 2 (OMIP-2). *Geosci. Model. Dev.* 13 (8), 3643–3708. doi:10.5194/gmd-13-3643-2020

Turner, J., Bracegirdle, T. J., Phillips, T., Marshall, G. J., and Hosking, J. S. (2013). An Initial Assessment of Antarctic Sea Ice Extent in the CMIP5 Models. *J. Clim.* 26 (5), 1473–1484. doi:10.1175/jcli-d-12-00068.1

Turner, J., Hosking, J. S., Bracegirdle, T. J., Marshall, G. J., and Phillips, T. (2015). Recent Changes in Antarctic Sea Ice. *Phil. Trans. R. Soc. A.* 373, 20140163. doi:10.1098/rsta.2014.0163

Uotila, P., Goosse, H., Haines, K., Chevallier, M., Barthélemy, A., Bricaud, C., et al. (2019). An Assessment of Ten Ocean Reanalyses in the Polar Regions. *Clim. Dyn.* 52 (3), 1613–1650. doi:10.1007/s00382-018-4242-z

Valdivieso, M., Haines, K., Balmaseda, M., Chang, Y.-S., Drevillon, M., Fujii, Y., et al. (2017). An Assessment of Air-Sea Heat Fluxes from Ocean and Coupled Reanalyses. *Clim. Dyn.* 49 (3), 983–1008. doi:10.1007/s00382-015-2843-3

Venables, H. J., and Meredith, M. P. (2014). Feedbacks between Ice Cover, Ocean Stratification, and Heat Content in Ryder Bay, Western Antarctic Peninsula. *J. Geophys. Res. Oceans* 119 (8), 5323–5336. doi:10.1002/2013jc009669

Vichi, M. (2021). A Statistical Definition of the Antarctic Marginal Ice Zone. *Cryosphere Discuss.* 1, 1–23. [preprint].

Vichi, M., Eayrs, C., Alberello, A., Bekker, A., Bennetts, L., Holland, D., et al. (2019). Effects of an Explosive Polar Cyclone Crossing the Antarctic Marginal Ice Zone. *Geophys. Res. Lett.* 46 (11), 5948–5958. doi:10.1029/2019gl082457

Wachter, P., Reiser, F., Friedl, P., and Jacobeit, J. (2021). A New Approach to Classification of 40 Years of Antarctic Sea Ice Concentration Data. *Int. J. Climatology* 41, E2683–E2699. doi:10.1002/joc.6874

Wang, M. J., Liu, T. T., Yang, Z. J., Wu, B., and Zhu, X. (2021). Variation of Antarctic Marginal Ice Zone Extent (1989–2019). *Adv. Polar Sci.* 32 (4), 341–355. doi:10.13679/j.advps.2021.0042

WMO (2009). WMO Sea-Ice Nomenclature. *WMO/OMM/BMO* 259 (Suppl. 5), 23.

Zuo, H., Balmaseda, M. A., Tietsche, S., Mogensen, K., and Mayer, M. (2019). The ECMWF Operational Ensemble Reanalysis-Analysis System for Ocean and Sea Ice: a Description of the System and Assessment. *Ocean Sci.* 15 (3), 779–808. doi:10.5194/os-15-779-2019

Conflict of Interest: The authors declare that the research was conducted in the absence of any commercial or financial relationships that could be construed as a potential conflict of interest.

Section 2.4. Changes in the Antarctic marginal ice zone

Authors: Doroteaciro Iovino, Julia Selivanova, Thomas Lavergne, Andrea Cipollone, Simona Masina, Gilles Garric

Statement of main outcome: The Southern Ocean plays a crucial role in the regulation of the global climate system, and the variation of its ice-covered area modifies the exchange of heat, mass and momentum between ocean and atmosphere. Therefore, knowledge of ice extent and its variability is necessary for an adequate simulation of those fluxes and thus for climate modelling. This section uses an ensemble of global eddy-permitting reanalyses (GREP) together with a Climate Data Record of Passive Microwave Sea Ice Concentration to investigate changes of Antarctic extent of the Marginal Ice Zone (MIZ) over the period 1993–2020. We assess the accuracy of GREP in discriminating the MIZ from the consolidated pack ice, and in reproducing their evolution in space/time. Although the ensemble reanalysis product tends to slightly overestimate summer MIZ, results show that it properly represents the variability of minima and maxima in MIZ extent as well as its interannual variability during the growing and melting seasons, particularly over the winter season. On average, the MIZ advance needs about 10 months to progress from near the coast in February to its most equatorward maximum and about only 2 months to return to a minimum. The MIZ extent did not experience a significant average trend over the study period, but the results further highlight substantial regional trends, particularly for regions covered by marginal ice.

2.4.1. Introduction

The Antarctic sea ice plays a crucial role in the regulation of the global climate system, and the variation of the ice-covered area modifies the exchange of heat, mass and momentum between ocean and atmosphere. Therefore, knowledge of ice extent and its variability is necessary for an adequate simulation of those fluxes and thus for climate modelling.

Unlike the Arctic, where sea ice extent (SIE) is decreasing in the entire region in all seasons, Antarctic trends are less noticeable and less clear (Simmonds 2015; Maksym 2019). While the Southern Ocean around Antarctica has been warming at an alarming rate contributing to ice sheet melt and consequently to sea-level rise, Antarctic SIE has remained stable (Parkinson 2019): the long-term SIE trend, on hemispheric scale, is nearly flat, for the winter maximum, summer minimum and annual average, although some regions experienced declines. Since the late 1970s, satellite record of total annual-mean extent shows a slight overall positive trend (Eayrs et al. 2021), which masks significantly larger opposing regional trends. The total Antarctic SIE has increased at a rate of approximately 1.5% per decade for the 1979–2015 period (e.g. Comiso et al. 2017), with a record high (of 12.8×10^6 km^2) reached in 2014 (Parkinson 2019). Many extreme events have been observed in recent years, with record-high winter maxima (occurring in decline with record low summer minimum extents (occurring in February/March) in 2016–2018 – the lowest value of 10.7×10^6 km^2 reached in 2017 (Parkinson 2019). Despite this marked decrease since late 2016, the overall long-term trend (1979–2021) remains positive, but it is of lower magnitude than the 1979–2016 trend, and is no longer significantly different from zero. Although several explanations have been proposed for Antarctic sea ice changes, as changes in upper ocean stratification and in the atmospheric dynamics and winds (e.g. Hobbs et al. 2016), how these changes link with polar and global climate change is still puzzling.

While the reasons for variability in total extent remain not completely understood, it is likely that these changes are not just affecting the total Antarctic SIE but also the distribution and variability of pack ice, marginal ice zone (MIZ) and sparse ice, in other ways (Stroeve et al. 2016). Knowledge of the spatial pattern of these different ice classes may help to elucidate the mechanisms contributing towards the expansion of Antarctic ice in some regions and contraction in others (Maksym et al. 2012). In spite of the vast winter cover, sea ice around Antarctica forms a very thin layer on the ocean, with less than 1 m thickness on average, and more compact ice remains all year around only in a few coastal regions (Worby et al. 2008; Holland et al. 2014).

Several criteria for characterising the MIZ have emerged over the past decades, but finding a coherent definition is still a challenge. The MIZ was originally described as the region where polar air, ice and water masses interact with the ocean temperature and subpolar climate system (Wadhams et al. 1981). Now, it is commonly defined as the portion of the ice-covered ocean where surface gravity waves significantly impact the dynamics of sea ice (e.g. Wadhams 2000; Dumont et al. 2011), often characterised by highly variable ice conditions. Given the unknowns in wave-ice interaction and the large uncertainties in both observed and forecasted waves within sea ice, the MIZ can be operationally defined through sea ice concentration thresholds, as the transition zone between open water and consolidated pack ice, where the total area of ocean is covered by 15–80% sea ice (e.g. Paul et al. 2021; Vichi 2021).

The MIZ is fundamental for climate dynamics and polar ecosystems, as a region of intense atmosphere-sea ice interactions that forms a physical buffer for the consolidated pack ice zone from the effects of open ocean dynamics (e.g. Squire 2007). The MIZ supports relevant

processes, such as air–sea gas exchange, and carbon exchange at the air–sea interface, marine primary production and delivery of nutrients to the euphotic zone (Barber et al. 2015). Monitoring changes of the MIZ environment can help us understand the associated changes in the climate system. Due to the thin and small broken ice floes, the MIZ region is highly dynamic and responsive to external forcing, and its response to climate variability differs from the inner pack ice (Stroeve et al. 2016). An accurate assessment of variability of dynamics in the MIZ is still missing, as well as a deep insight into how surface ocean/waves and atmospheric fields correlate with ice conditions, such as ice thickness, strength, and viscosity (Meylan et al. 2014; Sutherland and Balmforth 2019).

There are few in-situ data available on the Antarctic MIZ properties and still significant differences in estimates from satellite data sets depending on the algorithm employed (Stroeve et al. 2016). Numerous methods have been developed to estimate SIC from passive microwave instruments (including SMMR, SSMI, SSMIS, AMSR-E and AMSR-2) flying on various satellite platforms. The algorithms applied to the microwave brightness temperatures employ different channel combinations, with different corrections for weather, satellite drift, and other factors (Ivanova et al. 2015; Tonboe et al. 2016). When using estimates of sea ice properties, we should be conscious of the differences among algorithms and their attributes (Wright and Polashenski 2018), and the methods for combining different source data into long-term records (Stroeve et al. 2016).

Therefore, ocean/sea ice reanalysis data are essential in increasing our ability to comprehend total and marginal ice variability and to monitor their current state and predict their future changes. In this contribution, we aim to investigate how the Antarctic extent of MIZ is actually changing, using sea ice concentration from an ensemble of global eddy-permitting reanalyses (GREP), and to determine how realistically this product can capture the time/space variability of the Antarctic ice in the marginal ice zone over the period 1993-onward.

2.4.2. Methodology

The Global Reanalysis Ensemble Product (GREP version 2, product ref 2.4.1) is based on four global ocean reanalyses ORAs (GLORYS2v4, Lellouche et al. 2013; GloSea5, MacLachlan et al. 2015; C-GLORSv7, Storto et al. 2016; ORAS5, Zuo et al. 2019), constrained by satellite and in-situ observations and driven by ERA-Interim atmospheric reanalysis (Dee et al. 2011).

Each ORA uses the ocean component of the state-of-the-art NEMO model at eddy-permitting resolution (1/4° horizontal resolution), but the data assimilation techniques and the sea ice models differ (three ORAs employ the LIM2 sea ice model, one CICE4.1 that includes more complex physics compared to LIM2). Each of the reanalyses assimilates satellite sea surface temperature (SST), sea level anomalies, sea-ice concentrations and in-situ temperature and salinity. Details of each reanalysis product are in the above-mentioned studies. Single products as well as the multi-model ensemble are available from the beginning of the satellite altimetric era, January 1993 up to December 2020 (only Near Real Time altimetry data are ingested by the assimilation systems for the last six months).

The total ice is here split into three different zones. Due to the lack of wave estimations in the region and the availability of SIC observed-data, we use the concentration-based definitions for the GREP (product ref 2.4.1) output as well as the observational dataset (product ref 2.4.2), on their original grids. The consolidated pack ice is then defined by a SIC from 0.80 to 1. The MIZ is identified by SIC in the 0.15–0.80 range. Sparse sea ice covers regions with SIC lower than 0.15; it is worth mentioning that such low SIC can appear inside the pack ice region as well, in areas of potential polynyas.

To map Antarctic MIZ from satellite data record, we use the NOAA/NSIDC Climate Data Record (hereafter CDR, Meier et al. 2017, product ref. 2.4.2) that provides a combination of SIC estimates from two well-established algorithms (NASA Team and Bootstrap), reducing the overall low bias in a fully automated procedure (Peng et al. 2013). We use the merged product as each algorithm has different pros and cons. Stroeve et al. (2016) analysed the Antarctic MIZ from the NASA Team (NT) and Bootstrap (BT) data, and showed that (1) the BT algorithm halves the MIZ and doubles the consolidated pack ice area compared to the NT algorithm; (2) trends are also different with the BT indicating no statistically significant trends in the MIZ, and NT statistically significant positive MIZ trends in spring. The root mean square errors of SIC between the ensemble mean and NOAA/NSIDC CDR (product ref 2.4.2) is presented for September and February climatology over the period 1993–2019 (Figure 2.4.1). A RMSE up to 10% is visible in winter time over the Antarctic Circumpolar Current location, while summer SIC differs from satellite estimates mainly along the coastline of Eastern Antarctica where polynyas and ice sheets are present. CMEMS distributes global reprocessed SIC data from EUMETSAT OSISAF CDR and Interim CDR. This data set is ingested by some of the data assimilation systems employed in the ORAs constituting GREP (product ref 2.4.1), and hence not used for comparison in this study.

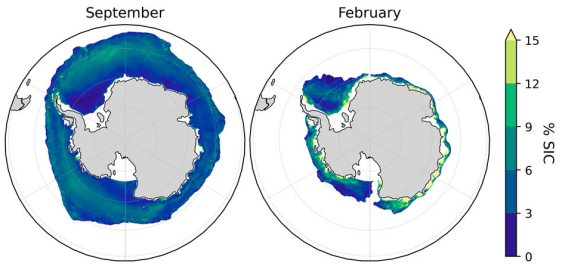

Figure 2.4.1. GREP SIC root mean square error for September (left), and February (right) averaged over 1993–2020 as derived from NOAA/NSIDC CDR (product ref. 2.4.2).

For all products, we analyse monthly means of SIC (the fractional coverage of an ocean grid-cell area covered with sea ice) to compute SIE as the total ocean area of all grid-cells with SIC exceeding 0.15. Thus, the MIZ extent represents the total area of ocean where SIC is comprised between 0.15 and 0.80. SIE is widely used as polar climate indicator minimising the effects of uncertainties in passive microwave estimates (e.g. Meier and Stewart 2019) compared to sea ice fraction and area. Our results are presented as hemispheric average, but we also show that sea ice variability and trends can regionally differ from the circumpolar ones.

2.4.3. Results

The climatological mean seasonal cycle of Antarctic MIZ does not follow total extent seasonality (Figure 2.4.2). While both reach minima in February, the MIZ extent peaks after the annual total (and pack) sea-ice maximum, generally occurring in September. On average, the MIZ advance needs about 10 months to progress from near the coast in February to its most equatorward maximum and about only 2 months to return to a minimum. The seasonal cycle of total SIE is dominated by the pack ice variability, with a shorter advance period (about 7 months) and longer retreat (about 5 months).

Figure 2.4.3 compares GREP (product ref 2.4.1) and CDR (product ref 2.4.2) time evolutions of MIZ and total SIE in four specific months [February (summer extent), May (growing season), September (winter extent) and December (melting season)]. There is a general good agreement between the observational estimates and the ensemble mean. For each month, GREP (product ref 2.4.1) is able to correctly reproduce the amounts of marginal ice and their interannual variability. GREP (product ref 2.4.1) SIE stays always within observational uncertainties. From the melting period to the summer minimum, GREP (product ref 2.4.1) MIZ interannual variability is consistent with satellite estimates, but overestimates MIZ extent indicating overall lower pack ice extent compared to observed data (product ref 2.4.2).

While total SIE (and pack ice extent) ranges from a summer minimum in February (always well under 5×10^6 km^2) to a winter maximum in September (always well over 18×10^6 km^2) in both GREP (product ref 2.4.1) and CDR (product ref 2.4.2) (Figures 2.4.2 and 2.4.3), the MIZ presents a minimum in February

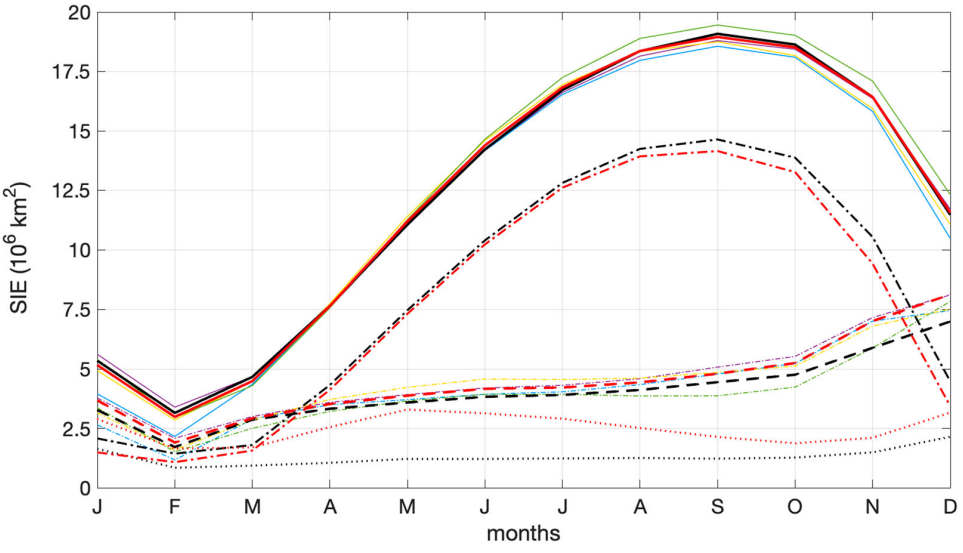

Figure 2.4.2. Mean seasonal cycle of total SIE (solid) and MIZ extent (dashed), from GREP (red, product ref. 2.4.1) and satellite estimates (black, product ref. 2.4.2), with individual ORA products (thin lines), for the 1993–2020 period. The seasonal cycles of pack ice (dash-dotted lines) and sparse ice (dotted lines) are also presented.

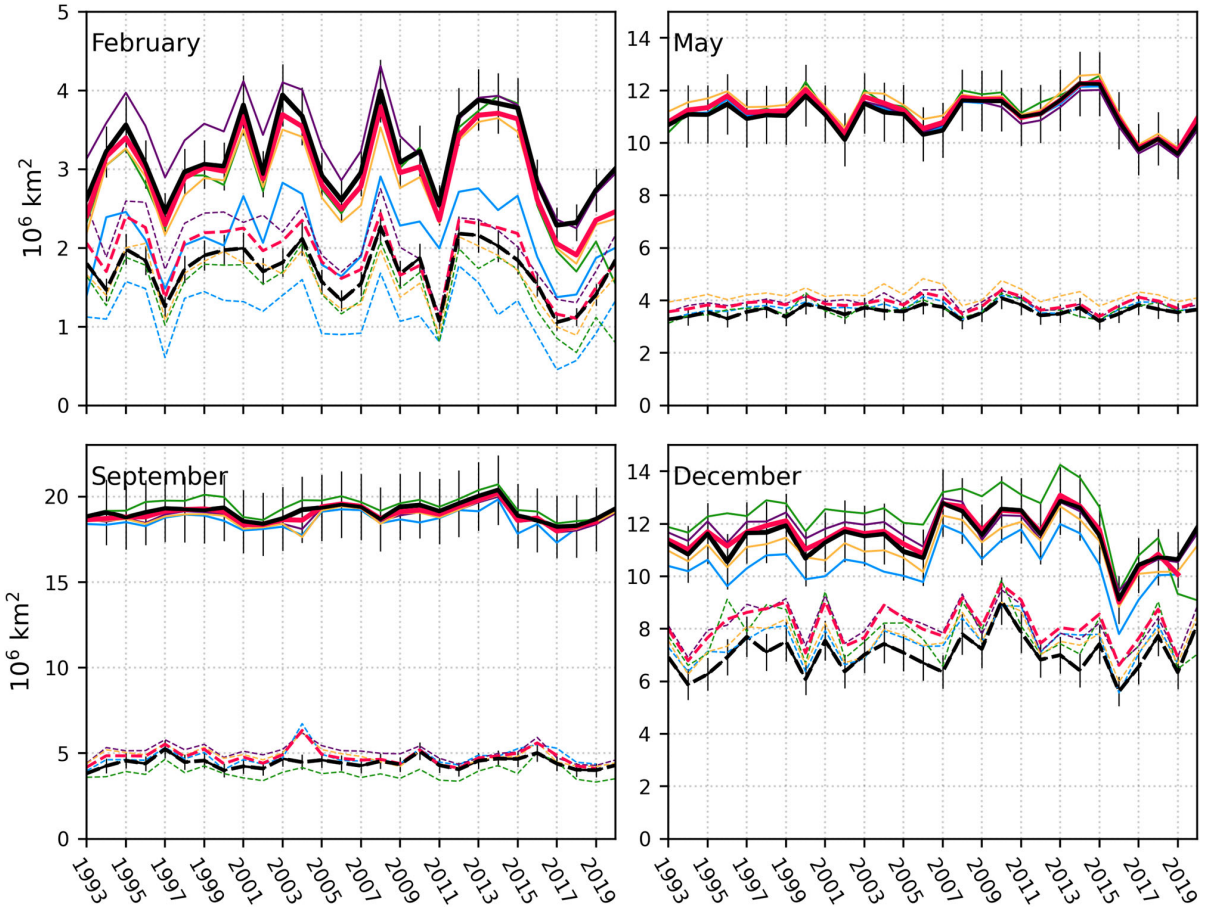

Figure 2.4.3. Time-series of Antarctic SIE (solid) and MIZ extent (dashed) from GREP (red, product ref 2.4.1) and CDR (black, product ref. 2.4.2) for February, May, September, and December. Thin lines represent the single ORAs. An error bar of 10% has been applied to the observational output (product ref. 2.4.2).

(generally higher than the minimum pack ice extent), to expand during the growing season when sea ice tends to aggregate and get denser, rapidly increasing the pack ice zone. In September, MIZ comprises about 25% of the total maximum extent but it does not reach its widest extent; it continues to expand toward the end of the year, to exceed again the pack ice extent during the melting season. The fraction of MIZ related to the total SIE is slightly overestimated in December and February by GREP (product ref 2.4.1), to follow more closely observed data in the growing season.

Time evolution of MIZ extent in each month has experienced no or little significant trends for 1993–2020 in both CDR (product ref 2.4.2) and GREP (product ref 2.4.1) – monthly-mean trends are listed in Table 2.4.1. The reduction in the minimum MIZ extent after 2016 is clearly visible and properly reproduced in GREP (product ref 2.4.1), as the extent increase in 2020. Trends in GREP (product ref 2.4.1) generally follow CDR (product ref 2.4.2). The hemispheric-wide SIE trends for February are negative in both products, driven by the MIZ decrease. During the ice expansion phase (in May), the negative trends in total SIE result from the reduction of the consolidated pack ice. In September, CDR (product ref 2.4.2) and GREP (product ref 2.4.1) exhibit opposing trends in the pack ice and MIZ, they compensate each other to result in a lack of trend in the total extent. During the melting period (in December), negative trends in the pack ice are comparable between the two products, but GREP (product ref 2.4.1) reproduces no trend in the MIZ too, with a larger decline in the total extent.

As a consequence of the similarities between CDR (product ref 2.4.2) and GREP (product ref 2.4.1) in estimating total and MIZ extent, the two products agree also in terms of the average locations of the MIZ. We illustrate the MIZ expansion and contraction, and assess the consistency between reanalysis products and observed estimates of MIZ locations, as shown in Figure 2.4.4. There is close agreement in the average latitude

Table 2.4.1. Slopes of trend lines (computed as linear least-squares regression) for the extent of marginal ice, consolidated pack ice and total ice for February–December (1993–2020) for both GREP (product ref 2.4.1) and CDR (product ref. 2.4.2).

Month	Ice classes	CDR	GREP
February	MIZ extent	−7.69	**−18.65**
	Pack ice extent	4.32	5.97
	Total extent	−3.37	−12.68
May	MIZ extent	5.36	1.58
	Pack ice extent	−18.79	−21.56
	Total extent	−13.42	−19.97
September	MIZ extent	1.13	−11.35
	Pack ice extent	−0.39	14.12
	Total extent	−0.73	−2.77
December	MIZ extent	14.65	−0.032
	Pack ice extent	−14.96	−17.13
	Total extent	−0.303	17.162

Notes: Values are listed in 10^3 km^2 per year. Bold indicates a significant slope with $p < 0.05$. The ensemble-mean MOC trend over 1993–2019 is also shown. All volume transports are referenced to zero at the surface to allow comparison with observations from Li et al. (2021). The ensemble-mean is calculated over the OSNAP observational period and over the full 1993–2019 ensemble period. The ensemble-mean uncertainty is equal to two times the standard deviation of the time-mean transport across the ensemble and its monthly-mean variability (and that of the observations) is equal to two times the standard deviation of the monthly-mean transports over the timeseries. ORAS5 is excluded from the ensemble-mean and uncertainty across all sections (see text). OSNAP observational estimates and uncertainties of the MOC (Li et al. 2021), and MHT and MFT (Lozier et al. 2017) are calculated using a Monte Carlo simulation. Estimates using the observed monthly-mean transports are in brackets. The OSNAP observational period is 2014–2018 for the MOC, and 2014–2016 for the MHT and MFT.

changes between the two products. The time evolution of the monthly-averaged position of the MIZ shows that the spatial pattern of the MIZ in GREP (product ref 2.4.1) and CDR (product ref 2.4.2), and its seasonal and interannual variability are again consistent, as well as the timing of MIZ advance and retreat. The location of the minimum MIZ extent slightly moves toward the equator in the last decade, while May and December show a contraction of the MIZ in the most recent years, from 2016. In the growing season, this is mainly due to the reduction of total SIE. The averaged latitude of MIZ is relatively constant in September and persistent at ∼62°S. Although the extent of marginal ice increases until the end of November/December and then its percentage stays nearly constant at this maximum extent, the December-average MIZ position and the outer ice edge move poleward. This is explained by the quick retreat of the inner pack ice starting in the end of September.

Satellite observations show that the small changes in total Antarctic sea ice over the last three decades mask a dipole pattern of regional changes, with substantial regional trends of increasing ice extent, primarily in the Ross and Weddell Seas, and decreasing ice extent in the Bellingshausen and Amundsen Seas (Parkinson 2019). There are complex spatial patterns of change in advance, retreat and duration, forced by wind-driven sea ice drift and ice-ocean heat fluxes. The accuracy of GREP (product ref 2.4.1) performances is investigated also on regional scales using maps of seasonal trends in sea ice concentration during 1993–2020 (Figure 2.4.5). The trends of simulated Antarctic SIC have large spatial differences that greatly agree with observed ice. They both show that the largest trends are present in the regions covered by marginal ice (see contour lines in Figure 2.4.5). From a seasonal perspective, summer (DJF) and autumn (MAM) have the largest and significant trends in both products. GREP (product ref 2.4.1) SIC exhibits negative trends in the Bellingshausen-Amundsen Sea and in Ross Sea, areas showing rapid regional warming. In summer and autumn, pronounced positive trends occur on the western Weddell Sea and north of the Antarctic Peninsula – they are due to a combination of processes, as changes in the atmospheric dynamics and wind patterns (e.g. Holland and Kwok 2012; Meehl et al. 2016; Vichi et al. 2019; Blanchard-Wrigglesworth et al. 2021), changes in the vertical structure of the near-surface water column (Goosse and Zunz 2014; Venables and Meredith 2014), freezing of low-salinity surface water from the ice sheet (Bintanja et al. 2013; Pauling et al. 2016; Haid et al. 2017). In all regions, the trends start to grow in spring (SON) resulting in the maximum summer trends. In winter (JJA), where the extent of the consolidated pack ice dominates, the largest positive/negative trends are located close to the ice edge (where ice distribution is mostly constrained by ocean dynamics). The spring Antarctic sea ice also shows a zonal wave-number-two structure, with a maximum in the Pacific sector and a minimum close to Davis Station (located on the Ingrid Christensen Coast in East Antarctica), similar to those in spring, except for the difference in the value.

2.4.4. Discussion and conclusions

The region covered by marginal ice is highly sensitive to atmospheric and oceanic forcing, changes in the MIZ extent can affect the level of atmosphere-ocean heat and gas exchanges the area of partially ice-covered ocean and can have implications for the polar ecosystems. Thus, investigation of changes of Antarctic MIZ supports understanding the Antarctic sea ice variability on different spatial and temporal scales.

We have analysed the evolution of the Antarctic MIZ as represented in the Global Reanalysis Ensemble Product (product ref 2.4.1) and compared it to a satellite-derived dataset (product ref 2.4.2). A detailed

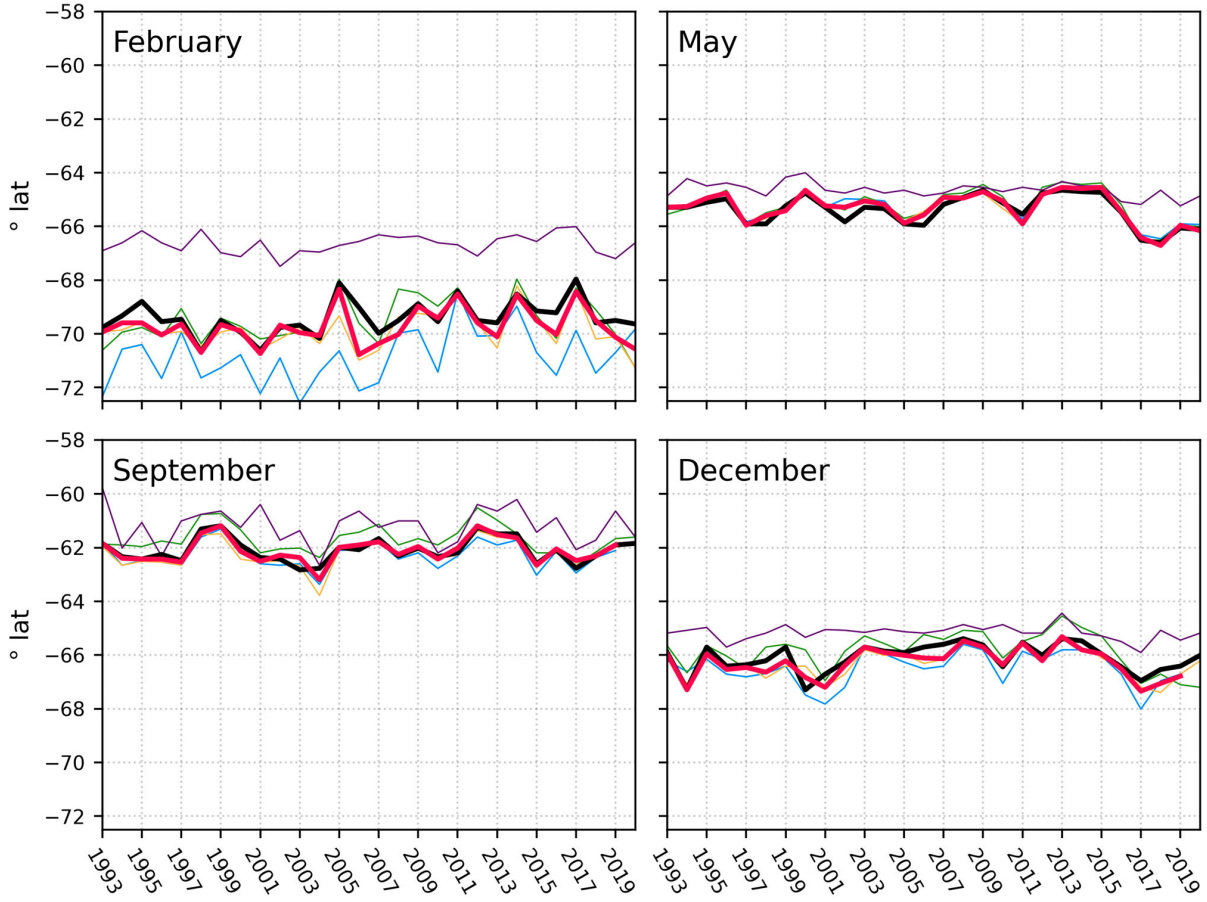

Figure 2.4.4. Time series of monthly-averaged latitudes of MIZ for GREP (red, product ref. 2.4.1) and CDR (black, product ref. 2.4.2) in February, May, September, and December.

understanding of mechanisms driving Antarctic sea ice classes is out of the scope of this contribution. Here, we want to assess the reliability of the sea ice concentration provided by the GREP ensemble mean (product ref 2.4.1) in discriminating the MIZ from the consolidated pack ice, and in reproducing the space/time evolution of the Antarctic MIZ from 1993 through 2020.

A challenge in the validation arises as to which long-term sea ice concentration data record to use. There are dozens of algorithms available, whose SICs are not necessarily consistent with each other (e.g. Ivanova et al. 2015; Stroeve et al. 2016). We derived monthly SIC fields from NOAA and the National Snow and Ice Data Center Climate Data Record (product ref 2.4.2), a long-term, consistent, satellite-based passive microwave record of sea ice concentration that leverages two well-validated concentration algorithms. This data set is not directly included in the data assimilation systems of the GREP (product ref 2.4.1) components.

GREP (product ref 2.4.1) is shown to properly represent the variability of minima and maxima in MIZ extent as well as its interannual variability during the growing and melting seasons. More evident discrepancies between GREP (product ref 2.4.1) and CDR (product ref 2.4.2) occur during summer, when the spread among individual ORA increases: one product tends to underestimate MIZ extent and another to overestimate pack ice extent.

The accuracy of the GREP ensemble mean (product ref 2.4.1) has already been assessed for a range of ocean applications (Storto et al. 2019). Although the four reanalyses included in GREP (product ref 2.4.1) employ the same ocean model and atmospheric forcing dataset, differences in ice models, data assimilation systems and observational datasets, air–sea flux formulations, initialisation strategy, and model configuration parameters, contribute to the ensemble dispersion. The ensemble-mean GREP always beats individual members in representing changes in the extent of total and marginal ice, in the Southern Ocean. The quality of GREP (product ref 2.4.1) is comparable to that of satellite data sets and the differences between GREP

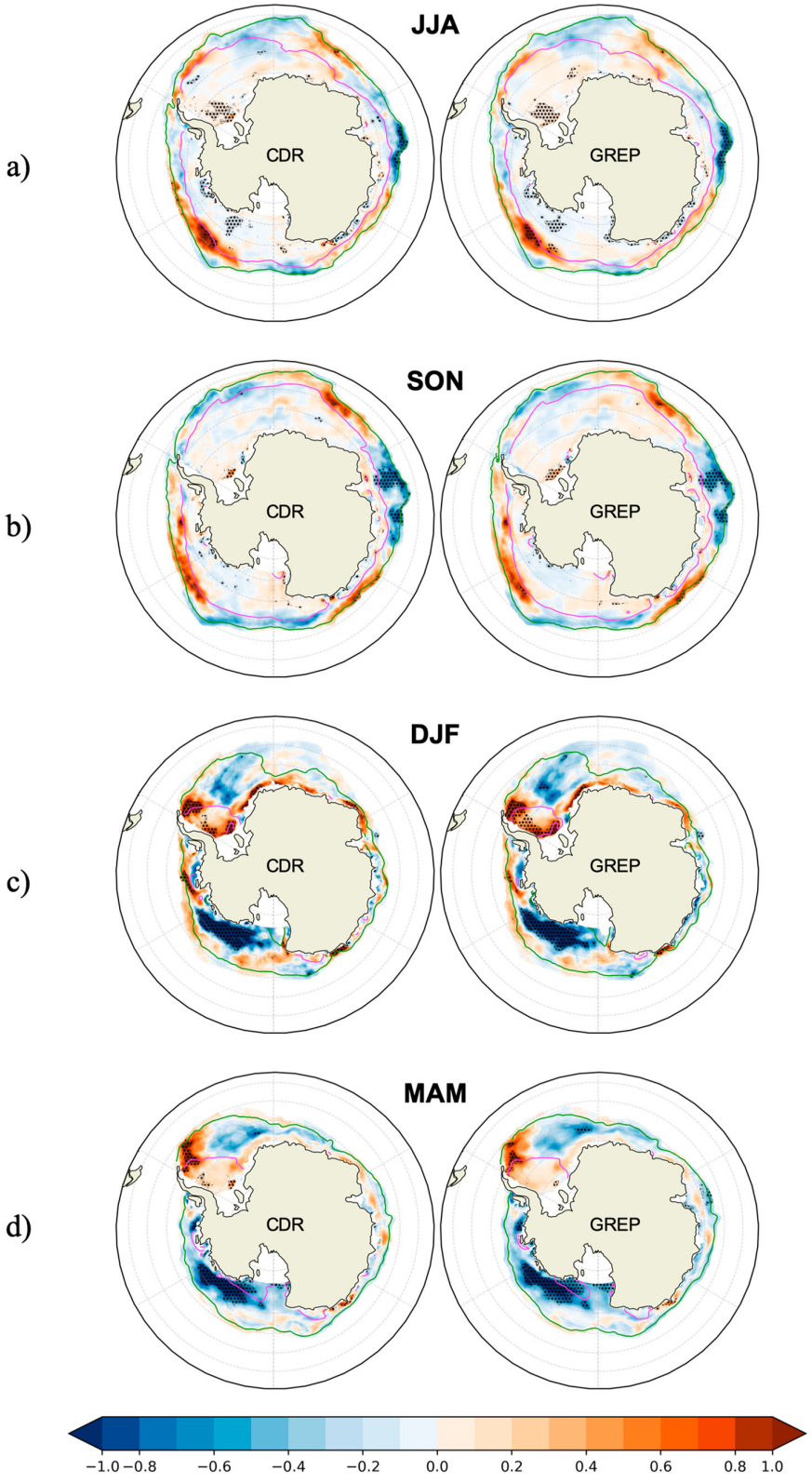

Figure 2.4.5. Map of seasonal trend in sea ice concentration (% yr^{-1}) from CDR (product ref. 2.4.2) and GREP (product ref. 2.4.1) in (a) winter (JJA), (b) spring (SON), (c) summer (DJF), and (d) autumn (MAM), for the 1993–2020 period. Contours indicate the SIC at 0.15 (green) and 0.8 (magenta). Dots show 95% significance. JJA: June-July-August; SON: September-October-November, DJF: December-January-February; MAM: March-April-May.

(product ref 2.4.1) and CDR (product ref 2.4.2) are comparable or even smaller than differences between different algorithms (Stroeve et al. 2016).

Nevertheless, the potential of the reanalysis ensemble emerged, but with a list of caveats that might be overcome in future works. The MIZ is very dynamic, making it challenging to provide precise delimitations using monthly SIC that are in turn sensitive to growth/melt processes and air–sea interface conditions. Future investigation of the ice classes variability in GREP (product ref 2.4.1) might benefit from reanalyses and observed values at higher time resolution, and focus on regional changes to better link MIZ extent to dynamical interactions with ocean and atmosphere, and feedback from rapid extreme events on seasonal and sub-seasonal scales. Improvement in data assimilation techniques, space–time data coverage the ice-covered Southern Ocean regions, and availability of other ice properties (such as thickness and drift) from satellite measurements will most probably boost the quality of ORAs and GREP (product ref 2.4.1) in polar regions.

Products used:

Ref. No.	Product name & type	Documentation
2.4.1	GLOBAL_REANALYSIS_PHY_001_031	PUM: https://marine.copernicus.eu/documents/PUM/CMEMS-GLO-PUM-001-031.pdf QUID: https://marine.copernicus.eu/documents/QUID/CMEMS-GLO-QUID-001-031.pdf
2.4.2	non-CMEMS remote sensing product: NOAA/NSIDC Climate Data Record of Passive Microwave Sea Ice Concentration, https://nsidc.org/data/g02202	Meier et al. 2017

Chapter 4
Antarctic sea ice in HighResMIP climate models

Abstract

Coupled climate models present low confidence in the simulation of the Antarctic sea ice state and historical evolution. Increasing horizontal resolution in the models can improve the representation of complex processes at high latitudes. Here, we examine the historical changes in the Antarctic sea ice cover in HighResMIP models over 1979-2014 with the objective to assess the realism of the main aspects of the Antarctic sea ice cover in coupled climate models. All models can adequately reproduce asymmetric seasonal cycle in sea ice area (SIA) but most of them delay the timing of the seasonal maximum in sea ice volume (SIV). All but one model fails to simulate overall SIA and SIV expansion over the satellite era and produces decreasing trends in response to global warming. Our results show no considerable improvements in the representation of Antarctic sea ice in coupled climate models with finer horizontal resolution (up to 0.25° in the ocean and 50 km in the atmosphere). Given the high computational cost of climate-scale simulations at increased spatial resolution, we assume that greater emphasis should be placed on improving the sea ice model description. The model skill to simulate the ocean and the atmosphere characteristics also could not explain the relatively good representation of the Antarctic sea ice mean state in a few models. We suggest that the realism of sea ice simulations rather depends on the interplay of the ocean and the atmosphere components in the coupled system.

4.1 Introduction

Sea ice is an iconic feature of the polar climate system which allows fluxes between the atmosphere and the underlying ocean in the form of heat, moisture, gas, and momentum exchanges. Variations of ice-covered area affect surface albedo, thermo-haline circulation, and biological productivity. The Southern Ocean witnesses the largest annual extension of the sea ice area on Earth: each year nearly 15x10^6 km^2 grow and melt which influences global climate dynamics (Abernathey et al., 2016; Pellichero et al., 2018), regional climate (Bracegirdle et al., 2013) and local ecosystems (Cavanagh et al., 2017). The long-term evolution of the Antarctic sea ice cover is quite distinct from its northern counterpart: while the Arctic has experienced continuous and stable sea ice loss over the recent decades (Onarheim et al., 2018), the Antarctic does not follow the trend, displaying weakly positive sea ice expansion (Parkinson, 2019), yet with considerable inter-annual

variability (Stammerjohn and Maksym, 2017). Moreover, the overall expansion masks high-magnitude seasonal (Holland, 2014) and regional (Hobbs et al., 2016; Stroeve et al., 2016) variability. The modest increase of sea ice area until 2014 has been interrupted by sea ice decreases between 2014 and 2016 followed by dramatic sea ice loss at the end of 2016, with the largest sea ice retreat in the Weddell and the Ross Seas. The puzzling behaviour of the Antarctic sea ice cover produced several explanations of the phenomenon with relation to large-scale atmospheric variability (Turner et al., 2015; Meehl et al., 2016), wind forcing (Holland and Kwok, 2012; Blanchard-Wrigglesworth et al., 2021), ice-ocean feedbacks (Goosse and Zunz, 2014), loss of Antarctic ice sheets (Bintanja et al., 2013; Haid et al., 2017), suggesting that multiple oceanic and atmospheric processes amplified by various climate feedbacks contribute differently to different sectors of the Southern Ocean, creating complex pattern of sea ice change throughout the satellite era.

Global coupled models represent a useful tool to investigate sea ice evolution and analyze the processes controlling its temporal and spatial variability. Providing a single framework, the Coupled Model Intercomparison Project (CMIP) helps to evaluate the realism of the simulations. It is generally viewed that in the Antarctic in comparison to the Arctic, the models have less credibility in simulating the main aspects of sea ice and the advancement across CMIP generations is much less noticeable (Roach et al., 2020; Shu et al., 2020). CMIP6 models exhibit huge inter-model spread in the SIA seasonal cycle, which in summer is twice as much as in the Arctic. Despite high uncertainties, the models in general can properly capture the asymmetry of the seasonal cycle with a slow advance and rapid retreat (Roach et al., 2020). The coupled climate models struggle to reproduce positive trends in the sea ice area over the satellite era: only 11% of CMIP6 models are able to capture observed expansion trends compared to 15% in CMIP5 (Shu et al., 2020). CMIP6 models predict sea ice loss in future projections at a higher rate compared to their predecessors from the fifth generation of CMIP (Holmes et al., 2022). A plausible representation of sea ice is essential to simulate air-sea fluxes at the ocean-atmosphere interface and to improve climate projections. However, sea ice is highly sensitive to oceanic and atmospheric forcing so the errors in sea ice representation can be composed of the errors in the simulation of the ocean (Docquier et al., 2019; Khosravi et al., 2022; Schroeter and Sandery, 2022) and atmosphere features (Lecomte et al., 2016; Lin et al., 2023). In fact, the coupled climate models suffer from systematic biases which affect other aspects of the climate and lead to error growth due to exchanges in the coupled system. Several systematic model biases have been identified in the Southern Ocean simulation (Meijers, 2014). One of the well-known biases is driven by cloud forcing (Zelinka et al., 2020): cloud effects introduce a great uncertainty and generate further biases such as surface warm bias (Beadling et al., 2020) and equatorward shift of the jet stream (Ceppi et al., 2012) which might translate into biases in sea ice area. The equatorward bias

of the westerly jet position has persisted over model generations (Gupta et al., 2021; Beadling et al., 2019) with improvement in the 6th phase of CMIP (Bracegirdle et al., 2020). Another consistent bias in the Southern Ocean simulation is too warm upper-ocean temperatures which affects air-sea heat fluxes, ocean circulation, water mass formation and Antarctic sea ice cover (Beadling et al., 2019; Hyder et al., 2018). One of the widely recognized ways to reduce the biases in the model simulations is to increase the horizontal resolution of the ocean and the atmosphere. The added value of enhanced horizontal resolution was demonstrated with regards to many aspects of Southern ocean climate, for example, Southern Ocean circulation and sea ice trends (Rackow et al., 2022), Antarctic Circumpolar Current (ACC) structure (Beadling et al., 2019), jet stream position (Curtis et al., 2020).

To explore the impact of the enhanced horizontal resolution on the accuracy of model simulations, The High Resolution Model Intercomparison Project (HighResMIP; Haarsma et al., 2016) was designed within the EU Horizon 2020 PRIMAVERA project (PRocess-based climate sIMulation: AdVances in high-resolution modelling and European climate Risk Assessment, https://www.primavera-h2020.eu/). The main focus of the HighResMIP ocean studies was the North Atlantic region and the Arctic (e.g. Docquier et al., 2019, 2020; Koenigk et al., 2021; Meccia et al., 2021). The only publication within HighResMIP with a focus on the Southern hemisphere has been Moreno-Chamarro et al., 2022, who investigated the warm Southern Ocean bias. They showed a mixed impact of increased resolution on the biases in surface air temperature and almost no difference between configurations for cloud radiative effect and precipitation.

In this paper, we explore the representation of Antarctic sea ice cover over the period 1979-2014 using the outputs of six coupled climate models participating in HighResMIP with the objective to assess the realism of the main aspects of the Antarctic sea ice cover. We investigate seasonal and long-term variability of sea ice area and volume in the model simulations against satellite estimates and reanalyses. We also seek to find out whether there is any impact of enhanced ocean/atmosphere horizontal resolution on the accuracy of simulated sea ice cover in the Southern Ocean by comparing it against observations and reanalyses.

4.2 Methods

In this study, we use the model outputs from the six coupled climate models participating in the HighResMIP, which is one of the CMIP6-endorsed Model Intercomparison Projects (MIPs). We focus on the historical runs ("hist-1950", 1950-2014) and chose for analysis period from 1979 to 2014 to compare the results with satellite observations and reanalyses. Every model has at least two resolution configurations and few of them have

Table 4.1: The model configurations used in the study.

Model configuration		nominal ocean res. (°)	nominal atm. res. (km)	model components	
				ocean-sea ice	atmosphere
CMCC-CM2 (Cherchi et al., 2019)	HR	0.25	100	NEMO3.6 +CICE4.0	CAM4
	VHR	0.25	25		
CNRM-CM6 (Voldoire et al., 2019)	LR	1	250	NEMO3.6 +GELATO6	ARPEGE6.3
	HR	0.25	100		
ECMWF-IFS (Roberts et al., 2018)	LR	1	50	NEMO3.4 +LIM2	IFS cycle43r1
	MR	0.25	50		
	HR	0.25	25		
EC-Earth3P (Haarsma et al., 2020)	LR	1	100	NEMO3.6 +LIM3	IFS cycle36r1
	HR	0.25	50		
HadGEM3 (Williams et al., 2018)	LM	1	250	NEMO3.6 +CICE5.1	UM
	MM	0.25	100		
	HM	0.25	50		
MPI-ESM (Müller et al., 2018)	HR	0.4	100	MPIOM1.6.3	ECHAM6.3
	XR	0.4	50		

intermediate resolution configurations: in four of the models (ECMWF-IFS; HadGEM3; EC-Earth3P; CNRM-CM6) both ocean and atmosphere vary between the configurations while in two of them (CMCC-CM2; MPI-ESM) only the atmosphere resolution varies. Note that ECMWF-IFS and HadGEM3 have several ensemble members and in this study, we use only the first ensemble member. The main characteristics of the models are given in Table 5.1. A more detailed description of the model configurations can be found in the respective documentations.

In this study, we compute sea ice area (SIA) using the variable "siconc", i. e. the integral area of ocean grid cells covered by sea ice with consideration of SIC in each of them. We focus on sea ice area instead of sea ice extent (total area of grid cells with at least 15% SIC; SIE) due to the large grid-dependency of the latter (Notz, 2014). The fields of sea ice thickness (SIT) are derived using the equivalent sea ice thickness "sivol", which refers to the sea ice volume per grid-cell area. To obtain sea ice volume (SIV), we multiply "sivol" with the individual grid-cell area, and then sum over the Antarctic region. To derive integrative metrics, only the grid cells with at least 15% SIC are considered owing to higher uncertainty in passive microwave retrievals in low sea ice conditions. Apart from sea ice variables, we retrieve monthly mean SST ("tos"), SSS ("sos"), ocean components of sea surface velocity ("uo","vo"), zonal component of wind at 925 hPa ("ua"). The mean metrics of the above-mentioned variables we use as the area-averaged field south of 60°S. Jet stream strength is determined as the highest zonal wind at 925 hPa level between 35 and 75°S where a cubic spline approximation is applied to the zonal-mean zonal wind and the jet position is defined as the latitude of this maximum (Bracegirdle et al., 2013).

In order to evaluate model results we use set of satellite products and reanalyses. For sea ice concentration, NOAA/NSIDC Climate Data Record (version 4, (Meier et al.,

2021), hereafter CDR) and EUMETSAT OSISAF Climate Data Record and Interim Climate Data Record (release 2, products OSI-450 and OSI-430-b, Lavergne et al., 2019) are used. In the present analysis, we use the reprocessed version of CDR which removes spatial and temporal filtering following Vichi (2022). Given the scarcity of SIT observations, the monthly means of SIT and SIV are obtained from reanalysis products: Global Ice-Ocean Modeling and Assimilation System (GIOMAS; Zhang and Rothrock, 2003) and the CMEMS ensemble of global ocean reanalyses (GREP; (Storto et al., 2019)). GIOMAS comprises a global Parallel Ocean and sea Ice Model (POIM) with data assimilation capabilities: the models are driven by SIC from the NSIDC near-real time product (Brodzik and Stewart, 2016) and SST from NCEP/NCAR reanalysis (Kalnay et al., 1996). Despite GIOMAS having uncertainties we use this product as a reference in the present analysis considering its persistence and spatial and temporal coverage. GREP is the ensemble mean of four global ocean eddy-permitting reanalyses available from 1993 (C-GLORSv7, Storto et al., 2016; FOAM-GloSea5, MacLachlan et al., 2015; GLORYS2v4, Lellouche et al., 2013; ORAS5, Zuo et al., 2019), all are composed of NEMO ocean model and forced by atmospheric reanalysis ECMWF Era Interim (**?**) on a 0.25° tripolar grid. GREP performance has already been assessed with respect to a range of ocean variables (Masina et al., 2015; Storto et al., 2019) as well as the Antarctic sea ice area (Iovino et al., 2022). For SST, SSS, ocean components of sea surface velocity, we use GREP. All GREP ensemble members assimilate SST and SSS observations (Storto et al., 2019) which permits us to use this product as a reference for inter-model comparison. For zonal wind, we use atmospheric reanalyses ERA5 (Hersbach et al., 2020) and JRA55 (Kobayashi et al., 2015). The fifth generation in the European Centre for Medium-range Weather Forecasts (ECMWF), ERA5 employs the operational ECMWF Integrated Forecasting System (IFS) model (cycle 41r2). The Japanese 55-year Reanalysis (JRA-55) is the update of JRA-25 developed by the Japan Meteorological Agency (JMA). JRA-55 uses the JMA global spectral model. Both reanalyses use a four-dimensional variational assimilation system. The level-pressure data in ERA5 is available at 0.25° while JRA55 provides a resolution of 1.25°. These atmospheric reanalyses have been successfully validated in the Southern Ocean with regard to surface air temperature (Huai et al., 2019; Zhu et al., 2021; King et al., 2022) and low-level winds (Tetzner et al., 2019; Caton Harrison et al., 2022).

4.3 Results

4.3.1 Mean state

Figure 4.1 illustrates the climatology of the Antarctic SIA (a) and SIV (b) in HighResMIP models against satellite observations and reanalyses for the period 1979-2014. The observed SIA has a distinct asymmetric seasonal cycle with slow autumn growth from

its minimum in February (~2.5x10^6 km^2) to its peak in September (16.2x10^6 km^2) and rapid spring retreat. The models are generally in good agreement with CDR in capturing the timing of the seasonal minima and maxima, however, the range of sea ice area varies from ~3x10^6 km^2 in summer to ~6x10^6 km^2 in winter excluding low the two outliers which simulate unrealistic seasonal cycle (HR and MR configurations of ECMWF-IFS).

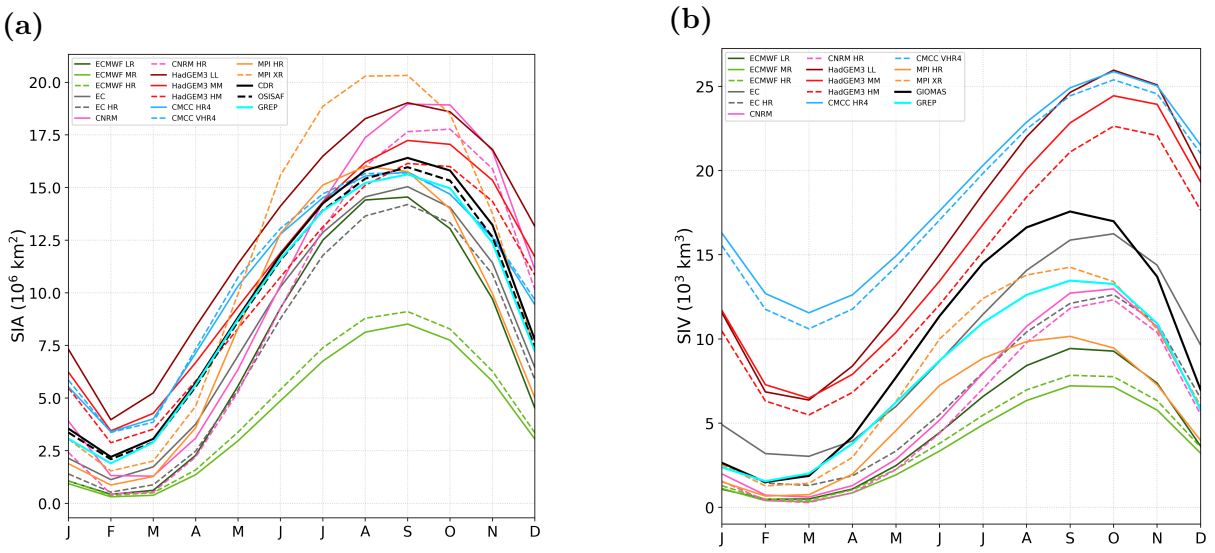

Figure 4.1: The 1979-2014 mean seasonal cycle in the Antarctic SIA (a) and SIV (b) from the model outputs against NSIDC CDRv4 for SIA and GIOMAS and GREP for SIV. GREP seasonal cycle is based on 1993-2014 data.

Few models miss the month of the observed annual maximum: both configurations of MPI-ESM reach the peak in August while CNRM has the maximum in October. Most products do not have enough sea ice in summer except two models which slightly overestimate SIA compared to observations. In winter, there is a substantial inter-model spread reaching ~12x10^6 km^2. Three out of six models are able to reproduce the amplitude of seasonal SIA variability (HadGEM3, EC-Earth3P, CMCC-CM2) whereas two models overestimate the annual cycle (CNRM, MPI-ESM XR), and the last one heavily underestimates it (ECMWF-IFS). Generally, with increased ocean resolution, there is a decrease of SIA and a closer fit to observations in winter while in summer the difference between configurations is very small. There is almost no effect of atmosphere resolution for ECMWF-IFS and CMCC-CM2, while for MPI-ESM we note the huge expansion of winter SIA with enhanced atmosphere resolution. Considering that SIT observations in the Southern Ocean are limited and not validated, for SIV we rely on data from GIOMAS and GREP reanalyses. The two reference products are in close agreement in summer (~2x10^3 km^3 in February) but simulate different amount of sea ice in winter: GIOMAS SIV grows up to ~17.5x10^3 km^3 while GREP SIV reaches ~12.5x10^3 km^3 in September. Compared to SIA, the inter-model spread in SIV is relatively larger and persistent throughout the year varying from ~15x10^3 km^3 in February to 23x10^3 km^3 in September. Two models

(a)

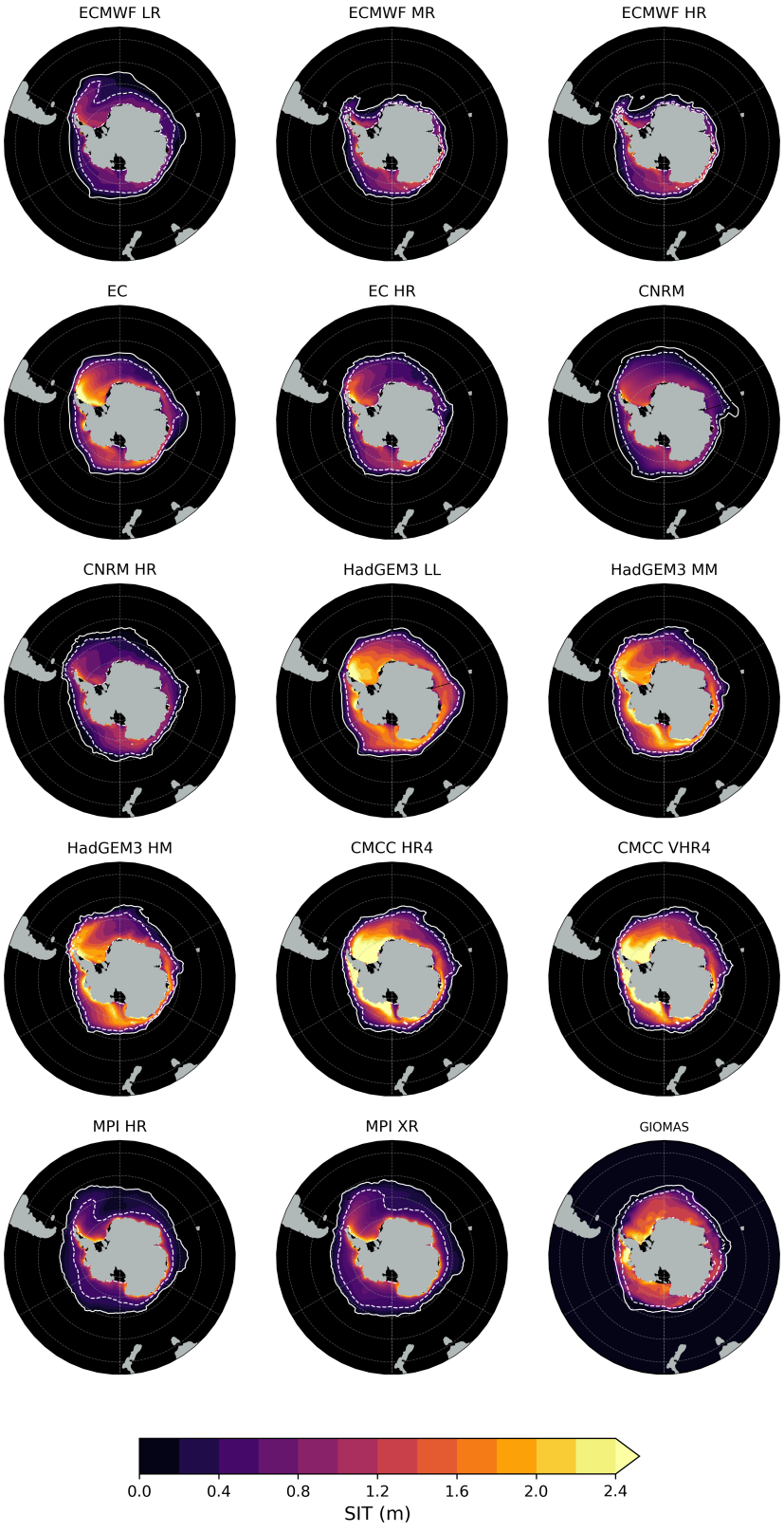
ECMWF LR
ECMWF MR
ECMWF HR
EC
EC HR
CNRM
CNRM HR
HadGEM3 LL
HadGEM3 MM
HadGEM3 HM
CMCC HR4
CMCC VHR4
MPI HR
MPI XR
GIOMAS
0.0
0.4
0.8
1.2
1.6
2.0
2.4
SIT (m)

(b)

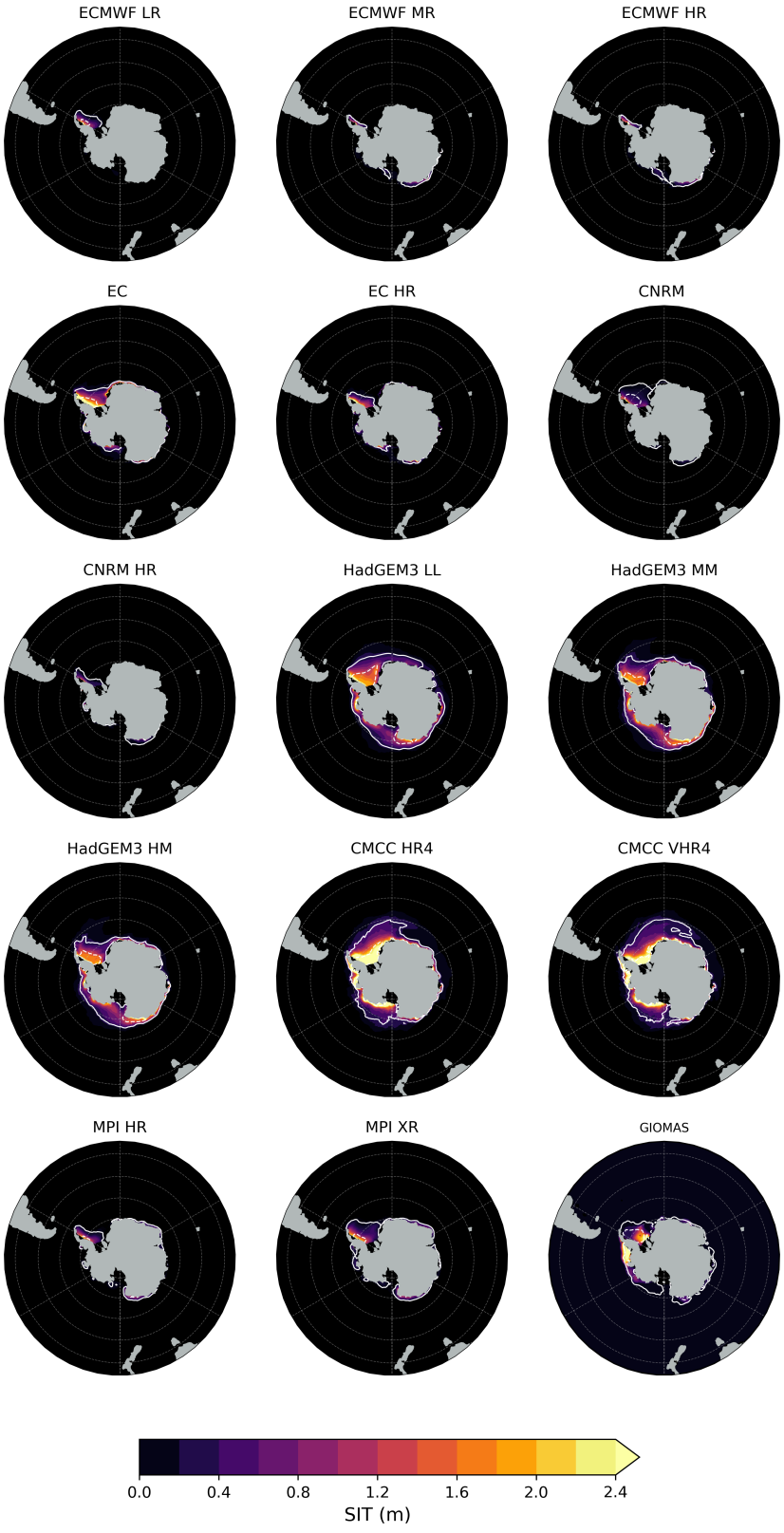

Figure 4.2: The 1979-2014 climatological mean sea ice thickness from the model outputs and GIOMAS in September (a) and February (b). White lines show 15% and 80% sea ice edges from corresponding models (SIC from NSIDC CDR for GIOMAS).

which are pretty good in reproducing SIA (HadGEM3, CMCC-CM2) largely overestimate SIV all year round due to great proportion of thick ice. Other models are close to the reanalyses in summer but underestimate SIV in other seasons relative to both reanalyses or remain close to GREP. All models simulate longer SIV growth compared to the reanalyses, with SIV maximum in October. Most models underrepresent the amplitude of SIV annual cycle since they simulate thinner ice compared to reanalyses, particularly in winter. CMCC-CM2 and HadGEM3 LL overestimate SIV in all seasons, however despite these persistent positive bias they agree well with GIOMAS on the amplitude of SIV seasonal cycle. In general, Antarctic SIV decreases with enhanced ocean resolution, while using the finer atmosphere resolution has different effects on the simulated SIV for different models: for HadGEM3 and CMCC-CM2 SIV decreases at higher atmospheric resolution while ECMWF-IFS and MPI-ESM have higher SIV in the finer atmospheric resolutions.

Next, we examine the spatial patterns of Antarctic SIC and SIT for the period 1979-2014. The climatological mean distribution of SIT and the sea ice edges (15% and 80% SIC) in September and February are shown in Figure 4.2. In September, the sea ice edge position is similar across the models. However, ECMWF-IFS clearly lacks sea ice in the Weddell Sea, while CNRM and MPI-ESM extend sea ice edge too far equatorward in the Weddell Sea and the Indian Ocean sector. HadGEM3 LL also grows more sea ice by September compared to GIOMAS, particularly in the eastern Indian Ocean. The location of 80% SIC identifies the ability of the models to simulate the MIZ (usually identified as the region between 15% and 80% SIC) and consolidated pack ice. Most models have a narrow band of marginal ice encircling the inner pack ice, similar to GIOMAS. ECMWF-IFS LR has a tail of pack ice in the Weddell Sea most probably as a result of underrepresented Weddell Gyre. MPI-ESM is the only model with a higher fraction of the MIZ, which is most prominently seen in the Atlantic and Indian Ocean sectors. In February, the major part of the models clearly melt too much sea ice: all models but HadGEM3 and CMCC-CM2 lack sea ice in the Ross, Amundsen and Bellinghausen Seas, some of them have not enough sea ice in the Weddell Sea (EC-Earth HR, CNRM HR, MPI-ESM HR) or melt down sea ice cover almost completely (ECMWF-IFS). The models also simulate different proportion of the MIZ and consolidated pack ice. Generally, only marginal ice survives in the models by February while pack ice is melted away. The models with thicker ice all year round (HadGEM3 and CMCC-CM2) retain pack ice in the Weddell Sea in summer.

There is great variability across the models in the spatial distribution of SIT in September: some of them simulate too thin ice everywhere in the domain (ECMWF-IFS, CNRM, MPI-ESM), while others exhibit clear thickening of the ice in the Weddell and the Ross Sea (HadGEM3 and CMCC-CM2). Different patterns of SIT in the models can be attributed to the different sea ice models: HadGEM3 and CMCC-CM2 use differ-

ent versions of CICE which includes five ice thickness categories in the parameterization schemes. EC-Earth3P exhibits a very close agreement with GIOMAS on the spatial distribution of SIT with the caveat that there is no reliable reference for SIT in the Southern Ocean. In February, most models remain only thin marginal ice, if any. In EC-Earth3P LR, a tongue of thicker ice maintains along the Antarctic Peninsula while in HadGEM3 and CMCC-CM2 thick or very thick ice covers a large part of the Weddell Sea produced by ridging. We do not observe any impact of the increased ocean resolution on the SIT spatial pattern: most models demonstrate similar SIT distribution in their different configurations. However, for EC-Earth3P and HadGEM3, enhanced ocean resolution leads to slightly thinner ice near the Antarctic Peninsula in the Weddell Sea. The increase of atmosphere resolution in CMCC-CM2 leads to thinner ice in the Weddell Sea reflecting the atmospheric enhancement of the sea ice drift.

4.3.2 Interannual variability and trends

Next, we investigate the long-term variability of Antarctic sea ice cover. Figure 4.3 shows the monthly anomalies of SIA (upper panel) and SIV (lower panel) with a comparison to CDR, OSISAF, and GREP for SIA and GIOMAS and GREP for SIV from 1979 to 2014 (1993-2014 for GREP).

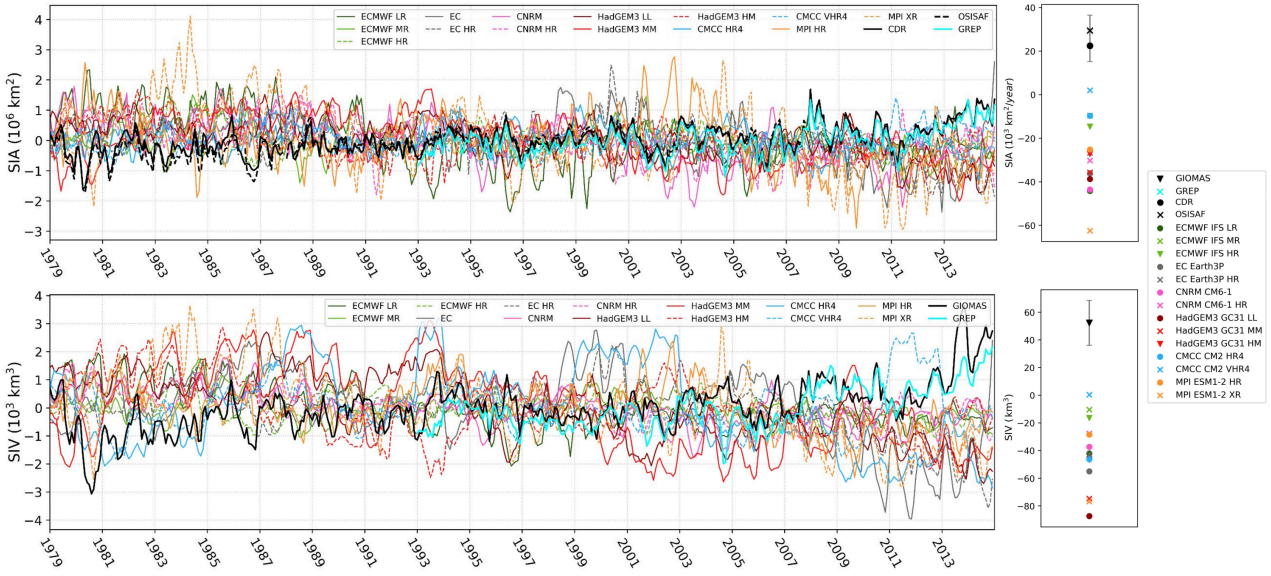

Figure 4.3: Monthly anomalies of SIA (upper panel) and SIV (lower panel) over 1979-2014 from HighResMIP model outputs and reference products. CDR and GIOMAS are indicated by a black line and GREP is shown by a cyan line. The plots on the right show linear trends in annual mean SIA (10^3 km^2/year) and SIV (km^3/year) over 1979-2014. The standard deviation for CDR is indicated by the vertical gray line.

Satellite products and GREP display modest growth of SIA with large inter-annual variability. The standard deviations in detrended Antarctic SIA over 1979-2014 are 0.28 (0.25)x10^6 km^2 in February and 0.33 (0.35)x10^6 km^2 in September in CDR (OSISAF). The models show a vast range of possible sea ice states and generally overestimate the interannual variability in SIA. The models are not able to capture the positive trends in SIA: the range of negative trends in SIA varies from -62.43 for MPI-ESM XR to -9.66x10^3 km^2/year for CMCC-CM2 HR. Only CMCC-CM2 XR simulates a positive trend at the rate of 2x10^3 km^2/year, which is still below the rate from CDR and OSISAF (22.5 and 29.45x10^3 km^2/year, respectively). By comparing trends in the annual mean SIA over the periods 1979-2014 and 1993-2014 (Table 5.1), we note that the models generally simulate higher sea ice loss for the more recent period, while satellite products show a similar rate of SIA expansion with slightly lower (OSISAF) or higher (CDR) trend for 1993-2014 period. Two models can capture SIA expansion over the years 1993-2014 (ECMWF-IFS LR and CMCC-CM2 VHR) and their trends fit well with satellite observations.

GIOMAS and GREP simulate similar SIV evolution (Table 4.3, lower panel) and both produce increasing trends but they are not in very close agreement for the inter-annual variability. The models demonstrate inter-model spread and all but one lose sea ice at the rate between -87.38 and -10.43 km^3/year. Only CMCC-CM2 VHR has a positive trend in the annual mean SIV but it is very weak (0.39 km^3/year). For the 1993-2014 period, two models have positive trends in SIV (15.09 km^3/year in ECMWF-IFS LR and 9.37 km^3/year in CMCC-CM2 VHR). The enhanced horizontal resolution of the ocean grid generally leads to less negative trends in SIA and SIV for the period 1979-2014 while for the years 1993-2014 ECMWF-IFS and HadGEM3 models have more negative trends with increased ocean resolution. The impact of the increased atmosphere resolution on the trends is less clear: enhanced atmosphere resolution leads to more negative trends in ECMWF-IFS and MPI-ESM and less negative or positive trends in HadGEM3 and CMCC-CM2.

4.3.3 Surface ocean properties

This section and the following one explore what aspects of the coupled models contribute to the biases in the representation of sea ice cover and why some models (CMCC-CM2, EC-Earth3P, HadGEM3) simulate fairly plausible mean sea ice state. Here we investigate the role of the ocean through the relationship between SIA, SST and SSS. From the top row in Figure 4.4 it is evident that the relationship between SIA and SST is strong: the models with higher SST have less SIA. In September, most models have SST lying between -1.6° and -1.2° not too different from GREP which has SST of around -1.5°. Moreover, the models do not exhibit large inter-annual variability in SST and SIA and stay in a relatively narrow range of values. There are two outliers in September:

Table 4.2: Linear trend in SIA and SIV and their standard deviations for 1979-2014 and 1993-2014 periods.

Model	1979-2014 SIA trend (10^3 km^2/yr)	1993-2014 SIA trend (10^3 km^2/yr)	1979-2014 SIV trend (km^3/yr)	1993-2014 SIV trend (km^3/yr)
ECMWF-IFS LR	-44.22 ± 16.8	27.85 ± 21.5	-42.08 ± 13.8	15.09 ± 18.5
ECMWF-IFS MR	-9.58 ± 9.6	-20.09 ± 13.7	-10.43 ± 10.6	-24.04 ± 13.9
ECMWF-IFS HR	-14.62 ± 10.6	-31.24 ± 18.4	-16.36 ± 11.1	-43.75 ± 19.2
EC-Earth3P	-36.07 ± 15.8	-69.55 ± 37.7	-55.01 ± 32.3	-129.44 ± 65.91
EC-Earth3P-HR	-26.71 ± 12.6	-65.36 ± 25.8	-42.72 ± 23.05	-111.47 ± 44.5
CNRM	-43.57 ± 14	-31.82 ± 34.5	-37.27 ± 12.8	-15.93 ± 28.3
CNRM HR	-30.2 ± 11.1	-16.64 ± 23.4	-27.78 ± 8.9	-23.63 ± 19.6
HadGEM3 GC31-LR	-38.7 ± 11.3	-54.6 ± 27	-87.38 ± 21.8	-102.04 ± 46.1
HadGEM3 GC31-MM	-35.71 ± 19.2	-68.24 ± 30	-74.79 ± 38	-116 ± 71.7
HadGEM3 GC31-HM	-27.2 ± 13.6	-7.5 ± 20.4	-46.57 ± 27.9	-14.22 ± 52
CMCC-CM2 HR	-9.66 ± 10.4	-39.67± 20.5	-46.31 ± 44.7	-198.55 ± 65.8
CMCC-CM2 VHR	2 ± 10.9	30.16 ± 16.9	0.39 ± 24.7	9.37 ± 65.77
MPI-ESM1-HR	-25.16 ± 18.4	-62.67 ± 37.8	-28.5 ± 17.7	-82.99 ± 34
MPI-ESM1-XR	-62.43 ± 23.6	-72.68 ± 44.4	-76.86 ± 25.4	-93.1 ± 43.4
CDR	22.5 ± 7.3	29.56 ± 17.5		
OSISAF	29.45 ± 7.3	23.2 ± 16.6		
GREP		32.14 ± 17		76.59 ± 29.6
GIOMAS			52.32 ± 16.2	67.15 ± 34.9

MPI-ESM HR and XR have cold SST close to or below -1.8° with a wide range of SIA stretching from 13 to 18x10^6 km^2 in the HR configuration and 18 to 22.5x10^6 km^2 in XR configuration. ECMWF-IFS MM and HR are warmer and with little ice, within the range of 8 and 10.5x10^6 km^2 for SIA and with SST between -1.2° and -0.9°. In February, there are two clear clusters. The first one includes the HadGEM3 and CMCC-CM2 configurations with high SIA up to 5x10^6 km^2 and low SST, which agrees well with GREP (0°-0.8°). The second cluster consists of the models with too warm ocean (1.4° - 3.7°) and lower SIA compared to GREP.

The representation of SSS is largely diverse across the models and there is no clear relationship between SIA and SSS in both seasons (Figure 4.4). In September, three models simulate salinity of around 34.1-34.15 (HadGEM3 LL, EC-Earth3P, CMCC-CM2 HR), similar to GREP. CMCC-CM2 XR has slightly higher SSS compared to GREP while three models simulate extremely high salinity (34.25 - 34.34 in two configurations of MPI-ESM and up to 34.8 in EC-Earth3P HR). The rest of the models have too fresh surface ocean up to 33.9 and below. In February, half of the models fall within the range of GREP SSS, which varies from roughly 33.25 to 33.61. The rest of the models have higher salinity, and all configurations of HadGEM3 and CMCC-CM2 have a narrow salinity range.

To examine the relationship between SIA and SST on a long-term scale we compare

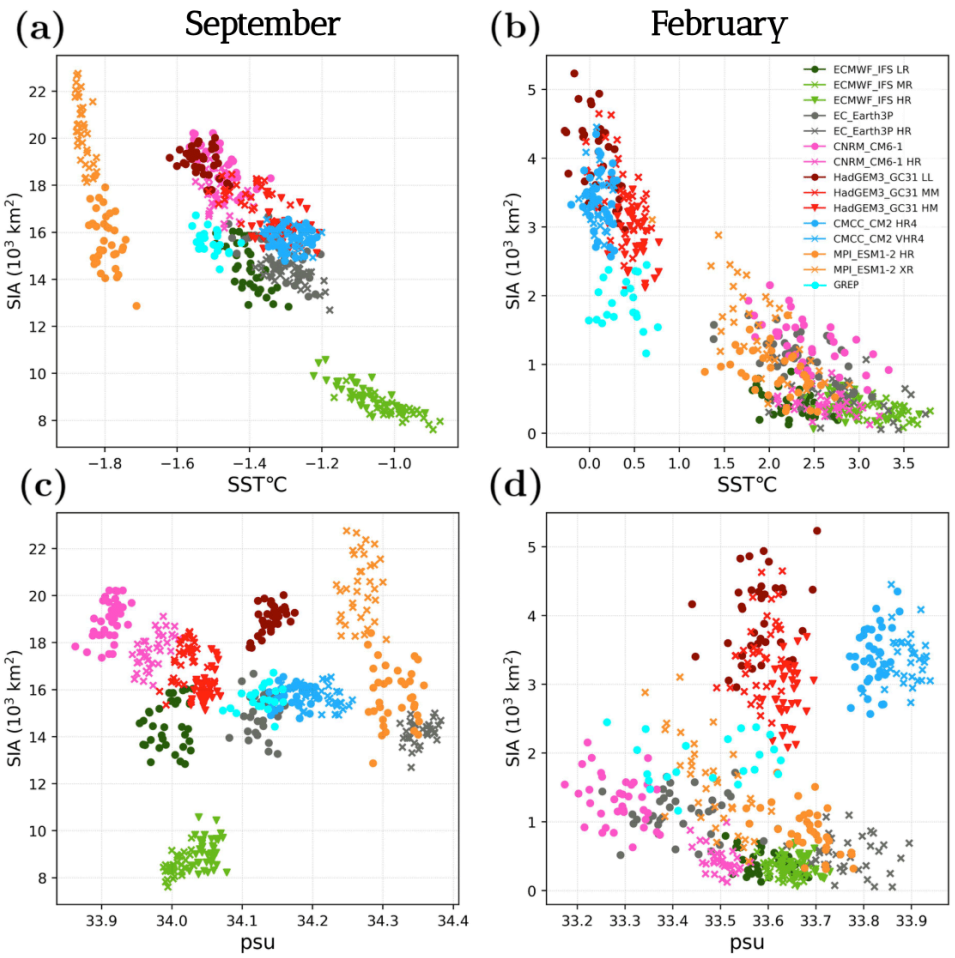

Figure 4.4: 1979-2014 average SST (a, b) and SSS (c, d) south of 60°S against SIA in September (left) and February (right) against estimates from GREP reanalysis for 1993-2014 (cyan).

linear trends in SIA and SST (Figure 4.5). From the plot, it is evident that generally, the models with stronger warming have more negative trends in SIA. However, there are also models with a weak SST trend and strong negative SIA trend (all configurations of HadGEM3) or, vice versa, a modest negative trend in SIA with a strong warming trend in the surface ocean (EC-Earth3P). In contrast to other models, CMCC-CM2 VHR produces a slightly positive trend in SIA together with weak cooling of the upper ocean.

4.3.4 Jet stream

Given the relationship between sea ice cover and the Southern Hemisphere jet stream through SST (Purich et al., 2016), we focus on the skill of the models at reproducing the westerly wind jet stream aiming to understand whether the large-scale atmosphere dynamics drives surface ocean temperature in the models. Figure 4.6a shows the climatology of the westerly jet strength.

Compared with ERA5 and JRA55, the major part of the models is able to simulate the annual cycle of the jet strength with two maximums in March and October reflecting

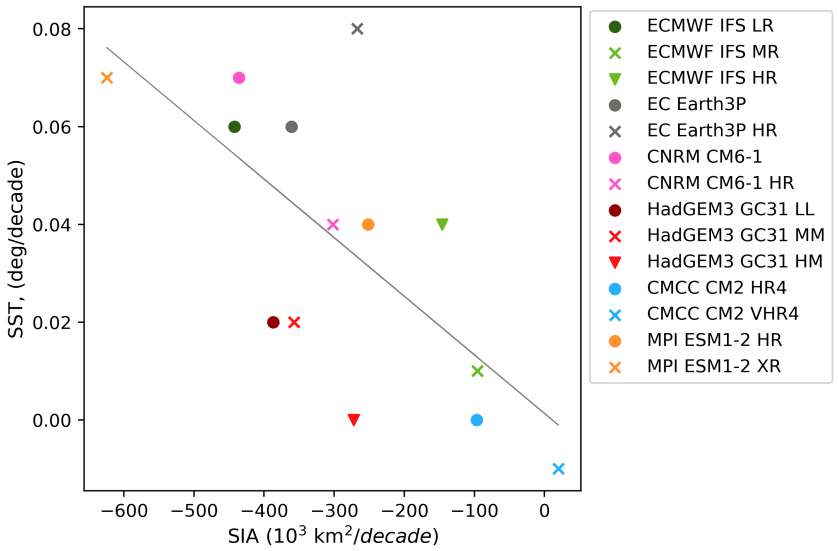

Figure 4.5: 1979-2014 trends in annual mean SST against trends in annual mean SIA.

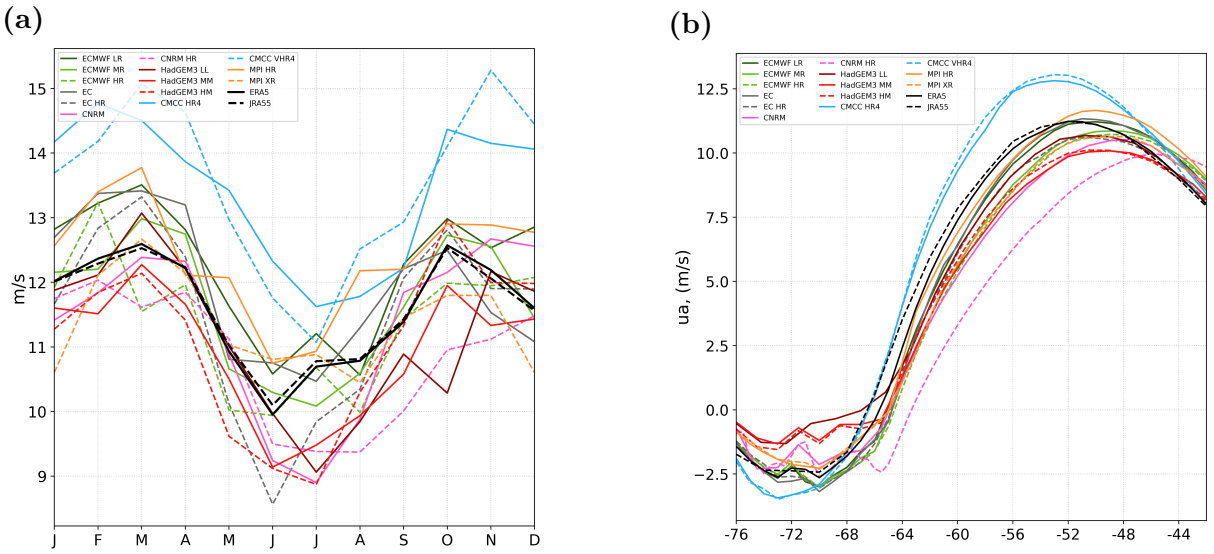

Figure 4.6: The 1979-2014 mean seasonal cycle in the jet strength (maximum zonal wind at 925 hPa level) (a). The annual mean zonal wind at 925 hPa level for the period 1979-2014 as a function of latitude (b).

a half-yearly pattern in surface pressure and temperature gradient, which controls the position of the ice edge (Eayrs et al., 2019). There is less agreement on the timing of the annual minimum which is delayed in many models to July or August. Some models do not have pronounced spring peak in the jet strength which might affect the timing of sea ice retreat. For example, CNRM with a delayed peak in the jet strength starts to melt sea ice later compared to other models (Figure 4.1a). In general, nearly half of the models underestimate the jet strength and another half tend to simulate stronger westerly wind compared to reanalyses. CMCC-CM2 model configurations have the highest bias in the wind speed among other models reaching ∼3 m/s relative to the reanalyses. Figure 4.6b illustrates the annual mean westerly wind at 925 hPa as a function of latitude. There is

a clear equatorward shift of the jet stream position in most of the models of up to 2° - 4°. On contrary, CMCC-CM2 simulates ∼2° poleward bias and ∼2 m/s higher speed of the jet stream with respect to the reanalyses.

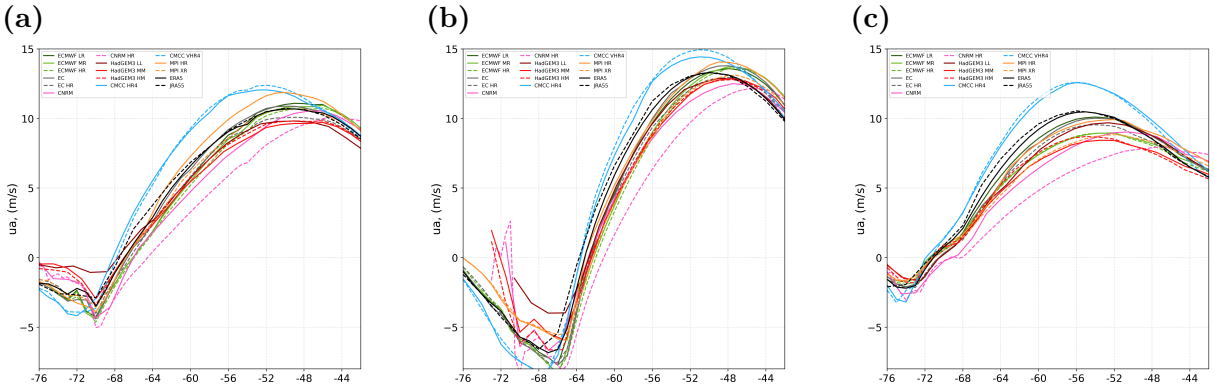

Figure 4.7: The annual mean zonal wind at 925 hPa level for the period 1993-2014 as a function of latitude for the Atlantic (a), Indian (b) and Pacific (c) sectors.

The model's skill to reproduce characteristics of the westerly wind varies across different regions. We analyze the position and strength of jet stream in different ocean basins: the Atlantic (290° - 20°), Indian (20° - 150°) and Pacific (150° - 290°) oceans are illustrated in Figure 4.7. The most accurate simulation of the jet strength and position is observed in the Atlantic sector. The models in general are in good agreement with the reanalyses on the jet strength (∼10.5 m/s) and reasonably capture the jet position. The jet stream position in CMCC-CM2 is shifted ∼4° poleward relative to reanalyses and its strength is ∼2 m/s higher. From the plot, it is clear that the Atlantic sector contributes the most to the error in the CMCC-CM2 representation of the mean jet stream position (Figure 4.7a). The Indian Ocean has the largest amplitude of the zonal wind across the ocean basins with stronger coastal easterlies along the Antarctic continent. Four out of five models are biased northward for the jet stream and all of them tend to overestimate the jet strength compared to the reanalyses. In the Indian Ocean sector, CMCC-CM2 is the only one that properly captures the latitude of the jet, yet slightly overestimates its strength. And finally, in the Pacific Ocean, we observe an increased inter-model spread in the representation of the wind speed stretching from ∼ 6 to ∼ 12 m/s at its peak. The models are also in better agreement on the latitude of the westerly jet and only CNRM still has equatorward bias.

Next, we investigated the time evolution of the jet stream over 1979-2014. Figure 4.8 shows the relationship between the linear trend in the annual mean jet position and its strength. Reanalyses show close to zero trend in the jet position and its strength. There are models that are well agreed with reanalyses on jet position trend (ECMWF-IFS HR, EC-Earth3P HR, CNRM-CM6) while the vast majority of the models exhibit weak poleward trend. Two models simulate an equatorward trend (ECMWF-IFS LR and

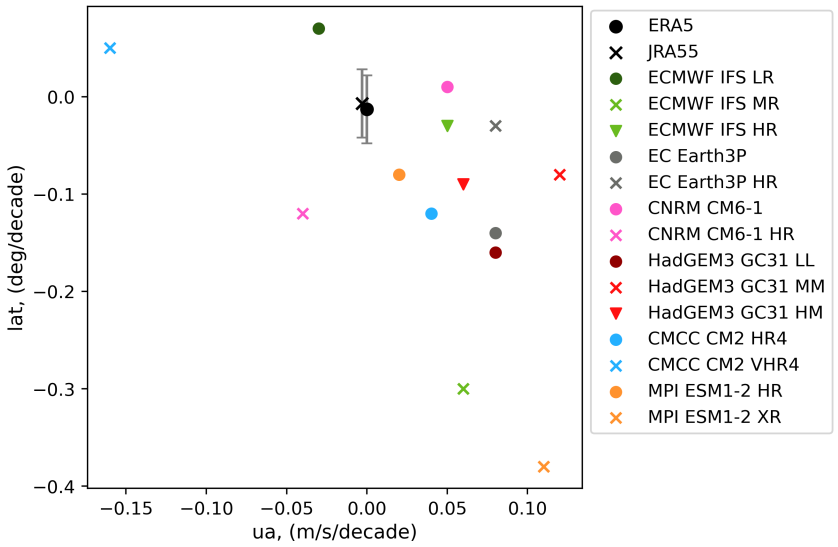

Figure 4.8: 1979-2014 trends in annual mean jet strength against linear trends in annual mean jet stream position.

CMCC-CM2 VHR) and the other two models simulate too negative trend in westerly jet position compared to reanalyses (ECMWF-IFS MM and MPI-ESM XR). The models generally produce strengthening of the zonal wind throughout 1979-2014: with the higher trend in zonal wind speed models show a stronger poleward shift of the jet stream which is a response to increased warming. Two models produce slight weakening of the jet stream and one model with the highest mean state (CMCC-CM2 VHR) simulates the most negative trends in the westerly jet strength. To check if there is any response of SST to jet stream on a long-term scale we examine the relationship between the linear trend in the annual mean SST and jet strength (not shown). We do not find a strong link between both variables which might be due to seasonal variability of trends disguised in the annual mean trend.

To examine the ocean response to momentum transfer from the westerly winds we analyze the zonally averaged zonal component of surface ocean currents (Figure 4.9). The models compare well with GREP both in the total Antarctic and in the different ocean basins. This is attributed to the fact that all models and GREP share the same ocean model NEMO. On contrary, MPI-ESM has distinct from other models profile north of 58°S for the Antarctic-averaged zonal current while it has similar velocity close to the sea ice edge and under sea ice. The models generally capture the position of ACC and simulate slightly weaker easterly current and stronger coastal westerly current in comparison to reanalysis. For the Antarctic-wide profile, the annual mean position of ACC is diverse across the models, ranging between ∼42°S for CNRM HR to ∼56°S for CMCC-CM2. The Atlantic sector has two peaks: the first is attributed to the northern flank of the Weddell Gyre (∼56°S) and the second is the ACC (∼48°S). In the Indian sector, the maximum

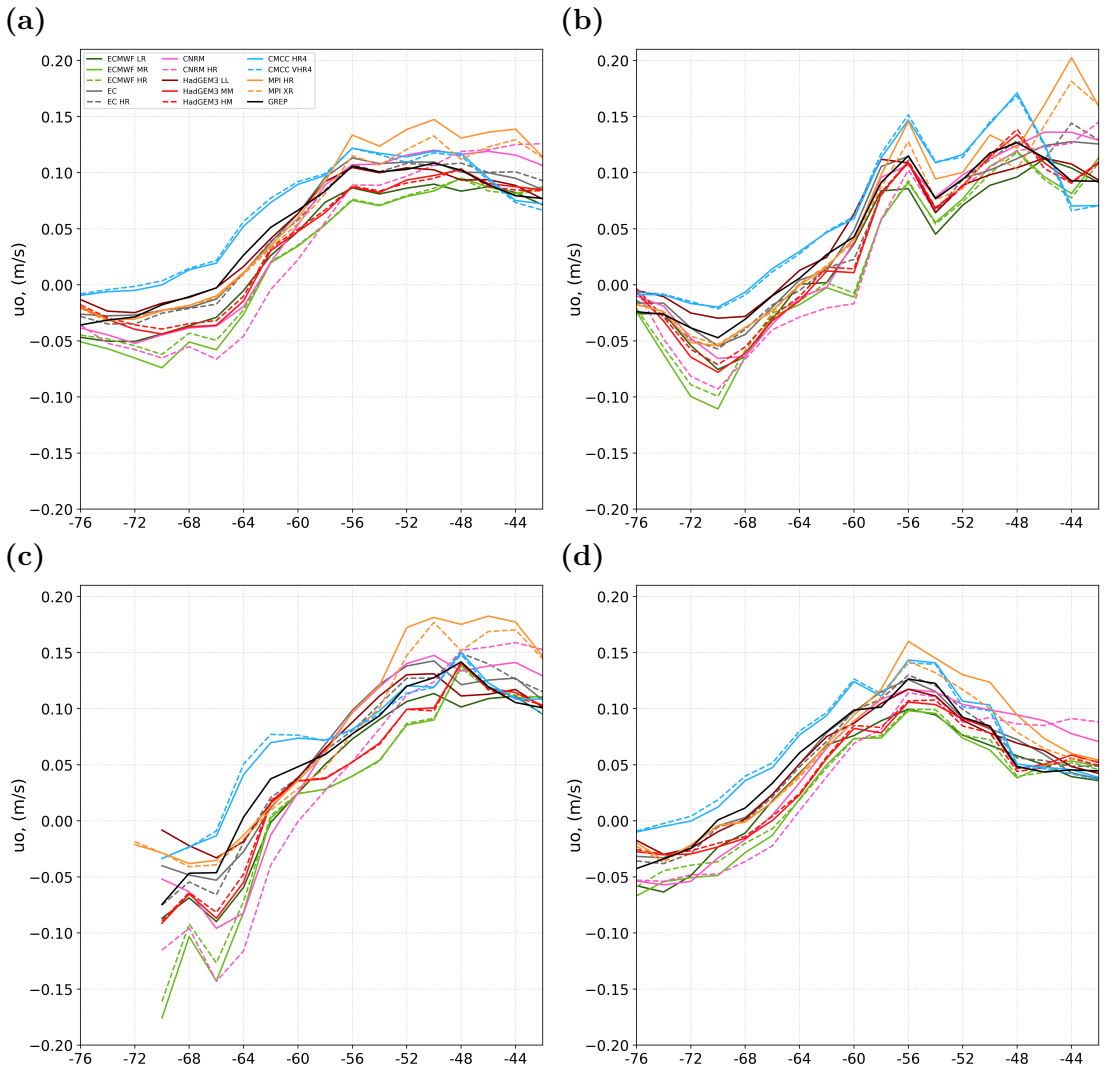

Figure 4.9: The annual mean zonal component of surface ocean currents for the period 1993-2014 as a function of latitude for the total Antarctic (a), Atlantic (b), Indian (c) and Pacific (d) sectors.

of the ocean current is located at ∼48°S while in the Pacific sector, the latitude of ACC is ∼56°S. There is a high inter-model spread on the westerly coastal currents along the Antarctic continent. The strongest coastal currents are produced by ECMWF-IFS and CNRM model configurations, particularly in the Atlantic basin. CMCC-CM2, on the contrary, underestimates westerly current and simulates stronger easterlies in response to strengthened zonal wind. Notably, the ACC strength in CMCC-CM2 configurations is well represented in the Indian Ocean basin while in the rest of the sectors, the model has a higher zonal current speed at its maximum.

To illustrate the spatial pattern of the zonal current component we show the climatology of the zonal surface current in the Atlantic sector in February (Figure 4.10). All models regardless of the horizontal resolutions are able to capture the general pattern of the zonal current with strong easterly ACC and coastal westerlies. Nevertheless, the use of 0.25° ocean resolution indeed allows to generate the eddies and provides a more

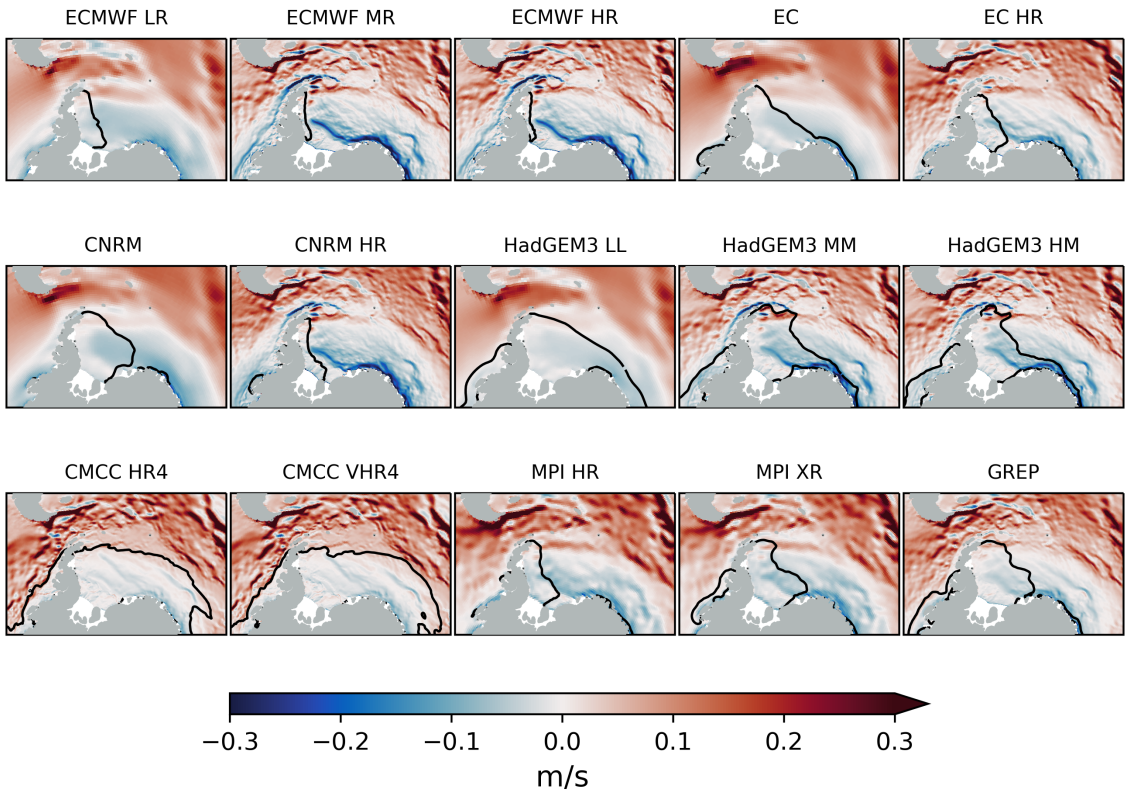

Figure 4.10: Climatological mean zonal component of surface currents in the Atlantic sector in February, averaged over 1993-2014. Sea ice edge position (15% SIC) is shown by black line.

realistic surface currents representation. From the plot, it is clear that for some models strengthened coastal current pushes sea ice towards the Antarctic Peninsula which results in too low SIA in the eastern Weddell Sea (ECMWF-IFS MM and HM, CNRM HR). In the case of HadGEM3, which on average grows thick ice, the sea ice edge does not respond to the ocean forcing as much as in the other models with thin ice since the thick ice is not so easily moved by currents. CMCC-CM2 configurations and HadGEM3 LL have slower coastal currents, which together with strengthened westerly zonal wind prevent the ice edge to move towards the Antarctic Peninsula. The thick mean state of sea ice in CMCC-CM2 also enhances multi-year ice persistence in the Weddell Sea during the melting season.

4.3.5 Discussion

The Antarctic is a region of interest due to the baffling behaviour of sea ice cover in recent years (e.g. Hobbs et al., 2016; Eayrs et al., 2019; Turner et al., 2022). The historical representation of the Antarctic sea ice cover in the coupled climate models is important for the plausible simulation of fluxes at the interface between the ocean and the atmosphere, which influences climate dynamics. The reasonable simulation of Antarctic sea ice is also critical for the model's response to radiative forcing and accurate predictions of future

conditions in the Southern Ocean which plays a major role in storing anthropogenic heat and carbon (Tjiputra et al., 2010). Thus, it is important to systematically evaluate simulated Antarctic sea ice in order to better understand mean state bias with respect to historical observations. The simulation of the mean state and time evolution of sea ice in coupled climate models is particularly challenging due to the complex nature of the Southern Ocean. The realism of simulated sea ice cover is highly sensitive to biases in individual model components. Errors in sea ice representation can be attributed to errors in thermohaline structure, surface winds, water mass properties, and radiative forcing. On the other hand, the atmosphere and ocean features are largely impacted by sea ice representation. To demonstrate the effects of sea ice on the upper ocean we show Figure 4.11 which represents how the models are different on salinity anomalies originating from sea ice in the eastern part of the Weddell Sea. It is clear that many models overestimate the northward propagation of salinity anomalies which has an effect on the upper ocean structure of the mid-latitudes. The errors in freshwater input and in brine release during sea ice melt and sea ice formation translate into biases in the upper ocean conditions and water mass formation in the model simulations.

In this study, we find that three models appear to be performing best in the mean state representation of sea ice characteristics (EC-Earth3P, HadGEM3 MM and HM, both configurations of CMCC-CM2). Given that the large-scale circulation controls dynamic and thermodynamic processes in the Antarctic (Purich et al., 2016), we first investigated the model performance in the jet stream representation. All models but one exhibit equatorward bias in the jet stream position. The CMCC-CM2 configurations show a strengthened westerly jet with poleward bias. This distinctive representation of zonal

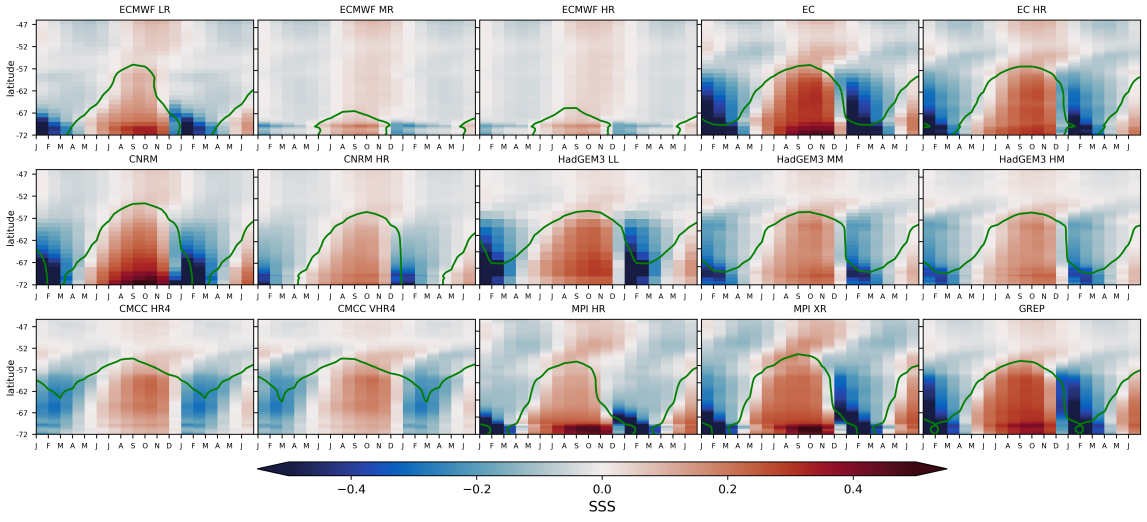

Figure 4.11: Zonally averaged (from 20°W to 20°E) surface salinity anomalies plotted as a function of time for all models and GREP, averaged over 1979-2014. The green line defines the location of the ice edge.

wind in CMCC-CM2 model might contribute to plausible SIA simulation: strong zonal wind drives strengthened Ekman transport and upwelled at high latitudes cold waters propagate equatorward which results in higher SIA in summer when almost all models lack sea ice. In addition, from the ocean side, weak coastal currents in CMCC-CM2 promote sea ice to sustain in summer over the great part of the Weddell Sea by not pushing the ice floes towards the Antarctic Peninsula. Coupled ocean-atmosphere dynamics contributes to the increased summer sea ice cover in CMCC-CM2 model. In winter, the strong zonal wind might also be beneficial for SIA simulation since intensified Antarctic Circumpolar Current driven by jet stream hamper sea ice expansion. However, other models with a fairly good mean sea ice state have similar jet stream characteristics as the models with poor sea ice representation. This suggests that the reasonable sea ice mean state in model simulations can be a result of compensating biases (Holmes et al., 2019).

We find that only one model configuration is able to capture a positive SIA trend over the satellite era (CMCC-CM2 VHR) while other models simulate a decline in sea ice cover. We also find that the models with stronger upper-ocean warming have more negative trends in SIA while CMCC-CM2 VHR has close to zero SST trend. We test a hypothesis that changes in the jet stream drive SST trend and thus affect the realism of SIA trends in the model simulations. We show that a major part of the models produces a strengthening of the jet stream over the years 1979-2014. On the long-term scale, stronger zonal wind leads to increased upwelling of Circumpolar Deep Water and consequently to sea ice loss (Newsom et al., 2016). Our results do not provide evidence of SST response to changes in the jet stream characteristics. However, for some models, the strengthened jet might affect SST and contribute to the inability of the models to produce positive trends in SIA over the historical period. On the other hand, the equatorward shift in the jet stream, vice versa, might be caused by sea ice loss (Screen et al., 2022). We suggest that other reasons can be responsible for disagreement on historical trends in SIA between observations and models, including high climate sensitivity (Zelinka et al., 2020), internal climate variability (Polvani and Smith, 2013), and model biases (Schroeter et al., 2017; Schroeter and Sandery, 2022; Roach et al., 2018, 2020; Sun and Eisenman, 2021).

This study investigates the added value of increased model horizontal resolution in the representation of Antarctic sea ice using historical simulations of six coupled climate models participating in HighResMIP. Our results do not show the systematic effect of the increased ocean/atmosphere resolution on the realism of simulated Antarctic sea ice cover over the satellite era. The representation of the mean state and long-term variability of Antarctic SIA and SIV is rather model-dependent. However, there is evidence of a weak positive effect of increased ocean resolution from 1° to 0.25° such as reduced bias in winter SIA and less negative trends in annual mean SIA and SIV. This reflects a major role of ocean resolution affecting simulated sea ice, which is also confirmed by other studies

focused on the Arctic sea ice (e.g. Grist et al., 2018; Roberts et al., 2018; Docquier et al., 2019). A great constraint for high-resolution global simulations is the requirement of large computer resources. Our study suggests that a few minor improvements in sea ice representation with enhanced horizontal resolution are not worth the major effort of costly computations. We assume that the focus of the modelling community should evolve firstly towards the improvement of the sea ice model physics and parameterizations. However, it can be the case that eddy-permitting configurations (0.25°) might be still not sufficient for the improvement of the Southern Ocean dynamics since the baroclinic Rossby radius in the high latitudes is on the order of kilometers. Rackow et al., 2022 showed that model simulation with a nested eddy-rich grid over ACC improves the representation of the Southern Ocean circulation and leads to more realistic historical sea ice trends. It is likely that performing simulations with variable horizontal resolution might offer a trade-off solution between computation cost and better representation of the ocean.

4.3.6 Summary and conclusions

In this study, we evaluate Antarctic sea ice simulated by coupled climate models that follow the protocol of the High Resolution Model Intercomparison Project (HighResMIP). We compare the historical simulations of six different coupled climate models (ECMWF-IFS, EC-Earth3P, CNRM, HadGEM3, CMCC-CM2, MPI-ESM) with satellite observations and reanalyses over 1979-2014. All models can adequately reproduce asymmetric seasonal cycle in SIA with slow sea ice growth and rapid sea ice retreat and properly capture the annual minimum of February and maximum of September. However, the models produce a wide inter-model spread in SIA, particularly in winter. Most models underestimate SIA in February as a result of the too warm ocean except HadGEM3 and CMCC-CM2 which instead overestimate summer SIA. The climatology of SIV in the model simulations shows less agreement with reference products compared to SIA: most of the models delay the timing of the seasonal maximum and generally have less SIV than reanalyses. The models which include sea ice model CICE (HadGEM3 and CMCC-CM2) grow too thick ice in the Weddell and the Ross Seas and retain more sea ice in the melting season which leads to high bias in SIV. All but one model cannot simulate overall SIA and SIV expansion over the satellite era and produce decreasing trends in response to the warming. We show a strong relationship between SIA and SST and with larger warming of the surface ocean the models have a stronger sea ice loss. Only CMCC-CM2 VHR simulates a weak positive trend throughout 1979-2014 which is also consistent with a little negative trend in SST. We also find the equatorward bias of the jet stream position in the mean state of most of the models with poleward shift and increases in its strength over the satellite era. Only CMCC-CM2 model configurations are in agreement with atmospheric reanalyses and exhibit poleward bias of the jet stream with close to zero

changes in its position and strength from 1979 to 2014. The model skill in the westerly jet stream representation varies with the ocean basins with the most accurate performance over the Atlantic sector and the largest equatorward shift in the Indian Ocean. We conclude that increased horizontal resolution does not improve the representation of Antarctic sea ice for most of the models: it rather depends on the model and examined variable. Our results do not provide evidence that the large-scale atmospheric circulation could explain the relatively good representation of the Antarctic sea ice mean state in a few models. We suggest that the realism of sea ice simulation rather depends on the interplay of ocean and atmosphere components in the coupled system. The detailed evaluation of ocean-atmosphere coupling in HighResMIP models we leave for further analysis.

Chapter 5

The past and future of the Arctic sea ice in HighResMIP climate models

Abstract

We examine the past and projected changes in Arctic sea ice properties in 6 climate models participating in the High Resolution Model Intercomparison Project (HighResMIP) in the Coupled Model Intercomparison Project Phase 6 (CMIP6). Within HighResMIP each of the experiments is run using a reference resolution configuration (consistent with typical CMIP6 runs) and higher resolution configurations. The role of horizontal grid resolution in both the atmosphere and ocean model components in reproducing past and future changes in the Arctic sea ice cover is analysed. Model outputs from the coupled historical (hist-1950) and future (highres-future) runs are used to describe the multi-model, multi-resolution representation of the Arctic sea ice and to evaluate the systematic differences (if any) that resolution enhancement causes. Our results indicate that there is not a strong relationship between the representation of sea ice cover and the ocean/atmosphere grid: the impact of horizontal resolution depends rather on the examined sea ice characteristic and the model used. However, the refinement of the ocean grid has a more prominent effect compared to the atmosphere: eddy-permitting ocean configurations provide more realistic representations of sea ice area and sea ice edge. All models project substantial sea ice shrinking: the Arctic loses nearly 95% of sea ice volume from 1950 to 2050. The model selection based on historical performance potentially improves the accuracy of the model projections and predicts the Arctic to turn ice-free as early as in 2047. Along with the overall sea ice loss, changes in the spatial structure of the total sea ice and its partition in ice classes are noticed: the marginal ice zone (MIZ) dominates the ice cover by 2050 suggesting a shift to a new sea ice regime much closer to the current Antarctic sea ice conditions. The MIZ-dominated Arctic might drive developments and modifications of model physics and parameterizations in the new generation of GCMs.

5.1 Introduction

Sea ice is the key feature of high-latitude climate through its role in the surface energy budget, ocean and atmosphere dynamics, and marine ecosystems. Over the recent decades, the Arctic has witnessed unprecedented sea ice loss, which is a key indicator of global climate change (e.g. Onarheim et al., 2018; Serreze and Meier, 2019), driven

both by anthropogenic activities and internal climate variability (e.g. Notz and Stroeve, 2016). Arctic sea ice has declined in every month of the year with the strongest trends in September, a sea ice extent (SIE) reduction of 79000 km^2yr^{-1} in the period 1979-2022, and in March, with -39200 km^2yr^{-1} over 1979-2022 (http://nsidc.org/arcticseaicenews/2022/). The overall decrease in SIE reveals large seasonal and regional variability. Although winter sea ice loss is dominated by the reduction in the Barents Sea (Árthun et al., 2021), the most pronounced summer sea ice decrease occurs in the East Siberian Sea (that explains more than 20% of the September trend, (Watts et al., 2021) and in the Beaufort, Chukchi, Laptev and Kara seas (Onarheim et al., 2018). Along with a severe reduction in sea ice coverage, Arctic sea ice has also thinned, with a ∼70% reduction in summer sea ice volume (SIV) over 1979-2021 (https://nsidc.org/). As a consequence, the Arctic ice is getting younger: the portion of the multi-year ice, which previously was the iconic feature of the Arctic, has decreased from ∼30% in 1985 (beginning of the satellite era) to ∼4.4% in 2020 in winter months (Perovich et al., 2020). The Arctic transition toward a first-year ice regime might substantially alter the interactions in the ocean-atmosphere-ice system (Aksenov et al., 2017). The changes in total SIE and sea ice thickness (SIT) cause redistribution of the sea ice classes, in particular the marginal ice zone (MIZ) is strongly affected (Rolph et al., 2020). The Arctic MIZ has held interest as the fundamental region supporting many physical, biological and biogeochemical processes (Tápias et al., 2021). The MIZ is traditionally defined as the region where polar air, ice, and water masses interact with the ocean temperature and subpolar climate system (Wadhams and Deacon, 1981). It corresponds to the portion of the ice-covered ocean often characterised by highly variable ice conditions, where surface gravity waves significantly impact the dynamics of sea ice (e.g. Dumont et al., 2011). Due to the large uncertainties in observed and forecasted waves within sea ice, the MIZ is still operationally defined through a sea ice concentration (SIC) thresholds, as the transition zone between open water and consolidated pack ice, where the total area of ocean is covered by 15-80% of sea ice (e.g. Strong et al., 2017; Paul et al., 2021; Rolph et al., 2020). While there are no significant changes in the area of the Arctic MIZ during the satellite era (Rolph et al., 2020), the marginal ice zone fraction (MIZF) defined as the percentage of total sea ice area (SIA) covered by MIZ (Horvat, 2021) increases by more than 50% in August and September as the total SIA drastically decreases (Rolph et al., 2020; Horvat, 2021). Since the MIZ differs from the pack ice in higher sensitivity to the dynamic and thermodynamic forces, the growing MIZF changes the Arctic response to warming, which may worsen the pace of sea ice melt and pose repercussions for local and global climate.

Assuming that the Arctic Ocean will continue to lose sea ice, a relevant question is how fast the Arctic will turn ice-free in summer. Coupled climate models can be used in the prediction and projection of the climate system, including the sea ice conditions. In

the majority of simulations from CMIP6 (Eyring et al., 2016), the Arctic Ocean becomes practically sea ice free (SIA $<$ 1 million km^2) in September for the first time before 2050 in all scenarios (Notz and Community, 2020) or even by 2035 when selecting only the models that best represent the present Arctic sea ice state and northward ocean heat transport (Docquier and Koenigk, 2021). Besides, the accurate simulation of past and present Arctic sea ice is still challenging. Although the CMIP6 multi-model ensemble mean is closer to the observed sensitivity of Arctic sea ice to global warming (Notz and Community, 2020; Shu et al., 2020), there is little difference in overall model performance among CMIP3, CMIP5 and CMIP6. CMIP6 models still simulate a wide spread of mean sea ice area and volume in March and September (Davy and Outten, 2020; Notz and Community, 2020; Watts et al., 2021). Among the model developments and improvements needed to produce more accurate future projections, the increase in horizontal spatial resolution is recognized to be a key step to enhance the representation of the complex processes at high latitudes and to obtain trustworthy projections of ice variability. In order to address the impact of the model grid resolution on the simulated oceanic and atmospheric phenomena, the High Resolution Model Intercomparison Project (HighResMIP; Haarsma et al., 2016) was designed within the EU Horizon 2020 PRIMAVERA project (PRocess-based climate sIMulation: AdVances in high-resolution modelling and European climate Risk Assessment, https://www.primavera-h2020.eu/). HighResMIP is one of the CMIP6-endorsed model intercomparison projects, which provides a useful framework to investigate the role of the enhanced horizontal resolution in representing the features of the climate system. A number of climate modelling groups contributed to the project providing the same simulations in at least two different configurations. The impact of the increased resolution within the HighResMIP is examined in many studies with regard to atmosphere, sea ice, and ocean components of the climate systems Fuentes-Franco and Koenigk, 2019; Docquier et al., 2019; Bador et al., 2020; Roberts et al., 2020; Jackson et al., 2020; Lohmann et al., 2021; Meccia et al., 2021). Despite the fact that high-resolution models can resolve specific dynamical features, the role of the enhanced horizontal resolution is not uniform across ocean regions and models. Grist et al. (2018) demonstrated that refining the ocean grid to eddy-permitting resolution raises the Atlantic meridional heat transport and improves the agreement with observational estimates - they also show the significantly smaller impact of atmosphere resolution on the strength of the heat transport. Docquier et al. (2019) confirmed this finding and showed that a better representation of Atlantic surface characteristics, velocity fields, and sea surface temperature (in addition to transports toward the Arctic) improves the representation of the Arctic SIA and SIV. Nevertheless, the role of ocean resolution in the representation of ocean heat transport (OHT) and SIA is less clear when considering the regional effect on specific Arctic sectors, as shown for the Barents Sea in Docquier et al. (2020). Here, we focus on the impact of horizontal resolution on

the Arctic sea ice properties in the past and future at hemispheric and regional scales using the model outputs from coupled historical (hist-1950) and future (highres-future) runs from HighResMIP. We assess seasonal and interannual variability and trends in the SIA and SIV, and examine when the Arctic will see its first ice-free summer. We aim to explore the role of enhanced ocean/atmosphere horizontal resolution in the representation of past and current sea ice and to provide some insight into whether the grid refinement improves the model performance in predicting future Arctic sea ice conditions.

5.2 Data

In this study, we analyse the outputs from the six coupled climate models participating in the HighResMIP. We use coupled runs with historical forcing (hist-1950) covering the period 1950-2014 and future projections (highres-future) from 2015 to 2050 based on the Fossil-fueled development SSP5 scenario. For the past sea ice properties, we mainly focus on the time period from 1979 to compare model results with available satellite records. For the ocean, five models use the Nucleus for European Modelling of the Ocean framework (NEMO, Madec et al., 2016), yet different versions, whereas MPI-ESM is based on the Max Planck Institute Ocean Model (MPIOM, Jungclaus et al., 2013). The basic characteristics of the models are given in Table 5.1. Because each of the models uses at least two different resolutions, we evaluate 14 configurations in total. CMCC-CM2 and MPI-ESM use one ocean (eddy-permitting) resolution with two different atmospheric grids. ECMWF-IFS and EC-Earth3P run two of three configurations with an eddy-permitting ocean and different atmosphere resolutions. In other models, ocean and atmosphere resolutions vary in concert among configurations. Note that ECMWF-IFS and HadGEM3 provide several ensemble members, however we use only the first ensemble member in this study; ECMWF-IFS is not considered in the analysis of future projections since it does not provide the outputs from highres-future experiments.

The simulated SIA is validated against satellite observations. We use monthly SIC from two satellite-based products: the NOAA/NSIDC Climate Data Record (version 4, Meier et al., 2021, hereafter CDR) and EUMETSAT OSISAF Climate Data Record and Interim Climate Data Record (release 2, products OSI-450 and OSI-430-b, Lavergne et al., 2019) both for the period 1979-2021. CDR uses gridded brightness temperatures in low frequencies from the Nimbus-7 SMMR (18, 37 GHz) and the DMSP series of SSM/I and SSMIS passive microwave radiometers (19.4, 22.2, 37 GHz). Different ratios of frequencies are used to filter weather effects. The output data are distributed on a 25 km x 25 km polar stereographic grid. CDR algorithm blends the NASA Team (NT; Cavalieri et al., 1984) and the Bootstrap (BT; Comiso, 1986) by selecting the higher concentration value for each grid cell, so taking advantage of the strengths of each algorithm to produce concentration

Table 5.1: The model configurations used in the study.

Model configuration		nominal ocean res. (°)	nominal atm. res. (km)	model components	
				ocean-sea ice	atmosphere
CMCC-CM2 (Cherchi et al., 2019)	HR	0.25	100	NEMO3.6 +CICE4.0	CAM4
	VHR	0.25	25		
CNRM-CM6-1 (Voldoire et al., 2019)	LR	1	250	NEMO3.6 +GELATO6	ARPEGE6.3
	HR	0.25	100		
ECMWF-IFS (Roberts et al., 2018)	LR	1	50	NEMO3.4 +LIM2	IFS cycle43r1
	MR	0.25	50		
	HR	0.25	25		
EC-Earth3P (Haarsma et al., 2020)	LR	1	100	NEMO3.6 +LIM3	IFS cycle36r1
	HR	0.25	50		
HadGEM3 (Williams et al., 2018)	LM	1	250	NEMO3.6 +CICE5.1	UM
	MM	0.25	100		
	HM	0.25	50		
MPI-ESM (Müller et al., 2018)	HR	0.4	100	MPIOM1.6.3	ECHAM6.3
	XR	0.4	50		

fields that are more accurate than those from either algorithm alone (Meier et al., 2014). OSISAF comprises two SIC products based on passive microwave sensors: OSI-450 (from 1979 to 2015) and OSI-430-b, extension from 2016 onwards. OSI-450 uses data from the SMMR 1979-1987), SSM/I (1987-2008), SSMIS (2006-2015) instruments (19.35 and 37 GHz frequencies) together with Era Interim reanalysis (**?**), while OSI-430-b is based on SSMIS and operational analysis and forecast from ECMWF. We use estimates of SIT and SIV from the Pan-Arctic Ice Ocean Modeling and Assimilation System (PIOMAS; Zhang and Rothrock, 2003) that comprises the global Parallel Ocean and sea Ice Model (POIM) coupled to eight-category thickness and enthalpy distribution sea ice model and a data assimilation of SST (from NCEP/NCAR reanalysis, Kalnay et al., 1996) and SIC (from the NSIDC near-real time product; Brodzik and Stewart, 2016). PIOMAS proved its credibility against in-situ measurements (Stroeve et al., 2014; Wang et al., 2016) and therefore it is widely used in numerous intercomparison studies as the observational proxy (e.g. Labe et al., 2018). Note that PIOMAS tends to underestimate the thick ice North to Greenland and the Canadian Arctic Archipelago and underestimate SIT in the areas of thin ice (Stroeve et al., 2014; Wang et al., 2016). Monthly fields of SIC and effective SIT from 1979 to 2021 are used in this work. We describe sea ice coverage in terms of SIA (the integral sum of the product of ocean grid-cell areas and the corresponding sea ice concentration), instead of SIE (the integral sum of the areas of all grid cells with at least 15% of SIC). To compute SIV, the equivalent SIT (the sea ice volume per grid-cell area) is multiplied by the individual grid-cell area, and then summed over the Arctic region. To derive integrative metrics, only the grid cells with at least 15% SIC are considered owing to the high uncertainty in passive microwave retrievals in low sea ice conditions. Apart from model evaluation at the hemispheric scale, we provide a regional analysis of sea ice

variability in six subregions of the Arctic Ocean as defined in Figure 5.1.

Figure 5.1: Map of sub-regions used in the regional analysis: Central Arctic Basin (CA), Barents and Kara Seas (B-K), Laptev Sea (LV), East Siberian Sea (ESS), Beaufort and Chukchi Seas (B-C), Canadian Arctic Archipelago and Greenland coast (GD).

5.3 Results

5.3.1 Mean state

First, we assess the spatial patterns of simulated ice properties against observational-based estimates over the historical period restricted from 1979 to 2014. Figure 5.2 shows the climatological mean distribution of SIT in March and September for model outputs and PIOMAS. The mean position of 15% and 80% SIC edges is also shown from each model and CDR (over PIOMAS). In general, most models struggle to reasonably simulate the spatial pattern of SIT and produce either thicker (ECMWF-IFS, EC-Earth3P, CMCC-CM2 VHR4) or thinner (CNRM-CM6, MPI-ESM) ice over a vast area compared to PIOMAS. Some models are able to correctly locate the thickest ice north of Greenland and the Canadian Arctic Archipelago and the thinner ice in the Siberian Shelf Seas (HadGEM3, CMCC-CM2 HR4), but the simulated ice can thicken up to 7 m. EC-Earth3P HR and ECMWF-IFS MR, despite capturing the overall SIT pattern, simulate high thickness also in the East Siberian and Chukchi Seas, which is clearly visible in March. This might be related to unrealistic sea ice drift. As in PIOMAS, most models reproduce changes in the SIT between March and September with a more pronounced

seasonal retreat in the Siberian sector. There is no direct effect of horizontal resolution on the spatial distribution of SIT. Increasing ocean resolution, the mean SIT decreases for ECMWF-IFS, does not change significantly for HadGEM3 and CNRM-CM6, and increases for EC-Earth3P. The role of atmosphere resolution also depends on the model: for example, the finer atmosphere resolution MPI-ESM reproduces on average slightly thinner ice compared to LR configuration, while the finer CMCC-CM2 simulates thicker ice over a larger area. Biases in the representation of SIT pattern can be related to poor representation in surface pressure and large-scale atmospheric patterns (Kwok and Untersteiner, 2011; Stroeve et al., 2014), sea ice motion and ocean forcing (Watts et al., 2021).

Most models tend to realistically simulate the position of the sea ice edge both in March and September. Configurations with finer ocean resolution have a better fit to CDR in the location of the 15% SIC ice edges. The LR configurations of ECMWF-IFS and HadGEM3 tend to overestimate the sea ice cover far south in the North Atlantic and the North Pacific Oceans compared to CDR. The bias can be explained by the poor representation of the ocean advection. In fact, Docquier et al. (2019) showed that the northward OHT is improved when ocean resolution increases from 1° to 0.25°, both across the Bering Strait (83 km wide) and through the Nordic Seas establishing the Atlantic warm inflow into the Arctic Ocean. Similarly as for SIT, the effect of the atmospheric grid resolution on the sea ice extent is model dependent. When it is enhanced, there are no notable changes in the location of the March ice edge in the ECMWF-IFS and HadGEM3 models, while it is largely overestimated in CMCC-CM2 and MPI-ESM, particularly in the Nordic Seas. Specifically, CMCC-CM2 HR4 underestimates March sea ice coverage in the northern Barents Sea, the Bering Sea, and the Sea of Okhotsk, whereas the VHR4 version (with finer atmospheric grid) reproduces a reasonable amount of winter ice in marginal seas. In September, higher atmosphere resolution leads to a larger SIA in ECMWF-IFS and CMCC-CM2, conversely, it has an opposite effect in HadGEM3 and MPI-ESM models. In Addition, MPI-ESM XR does significantly melt sea ice in the Siberian seas which are almost ice-free in summer. The width of the MIZ (marked in Figure 5.2 by the area capped between 15% and 80% SIC contours) also varies among different models. In many of them, March MIZ similarly surrounds the inner ice pack, comparing well with CDR. In September, most models fairly simulate an extension of MIZ comparable to the observed one. Exceptions are MPI-ESM runs that lose all consolidated pack ice in summer and ECMWF LR that tends to overestimate the total and pack ice, with a small portion covered by marginal ice in the Barents Sea and Nordic Seas.

5.3.2 Seasonal variability

Figure 5.3 shows the mean seasonal cycle of the total Arctic SIA and SIV, computed over the 1979-2014 period. Satellite estimates from both OSISAF and CDR are included

(a)

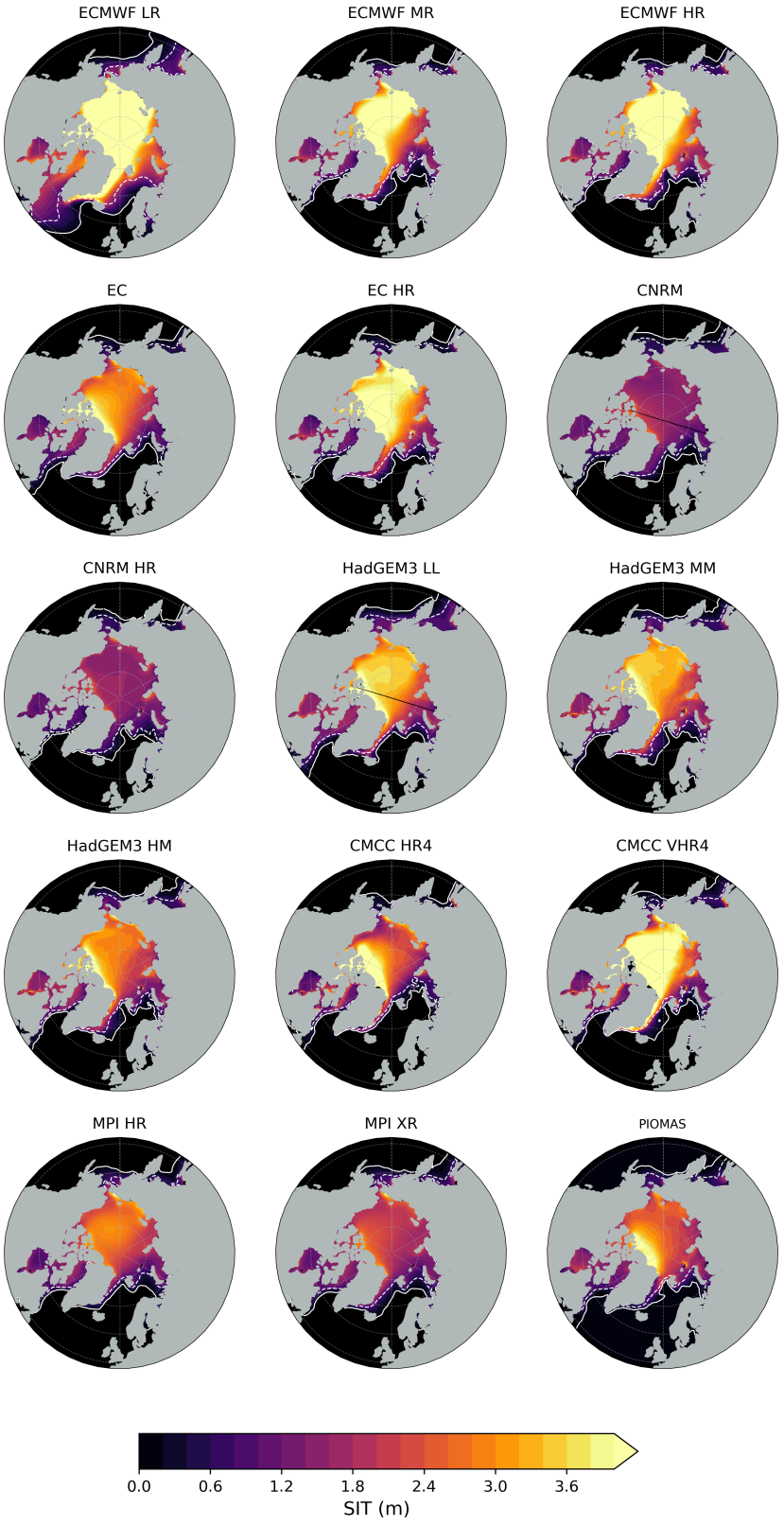
ECMWF LR
ECMWF MR
ECMWF HR
EC
EC HR
CNRM
CNRM HR
HadGEM3 LL
HadGEM3 MM
HadGEM3 HM
CMCC HR4
CMCC VHR4
MPI HR
MPI XR
PIOMAS
0.0
0.6
1.2
1.8
2.4
3.0
3.6
SIT (m)

(b)

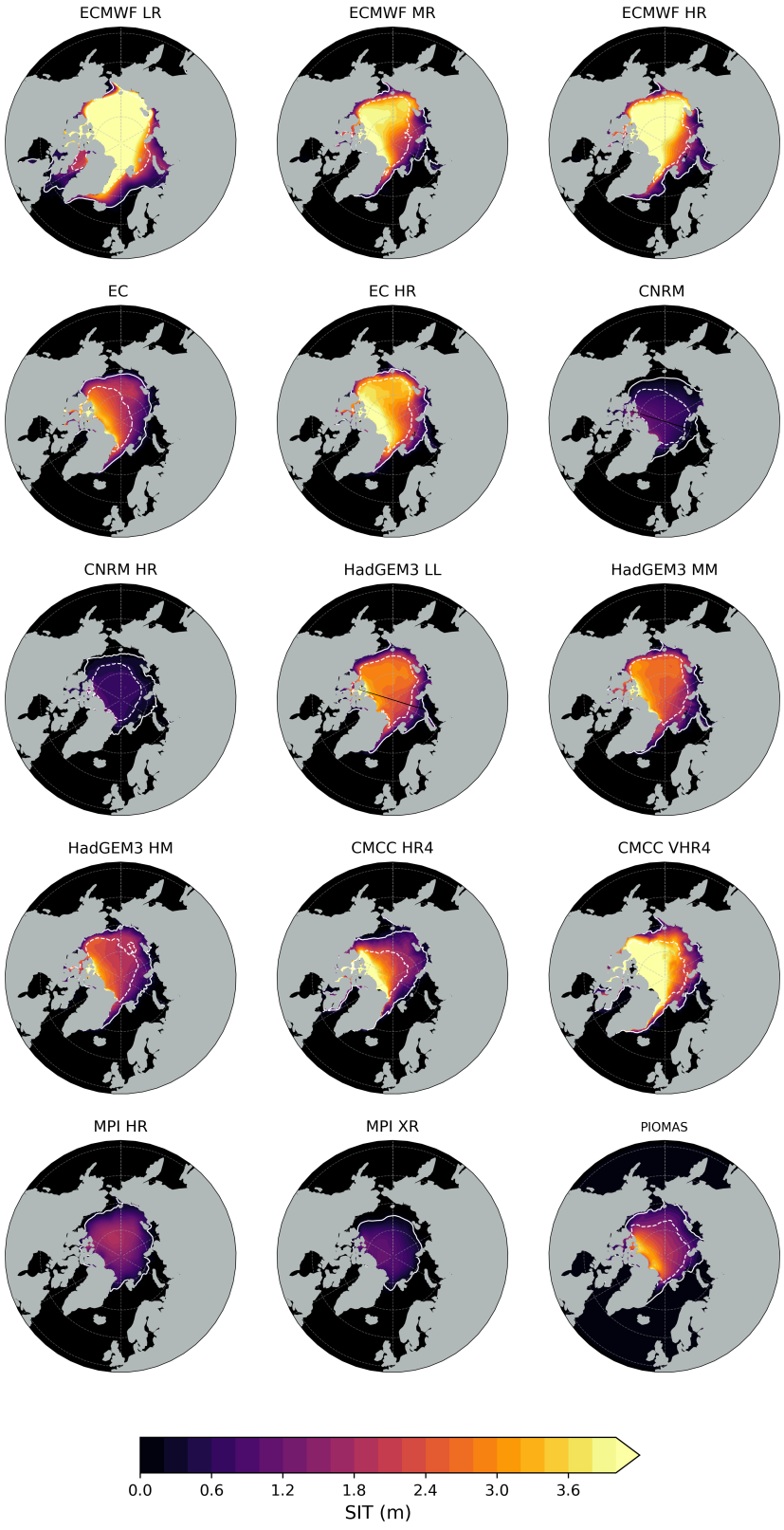

Figure 5.2: The 1979-2014 climatological mean sea-ice thickness from the model outputs and PIOMAS in March (a) and September (b). White contours show the edges of 15% (solid) and 80% (dashed) sea-ice concentration from each model. SIC from NSIDC CDR is used for PIOMAS.

to validate the models' outputs. The CDR Arctic ice area expands to its maximum in March, with coverage of nearly 14x10^6 km^2, and returns to its minimum in September at around 6x10^6 km^2. Similar seasonality is displayed by the OSISAF dataset, which has just a slightly smaller SIA in all months. As in CMIP5 and CMIP6 low-resolution models (Shu et al., 2020; Notz and Community, 2020), most HighResMIP models adequately reproduce the mean seasonal cycle of SIA with the melt season starting in March, and lasting until September where a minimum is reached (Figure 5.3a).

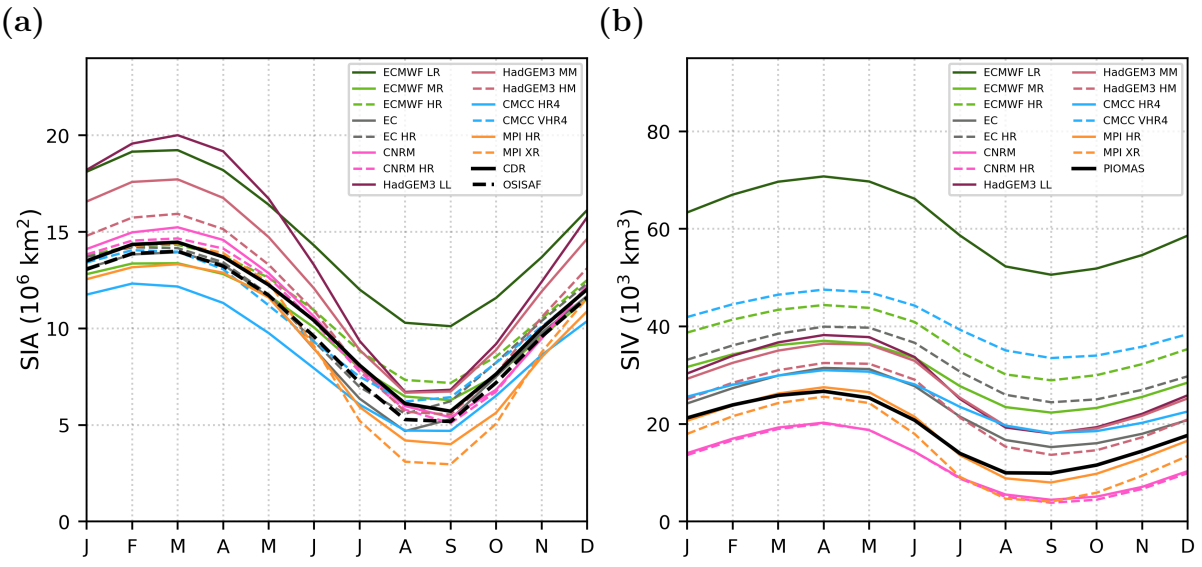

Figure 5.3: The 1979-2014 seasonal cycle in SIA (a) and SIV (b) from HighResMIP hist-1950 model outputs.

There is a considerable spread among models, it is relatively larger in winter than in summer. March SIA ranges from 12 to 20x10^6 km^2, while September values in all but one model lie in the range between 3 and 7.5x10^6 km^2. The ECMWF-ISF LR overestimates the Arctic SIA all year round, but it can properly represent the amplitude of SIA seasonal variability and hence correctly reproduces the ice advance and retreat phases. The comparison between the model configurations indicates that finer resolution generally results in simulated SIA closer to satellite products. The effect of the changing atmosphere resolution varies among models, though. For instance, the CMCC-CM2 HR constantly stays in the lower bound of the model ensemble and reproduces a weaker amplitude of the seasonal cycle compared to observations; applying the atmospheric grid refinement (CMCC-CM2 VHR4 configuration) favourably increases sea ice coverage and does not significantly change the seasonal cycle amplitude. A different impact is for the MPI-ESM model, for which the finer atmospheric grid improves the winter SIA but increases the spring/summer melting and underestimates the September minimum by ∼50% compared to observations. In general, in other HighResMIP runs, the atmosphere grid refinement gives smaller changes to Arctic sea ice coverage compared to the ocean resolution enhancement. In the ECMWF-IFS, the LR shows a constant SIA overestimation, that is largely

resolved in the model configuration with an eddy-permitting ocean (HR) whose Arctic SIA is in good agreement with observations, particularly in summer. As for the CMCC-CM2 model, a further refinement in the atmosphere resolution increases the SIA in the whole year with the best agreement with observations from October to July. The HadGEM3 runs are relatively close to observations in summer but they tend to overestimate the sea ice growth - the impact of increased ocean and atmosphere resolution is evident for this model with a strong reduction of winter sea ice of ∼25% from LL to HM and a smaller but still remarkable contraction in summer. Here, the increase in the atmosphere resolution further reduces SIA in contrast to previous models. Finally, EC-Earth3P and CNRM-CM6 models show negligible differences between model configurations, despite ocean and atmosphere grid resolution.

In our reference PIOMAS product, the Arctic SIV ranges from ∼25x10^3 km^3 at its peak in April, to ∼10x10^3 km^3 at its minimum in August/September (Figure 3b). All models capture the timing of the SIV maximum in April/May and the minimum in August/September with a realistic seasonal cycle amplitude that ranges between 15 and 20x10^3 km^3. However, there is a large spread among different models, with most models overestimating PIOMAS - ECMWF-ISF LR is a clear "outlier" exceeding 70x10^3 km^3 in April and 50x10^3 km^3 in September. Although in some models the bias in SIA is seasonally dependent with larger errors in winter, bias in simulated SIV is consistent throughout the year in all models. In general, the large SIV is mainly due to poorly simulated SIT rather than incorrect sea ice cover (Figure 5.2, 5.3a). Only in ECMWF-IFS LR, the combination of large ice expansion and extremely thick ice leads to unrealistically high SIV. The SIV overestimation in the CMCC-CM2 and EC-Earth3P models is caused by too thick sea ice, even though their SIA is well compared well with observations. Only one model (both configurations of CNRM-CM6) has thin ice and hence low bias in SIV compared to PIOMAS, all year round. The changes in resolution have no visible impact in the CNRM-CM6 runs. The increase of only ocean resolution largely improves the representation of SIV (as for SIA) in ECMWF-IFS with a large volume reduction, but does not affect the volume seasonality in HadGEM3. Finer atmosphere resolution or the combined resolution increase in both model components tends to increase the ice volume except in HadGEM3 and MPI-ESM. MPI-ESM has a good fit to PIOMAS for SIV although this model underestimates SIA and cannot simulate consolidated pack ice (SIC $>$ 80%, Figure 5.2).

In addition to the total SIA, we show the seasonal variability of the area covered by marginal ice, over the same 1979-2014 period (Figure 5.4a). First, it is worth noting the evaluation of the simulated MIZ area is highly dependent on the reference product used. The difference between CDR and OSISAF in the estimates of MIZ area. This can be mainly ascribed to the treatment of the wet surface (e.g. melt ponds, snow wetness) that

poses difficulty to retrieve the SIC using passive microwave radiometers (Ivanova et al., 2015). OSISAF has a small portion of MIZ in winter, while it overestimates CDR from May to November. The maximum difference between the two products is up to nearly $1.1x^6$ km^2 in July. The observed MIZ seasonal variability contrasts with the one shown by total ice area: the MIZ expands in spring, when the consolidated pack ice starts to melt, which leads to the MIZ area peak occurring in summer. After reaching its maximum in July, the marginal ice starts to melt and its area decreases until September, simultaneously with the total and consolidated pack ice cover. Before the next year's melt season, the MIZ stays relatively stable but with a secondary peak in October. Models are overall able to simulate the seasonal cycle, reasonably capturing the phases of the MIZ expansion and retreat. However, they tend to overestimate the MIZ in winter, but most of them are within the observational uncertainty lying between the OSISAF and CDR summer estimates. However, models struggle to properly simulate the timing and magnitude of the MIZ maximum ECMWF-IFS LR is higher than observations from November to May due to a large overestimation of the total ice area, but it lies between CDR and OSISAF in the rest of the year. The ECMWF-IFS finer resolution configurations are in much better agreement with observed values. In the HadGEM3 LL, the marginal ice expansion starts earlier, with a large bias of the MIZ area from March to June. The resolution has no visible impact for the rest of the year. The impact of changes in the ocean and atmosphere resolution is small for other models. Both MPI-ESM configurations fail to reproduce the MIZ seasonal cycle, from June to November. This is confirmed in Figure 5.2, which reflects SIC underestimation within the consolidated pack ice, resulting in the MIZ predominance in the MPI-ESM runs.

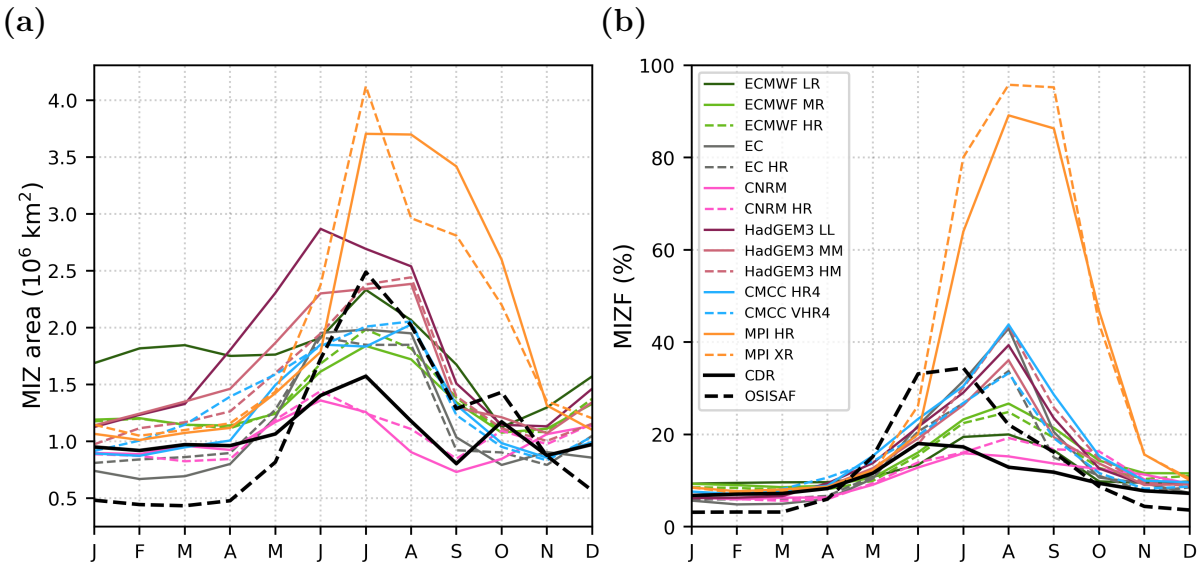

Figure 5.4: The 1979-2014 seasonal cycle in the MIZ area (a) and MIZF (b) from HighResMIP hist-1950 model outputs.

We also show the seasonal cycle of the MIZ area fraction (MIZF) from 1979 to 2014, calculated from the model and satellite products outputs (Figure 5.4b). The MIZF is defined as the percentage of the ice cover that is MIZ (Horvat, 2021), and it reflects the relative changes of the MIZ, which are more obvious since the total ice experiences substantial seasonal variability. The observed MIZF ranges from 5-10% in winter to 20-40% at its maximum between June/July. The simulated MIZF maxima are delayed compared to satellite estimates and to the MIZ area by about one month, when the total ice area approaches the September minimum but the MIZ area is still large. It is notable that the HighResMIP models are in better agreement when considering the MIZF rather than the MIZ area since the MIZ area in model simulations depends on the representation of total ice area. Excluding the MPI-ESM configurations, all models are in general agreement from November to May; the model spread enlarges in spring/summer but the models lie anyway within the observation envelope. The use of the MIZF metric highlights the peculiar representation of Arctic sea ice in the MPI-ESM: up to 95% of sea ice in the model consists of marginal ice.

5.3.3 Seasonal variability in the sub-regions

Since sea ice changes in the Arctic region are not uniform in space and time as a result of local climate effects (e.g. Parkinson et al., 1999; Meier et al., 2007; Peng and Meier, 2017), it is important to monitor the sea ice change also on regional scales to better understand the Arctic vulnerability. We analyse the seasonal variability of SIA and SIV in six sub-regions and compare them to the reference products (Figure 5.5).

Satellite estimates of SIA are not shown in the Central Arctic sector (CA) due to the observation gap near the North Pole. In this region, all models simulate a pronounced seasonal cycle in SIA with a wide area between December and April, and a minimum in August. While most models agree in winter when the region is fully covered by sea ice, the inter-model spread increases in summer. HadGEM3 and CMCC-CM2 simulate similar seasonal cycle in all configurations with slightly lower values in HadGEM3 HM. The ECMWF-IFS LR is an outlier also in this region, with a large SIA all year round and a minimum in August that is as large as the autumn/winter values in other models. Also EC-Earth3P LR has large SIA from November to May comparable to ECMWF-IFS LR, but it overestimates the melting and growing phases with an August minimum comparable to other models. The CNRM-CM6 model produces the smallest seasonal cycle amplitude in both resolutions, with a decrease between the winter values and the minimum of $\sim$10%. On the contrary, both MPI-ESM configurations present the strongest seasonal cycle, with the largest area in winter and the smaller in summer. These differences among models do not clearly depend on the resolution changes. For SIV, PIOMAS shows an increase of $\sim$30% between the minimum in August/September and the maximum in May. The

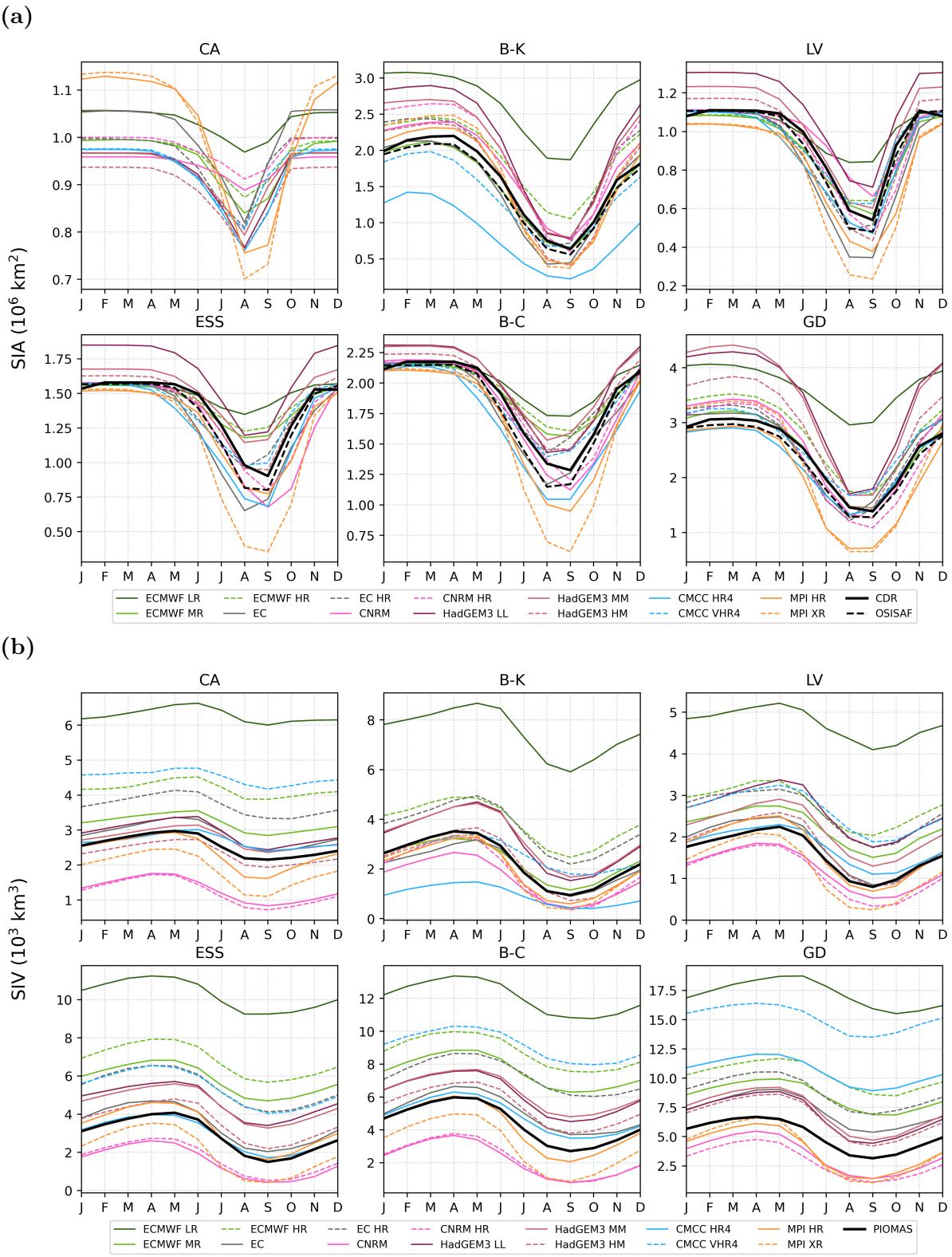

Figure 5.5: The 1979-2014 seasonal cycle in a) SIA and b) SIV from HighResMIP hist-1950 model outputs in the Arctic sub-regions.

seasonal cycle magnitude is captured by most models but with a large spread among them mainly driven by differences in the simulated thickness (Figure 5.2). The models generally perform similarly in simulating the SIV seasonal cycle in the sub-regions as at

the hemispheric scale (Figure 5.3b). To avoid repetitions, only the specific features of the SIV representation at the regional scale will be indicated below.

The Barents-Kara Seas (B-K) is the only sub-region where satellite products present a pronounced maximum peak that occurs in April (one month later the hemispheric SIA maximum). Except for CMCC-CM2, the models generally overestimate SIA in winter and reveal a large spread that is reduced in summer when models are in closer agreement with satellite estimates. The strong underestimation of SIA in CMCC-CM2 model could be attributed to the increased poleward Atlantic OHT simulated by this model Docquier et al. (2020). The warmer ocean temperatures not only promote sea ice melting in winter but also hinder its growth in autumn. The ocean and atmosphere resolution have generally the opposite effects on simulated SIA. Increasing only the ocean resolution in ECMWF-IFS (from LR to MR) and HadGEM3 (from LL to MM) results in lower SIA and a better fit to the observations. increasing the atmosphere resolution generally leads to larger SIA, except for a decrease in SIA for HadGEM3. The combined effect of enhanced resolution in both ocean and atmosphere in CNRM-CM6 and EC-Earth3P models increases the winter SIA, worsening the comparison with the observations. For SIV, nearly half of the model ensemble is very close to PIOMAS from January to June which is not the case for other sectors. The Barents-Kara Seas is the only region where CMCC-CM2 HR underestimates SIV as a result of too low SIA. In addition, both configurations of CMCC-CM2 underrepresent seasonal variation of SIV. At the same time, CNRM-CM6 has a better fit to PIOMAS in the Barents-Kara Sea sector compared to the rest parts of the Arctic Ocean, owing to improved representation of SIA. Notably, CNRM-CM6 has small regional differences in the amount of sea ice. The increased ocean resolution has a clear positive effect on SIV representation for ECMWF-IFS model while other models present similar values in their different configurations. The enhanced atmosphere resolution leads to higher SIV for ECMWF-IFS and CMCC-CM2, lower SIV for HadGEM3 and does not affect SIV in MPI-ESM.

In the Laptev (LV), East Siberian (ESS), and Beaufort-Chukchi Seas (B-C), there is no notable peak in the observed seasonal variability of SIA but instead, the annual maximum is extended between December and May since the winter sea ice expansion is constrained by land. In spring, the downward shortwave radiation increases, causing the rapid sea ice melt, which ends at the annual minimum in September. Notably, the disagreement between satellite estimates in summer SIA is higher in all three regions probably due to melt ponds, which complicate the SIC retrievals from passive microwave radiometers (Ivanova et al., 2015). In all three regions the models exhibit better agreement in winter while in summer, the spread across the models is large. This can be associated with the model differences in simulating the river discharge (Park et al., 2020) as well as the transport of Pacific waters through the Bering Strait (Watts et al., 2021), which

modify the thermo-haline structure of the upper-ocean and affect sea ice growth and melt. In all three regions, ECMWF-IFS LR is well compared with satellite estimates in winter, which is not the case for other sectors with a greater role of the Atlantic OHT where the model is biased high. HadGEM3 overestimates SIA, particularly in its lower-resolution configuration. This behavior is common also for other parts of the Arctic Ocean which points out that bias in HadGEM3 is similarly distributed across the regions. MPI-ESM underestimates SIA particularly in summer since the model is struggling to simulate consolidated pack ice (Figure 5.2). CNRM-CM6, CMCC-CM2 and HR of EC-Earth3P show a fairly good agreement with satellite estimates in all three regions. Lower resolution of EC-Earth3P presents an earlier and faster sea ice retreat in the Laptev and East Siberian Seas resulting in the second-lowest SIA among models while in the Beaufort-Chukchi Seas the model compares well with OSISAF estimates. Increased ocean resolution leads to lower SIA for all models except for EC-Earth3P which has higher values in its HR configuration. The effect of the ocean resolution is stronger in summer however for HadGEM3 the impact is seen all year round. Enhancement of the atmosphere resolution does not significantly affect ECMWF-IFS but leads to higher summer SIA in CMCC-CM2, as in the other regions. For MPI-ESM, the increase in atmosphere resolution has a larger impact on summer SIA in the Laptev, East Siberian, and Beaufort-Chukchi Seas compared to other sectors: MPI-ESM XR simulates SIA almost twice lower than other models in August and September. In the Laptev, East Siberian, and Beaufort-Chukchi Seas, SIV reaches the maximum in May (April-May in B-C) while the annual minimum occurs in September. Most models overestimate SIV with the highest bias in the East Siberian and Beaufort-Chukchi Seas. CMCC-CM2 HR and MPI-ESM HR have a very good fit to PIOMAS, even though the latter fails to reasonably simulate the SIC (Figure 5.2). The effect of the ocean resolution on SIV is clearly seen for ECMWF-IFS and EC-Earth3P in all three regions and for HadGEM3 in the Laptev Sea - the only regions where LL and MM configurations of HadGEM3 differ. Other models do not have considerable differences in SIV with changing ocean resolution. Increased atmosphere resolution results in higher SIV for ECMWF-IFS, EC-Earth3P and CMCC-CM2 and lower SIV for HadGEM3 and MPI-ESM.

The Greenland region (GD) holds the largest area of sea ice both in winter and summer (3 and 1.5x10^6 km^2 respectively according to the satellite estimates). Most models tend to overestimate SIA all year round with the highest bias in winter in ECMWF-IFS LR and HadGEM3. This is confirmed by the mean March location of the ice edges extended far south (Figure 5.2). The models are generally capable of melting away the excess of sea ice by September, so there is more consistency among most models in summer. MPI-ESM again tends to underestimate SIA and has the strongest low bias in summer. An increase in the ocean resolution from 1° to 0.25° improves the representation of SIA in

ECMWF-IFS and does not give notable changes in HadGEM3 and EC-Earth3P. The effect of atmosphere resolution again depends on the model. ECMWF-IFS and CMCC-CM2 produce slightly higher SIA in their finer atmosphere configurations, particularly in winter. Conversely, HadGEM3 has lower SIA in its HM configuration in winter, which fits better to the observations. For MPI-ESM, there are no differences between different configurations, as in the Barents-Kara Seas region. For SIV, both configurations of CMCC-CM2 have a large error in the Greenland region owing to high bias in SIT (Figure 5.2) whilst, in other sectors, at least one configuration of the model is in good agreement with PIOMAS. Enhanced ocean resolution leads to lower SIV for ECMWF-IFS and higher SIV for EC-Earth3P. At the same time, for HadGEM3 and CNRM-CM6, there are no significant differences between configurations with changing ocean resolution. An increase in the atmosphere resolution has no effect on SIV in HadGEM3 and MPI-ESM but leads to higher SIV in CMCC-CM2.

The regional analysis of the seasonal variability reveals that the model performance and the accuracy of simulated SIA largely depend on the region and season. While Barents-Kara Seas and Greenland regions contribute mainly to the winter inter-model spread, the largest summer differences among models are seen in the Laptev, East Siberian and Beaufort-Chukchi Seas. At the same time there are no considerable differences in the model's ability to simulate SIV at regional scale: the biases are generally uniform across the regions and seasons. We find no strong dependence of sea ice realism in the models at the regional scale from the horizontal resolution. The impact of the ocean resolution on the representation of SIA is most pronounced in the Barents-Kara Seas and Greenland sea ice regions that are strongly influenced by the Atlantic OHT. The effect of the atmosphere resolution is less clear but there is evidence that the atmosphere resolution has a stronger impact on SIV rather than on SIA and particularly in the regions of thicker ice.

5.3.4 Interannual variability

Next, we evaluate the long-term variability of the Arctic SIA and SIV from the hist-1950 simulations from 1979 to 2014. Figure 5.6a illustrates monthly anomalies of SIA (with respect to 1979-2014 climatologies) simulated by the models and derived from satellite data sets.

The inter-model spread is relatively similar throughout the period but it slightly increases from the mid-2000s when the ice reduction has accelerated. The interannual variability of the simulated SIA is weakly correlated with the CDR estimates (correlation is lower than 0.2). All models are able to reproduce sea ice shrinking but with varying intensity: ECMWF-IFS LR, HadGEM3 LL, MPI-ESM HR show larger negative trends compared to observations (-44x10^3 km^{2}yr^{-1} in CDR and -46x10^3 km^{2}yr^{-1} in OSISAF)

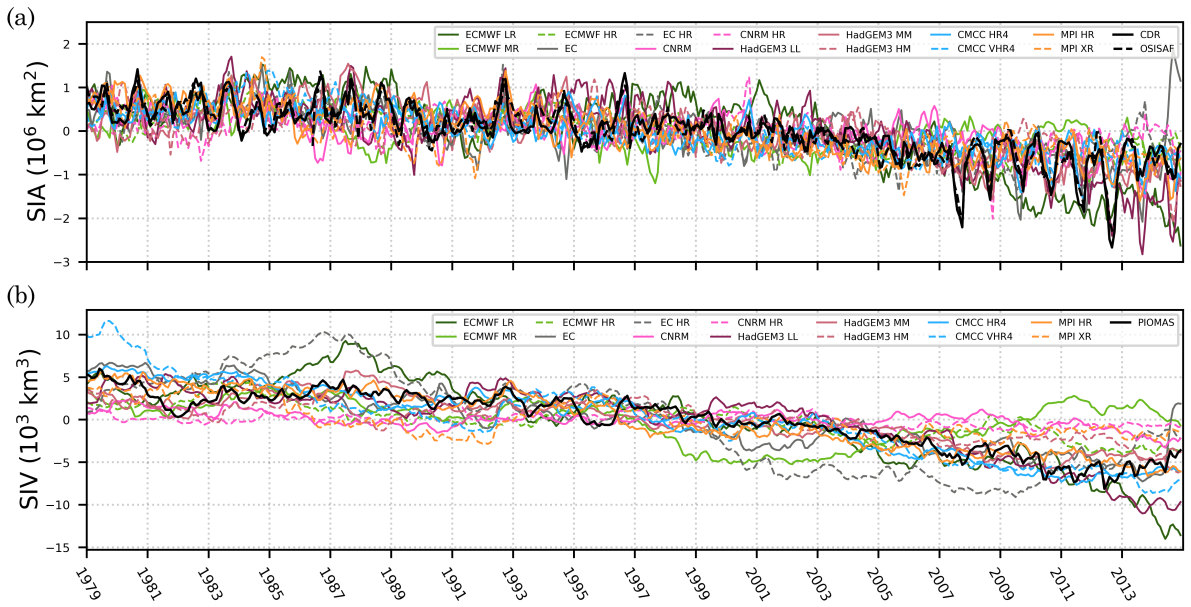

Figure 5.6: Monthly anomalies of SIA (a) and SIV (b) over 1979-2014 from HighResMIP model outputs and reference products.

while the MR and HR versions of ECMWF-IFS, both configurations of CNRM-CM6, EC-Earth3P, HadGEM3 HM, CMCC-CM2 HR present weaker negative trends. None of the models can capture the record lows of 2007 and 2012. An increase in the ocean resolution generally results in smaller negative trends except for EC-Earth3P which shows a similar rate of decline in both configurations. The effect of finer atmosphere resolution is different among models: the SIA decrease is stronger in ECMWF-IFS and CMCC-CM2 and weaker in HadGEM3 and MPI-ESM.

Figure 5.6b shows monthly anomalies of SIV (with the seasonal cycle removed) over 1979-2014 in HighResMIP models and PIOMAS. There is a substantial inter-model spread for SIV compared to SIA, particularly at the beginning and the end of the observed period. The biases from few models are not consistent throughout the years varying significantly from positive to negative (EC Earth-3P HR, ECMWF MR, HadGEM3 LL). Models are generally in agreement with PIOMAS interannual variability of SIV (the correlation coefficient for most models is higher than 0.75). The weakest agreement is found for ECMWF-IFS MR (R=0.28) and CNRM-CM6 (R=0.51 in LR and R=0.61 in HR). Increasing atmosphere resolution results in a weaker correlation with PIOMAS (for HadGEM3, the correlation ranges from 0.91 (MM) to 0.82 (HM); for CMCC-CM2, 0.93 (HR) and 0.87 (VHR); for MPI-ESM, 0.9 (HR) and 0.54 (XR)).

PIOMAS simulates sea ice shrinking at the rate of -291 km^{3}yr^{-1} while the models disagree on the intensity of SIV decrease. There is no straightforward impact of changing resolution in ocean and atmosphere on the linear trends in SIV since the impact of horizontal resolution on SIA and SIT is different and depends on the model. We find

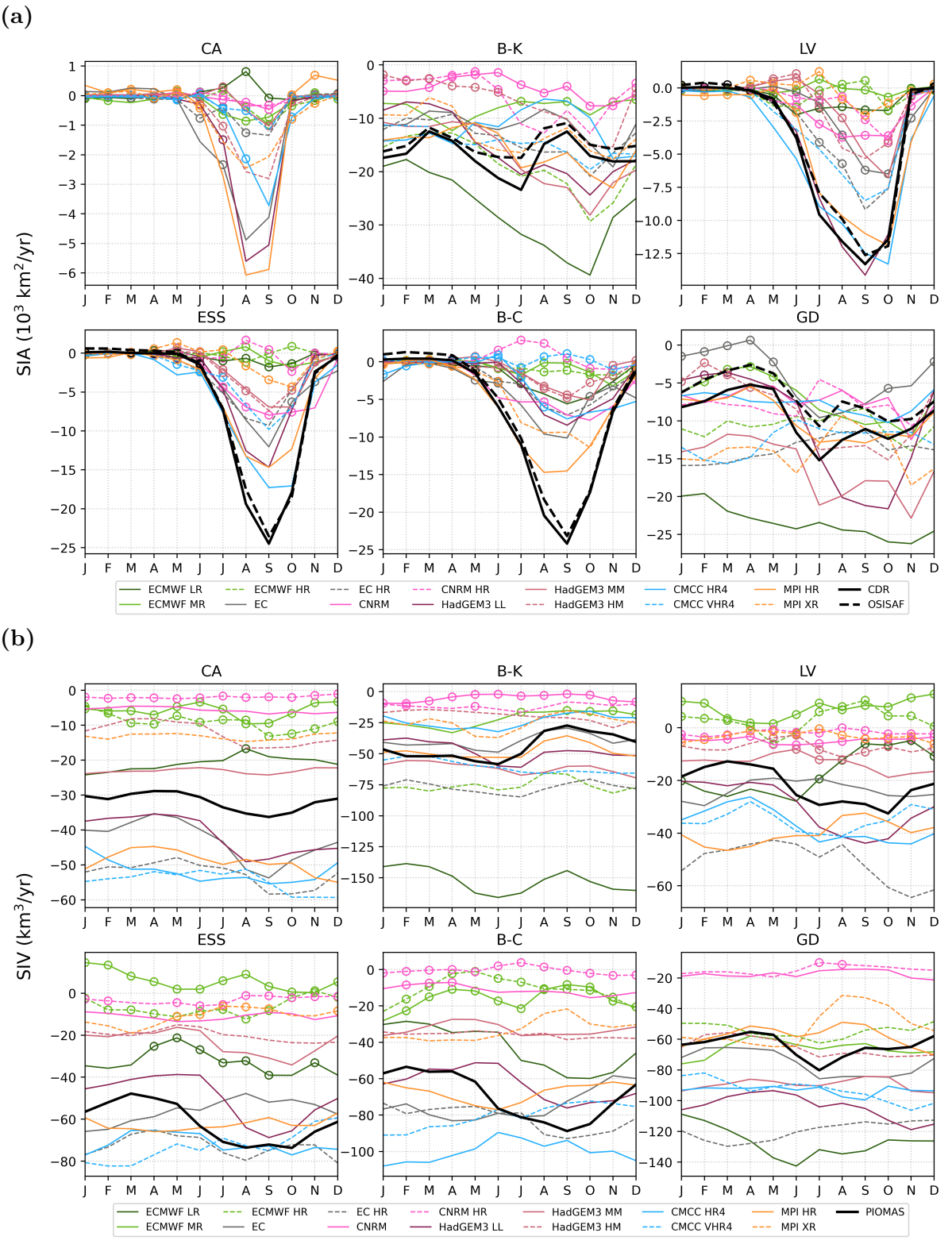

Figure 5.7: The 1979-2014 monthly trends in SIA (a) and SIV (b) in the Arctic subregions. Dots indicate non-significant trends.

that configurations with coarse ocean resolution tend to simulate more negative trends (-424 km^{3}yr^{-1} in ECMWF LR compared to -105 and -157 km^{3}yr^{-1} in its finer configurations; for HadGEM3, the trend ranges from -355 km^{3}yr^{-1} in lower resolution to -257 and -174 km^{3}yr^{-1} in finer resolution configurations). Here, the exception is EC-Earth3P

in which the eddy-permitting configuration has a larger negative trend in SIV (-322 and -460 km^3yr^{-1}). In CNRM-CM6, the SIV decrease is very weak for both configurations (-62 and -36 km^3yr^{-1} for LR and HR, respectively), which might reflect the negative ice growth-ice thickness feedback: thin ice allows sea ice to grow more rapidly, mitigating the ice loss. The finer atmosphere resolution has a different impact on the pace of sea ice retreat in different models: CMCC-CM2 VHR4 and ECMWF-IFS HR simulate slightly stronger trend compared to their coarser counterparts (-384 and -411 km^3yr^{-1} in CMCC-CM2; -105 and -158 km^3yr^{-1} in ECMWF-IFS). On the other hand, in MPI-ESM and HadGEM3, the finer configuration has less negative trend compared to the coarser one (337 km^3yr^{-1} and -144 km^3yr^{-1} in MPI-ESM; -174 and -257 km^3yr^{-1} in HadGEM3).

We also examine how the models simulate sea ice response to the external forcing on a seasonal scale. The monthly trends in the Arctic-wide SIA reveal that the models tend to underestimate the rate of sea ice loss in the melting season and in summer (not shown). Many models cannot reproduce the pronounced seasonal cycle of the trends but instead simulate a similar rate of decline in different months of the year. Most models reproduce more negative trends from November to May and underestimate the magnitude of trends in other seasons. MPI-ESM HR trends are found to have a closer fit to the observed trends for the total Arctic although the model is wrong in simulating SIC and sea ice classes. For SIV, the models vary greatly in the representation of trends. Despite all models are able to simulate SIV decline in all months, they cannot capture the observed magnitude of sea ice loss and have values ranging from almost 0 to -450 km^3yr^{-1}. They also struggle to reproduce the seasonal cycle in the trend which in PIOMAS has a slightly stronger signal in June and a weaker signal in winter months (-320 $km^3yr^{-1}$and -260 km^3yr^{-1} respectively).

Since there is a substantial difference in the models' performance in reproducing the seasonal variability on a regional scale, we analyse monthly trends in SIA and SIV in each sea ice zone over 1979-2014 (Figure 5.7). The magnitude and timing of sea ice loss strongly depend on season and region. According to observations, the winter decrease in SIA is most dramatic in the Barents-Kara Seas (nearly -17x10^3 km^2yr^{-1}) while the summer trends are dominated by the Eastern Siberian Sea and Beaufort, and Chukchi Seas (almost -25x10^3 km^2yr^{-1}). The Barents-Kara Seas and the Greenland region show a pattern of SIA trends that differs from the total Arctic and the rest of the regions which have one pronounced negative peak in September and close to zero trends in winter. Instead, in the Atlantic sector, sea ice loss is observed all year round with slighly stronger decreases in July. In the Central Arctic, the models simulate a weak SIA reduction with the strongest signal in August-September, which is not significant in most models (5% level). Generally, the models tend to underestimate the pace of sea ice loss indicated by satellite estimates. The exception is the Barents-Kara Seas and Greenland where some

models produce more negative trends compared to the observations. In the Laptev, East Siberian, Beaufort, and Chukchi Seas some of the models do not simulate a reduction in summer SIA and even have weak positive trends, yet insignificant. Given that these regions all hold a large MIZF in summer (Figure 5.4), the inability to capture trends points to inaccurate sensitivity of sea ice to the external forcing, particularly within the MIZ.

The strongest negative trends in SIV are observed in the areas of thick ice: in the Beaufort and Chukchi Seas (up to -90 km^3yr^{-1} in September), in the Greenland sector (-80 km^3yr^{-1} in July), and the East Siberian Sea (-70 km^3yr^{-1} in summer months). The Barents-Kara Sea contrasts in the seasonality of SIV trends with other sectors where the highest rate of sea ice decline is observed in September. Notably, in the Laptev, East Siberian and Beaufort, and Chukchi Seas, SIV experiences a substantial decrease in the winter months while SIA stays nearly stable reflecting considerable ice thinning which points to the primary role of the basal melt. In the East Siberian Sea and Beaufort-Chukchi Seas, almost all models tend to underestimate trends in SIV while in the rest of the ice zones, PIOMAS is nearly in the middle of inter-model uncertainty. Both CNRM-CM6 configurations and two finer configurations of ECMWF-IFS deviate from the other models in the sense that they have close to zero changes in SIA and SIV, which in general are insignificant. CNRM-CM6 simulates very thin ice so the lack of trend is consistent with the concept of negative ice thickness-ice growth feedback. ECMWF-IFS MR and HR, conversely, underestimate sea ice reduction everywhere despite simulating very thick ice. HadGEM3 performs differently at a regional scale but at least one configuration has a very good fit to the PIOMAS estimates. Both configurations of CMCC-CM2 present the large SIV decrease in all sectors except for the Barents-Kara Sea and the rate of decline is similar between two resolutions despite a significant difference in the mean SIV. HR configuration of MPI-ESM is in fairly good agreement with PIOMAS in all regions except the Central Arctic and the Laptev Sea where it tends to produce more negative trends. MPI-ESM XR underestimates negative SIV trends in all parts of the Arctic Ocean except the Greenland zone where it is close to its HR configuration. There is no strong link between the strength of sea ice retreat and the ocean/atmosphere resolution. The relationship rather depends on the region and the model used. Given that the models generally underestimate SIA trends and produce less negative trends in their finer ocean configurations, we can conclude that enhanced ocean resolution does not improve representation of the SIA trends, particularly in the Laptev, East Siberian and Beaufort and Chukchi Seas in summer. Benefecial effect of increased ocean resolution for SIA trends is especially evident for ECMWF-IFS in the Barents-Kara Seas and the Greenland area, where LR configuration tends to overestimate negative trends. Other models in these regions do not considerably differ between their configurations and both low and high-resolution configurations show closer

fit to the observations in different months of the year. The increased atmosphere resolution also does not improve representation of SIA trends. For HadGEM3, CMCC-CM2 and MPI-ESM, the finer atmosphere resolution leads to less negative SIA trends compared to their counterparts at coarse resolution. The relationship between ocean/atmosphere resolution and SIV trends is less clear and depends on the region and the model.

5.3.5 Future projections

In this section, we assess the performance of HighResMIP models in simulating the Arctic sea ice future changes using highres-future model outputs from 2015 up to 2050. All models produce sea ice loss in future runs with generally stronger negative trends compared to historical runs. The model simulations can elucidate when the Arctic will reach its first ice-free summer, the conditions typically defined as the timing when September sea ice drops below 10^6 km^2. Reaching ice-free conditions symbolizes the unprecedented change in the Arctic environment and the tipping-point in the Earth's climate system. Considering large inter-model spread in simulating observed mean sea ice state and trends we assume that the selection of the models which better agree with observations can narrow down the spread and decrease uncertainty in the model projections. We select models based on their historical performance by comparing simulated September SIA and SIV mean state and trends with those from CDR and PIOMAS, respectively (Figure 5.8). To exclude the outliers we define the 75th percentile threshold and pick out the models whose values do not exceed the threshold for both variables. The resulting subset includes four models: low configuration of EC-Earth3P, HadGEM3 MM and HM, and CMCC-CM2 HR. These models are used in the further analysis of the future sea ice evolution.

Figure 5.9 illustrates the September SIV time series from 1950 to 2050 computed for the total Arctic and sub-regions. The vertical lines mark first ice-free September in the multi-model mean with and without model selection (yellow and green, respectively) and in CDR (black) if it has already happened before 2021 in the given region. Since we examine the Arctic sea ice changes also at the regional scale, the timing of the ice-free conditions in the sub-regions refers to the threshold of 25% of the CDR SIA averaged over the 1980-2010 period in the given region. It is evident that huge sea ice reduction takes place in all sea ice zones but the pace of sea ice loss varies across the regions owing to differences in the initial state and dominant processes driving the change. We can note that applying model selection results in earlier timing of the ice-free conditions in the sub-regions (Barents-Kara, Laptev, East Siberian, Beaufort-Chukchi Seas). The model selection also results in reaching ice-free conditions in the total Arctic and all sub-regions while multi-model mean without model selection does not predict the event everywhere before 2050. The comparison between the model configurations in simulating the timing of ice-free conditions shows that there is no clear link between the model resolution and

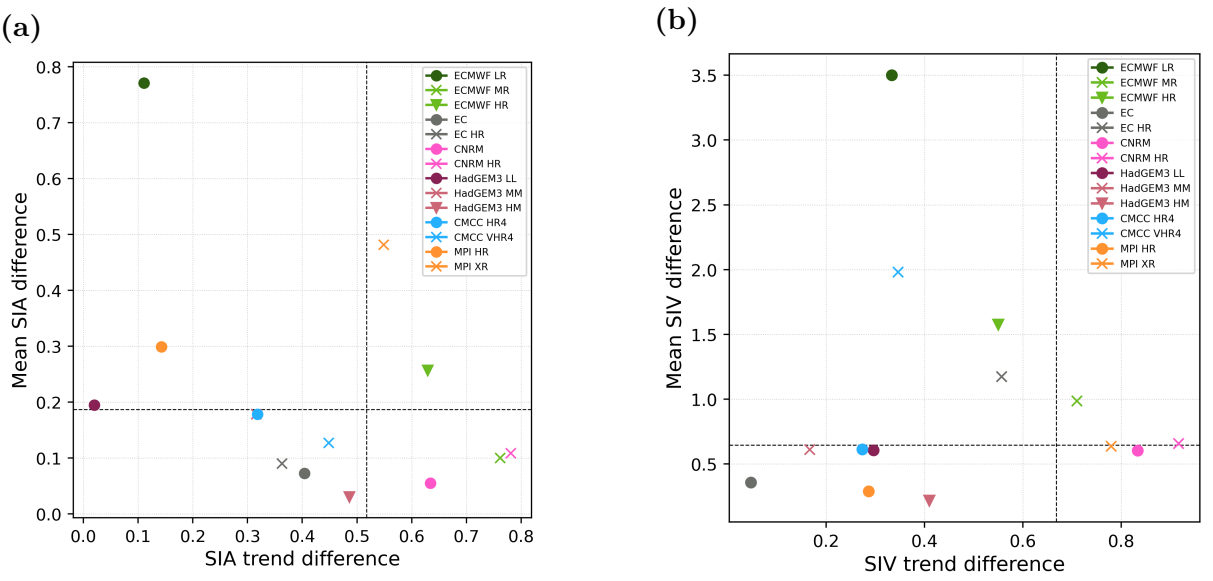

Figure 5.8: Normalized difference in mean September SIA against September SIA trend over 1979-2014 (a). Same for SIV (b). The difference is computed with reference to CDR (for SIA) and PIOMAS (for SIV). Vertical lines indicate the 75th percentile for a set of the model outputs excluding ECMWF-IFS.

the pace of sea ice loss (not shown).

The September Arctic-wide sea ice from the multi-model mean (with model selection) shrinks by 95% from 1950 to 2050. The inter-model spread decreases throughout the century from 14x10^3 in 1950 to 1.64x10^3 km^3 in 2050. The Arctic does not reach ice-free conditions within 2050 in the multi-model mean without model selection, although applying selection criteria advances the timing of the event up to 2047. The Central Arctic September sea ice loses 96% of its volume by 2050 in the multi-model ensemble, which is in good agreement with PIOMAS in the overlapping period. The inter-model spread again narrows substantially from nearly 2.58x10^3 km^3 in 1950 to 0.23x10^3 km^3 in 2050. The Arctic ice-free conditions in the Central Arctic are not reached before 2050 in the multi-model mean when considering all models. However, excluding the outliers results in approaching the threshold in 2042. In the Barents-Kara Seas, the spread among models is relatively small compared to the rest of the sectors due to the thin ice, decreasing from 1.46x10^3 km^3 in 1950 to almost 0 in 2050.

The Barents-Kara Seas experience the most dramatic sea ice loss accounting for almost 100% of SIV from 1950 to 2050 in the ensemble of the models. First ice-free September in the Barents-Kara Seas is accurately simulated by the multi-model mean with model selection: the event occurs in 2012. The multi-model mean without model selection postpones the event by 19 years. The multi-model mean SIV in the Laptev Sea shrinks by 99% during 100 years. The inter-model spread is also relatively small in this region and it narrows from nearly 0.9x10^3 km^3 at the beginning of the run to 0.05x10^3 km^3 in the end.

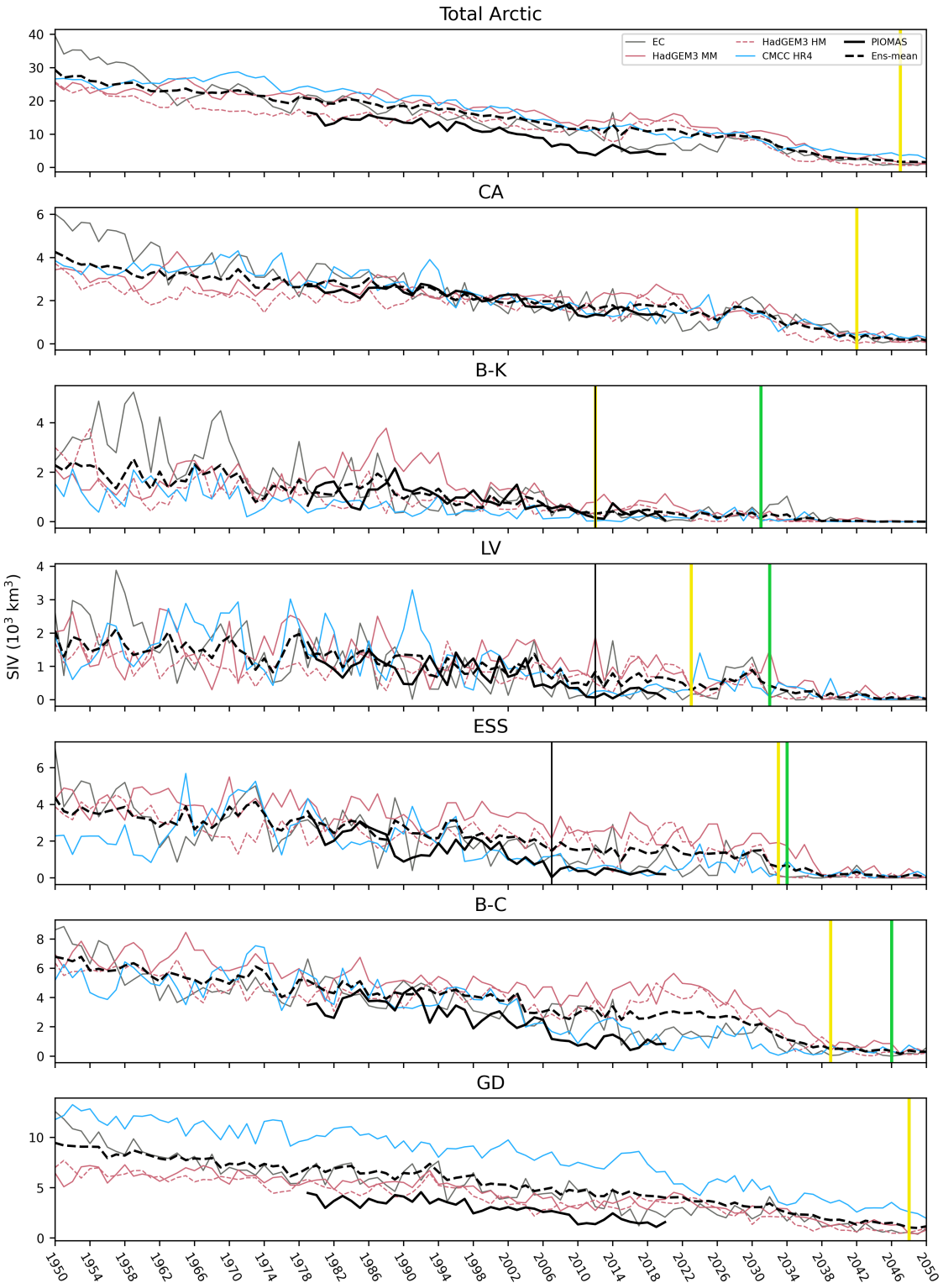

Figure 5.9: Time series of September SIV from 1950 to 2050 using HighResMIP historical and future runs and PIOMAS for the full Arctic and sub-regions. The multi-model mean SIV with model selection is shown by dashed line. The vertical line indicates the timing of ice-free conditions: in the multi-model mean without model selection (green), in the multi-model mean with model selection (yellow), and in CDR (black). Free-ice conditions refer to first September SIA to fall below 10^6 km^2 for the total Arctic (25% of the CDR SIA averaged over 1980-2010 for the sub-regions).

The timing of first ice-free summer is similar to that in the Barents-Kara Seas: SIA drops below the threshold in 2012 for CDR and in 2032 for the multi-model mean without model selection. When applying selection criteria, the timing of the ice-free conditions advances to 2023. In the East Siberian Sea, September ensemble-mean SIV is reduced by 99% by the middle of this century. The inter-model spread ranges between 4.76x10^3 km^3 in 1950 and 0.1x10^3 km^3 in 2050. The East Siberian Sea reaches the threshold in SIA earlier compared to the other regions. CDR produces the event in 2007 when the Arctic broke the first record low while the multi-model mean with model selection simulates first ice-free conditions in 2033 (2034 without model selection). The Beaufort-Chukchi Seas lose nearly 96% of SIV in 100 years in the ensemble-mean. The inter-model spread decreases from 3.44x10^3 km^3 at the beginning to 0.37x10^3 km^3 at the end of the run. The multi-model mean reaches first ice-free September in 2046. When adopting the model selection, the Beaufort-Chukchi Seas will be ice-free in 2039. The Greenland region is undergoing the least prominent sea ice loss accounting for 88% throughout the period from 1950 to 2050. However, there is a great narrowing of the inter-model spread from 6.12x10^3 km^3 in the middle of the last century to 1.15x10^3 km^3 100 years after. The multi-model mean with and without model selection projects that Greenland SIA might turn ice-free in 2048. Considering that the models generally postpone first ice-free September when comparing to CDR in the sub-regions, we assume that the total Arctic will probably meet its first ice-free summer earlier than predicted by the multi-model mean.

Along with overall sea ice loss, there are substantial changes in the structure of sea ice cover. Figure 5.9 displays the time series of September SIA and the MIZF from 1950 to 2050. For SIA, the models are in fairly good agreement with the observations, yet have systematic biases and underestimate the negative trend. In addition, the inter-model spread is large but relatively similar throughout the years (4x10^6 km^2). For the MIZF, the spread among models increases considerably with time from 10% in 1950 to 75% in 2050. Most models simulate the MIZF growth, which reflects the transition of the sea ice state to the marginal ice-dominated. The MIZ in the 2040s is projected to account for up to 80% of the total ice area in September, although the interannual variability at the end of the run is large in most models. CNRM-CM6 and MPI-ESM are two outliers in the sense that CNRM-CM6 has a nearly constant MIZ fraction during the whole period while MPI-ESM has the MIZF with close to 100% values from the beginning of the run, which however drops to 0 in certain years in the end of the run. This highlights the importance to examine the variability of the MIZ together with the total SIA: the accurate representation of the total SIA does not guarantee the same for sea ice classes.

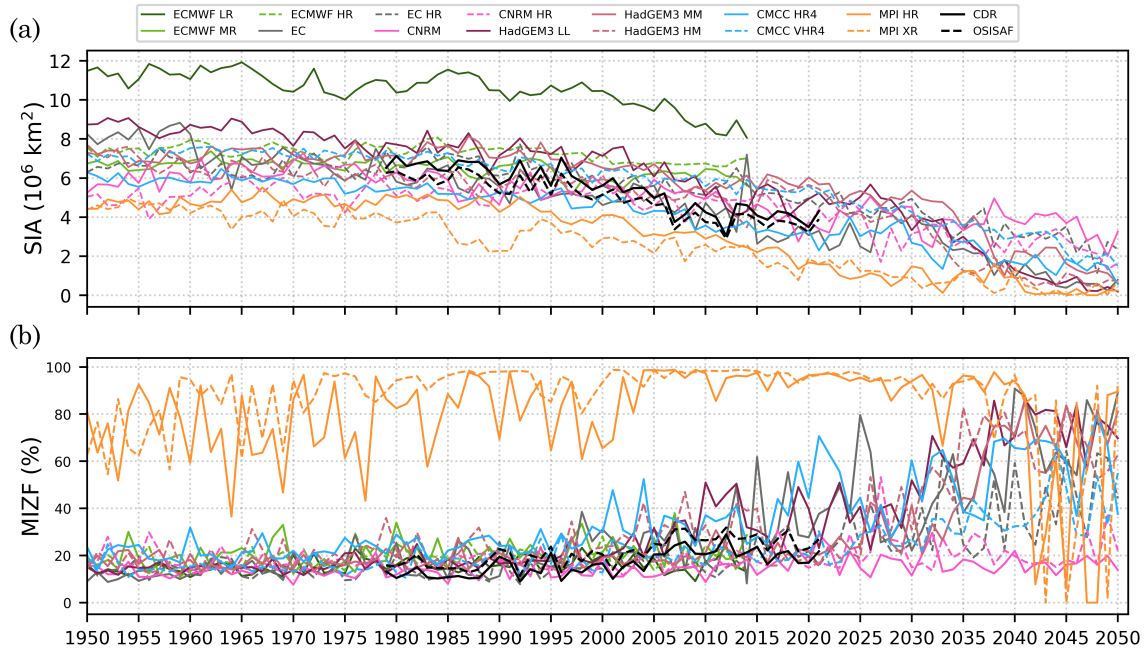

Figure 5.10: Time series of September SIA (a) and MIZF (b) from 1950 to 2050 using HighResMIP historical and future runs and satellite products (CDR and OSISAF).

5.4 Discussion

Although the latest generation of the models does a fairly reasonable job in simulating the mean state and long-term variability of sea ice cover (Notz and Community, 2020), the models still suffer from biases, which decrease the model's trustworthiness in projecting the future sea ice state in the Arctic. The enhancement in the horizontal resolution in model components is used in the CMIP6 HighResMIP as one of the factors capable of improving the realism of the model simulations and reducing biases also in polar regions. In this study, we investigate the ability of HighResMIP in simulating Arctic sea ice variability and the impact of the ocean and atmosphere horizontal resolution on the representation of sea ice properties in the recent past and future climate. We do not find a strong link between ocean/atmosphere resolution and the representation of sea ice properties and the realism of model performance rather depends on the model used. However, there is evidence that enhanced ocean resolution leads to improved representation of winter SIA in some models. This is associated with a more accurate meridional heat transport (Docquier et al., 2019) which is a key process that can regulate the location of the ice edge and SIA (Li et al., 2017; Muilwijk et al., 2019) in the models. The Atlantic Ocean is the main heat source entering the Arctic, accounting for 73 TW on average per year (Smedsrud et al., 2010), therefore the adequate simulation of the boundary currents is particularly important in the Atlantic sector of the Arctic Ocean which is confirmed by the regional analysis in our study. Another process that might be sensitive to horizontal ocean resolution is the Arctic river discharge, which contributes

both to seasonal variations of sea ice cover and long-term sea ice variability. The freshwater input stabilizes the upper ocean stratification and isolates the warm Atlantic layer from the bottom of sea ice cover (Carmack et al., 2015), resulting in higher ice growth in winter. On the other hand, the heat input from the rivers accelerates sea ice melt and increases the ocean temperature, which has possible implications for the next year's growing season (Park et al., 2020). The representation of river discharge in HighResMIP models needs additional investigation. Our results do not show the systematic impact of atmosphere resolution on the representation of the Arctic sea ice. This is confirmed by other studies reporting the minor role of atmosphere resolution compared to the ocean (Roberts et al., 2020; Koenigk et al., 2021; Meccia et al., 2021). Increasing atmosphere resolution might permit a more realistic representation of precipitation, which can lead to increased snowfall (Strandberg and Lind, 2021) and consequently invoke cooling and sea ice expansion (Bintanja et al., 2018). SIT is less responsive to changes in the ocean grid resolution compared to SIA and its representation largely depends on sea ice model. Moreover, our results show that in some cases large biases in SIT reduce the beneficial effect of increased horizontal resolution with regard to SIA. Poor representation of SIT is a great obstacle to the robustness of sea ice projections. The high uncertainty cannot be overcome without constraining the model simulations with a sufficient number of in-situ measurements of the Arctic SIT, which are still sparse and unreliable (Massonnet et al., 2018). Apart from the horizontal resolution, there are other important factors affecting the model performance. The possible reasons for sea ice errors might be related to inaccurate representation in the models of the mixed layer depth (Watts et al., 2021), surface air temperature (Papalexiou et al., 2020), surface pressure and geostrophic winds (Kwok and Untersteiner, 2011; Stroeve et al., 2014), sea ice sensitivity to the global warming (Zhang, 2010). Another possible source of inaccurate simulation of the sea ice state is the physics and complexity of sea ice models itself including the thermodynamics schemes and parametrizations (Keen et al., 2021), sea ice dynamics components (Hunke, 2010) and coupling between the ocean and atmosphere components (Hunke et al., 2020). Given few improvements with increased horizontal resolution we argue that running the models at higher resolution might not be worth the major effort of costly computations. Our results suggest that the efforts of the modelling groups should be aimed rather at the improvement of the sea ice model physics and parameterizations.

In this study, with the means of HighResMIP outputs we try to understand when the Arctic will see its first ice-free summer. Models produce a wide range of possible timing of first ice-free conditions in the Arctic. To reduce the inter-model spread in sea ice projections we apply a widely used approach based on selection of the models according to their historical performance (Wang and Overland, 2012; Senftleben et al., 2020). Although close agreement with observations does not guarantee the realism of the models, we believe

that excluding the models that cannot reproduce present-day SIA and SIV mean state and trends might improve the accuracy of future sea ice projections. Different criteria to select best-performing models exist and almost always lead to earlier near-disappearance of sea ice compared to no selection (Docquier and Koenigk, 2021). The timing of first ice-free Arctic in our model selection compares well with similar criteria applied to CMIP6 models which predict the event between 2047 and 2052 while the process-based criteria advances the timing of first ice-free summer up to 2035 (Docquier and Koenigk, 2021). The investigation of model selection criteria is out of scope of this study. Our goal is to give an insight into when the Arctic might turn ice-free.

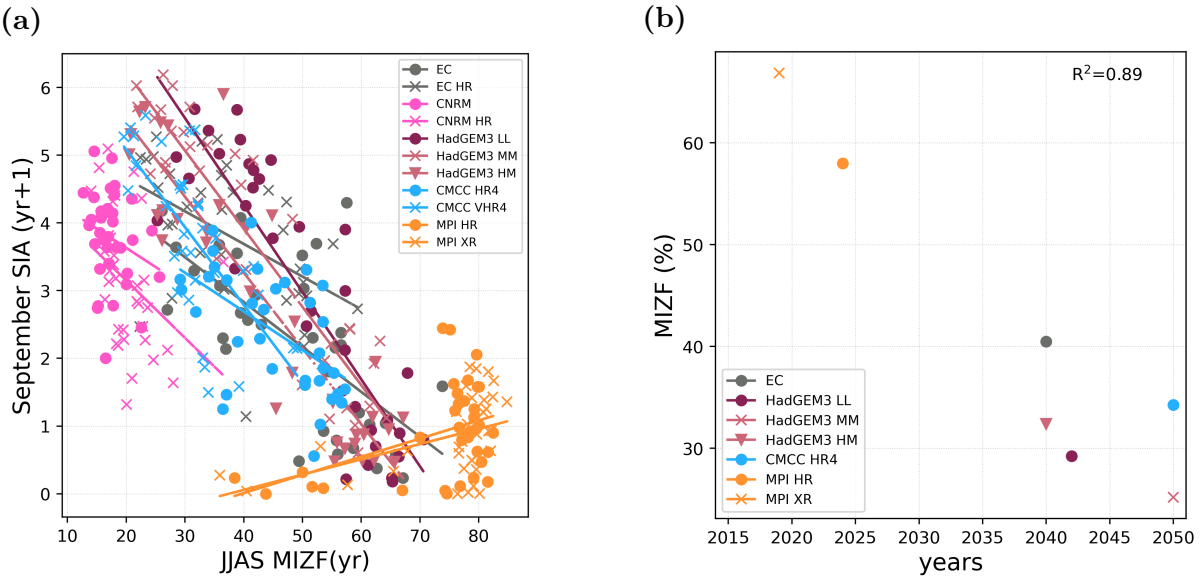

Figure 5.11: JJAS MIZF against September SIA with one year lag over 2015-2050 (a); The timing of the ice-free Arctic against JJAS MIZF in 2015 (b).

Our results also highlight the increasing role of the MIZ in the response of Arctic sea ice cover to climate change. We show that the MIZ will be the dominant sea ice class in the Arctic by 2050 which implies the shift to the new sea ice conditions, similar to the Antarctic. The chaotic interannual variability of the summer MIZF in the last years of the simulation points out that the current model physics might not be adapted to changing sea ice conditions (Figure 10). In order to realistically simulate (thermo)dynamical processes, the new sea ice regime requires modifications in the model physics and sea ice rheology which is formulated for thick pack ice (Aksenov et al., 2017). Additionally, the growing fraction of the MIZ requires changes in the parameterization of the lateral and basal melt (Smith et al., 2022). The proper simulation of the MIZ is essential for reasonable projections of future sea ice conditions because small and thin ice floes within the MIZ are more vulnerable compared to consolidated pack ice to external forces both dynamic and thermodynamic. The currents become stronger when the ice edge moves northward and the open ocean area expands which eventually promotes further sea ice retreat (Aksenov

et al., 2017). In addition, the water patches between the ice floes permit the absorption of solar radiation in the upper ocean, increasing the role of the ice-albedo effect which causes anticipation of the ice-advance onset and acceleration of the overall sea ice loss. To demonstrate positive feedback between summer MIZ and minimum SIA for the following year we plot JJAS MIZF against September SIA with a 1-year lag computed for the years 2015-2050 (Figure 5.11a). All models except one simulate negative regression ranging from $\sim$-0.13%/10^6 km^2 to -0.06%/10^6 km^2 which means that the larger summer MIZF leads to lower September SIA the following year. We suggest that the MIZ might act as a predictor of future sea ice conditions in the model simulations. Figure 5.11b shows JJAS MIZF in 2015 (start of highres-future run) against the first September when the Arctic becomes ice-free. Note that not all models simulate the event before 2050. Our analysis indicates that with the higher initial MIZF, the September sea ice disappears earlier. This points out that the reasonable representation of the MIZ at the beginning of the run might impact the pace of sea ice loss and potentially improve the accuracy of model projections. We assume that the MIZF might represent a robust criterion to examine the model performance. The impact of the MIZ on the accuracy of the model simulations needs further investigation.

5.5 Conclusions

In this study, we evaluate the historical and future variability of the Arctic sea ice area and volume using six coupled atmosphere-ocean general models participating in the HighResMIP experiments of the sixth phase of the Coupled Model Intercomparison Project (CMIP6). For the period 1979-2014, we find that all models can properly simulate maximum and minimum in SIA at hemispheric and regional scales. However, some models cannot correctly capture the magnitude of the mean annual cycle of SIA, failing to realistically reproduce the ice growth and retreat phases with systematic over- or underestimation of the seasonal variability. We find that the models generally are able to reproduce the seasonal cycle of the Arctic-wide MIZ area, although not all of them can capture the timing of the annual maximum. The models simulate different area of the MIZ, especially in summer, however, there is stronger agreement among models for MIZF, which suggests that the MIZ in the simulations is closely linked to the amount of the total SIA. We find different regional contributions to the inter-model spread at seasonal maximum and minimum: while the winter inter-model spread in SIA is associated with the Atlantic sector (Barents-Kara Seas and the Greenland ice zones), the summer differences are tied to the the Laptev, East Siberian, and Beaufort-Chukchi Seas. Models broadly vary on the spatial distribution of the mean SIT as well as its average values. Only a few models reveal a similar to PIOMAS pattern with thicker ice off the coast of Greenland and

the Canadian Archipelago. Most models simulate too thick ice which in turn affects the representation of sea ice volume: excluding one outlier, all but two models overestimate ice volume all year round up to 1.5 times in April and 3.5 times in August. However, regardless of large systematic biases, most models simulate a realistic seasonal cycle of SIV with a maximum in April and a minimum in August. All models capture declines in SIA and SIV over the historical period but they disagree on the pace of sea ice loss. The response to the external forcing does change with season and region: the winter trends are dominated by the Barents-Kara Seas and the Greenland ice zone, while the summer trends are driven by the East Siberian and Beaufort-Chukchi Seas. Most models underestimate ice loss in all regions particularly in summer while in the Greenland zone, they tend to simulate more negative trends which results in an overestimation of the Arctic-wide SIA trend in a few configurations. In this study, we find that there is no strong relationship between ocean/atmosphere resolution and sea ice cover representation: the impact of horizontal resolution rather depends on the examined characteristic and the model used. However, the ocean has a stronger effect than the atmosphere, and the increase in the ocean resolution from $\sim 1^{\circ}$ to $\sim 0.25^{\circ}$ has favourable impact on the representation of SIA and sea ice edges which is especially evident for ECMWF-IFS and HadGEM3. At the same time, the simulation of SIT does not directly rely on the grid spacing affecting simulated SIV, the variable which represents the real amount of sea ice. A finer ocean resolution leads to lower SIV for ECMWF-IFS and almost no differences for HadGEM3. Increasing resolution both in the ocean and atmosphere results in little difference between configurations in CNRM and higher SIV for EC-Earth3P. On the other hand, enhanced atmosphere resolution leads to higher SIV for ECMWF-IFS and CMCC-CM2 and lower SIV for HadGEM3 and MPI-ESM. We also find that the difference between the configurations varies from one region to another which highlights the importance to examine the model performance at the regional scale. For example, CMCC-CM2 HR4 has too low SIA and SIV in the Barents Sea, which is caused by increased OHT at the Barents Sea Opening (Docquier et al., 2020) while in the rest of the sectors the model performs well relative to the observations. On the other hand, MPI-ESM has similar SIA in two configurations in the Barents-Kara Seas and the Greenland ice zone, while in the rest of the regions, the finer atmosphere configuration produces less ice in summer. For the period 2015-2050, all models simulate a long-term decrease in SIA and SIV with a generally stronger rate of ice loss compared to the historical period. The Arctic loses nearly 95% of SIV from 1950 to 2050 in the model simulations. There is again no systematic impact of horizontal resolution on the timing of first ice-free conditions. The multi-model mean of all the models does not project the Arctic to become ice-free before 2050. However, applying the model selection based on historical performance advances the timing of the event up to 2047. Considering that the model selection leads to closer agreement

with CDR on the year of ice-free summer in the regions where it already happened based on our criteria (the East Siberian, Barents and Kara, and the Laptev Sea),s.we assume that applying model selection may potentially improve the accuracy of model projections of future Arctic sea ice evolution. Together with the overall ice shrinking, we find the changes in the structure of sea ice cover: by 2050 the MIZ constitutes up to 60-80% of the September SIA. This suggests a shift to a new sea ice regime similar to that in the Antarctic. Given that the MIZ will play a major role in the response of the Arctic sea ice to external forcing, modifications in the model physics and parametrizations are needed in new generations of coupled climate models.

Summary

The overall objective of this dissertation is to improve our knowledge of the temporal and spatial variability of sea-ice properties in the Arctic and Antarctic regions. The thesis examines the performance of state-of-the-art global ocean reanalyses and the last generation of coupled climate models to reproduce observed sea ice records and to project future sea ice evolution. The consistent evaluation of the model's ability in reproducing the sea-ice state and its temporal/spatial variability is needed to enhance the model representation of sea-ice properties and increase the trustworthiness of future projections. This dissertation identifies the shortcomings of numerical systems which can be useful for modelling community and can have implications for improving the model performance.

- The results of the thesis highlight the necessity to distinguish between sea ice classes both in order to investigate sea-ice changes and to assess the quality of numerical systems. The focus on sea-ice classes instead of total sea-ice cover improves our understanding of sea-ice changes and might shed the light on the mechanisms driving sea-ice variability.
- Global ocean reanalyses are able to reasonably simulate observed Antarctic sea-ice area variability in time and space within consolidated pack ice and marginal ice zone. The reanalysis performance varies with a sub-region which is attributed to the proportion of sea ice classes in the regions.
- The fidelity of the ensemble-mean approach is proved as it allows to minimize errors from individual ensemble members providing the most robust and consistent estimates of recent changes in Antarctica. The quality of GREP is generally comparable to that of satellite data sets with regard to sea ice concentration and associated metrics therefore GREP can be used in a wide range of applications.
- Coupled climate models can adequately reproduce historical seasonal variability in the sea-ice area and sea-ice volume capturing generally the winter maximum and summer minimum, although they exhibit a large inter-model spread, particularly in the Antarctic.
- There is no unambiguous relationship between ocean/atmosphere grid resolutions and sea ice representation: the impact of horizontal resolution rather depends on the examined ice characteristic and the model used. However, the refinement of the ocean mesh has a more prominent effect compared to the atmosphere. The evident impact of increased ocean resolution is observed in the Arctic for winter sea-ice area with more realistic values in high-resolution model configurations.

- All models are able to simulate sea-ice loss in recent years in the Arctic while they generally fail to reproduce the overall expansion trend in the Antarctic. The increased horizontal resolution does not improve the realism of the sea ice long-term variability in both hemispheres.
- A reasonable simulation of sea-ice thickness is still challenging in both hemispheres. Inaccurate sea-ice thickness is an obstacle to a realistic representation of sea-ice properties and reliable predictions of future sea-ice evolution.
- The proper simulation of the marginal ice zone is fundamental for robust predictions of sea ice conditions. Given that the marginal ice zone will dominate the Arctic sea ice cover in the near future, the model physics might require adaptation to a new sea-ice regime.

Bibliography

Abernathey, R. P., Cerovecki, I., Holland, P. R., Newsom, E., Mazloff, M., and Talley, L. D.: Water-mass transformation by sea ice in the upper branch of the Southern Ocean overturning, Nature Geoscience, 9, 596–601, doi:10.1038/ngeo2749, URL https://doi.org/10.1038/ngeo2749, 2016.

Aksenov, Y., Popova, E. E., Yool, A., Nurser, A. J., Williams, T. D., Bertino, L., and Bergh, J.: On the future navigability of Arctic sea routes: High-resolution projections of the Arctic Ocean and sea ice, Marine Policy, 75, 300–317, doi:10.1016/J.MARPOL.2015.12.027, 2017.

Alberello, A., Onorato, M., Bennetts, L., Vichi, M., Eayrs, C., MacHutchon, K., and Toffoli, A.: Brief communication: Pancake ice floe size distribution during the winter expansion of the Antarctic marginal ice zone, The Cryosphere, 13, 41–48, doi:10.5194/tc-13-41-2019, URL https://tc.copernicus.org/articles/13/41/2019/, 2019.

Alexandrov, V., Sandven, S., Wahlin, J., and Johannessen, O. M.: The relation between sea ice thickness and freeboard in the Arctic, The Cryosphere, 4, 373–380, doi:10.5194/tc-4-373-2010, URL https://tc.copernicus.org/articles/4/373/2010/, 2010.

Alizadeh, O.: Advances and challenges in climate modeling, Climatic Change, 170, 18, doi:10.1007/s10584-021-03298-4, URL https://doi.org/10.1007/s10584-021-03298-4, 2022.

Armour, K. C., Marshall, J., Scott, J. R., Donohoe, A., and Newsom, E. R.: Southern Ocean warming delayed by circumpolar upwelling and equatorward transport, Nature Geoscience, 9, 549–554, doi:10.1038/ngeo2731, 2016.

Árthun, M., Onarheim, I. H., Dörr, J., and Eldevik, T.: The Seasonal and Regional Transition to an Ice-Free Arctic, Geophysical Research Letters, 48, e2020GL090 825, doi:https://doi.org/10.1029/2020GL090825, URL https://agupubs.onlinelibrary.wiley.com/doi/abs/10.1029/2020GL090825, e2020GL090825 2020GL090825, 2021.

Bador, M., Boé, J., Terray, L., Alexander, L. V., Baker, A., Bellucci, A., Haarsma, R., Koenigk, T., Moine, M.-P., Lohmann, K., Putrasahan, D. A., Roberts, C., Roberts, M., Scoccimarro, E., Schiemann, R., Seddon, J., Senan, R., Valcke, S., and Vanniere, B.: Impact of Higher Spatial Atmospheric Resolution on Precipitation Extremes Over Land in Global Climate Models, Journal of Geophysical Research: Atmospheres, 125, e2019JD032 184, doi:https://doi.org/10.1029/2019JD032184, URL https://agupubs.onlinelibrary.wiley.com/doi/abs/10.1029/2019JD032184, e2019JD032184 2019JD032184, 2020.

Balsamo, G., Viterbo, P., Beijaars, A., van den Hurk, B., Hirschi, M., Betts, A. K., and Scipal, K.: A revised hydrology for the ECMWF model: Verification from field site to terrestrial water storage and impact in the integrated forecast system, Journal of Hydrometeorology, 10, 623–643, doi:10.1175/2008JHM1068.1, 2009.

Beadling, R. L., Russell, J. L., Stouffer, R. J., Goodman, P. J., and Mazloff, M.: Assessing

the Quality of Southern Ocean Circulation in CMIP5 AOGCM and Earth System Model Simulations, Journal of Climate, 32, 5915 – 5940, doi:10.1175/JCLI-D-19-0263.1, URL https://journals.ametsoc.org/view/journals/clim/32/18/jcli-d-19-0263.1.xml, 2019.

Beadling, R. L., Russell, J. L., Stouffer, R. J., Mazloff, M., Talley, L. D., Goodman, P. J., Sallée, J. B., Hewitt, H. T., Hyder, P., and Pandde, A.: Representation of Southern Ocean Properties across Coupled Model Intercomparison Project Generations: CMIP3 to CMIP6, Journal of Climate, 33, 6555 – 6581, doi:10.1175/JCLI-D-19-0970.1, URL https://journals.ametsoc.org/view/journals/clim/33/15/jcliD190970.xml, 2020.

Best, M. J., Pryor, M., Clark, D. B., Rooney, G. G., Essery, R. L. H., Ménard, C. B., Edwards, J. M., Hendry, M. A., Porson, A., Gedney, N., Mercado, L. M., Sitch, S., Blyth, E., Boucher, O., Cox, P. M., Grimmond, C. S. B., and Harding, R. J.: The Joint UK Land Environment Simulator (JULES), model description - Part 1: Energy and water fluxes, Geoscientific Model Development, 4, 677–699, doi:10.5194/gmd-4-677-2011, 2011.

Bintanja, R., Oldenborgh, G. J. V., Drijfhout, S. S., Wouters, B., and Katsman, C. A.: Important role for ocean warming and increased ice-shelf melt in Antarctic sea-ice expansion, Nature Geoscience, 6, 376–379, doi:10.1038/ngeo1767, 2013.

Bintanja, R., Katsman, C. A., and Selten, F. M.: Increased Arctic precipitation slows down sea ice melt and surface warming, Oceanography, 31, 118–125, URL https://www.jstor.org/stable/26542658, 2018.

Blanchard-Wrigglesworth, E., Roach, L. A., Donohoe, A., and Ding, Q.: Impact of Winds and Southern Ocean SSTs on Antarctic Sea Ice Trends and Variability, Journal of Climate, 34, 949 – 965, doi:10.1175/JCLI-D-20-0386.1, URL https://journals.ametsoc.org/view/journals/clim/34/3/JCLI-D-20-0386.1.xml, 2021.

Boeke, R. C. and Taylor, P. C.: Seasonal energy exchange in sea ice retreat regions contributes to differences in projected Arctic warming, Nature Communications, 9, doi:10.1038/s41467-018-07061-9, 2018.

Bracegirdle, T. J., Shuckburgh, E., Sallee, J.-B., Wang, Z., Meijers, A. J. S., Bruneau, N., Phillips, T., and Wilcox, L. J.: Assessment of surface winds over the Atlantic, Indian, and Pacific Ocean sectors of the Southern Ocean in CMIP5 models: historical bias, forcing response, and state dependence, Journal of Geophysical Research: Atmospheres, 118, 547–562, doi:https://doi.org/10.1002/jgrd.50153, URL https://agupubs.onlinelibrary.wiley.com/doi/abs/10.1002/jgrd.50153, 2013.

Bracegirdle, T. J., Krinner, G., Tonelli, M., Haumann, F. A., Naughten, K. A., Rackow, T., Roach, L. A., and Wainer, I.: Twenty first century changes in Antarctic and Southern Ocean surface climate in CMIP6, Atmospheric Science Letters, 21, e984, doi:https://doi.org/10.1002/asl.984, URL https://rmets.onlinelibrary.wiley.com/doi/abs/10.1002/asl.984, 2020.

Brodzik, M. J. and Stewart, J. S.: Near-Real-Time SSM/I-SSMIS EASE-Grid Daily Global Ice Concentration and Snow Extent, Version 5, 2016.

Bronselaer, B., Winton, M., Griffies, S. M., Hurlin, W. J., Rodgers, K. B., Sergienko, O. V., Stouffer, R. J., and Russell, J. L.: Change in future climate due to Antarctic meltwater, Nature, 564, 53–58, doi:10.1038/s41586-018-0712-z, URL https://doi.org/10.1038/s41586-018-0712-z, 2018.

Brouwer, J., Fraser, A. D., Murphy, D. J., Wongpan, P., Alberello, A., Kohout, A., Horvat, C., Wotherspoon, S., Massom, R. A., Cartwright, J., Williams, G. D., and AlexanderFraser, A. F.: Altimetric observation of wave attenuation through the Antarctic marginal ice zone using ICESat-2, doi:10.5194/tc-2021-367, URL https://doi.org/10.5194/tc-2021-367, 2021.

Carmack, E., Polyakov, I., Padman, L., Fer, I., Hunke, E., Hutchings, J., Jackson, J., Kelley, D., Kwok, R., Layton, C., Melling, H., Perovich, D., Persson, O., Ruddick, B., Timmermans, M. L., Toole, J., Ross, T., Vavrus, S., and Winsor, P.: Toward quantifying the increasing role of oceanic heat in sea ice loss in the new Arctic, Bulletin of the American Meteorological Society, 96, 2079–2105, doi:10.1175/BAMS-D-13-00177.1, 2015.

Caton Harrison, T., Biri, S., Bracegirdle, T. J., King, J. C., Kent, E. C., Vignon, E., and Turner, J.: Reanalysis representation of low-level winds in the Antarctic near-coastal region, Weather and Climate Dynamics, 3, 1415–1437, doi:10.5194/wcd-3-1415-2022, URL https://wcd.copernicus.org/articles/3/1415/2022/, 2022.

Cavalieri, D. and Martin, S.: THE CONTRIBUTION OF ALASKAN, SIBERIAN, AND CANADIAN COASTAL POLYNYAS TO THE COLD HALOCLINE LAYER OF THE ARCTIC-OCEAN, JOURNAL OF GEOPHYSICAL RESEARCH-OCEANS, 99, 18 343–18 362, doi:10.1029/94JC01169, 1994.

Cavalieri, D. J., Gloersen, P., and Campbell, W. J.: Determination of sea ice parameters with the NIMBUS 7 SMMR, Journal of Geophysical Research: Atmospheres, 89, 5355–5369, doi:https://doi.org/10.1029/JD089iD04p05355, URL https://agupubs.onlinelibrary.wiley.com/doi/abs/10.1029/JD089iD04p05355, 1984.

Cavalieri, D. J., Parkinson, C. L., Gloersen, P., Comiso, J. C., and Zwally, H. J.: Deriving long-term time series of sea ice cover from satellite passive-microwave multisensor data sets, Journal of Geophysical Research: Oceans, 104, 15 803–15 814, doi:https://doi.org/10.1029/1999JC900081, URL https://agupubs.onlinelibrary.wiley.com/doi/abs/10.1029/1999JC900081, 1999.

Cavanagh, R. D., Murphy, E. J., Bracegirdle, T. J., Turner, J., Knowland, C. A., Corney, S. P., Smith, W. O., Waluda, C. M., Johnston, N. M., Bellerby, R. G. J., Constable, A. J., Costa, D. P., Hofmann, E. E., Jackson, J. A., Staniland, I. J., Wolf-Gladrow, D., and Xavier, J. C.: A Synergistic Approach for Evaluating Climate Model Output for Ecological Applications, Frontiers in Marine Science, 4, doi:10.3389/fmars.2017.00308, URL https://www.frontiersin.org/articles/10.3389/fmars.2017.00308, 2017.

Ceppi, P., Hwang, Y.-T., Frierson, D. M. W., and Hartmann, D. L.: Southern Hemisphere jet latitude biases in CMIP5 models linked to shortwave cloud forcing, Geophysical Research Letters, 39, doi:https://doi.org/10.1029/2012GL053115, URL https://agupubs.

onlinelibrary.wiley.com/doi/abs/10.1029/2012GL053115, 2012.

Cherchi, A., Fogli, P. G., Lovato, T., Peano, D., Iovino, D., Gualdi, S., Masina, S., Scoccimarro, E., Materia, S., Bellucci, A., and Navarra, A.: Global Mean Climate and Main Patterns of Variability in the CMCC-CM2 Coupled Model, Journal of Advances in Modeling Earth Systems, 11, 185–209, doi:10.1029/2018MS001369, 2019.

Chevallier, M., Smith, G. C., Dupont, F., Lemieux, J.-F., Forget, G., Fujii, Y., Hernandez, F., Msadek, R., Peterson, K. A., Storto, A., Toyoda, T., Valdivieso, M., Vernieres, G., Zuo, H., Balmaseda, M., Chang, Y.-S., Ferry, N., Garric, G., Haines, K., Keeley, S., Kovach, R. M., Kuragano, T., Masina, S., Tang, Y., Tsujino, H., and Wang, X.: Intercomparison of the Arctic sea ice cover in global ocean-sea ice reanalyses from the ORA-IP project, Climate Dynamics, 49, 1107–1136, doi:10.1007/s00382-016-2985-y, URL https://doi.org/10.1007/s00382-016-2985-y, 2017.

Chung, E. S., Ha, K. J., Timmermann, A., Stuecker, M. F., Bodai, T., and Lee, S. K.: Cold-Season Arctic Amplification Driven by Arctic Ocean-Mediated Seasonal Energy Transfer, Earth's Future, 9, doi:10.1029/2020EF001898, 2021.

Comiso, J. C.: Characteristics of Arctic winter sea ice from satellite multispectral microwave observations, Journal of Geophysical Research: Oceans, 91, 975–994, doi:https://doi.org/10.1029/JC091iC01p00975, URL https://agupubs.onlinelibrary.wiley.com/doi/abs/10.1029/JC091iC01p00975, 1986.

Cullen, M. J. P.: The unified forecast climate model, Meteorological Magazine, 122, 81–94, 1993.

Curtis, P. E., Ceppi, P., and Zappa, G.: Role of the mean state for the Southern Hemispheric jet stream response to CO2 forcing in CMIP6 models, Environmental Research Letters, 15, 64 011, doi:10.1088/1748-9326/ab8331, URL https://dx.doi.org/10.1088/1748-9326/ab8331, 2020.

Davy, R. and Outten, S.: The Arctic Surface Climate in CMIP6: Status and Developments since CMIP5, Journal of Climate, 33, 8047 – 8068, doi:https://doi.org/10.1175/JCLI-D-19-0990.1, URL https://journals.ametsoc.org/view/journals/clim/33/18/jcliD190990.xml, 2020.

Day, J. J., Tietsche, S., and Hawkins, E.: Pan-Arctic and Regional Sea Ice Predictability: Initialization Month Dependence, Journal of Climate, 27, 4371 – 4390, doi:10.1175/JCLI-D-13-00614.1, URL https://journals.ametsoc.org/view/journals/clim/27/12/jcli-d-13-00614.1.xml, 2014.

Dee, D. P., Uppala, S. M., Simmons, A. J., Berrisford, P., Poli, P., Kobayashi, S., Andrae, U., Balmaseda, M. A., Balsamo, G., d P Bauer, et al.: The ERA-Interim reanalysis: Configuration and performance of the data assimilation system, Quarterly Journal of the royal meteorological society, 137, 553–597, 2011.

Dee, D. P., Balmaseda, M., Balsamo, G., Engelen, R., Simmons, A. J., and Thépaut, J.-N.: Toward a Consistent Reanalysis of the Climate System, Bulletin of the American Meteorological Society, 95, 1235 – 1248, doi:10.1175/BAMS-D-13-00043.1, URL https:

//journals.ametsoc.org/view/journals/bams/95/8/bams-d-13-00043.1.xml, 2014.

Dickson, R. R., Meincke, J., Malmberg, S.-A., and Lee, A. J.: The "great salinity anomaly" in the Northern North Atlantic 1968-1982, Progress in Oceanography, 20, 103–151, doi:https://doi.org/10.1016/0079-6611(88)90049-3, 1988.

Docquier, D. and Koenigk, T.: Observation-based selection of climate models projects Arctic ice-free summers around 2035, Communications Earth & Environment, 2, 144, doi:10.1038/s43247-021-00214-7, URL https://doi.org/10.1038/s43247-021-00214-7, 2021.

Docquier, D., Grist, J. P., Roberts, M. J., Roberts, C. D., Semmler, T., Ponsoni, L., Massonnet, F., Sidorenko, D., Sein, D. V., Iovino, D., Bellucci, A., and Fichefet, T.: Impact of model resolution on Arctic sea ice and North Atlantic Ocean heat transport, Climate Dynamics, 53, 4989–5017, doi:10.1007/s00382-019-04840-y, URL https://doi.org/10.1007/s00382-019-04840-y, 2019.

Docquier, D., Fuentes-Franco, R., Koenigk, T., and Fichefet, T.: Sea Ice-Ocean Interactions in the Barents Sea Modeled at Different Resolutions, Frontiers in Earth Science, 8, doi:10.3389/feart.2020.00172, URL https://www.frontiersin.org/articles/10.3389/feart.2020.00172, 2020.

Döscher, R., Vihma, T., and Maksimovich, E.: Recent advances in understanding the Arctic climate system state and change from a sea ice perspective: A review, doi:10.5194/acp-14-13571-2014, 2014.

Dumont, D., Kohout, A., and Bertino, L.: A wave-based model for the marginal ice zone including a floe breaking parameterization, J. Geophys. Res., 116, C04 001, 2011.

DuVivier, A. K., Holland, M. M., Kay, J. E., Tilmes, S., Gettelman, A., and Bailey, D. A.: Arctic and Antarctic Sea Ice Mean State in the Community Earth System Model Version 2 and the Influence of Atmospheric Chemistry, Journal of Geophysical Research: Oceans, 125, doi:10.1029/2019JC015934, 2020.

Eayrs, C., Holland, D., Francis, D., Wagner, T., Kumar, R., and Li, X.: Understanding the Seasonal Cycle of Antarctic Sea Ice Extent in the Context of Longer-Term Variability, Reviews of Geophysics, 57, 1037–1064, doi:https://doi.org/10.1029/2018RG000631, URL https://agupubs.onlinelibrary.wiley.com/doi/abs/10.1029/2018RG000631, 2019.

Eayrs, C., Li, X., Raphael, M. N., and Holland, D. M.: Rapid decline in Antarctic sea ice in recent years hints at future change, doi:10.1038/s41561-021-00768-3, 2021.

Enomoto, H. and Ohmura, A.: The influences of atmospheric half-yearly cycle on the sea ice extent in the Antarctic, Journal of Geophysical Research: Oceans, 95, 9497–9511, doi:https://doi.org/10.1029/JC095iC06p09497, URL https://agupubs.onlinelibrary.wiley.com/doi/abs/10.1029/JC095iC06p09497, 1990.

Eyring, V., Bony, S., Meehl, G. A., Senior, C. A., Stevens, B., Stouffer, R. J., and Taylor, K. E.: Overview of the Coupled Model Intercomparison Project Phase 6 (CMIP6) experimental design and organization, Geoscientific Model Development, 9, 1937–1958, doi:10.5194/gmd-9-1937-2016, 2016.

Ezraty, R., Girard-Ardhuin, F., Piolle, J.-f., Kaleschke, L., and Heygster, G.: Arctic & Antarctic sea ice concentration and Arctic sea ice drift estimated from Special Sensor MIcrowave data - User's manual V2.1, 2007.

Fichefet, T. and Maqueda, M. A.: Sensitivity of a global sea ice model to the treatment of ice thermodynamics and dynamics, Journal of Geophysical Research: Oceans, 102, 12 609–12 646, doi:10.1029/97JC00480, 1997.

Fuentes-Franco, R. and Koenigk, T.: Sensitivity of the Arctic freshwater content and transport to model resolution, Climate Dynamics, 53, 1765–1781, doi:10.1007/s00382-019-04735-y, URL https://doi.org/10.1007/s00382-019-04735-y, 2019.

Goessling, H. F., Tietsche, S., Day, J. J., Hawkins, E., and Jung, T.: Predictability of the Arctic sea ice edge, Geophysical Research Letters, 43, 1642–1650, doi:https://doi.org/10.1002/2015GL067232, URL https://agupubs.onlinelibrary.wiley.com/doi/abs/10.1002/2015GL067232, 2016.

Good, S., Fiedler, E., Mao, C., Martin, M. J., Maycock, A., Reid, R., Roberts-Jones, J., Searle, T., Waters, J., While, J., and Worsfold, M.: The Current Configuration of the OSTIA System for Operational Production of Foundation Sea Surface Temperature and Ice Concentration Analyses, Remote Sensing, 12, doi:10.3390/rs12040720, URL https://www.mdpi.com/2072-4292/12/4/720, 2020.

Goosse, H. and Zunz, V.: Decadal trends in the Antarctic sea ice extent ultimately controlled by ice-ocean feedback, Cryosphere, 8, 453–470, doi:10.5194/tc-8-453-2014, 2014.

Goosse, H., Kay, J. E., Armour, K. C., Bodas-Salcedo, A., Chepfer, H., Docquier, D., Jonko, A., Kushner, P. J., Lecomte, O., Massonnet, F., Park, H.-S., Pithan, F., Svensson, G., and Vancoppenolle, M.: Quantifying climate feedbacks in polar regions, Nature Communications, 9, 1919, doi:10.1038/s41467-018-04173-0, URL https://doi.org/10.1038/s41467-018-04173-0, 2018.

Gordon, A. L.: Seasonality of Southern Ocean sea ice, Journal of Geophysical Research: Oceans, 86, 4193–4197, doi:https://doi.org/10.1029/JC086iC05p04193, URL https://agupubs.onlinelibrary.wiley.com/doi/abs/10.1029/JC086iC05p04193, 1981.

Gorman, K. B., Ruck, K. E., Williams, T. D., and Fraser, W. R.: Advancing the Sea Ice Hypothesis: Trophic Interactions Among Breeding Pygoscelis Penguins With Divergent Population Trends Throughout the Western Antarctic Peninsula, Frontiers in Marine Science, 8, doi:10.3389/fmars.2021.526092, URL https://www.frontiersin.org/article/10.3389/fmars.2021.526092, 2021.

Graversen, R. G. and Burtu, M.: Arctic amplification enhanced by latent energy transport of atmospheric planetary waves, Quarterly Journal of the Royal Meteorological Society, 142, 2046–2054, doi:10.1002/qj.2802, 2016.

Grist, J. P., Josey, S. A., New, A. L., Roberts, M., Koenigk, T., and Iovino, D.: Increasing Atlantic Ocean Heat Transport in the Latest Generation Coupled Ocean-Atmosphere Models: The Role of Air-Sea Interaction, Journal of Geophysical Research: Oceans, 123, 8624–8637,

doi:https://doi.org/10.1029/2018JC014387, URL https://agupubs.onlinelibrary.wiley.com/doi/abs/10.1029/2018JC014387, 2018.

Guemas, V., Chevallier, M., Déqué, M., Bellprat, O., and Doblas-Reyes, F.: Impact of sea ice initialization on sea ice and atmosphere prediction skill on seasonal timescales, Geophysical Research Letters, 43, 3889–3896, doi:https://doi.org/10.1002/2015GL066626, URL https://agupubs.onlinelibrary.wiley.com/doi/abs/10.1002/2015GL066626, 2016.

Gupta, A. S., Stellema, A., Pontes, G. M., Taschetto, A. S., Vergés, A., and Rossi, V.: Future changes to the upper ocean Western Boundary Currents across two generations of climate models, Scientific Reports, 11, 9538, doi:10.1038/s41598-021-88934-w, URL https://doi.org/10.1038/s41598-021-88934-w, 2021.

Haarsma, R., Acosta, M., Bakhshi, R., Bretonniére, P. A., Caron, L. P., Castrillo, M., Corti, S., Davini, P., Exarchou, E., Fabiano, F., Fladrich, U., Franco, R. F., Garciá-Serrano, J., Hardenberg, J. V., Koenigk, T., Levine, X., Meccia, V. L., Noije, T. V., Oord, G. V. D., Palmeiro, F. M., Rodrigo, M., Ruprich-Robert, Y., Sager, P. L., Tourigny, E., Wang, S., Weele, M. V., and Wyser, K.: HighResMIP versions of EC-Earth: EC-Earth3P and EC-Earth3P-HR - Description, model computational performance and basic validation, Geoscientific Model Development, 13, 3507–3527, doi:10.5194/gmd-13-3507-2020, 2020.

Haarsma, R. J., Roberts, M. J., Vidale, P. L., Catherine, A., Bellucci, A., Bao, Q., Chang, P., Corti, S., ckar, N. S. F., Guemas, V., Hardenberg, J. V., Hazeleger, W., Kodama, C., Koenigk, T., Leung, L. R., Lu, J., Luo, J. J., Mao, J., Mizielinski, M. S., Mizuta, R., Nobre, P., Satoh, M., Scoccimarro, E., Semmler, T., Small, J., and Storch, J. S. V.: High Resolution Model Intercomparison Project (HighResMIP v1.0) for CMIP6, Geoscientific Model Development, 9, 4185–4208, doi:10.5194/gmd-9-4185-2016, 2016.

Haid, V., Iovino, D., and Masina, S.: Impacts of freshwater changes on Antarctic sea ice in an eddy-permitting sea-ice-ocean model, Cryosphere, 11, 1387–1402, doi:10.5194/tc-11-1387-2017, 2017.

Haine, T. W. N., Curry, B., Gerdes, R., Hansen, E., Karcher, M., Lee, C., Rudels, B., Spreen, G., de Steur, L., Stewart, K. D., and Woodgate, R.: Arctic freshwater export: Status, mechanisms, and prospects, GLOBAL AND PLANETARY CHANGE, 125, 13–35, doi:10.1016/j.gloplacha.2014.11.013, 2015.

Henderson, G. R., Barrett, B. S., Wachowicz, L. J., Mattingly, K. S., Preece, J. R., and Mote, T. L.: Local and Remote Atmospheric Circulation Drivers of Arctic Change: A Review, doi:10.3389/feart.2021.709896, 2021.

Hersbach, H., Bell, B., Berrisford, P., Hirahara, S., Horányi, A., noz Sabater, J. M., Nicolas, J., Peubey, C., Radu, R., Schepers, D., Simmons, A., Soci, C., Abdalla, S., Abellan, X., Balsamo, G., Bechtold, P., Biavati, G., Bidlot, J., Bonavita, M., Chiara, G. D., Dahlgren, P., Dee, D., Diamantakis, M., Dragani, R., Flemming, J., Forbes, R., Fuentes, M., Geer, A., Haimberger, L., Healy, S., Hogan, R. J., Hólm, E., Janisková, M., Keeley, S., Laloyaux, P., Lopez, P., Lupu, C., Radnoti, G., de Rosnay, P., Rozum, I., Vamborg, F., Villaume, S., and Thépaut,

J.-N.: The ERA5 global reanalysis, Quarterly Journal of the Royal Meteorological Society, 146, 1999–2049, doi:https://doi.org/10.1002/qj.3803, URL https://rmets.onlinelibrary.wiley.com/doi/abs/10.1002/qj.3803, 2020.

Hobbs, W. R., Massom, R., Stammerjohn, S., Reid, P., Williams, G., and Meier, W.: A review of recent changes in Southern Ocean sea ice, their drivers and forcings, Global and Planetary Change, 143, 228–250, doi:10.1016/j.gloplacha.2016.06.008, URL http://dx.doi.org/10.1016/j.gloplacha.2016.06.008, 2016.

Holland, P. R.: The seasonality of Antarctic sea ice trends, Geophysical Research Letters, 41, 4230–4237, doi:https://doi.org/10.1002/2014GL060172, URL https://agupubs.onlinelibrary.wiley.com/doi/abs/10.1002/2014GL060172, 2014.

Holland, P. R. and Kwok, R.: Wind-driven trends in Antarctic sea-ice drift, Nature Geoscience, 5, 872–875, doi:10.1038/ngeo1627, 2012.

Holmes, C. R., Holland, P. R., and Bracegirdle, T. J.: Compensating Biases and a Noteworthy Success in the CMIP5 Representation of Antarctic Sea Ice Processes, Geophysical Research Letters, 46, 4299–4307, doi:https://doi.org/10.1029/2018GL081796, URL https://agupubs.onlinelibrary.wiley.com/doi/abs/10.1029/2018GL081796, 2019.

Holmes, C. R., Bracegirdle, T. J., and Holland, P. R.: Antarctic Sea Ice Projections Constrained by Historical Ice Cover and Future Global Temperature Change, Geophysical Research Letters, 49, e2021GL097 413, doi:https://doi.org/10.1029/2021GL097413, URL https://agupubs.onlinelibrary.wiley.com/doi/abs/10.1029/2021GL097413, e2021GL097413 2021GL097413, 2022.

Holmes, R., McClelland, J., Peterson, B., Tank, S., Bulygina, E., Eglinton, T., Gordeev, V., Gurtovaya, T., Raymond, P., Repeta, D., Staples, R., Striegl, R., Zhulidov, A., and Zimov, S.: Seasonal and Annual Fluxes of Nutrients and Organic Matter from Large Rivers to the Arctic Ocean and Surrounding Seas, Estuaries and Coasts, 35, 369–382, doi:10.1007/s12237-011-9386-6, 2012.

Horvat, C.: Marginal ice zone fraction benchmarks sea ice and climate model skill, Nature Communications, 12, 2221, doi:10.1038/s41467-021-22004-7, URL https://doi.org/10.1038/s41467-021-22004-7, 2021.

Huai, B., Wang, Y., Ding, M., Zhang, J., and Dong, X.: An assessment of recent global atmospheric reanalyses for Antarctic near surface air temperature, Atmospheric Research, 226, 181–191, doi:https://doi.org/10.1016/j.atmosres.2019.04.029, URL https://www.sciencedirect.com/science/article/pii/S016980951930016X, 2019.

Hunke, E.: Thickness sensitivities in the CICE sea ice model, Ocean Modelling - OCEAN MODEL, 34, 137–149, doi:10.1016/j.ocemod.2010.05.004, 2010.

Hunke, E., Allard, R., Blain, P., Blockley, E., Feltham, D., Fichefet, T., Garric, G., Grumbine, R., Lemieux, J.-F., Rasmussen, T., Ribergaard, M., Roberts, A., Schweiger, A., Tietsche, S., Tremblay, B., Vancoppenolle, M., and Zhang, J.: Should Sea-Ice Modeling Tools Designed for Climate Research Be Used for Short-Term Forecasting?, Current Climate Change

Reports, 6, 121–136, doi:10.1007/s40641-020-00162-y, URL https://doi.org/10.1007/s40641-020-00162-y, 2020.

Huot, P. V., Kittel, C., Fichefet, T., Jourdain, N. C., and Fettweis, X.: Effects of ocean mesoscale eddies on atmosphere-sea ice-ocean interactions off Adlie Land, East Antarctica, Climate Dynamics, doi:10.1007/s00382-021-06115-x, 2022.

Hyder, P., Edwards, J. M., Allan, R. P., Hewitt, H. T., Bracegirdle, T. J., Gregory, J. M., Wood, R. A., Meijers, A. J. S., Mulcahy, J., Field, P., Furtado, K., Bodas-Salcedo, A., Williams, K. D., Copsey, D., Josey, S. A., Liu, C., Roberts, C. D., Sanchez, C., Ridley, J., Thorpe, L., Hardiman, S. C., Mayer, M., Berry, D. I., and Belcher, S. E.: Critical Southern Ocean climate model biases traced to atmospheric model cloud errors, Nature Communications, 9, 3625, doi:10.1038/s41467-018-05634-2, URL https://doi.org/10.1038/s41467-018-05634-2, 2018.

Ingvaldsen, R. B., Assmann, K. M., Primicerio, R., Fossheim, M., Polyakov, I. V., and Dolgov, A. V.: Physical manifestations and ecological implications of Arctic Atlantification, Nature Reviews Earth & Environment, 2, 874–889, doi:10.1038/s43017-021-00228-x, URL https://doi.org/10.1038/s43017-021-00228-x, 2021.

Iovino, D., Selivanova, J., Masina, S., and Cipollone, A.: The Antarctic Marginal Ice Zone and Pack Ice Area in CMEMS GREP Ensemble Reanalysis Product, Frontiers in Earth Science, 10, doi:10.3389/feart.2022.745274, URL https://www.frontiersin.org/articles/10.3389/feart.2022.745274, 2022.

Ivanov, V., Alexeev, V., Koldunov, N. V., Repina, I., Anne, ., Sandø, B., Lars, ., Smedsrud, H., and Smirnov, A.: Arctic Ocean Heat Impact on Regional Ice Decay: A Suggested Positive Feedback, doi:10.1175/JPO-D-15, URL http://dx.doi.org/10.1175/JPO-D-15-, 2016.

Ivanova, N., Pedersen, L. T., Tonboe, R. T., Kern, S., Heygster, G., Lavergne, T., Sørensen, A., Saldo, R., Dybkjær, G., Brucker, L., and Shokr, M.: Inter-comparison and evaluation of sea ice algorithms: towards further identification of challenges and optimal approach using passive microwave observations, The Cryosphere, 9, 1797–1817, doi:10.5194/tc-9-1797-2015, URL https://tc.copernicus.org/articles/9/1797/2015/, 2015.

Jackson, L. C., Roberts, M. J., Hewitt, H. T., Iovino, D., Koenigk, T., Meccia, V. L., Roberts, C. D., Ruprich-Robert, Y., and Wood, R. A.: Impact of ocean resolution and mean state on the rate of AMOC weakening, Climate Dynamics, 55, 1711–1732, doi:10.1007/s00382-020-05345-9, URL https://doi.org/10.1007/s00382-020-05345-9, 2020.

Jaiser, R., Dethloff, K., Handorf, D., Rinke, A., and Cohen, J.: Impact of sea ice cover changes on the northern hemisphere atmospheric winter circulation, Tellus, Series A: Dynamic Meteorology and Oceanography, 64, doi:10.3402/tellusa.v64i0.11595, 2012.

Jungclaus, J. H., Fischer, N., Haak, H., Lohmann, K., Marotzke, J., Matei, D., Mikolajewicz, U., Notz, D., and Storch, J. S. V.: Characteristics of the ocean simulations in the Max Planck Institute Ocean Model (MPIOM) the ocean component of the MPI-Earth system model, Journal of Advances in Modeling Earth Systems, 5, 422–446, doi:10.1002/jame.20023, 2013.

Kacimi, S. and Kwok, R.: Arctic Snow Depth, Ice Thickness, and Volume From ICESat-2 and

CryoSat-2: 2018-2021, Geophysical Research Letters, 49, doi:10.1029/2021gl097448, 2022.

Kalnay, E., Kanamitsu, M., Kistler, R., Collins, W., Deaven, D., Gandin, L., Iredell, M., Saha, S., White, G., Woollen, J., Zhu, Y., Chelliah, M., Ebisuzaki, W., Higgins, W., Janowiak, J., Mo, K. C., Ropelewski, C., Wang, J., Leetmaa, A., Reynolds, R., Jenne, R., and Joseph, D.: The NCEP/NCAR 40-Year Reanalysis Project, Bulletin of the American Meteorological Society, 77, 437 – 472, doi:10.1175/1520-0477(1996)077<0437:TNYRP>2.0.CO;2, URL https://journals.ametsoc.org/view/journals/bams/77/3/1520-0477_1996_077_0437_tnyrp_2_0_co_2.xml, 1996.

Keen, A., Blockley, E., Bailey, D. A., Debernard, J. B., Bushuk, M., Delhaye, S., Docquier, D., Feltham, D., Massonnet, F., O'Farrell, S., Ponsoni, L., Rodriguez, J. M., Schroeder, D., Swart, N., Toyoda, T., Tsujino, H., Vancoppenolle, M., and Wyser, K.: An inter-comparison of the mass budget of the Arctic sea ice in CMIP6 models, The Cryosphere, 15, 951–982, doi:10.5194/tc-15-951-2021, URL https://tc.copernicus.org/articles/15/951/2021/, 2021.

Khosravi, N., Wang, Q., Koldunov, N., Hinrichs, C., Semmler, T., Danilov, S., and Jung, T.: The Arctic Ocean in CMIP6 Models: Biases and Projected Changes in Temperature and Salinity, Earth's Future, 10, doi:10.1029/2021EF002282, 2022.

King, J. C., Marshall, G. J., Colwell, S., Arndt, S., Allen-Sader, C., and Phillips, T.: The Performance of the ERA-Interim and ERA5 Atmospheric Reanalyses Over Weddell Sea Pack Ice, Journal of Geophysical Research: Oceans, 127, e2022JC018 805, doi:https://doi.org/10.1029/2022JC018805, URL https://agupubs.onlinelibrary.wiley.com/doi/abs/10.1029/2022JC018805, e2022JC018805 2022JC018805, 2022.

Kobayashi, S., Ota, Y., Harada, Y., Ebita, A., Moriya, M., Onoda, H., Onogi, K., Kamahori, H., Kobayashi, C., Endo, H., Miyaoka, K., and Takahashi, K.: The JRA-55 Reanalysis: General Specifications and Basic Characteristics, Journal of the Meteorological Society of Japan. Ser. II, 93, 5–48, doi:10.2151/jmsj.2015-001, 2015.

Koenigk, T., Mikolajewicz, U., Haak, H., and Jungclaus, J.: Arctic freshwater export in the 20th and 21st centuries, Journal of Geophysical Research: Biogeosciences, 112, doi:10.1029/2006JG000274, 2007.

Koenigk, T., Fuentes-Franco, R., Meccia, V. L., Gutjahr, O., Jackson, L. C., New, A. L., Ortega, P., Roberts, C. D., Roberts, M. J., Arsouze, T., Iovino, D., Moine, M. P., and Sein, D. V.: Deep mixed ocean volume in the Labrador Sea in HighResMIP models, Climate Dynamics, 57, 1895–1918, doi:10.1007/s00382-021-05785-x, 2021.

Kwok, R.: Arctic sea ice thickness, volume, and multiyear ice coverage: losses and coupled variability (1958-2018), Environmental Research Letters, 13, 105 005, doi:10.1088/1748-9326/aae3ec, URL https://dx.doi.org/10.1088/1748-9326/aae3ec, 2018.

Kwok, R. and Cunningham, G. F.: ICESat over Arctic sea ice: Estimation of snow depth and ice thickness, Journal of Geophysical Research: Oceans, 113, doi:https://doi.org/10.1029/2008JC004753, URL https://agupubs.onlinelibrary.wiley.com/doi/abs/10.1029/2008JC004753, 2008.

Kwok, R. and Untersteiner, N.: The thinning of Arctic sea ice, Physics Today, 64, 36–41, doi: 10.1063/1.3580491, 2011.

Kwok, R., Spreen, G., and Pang, S.: Arctic sea ice circulation and drift speed: Decadal trends and ocean currents, Journal of Geophysical Research: Oceans, 118, 2408–2425, doi:https://doi.org/10.1002/jgrc.20191, URL https://agupubs.onlinelibrary.wiley.com/doi/abs/10.1002/jgrc.20191, 2013.

Labe, Z., Magnusdottir, G., and Stern, H.: Variability of Arctic Sea Ice Thickness Using PIOMAS and the CESM Large Ensemble, Journal of Climate, 31, 3233 – 3247, doi: 10.1175/JCLI-D-17-0436.1, URL https://journals.ametsoc.org/view/journals/clim/31/8/jcli-d-17-0436.1.xml, 2018.

Lang, A., Yang, S., and Kaas, E.: Sea ice thickness and recent Arctic warming, Geophysical Research Letters, 44, 409–418, doi:https://doi.org/10.1002/2016GL071274, URL https://agupubs.onlinelibrary.wiley.com/doi/abs/10.1002/2016GL071274, 2017.

Lavergne, T., Sorensen, A. M., Kern, S., Tonboe, R., Notz, D., Aaboe, S., Bell, L., r, G. D., Eastwood, S., Gabarro, C., Heygster, G., Killie, M. A., Kreiner, M. B., Lavelle, J., Saldo, R., Sandven, S., and Pedersen, L. T.: Version 2 of the EUMETSAT OSI SAF and ESA CCI sea-ice concentration climate data records, The Cryosphere, 13, 49–78, doi:10.5194/tc-13-49-2019, URL https://tc.copernicus.org/articles/13/49/2019/, 2019.

Laxon, S. W., Giles, K. A., Ridout, A. L., Wingham, D. J., Willatt, R., Cullen, R., Kwok, R., Schweiger, A., Zhang, J., Haas, C., Hendricks, S., Krishfield, R., Kurtz, N., Farrell, S., and Davidson, M.: CryoSat-2 estimates of Arctic sea ice thickness and volume, Geophysical Research Letters, 40, 732–737, doi:https://doi.org/10.1002/grl.50193, URL https://agupubs.onlinelibrary.wiley.com/doi/abs/10.1002/grl.50193, 2013.

Lecomte, O., Goosse, H., Fichefet, T., Holland, P., Uotila, P., Zunz, V., and Kimura, N.: Impact of surface wind biases on the Antarctic sea ice concentration budget in climate models, Ocean Modelling, 105, 60–70, doi:https://doi.org/10.1016/j.ocemod.2016.08.001, URL https://www.sciencedirect.com/science/article/pii/S1463500316300774, 2016.

Lellouche, J.-M., Galloudec, O. L., Drévillon, M., Régnier, C., Greiner, E., Garric, G., Ferry, N., Desportes, C., Testut, C.-E., Bricaud, C., Bourdallé-Badie, R., Tranchant, B., Benkiran, M., Drillet, Y., Daudin, A., and Nicola, C. D.: Evaluation of global monitoring and forecasting systems at Mercator Océan, Ocean Science, 9, 57–81, doi:10.5194/os-9-57-2013, URL https://os.copernicus.org/articles/9/57/2013/, 2013.

Li, D., Zhang, R., and Knutson, T. R.: On the discrepancy between observed and CMIP5 multi-model simulated Barents Sea winter sea ice decline, Nature Communications, 8, 14 991, doi:10.1038/ncomms14991, URL https://doi.org/10.1038/ncomms14991, 2017.

Li, J., Bao, Q., Liu, Y., Wang, L., Yang, J., Wu, G., Wu, X., He, B., Wang, X., Zhang, X., Yang, Y., and Shen, Z.: Effect of horizontal resolution on the simulation of tropical cyclones in the Chinese Academy of Sciences FGOALS-f3 climate system model, Geoscientific Model Development, 14, 6113–6133, doi:10.5194/gmd-14-6113-2021, 2021.

Liao, S., Luo, H., Wang, J., Shi, Q., Zhang, J., and Yang, Q.: An evaluation of Antarctic sea-ice thickness from the Global Ice-Ocean Modeling and Assimilation System based on in-situ and satellite observations, The Cryosphere, 16, 1807–1819, doi:10.5194/tc-16-1807-2022, 2022.

Lin, X., Massonnet, F., Fichefet, T., and Vancoppenolle, M.: Impact of atmospheric forcing uncertainties on Arctic and Antarctic sea ice simulations in CMIP6 OMIP models, The Cryosphere, 17, 1935–1965, doi:10.5194/tc-17-1935-2023, URL https://tc.copernicus.org/articles/17/1935/2023/, 2023.

Lindsay, R. and Schweiger, A.: Arctic sea ice thickness loss determined using subsurface, aircraft, and satellite observations, The Cryosphere, 9, 269–283, doi:10.5194/tc-9-269-2015, URL https://tc.copernicus.org/articles/9/269/2015/, 2015.

Lohmann, K., Putrasahan, D. A., von Storch, J.-S., Gutjahr, O., Jungclaus, J. H., and Haak, H.: Response of Northern North Atlantic and Atlantic Meridional Overturning Circulation to Reduced and Enhanced Wind Stress Forcing, Journal of Geophysical Research: Oceans, 126, e2021JC017 902, doi:https://doi.org/10.1029/2021JC017902, URL https://agupubs.onlinelibrary.wiley.com/doi/abs/10.1029/2021JC017902, e2021JC017902 2021JC017902, 2021.

Long, M., Zhang, L., Hu, S., and Qian, S.: Multi-Aspect Assessment of CMIP6 Models for Arctic Sea Ice Simulation, Journal of Climate, 34, 1515 – 1529, doi:10.1175/JCLI-D-20-0522.1, URL https://journals.ametsoc.org/view/journals/clim/34/4/JCLI-D-20-0522.1.xml, 2021.

MacLachlan, C., Arribas, A., Peterson, K. A., Maidens, A., Fereday, D., Scaife, A. A., Gordon, M., Vellinga, M., Williams, A., Comer, R. E., Camp, J., Xavier, P., and Madec, G.: Global Seasonal forecast system version 5 (GloSea5): a high-resolution seasonal forecast system, Quarterly Journal of the Royal Meteorological Society, 141, 1072–1084, doi:https://doi.org/10.1002/qj.2396, URL https://rmets.onlinelibrary.wiley.com/doi/abs/10.1002/qj.2396, 2015.

Madec, G., Bourdallé-Badie, R., Chanut, J., Clementi, E., Coward, A., Ethé, C., Iovino, D., Lea, D., Lévy, C., Lovato, T., Martin, N., Masson, S., Mocavero, S., Rousset, C., Storkey, D., Müeller, S., Nurser, G., Bell, M., Samson, G., Mathiot, P., Mele, F., and Moulin, A.: NEMO ocean engine, doi:10.5281/ZENODO.6334656, URL https://zenodo.org/record/6334656, 2016.

Madec, G., Bourdallé-Badie, R., Chanut, J., Clementi, E., Coward, A., Ethé, C., Iovino, D., Lea, D., Lévy, C., Lovato, T., Martin, N., Masson, S., Mocavero, S., Rousset, C., Storkey, D., Müeller, S., Nurser, G., Bell, M., Samson, G., Mathiot, P., Mele, F., and Moulin, A.: NEMO ocean engine, doi:10.5281/ZENODO.6334656, URL https://zenodo.org/record/6334656, 2022.

Maksym, T. and Markus, T.: Antarctic sea ice thickness and snow-to-ice conversion from atmospheric reanalysis and passive microwave snow depth, Journal of Geophysical Research: Oceans, 113, doi:https://doi.org/10.1029/2006JC004085, URL https://agupubs.

onlinelibrary.wiley.com/doi/abs/10.1029/2006JC004085, 2008.

Maksym, T., Stammerjohn, S. E., Ackley, S., and Massom, R.: Antarctic sea ice- A polar opposite?, Oceanography, 25, 140–151, doi:10.5670/oceanog.2012.88, 2012.

Martinson, D. G.: Antarctic circumpolar current's role in the Antarctic ice system: An overview, Palaeogeography, Palaeoclimatology, Palaeoecology, 335-336, 71–74, doi:10.1016/J.PALAEO.2011.04.007, 2012.

Masina, S., Storto, A., Ferry, N., Valdivieso, M., Haines, K., Balmaseda, M., Zuo, H., Drevillon, M., and Parent, L.: An ensemble of eddy-permitting global ocean reanalyses from the MyOcean project, Climate Dynamics, 49, doi:10.1007/s00382-015-2728-5, 2015.

Massom, R. A. and Stammerjohn, S. E.: Antarctic sea ice change and variability - Physical and ecological implications, Polar Science, 4, 149–186, doi:https://doi.org/10.1016/j.polar.2010.05.001, URL https://www.sciencedirect.com/science/article/pii/S1873965210000411, antarctic Biology in the 21st Century - Advances in and beyond IPY, 2010.

Masson, V., Le Moigne, P., Martin, E., Faroux, S., Alias, A., Alkama, R., Belamari, S., Barbu, A., Boone, A., Bouyssel, F., Brousseau, P., Brun, E., Calvet, J.-C., Carrer, D., Decharme, B., Delire, C., Donier, S., Essaouini, K., Gibelin, A.-L., Giordani, H., Habets, F., Jidane, M., Kerdraon, G., Kourzeneva, E., Lafaysse, M., Lafont, S., Lebeaupin Brossier, C., Lemonsu, A., Mahfouf, J.-F., Marguinaud, P., Mokhtari, M., Morin, S., Pigeon, G., Salgado, R., Seity, Y., Taillefer, F., Tanguy, G., Tulet, P., Vincendon, B., Vionnet, V., and Voldoire, A.: The SURFEXv7.2 land and ocean surface platform for coupled or offline simulation of earth surface variables and fluxes, Geoscientific Model Development, 6, 929–960, doi:10.5194/gmd-6-929-2013, URL https://gmd.copernicus.org/articles/6/929/2013/, 2013.

Massonnet, F., Vancoppenolle, M., Goosse, H., Docquier, D., Fichefet, T., and Blanchard-Wrigglesworth, E.: Arctic sea-ice change tied to its mean state through thermodynamic processes, Nature Climate Change, 8, 599–603, doi:10.1038/s41558-018-0204-z, URL https://doi.org/10.1038/s41558-018-0204-z, 2018.

Mathiot, P., Jenkins, A., Harris, C., and Madec, G.: Explicit representation and parameterised impacts of under ice shelf seas in the z∗-coordinate ocean model NEMO 3.6, Geoscientific Model Development, 10, 2849–2874, doi:10.5194/gmd-10-2849-2017, 2017.

Meccia, V. L., Iovino, D., and Bellucci, A.: North Atlantic gyre circulation in PRIMAVERA models, Climate Dynamics, 56, 4075–4090, doi:10.1007/s00382-021-05686-z, URL https://doi.org/10.1007/s00382-021-05686-z, 2021.

Meehl, G. A., Boer, G. J., Covey, C., Latif, M., and Stouffer, R. J.: The Coupled Model Intercomparison Project (CMIP), Bulletin of the American Meteorological Society, 81, 313–318, doi:10.1175/1520-0477(2000)081<0313:tcmipc>2.3.co;2, 2000.

Meehl, G. A., Arblaster, J. M., Bitz, C. M., Chung, C. T. Y., and Teng, H.: Antarctic sea-ice expansion between 2000 and 2014 driven by tropical Pacific decadal climate variability, Nature Geoscience, 9, 590–595, doi:10.1038/ngeo2751, URL https://doi.org/10.1038/ngeo2751,

2016.

Meehl, G. A., Senior, C. A., Eyring, V., Flato, G., Lamarque, J.-F., Stouffer, R. J., Taylor, K. E., and Schlund, M.: Context for interpreting equilibrium climate sensitivity and transient climate response from the CMIP6 Earth system models, URL https://pcmdi.llnl.gov/mips/cmip5/availability.html., 2020.

Meier, W., Stroeve, J., and Fetterer, F.: Whither Arctic sea ice? A clear signal of decline regionally, seasonally and extending beyond the satellite record, Annals of Glaciology, 46, 428–434, doi:10.3189/172756407782871170, 2007.

Meier, W. N., Ge, P., J., S. D., and H., S. M.: Verification of a new NOAA/NSIDC passive microwave sea-ice concentration climate record, 33, 2014.

Meier, W. N., Fetterer, F., Savoie, M., Mallory, S., Duerr, R., and Stroeve, J.: NOAA/NSIDC climate data record of passive microwave sea ice concentration, version 3, Boulder, Colorado USA. NSIDC: National Snow and Ice Data Center, 10, 2017.

Meier, W. N., Fetterer, F., Windnagel, A. K., and Stewart, J. S.: NOAA/NSIDC Climate Data Record of Passive Microwave Sea Ice Concentration, Version 4, doi:10.7265/efmz-2t65, URL https://nsidc.org/data/G02202/versions/4, 2021.

Meijers, A. J. S.: The Southern Ocean in the Coupled Model Intercomparison Project phase 5, Philosophical Transactions of the Royal Society A: Mathematical, Physical and Engineering Sciences, 372, 20130 296, doi:10.1098/rsta.2013.0296, URL https://royalsocietypublishing.org/doi/abs/10.1098/rsta.2013.0296, 2014.

Moreno-Chamarro, E., Caron, L.-P., Tomas, S. L., Vegas-Regidor, J., Gutjahr, O., Moine, M.-P., Putrasahan, D., Roberts, C. D., Roberts, M. J., Senan, R., Terray, L., Tourigny, E., and Vidale, P. L.: Impact of increased resolution on long-standing biases in HighResMIP-PRIMAVERA climate models, Geoscientific Model Development, 15, 269–289, doi:10.5194/gmd-15-269-2022, URL https://gmd.copernicus.org/articles/15/269/2022/, 2022.

Morioka, Y., Iovino, D., Cipollone, A., Masina, S., and Behera, S. K.: Summertime sea-ice prediction in the Weddell Sea improved by sea-ice thickness initialization, Scientific Reports, 11, 11 475, doi:10.1038/s41598-021-91042-4, URL https://doi.org/10.1038/s41598-021-91042-4, 2021.

Muilwijk, M., Ilicak, M., Cornish, S. B., Danilov, S., Gelderloos, R., Gerdes, R., Haid, V., Haine, T. W. N., Johnson, H. L., Kostov, Y., Kovács, T., Lique, C., Marson, J. M., Myers, P. G., Scott, J., Smedsrud, L. H., Talandier, C., and Wang, Q.: Arctic Ocean Response to Greenland Sea Wind Anomalies in a Suite of Model Simulations, Journal of Geophysical Research: Oceans, 124, 6286–6322, doi:https://doi.org/10.1029/2019JC015101, URL https://agupubs.onlinelibrary.wiley.com/doi/abs/10.1029/2019JC015101, 2019.

Müller, W. A., Jungclaus, J. H., Mauritsen, T., Baehr, J., Bittner, M., Budich, R., Bunzel, F., Esch, M., Ghosh, R., Haak, H., Ilyina, T., Kleine, T., Kornblueh, L., Li, H., Modali, K., Notz, D., Pohlmann, H., Roeckner, E., Stemmler, I., Tian, F., and Marotzke, J.: A Higher-resolution Version of the Max Planck Institute Earth System Model (MPI-ESM1.2-HR), Journal of

Advances in Modeling Earth Systems, 10, 1383–1413, doi:10.1029/2017MS001217, 2018.

Neale, R. B., Richter, J., Park, S., Lauritzen, P. H., Vavrus, S. J., Rasch, P. J., and Zhang, M.: The Mean Climate of the Community Atmosphere Model (CAM4) in Forced SST and Fully Coupled Experiments, Journal of Climate, 26, 5150 – 5168, doi:10.1175/JCLI-D-12-00236.1, URL https://journals.ametsoc.org/view/journals/clim/26/14/jcli-d-12-00236.1.xml, 2013.

Newsom, E. R., Bitz, C. M., Bryan, F. O., Abernathey, R., and Gent, P. R.: Southern Ocean Deep Circulation and Heat Uptake in a High-Resolution Climate Model, Journal of Climate, 29, 2597 – 2619, doi:10.1175/JCLI-D-15-0513.1, URL https://journals.ametsoc.org/view/journals/clim/29/7/jcli-d-15-0513.1.xml, 2016.

Notz, D. and Community, S.: Arctic Sea Ice in CMIP6, Geophysical Research Letters, 47, e2019GL086 749, doi:https://doi.org/10.1029/2019GL086749, URL https://agupubs.onlinelibrary.wiley.com/doi/abs/10.1029/2019GL086749, e2019GL086749 10.1029/2019GL086749, 2020.

Notz, D. and Stroeve, J.: Observed Arctic sea-ice loss directly follows anthropogenic CO^2 emission, Science, 354, 747–750, doi:10.1126/science.aag2345, 2016.

Notz, D., Jahn, A., Holland, M., Hunke, E., Massonnet, F., Stroeve, J., Tremblay, B., and Vancoppenolle, M.: The CMIP6 Sea-Ice Model Intercomparison Project (SIMIP): understanding sea ice through climate-model simulations, Geoscientific Model Development, 9, 3427–3446, doi:10.5194/gmd-9-3427-2016, URL https://gmd.copernicus.org/articles/9/3427/2016/, 2016.

Oleson, K. W., Lead, D. M. L., Bonan, G. B., Drewniak, B., Huang, M., Koven, C. D., Levis, S., Li, F., Riley, W. J., Subin, Z. M., Swenson, S. C., Thornton, P. E., Bozbiyik, A., Fisher, R., Heald, C. L., Kluzek, E., Lamarque, J.-F., Lawrence, P. J., Leung, L. R., Lipscomb, W., Muszala, S., Ricciuto, D. M., Sacks, W., Sun, Y., Tang, J., and Yang, Z.-L.: NCAR/TN-503+STR NCAR Technical Note Technical Description of version 4.5 of the Community Land Model (CLM) Coordinating Lead Authors, URL http://library.ucar.edu/research/publish-technote, 2013.

Onarheim, I. H., Eldevik, T., Smedsrud, L. H., and Stroeve, J. C.: Seasonal and Regional Manifestation of Arctic Sea Ice Loss, Journal of Climate, 31, 4917 – 4932, doi:10.1175/JCLI-D-17-0427.1, URL https://journals.ametsoc.org/view/journals/clim/31/12/jcli-d-17-0427.1.xml, 2018.

Ordoñez, A. C., Bitz, C. M., and Blanchard-Wrigglesworth, E.: Processes Controlling Arctic and Antarctic Sea Ice Predictability in the Community Earth System Model, Journal of Climate, 31, 9771 – 9786, doi:10.1175/JCLI-D-18-0348.1, URL https://journals.ametsoc.org/view/journals/clim/31/23/jcli-d-18-0348.1.xml, 2018.

Pang, X., Pu, J., Zhao, X., Ji, Q., Qu, M., and Cheng, Z.: Comparison between AMSR2 Sea Ice Concentration Products and Pseudo-Ship Observations of the Arctic and Antarctic Sea Ice Edge on Cloud-Free Days, Remote Sensing, 10, doi:10.3390/rs10020317, URL https:

//www.mdpi.com/2072-4292/10/2/317, 2018.

Papalexiou, S. M., Rajulapati, C. R., Clark, M. P., and Lehner, F.: Robustness of CMIP6 Historical Global Mean Temperature Simulations: Trends, Long-Term Persistence, Autocorrelation, and Distributional Shape, Earth's Future, 8, e2020EF001 667, doi:https://doi.org/10.1029/2020EF001667, URL https://agupubs.onlinelibrary.wiley.com/doi/abs/10.1029/2020EF001667, e2020EF001667 2020EF001667, 2020.

Parish, T. R. and Cassano, J. J.: The Role of Katabatic Winds on the Antarctic Surface Wind Regime, monthly Weather Review, 131, 317 – 333, doi:10.1175/1520-0493(2003)131<0317:TROKWO>2.0.CO;2, URL https://journals.ametsoc.org/view/journals/mwre/131/2/1520-0493_2003_131_0317_trokwo_2.0.co_2.xml, 2003.

Park, H., Watanabe, E., Kim, Y., Polyakov, I., Oshima, K., Zhang, X., Kimball, J. S., and Yang, D.: Increasing riverine heat influx triggers Arctic sea ice decline and oceanic and atmospheric warming, Science Advances, 6, eabc4699, doi:10.1126/sciadv.abc4699, URL https://www.science.org/doi/abs/10.1126/sciadv.abc4699, 2020.

Parkinson, C. L.: A 40-y record reveals gradual Antarctic sea ice increases followed by decreases at rates far exceeding the rates seen in the Arctic, Proceedings of the National Academy of Sciences of the United States of America, 116, 14 414–14 423, doi:10.1073/pnas.1906556116, 2019.

Parkinson, C. L. and DiGirolamo, N. E.: Sea ice extents continue to set new records: Arctic, Antarctic, and global results, Remote Sensing of Environment, 267, 112 753, doi:10.1016/J.RSE.2021.112753, 2021.

Parkinson, C. L., Cavalieri, D. J., Gloersen, P., Zwally, H. J., and Comiso, J. C.: Arctic sea ice extents, areas, and trends, 1978-1996, Journal of Geophysical Research, Washington, DC, 104, 20 837–20 856, 1999.

Paul, F., Mielke, T., Schwarz, C., Schröder, J., Rampai, T., Skatulla, S., Audh, R. R., Hepworth, E., Vichi, M., and Lupascu, D. C.: Frazil Ice in the Antarctic Marginal Ice Zone, Journal of Marine Science and Engineering, 9, doi:10.3390/jmse9060647, URL https://www.mdpi.com/2077-1312/9/6/647, 2021.

Pellichero, V., Sallée, J.-B., Chapman, C. C., and Downes, S. M.: The southern ocean meridional overturning in the sea-ice sector is driven by freshwater fluxes, Nature Communications, 9, 1789, doi:10.1038/s41467-018-04101-2, URL https://doi.org/10.1038/s41467-018-04101-2, 2018.

Peng, G. and Meier, W.: Temporal and regional variability of Arctic sea-ice coverage from satellite data, Annals of Glaciology, 59, 1–10, doi:10.1017/aog.2017.32, 2017.

Perovich, D., Meier, W., Tschudi, M., Hendricks, S., Petty, A. A., Divine, D., Farrell, S., Gerland, S., Haas, C., Kaleschke, L., Pavlova, O., Ricker, R., Tian-Kunze, X., Webster, M., and Wood, K.: NOAA Arctic Report Card 2020, doi:10.25923/n170-9h57, 2020.

Polvani, L. M. and Smith, K. L.: Can natural variability explain observed Antarctic sea ice trends? New modeling evidence from CMIP5, Geophysical Research Letters, 40, 3195–3199,

doi:https://doi.org/10.1002/grl.50578, URL https://agupubs.onlinelibrary.wiley.com/doi/abs/10.1002/grl.50578, 2013.

Polvani, L. M., Waugh, D. W., Correa, G. J., and Son, S. W.: Stratospheric ozone depletion: The main driver of twentieth-century atmospheric circulation changes in the Southern Hemisphere, Journal of Climate, 24, 795–812, doi:10.1175/2010JCLI3772.1, 2011.

Polyakov, I., Pnyushkov, A., Alkire, M., Ashik, I., Baumann, T., Carmack, E., Goszczko, I., Guthrie, J., Ivanov, V., Kanzow, T., Krishfield, R., Kwok, R., Sundfjord, A., Morison, J., Rember, R., and Yulin, A.: Greater role for Atlantic inflows on sea-ice loss in the Eurasian Basin of the Arctic Ocean, Science (New York, N.Y.), 356, doi:10.1126/science.aai8204, 2017.

Ponsoni, L., Massonnet, F., Fichefet, T., Chevallier, M., and Docquier, D.: On the timescales and length scales of the Arctic sea ice thickness anomalies: A study based on 14 reanalyses, The Cryosphere, 13, 521–543, doi:10.5194/tc-13-521-2019, 2019.

Previdi, M., Smith, K. L., and Polvani, L. M.: Arctic amplification of climate change: A review of underlying mechanisms, doi:10.1088/1748-9326/ac1c29, 2021.

Purich, A., Cai, W., England, M. H., and Cowan, T.: Evidence for link between modelled trends in Antarctic sea ice and underestimated westerly wind changes, Nature Communications, 7, 10 409, doi:10.1038/ncomms10409, URL https://doi.org/10.1038/ncomms10409, 2016.

Rackow, T., Danilov, S., Goessling, H. F., Hellmer, H. H., Sein, D. V., Semmler, T., Sidorenko, D., and Jung, T.: Delayed Antarctic sea-ice decline in high-resolution climate change simulations, Nature Communications, 13, 637, doi:10.1038/s41467-022-28259-y, URL https://doi.org/10.1038/s41467-022-28259-y, 2022.

Rampal, P., Weiss, J., Dubois, C., and Campin, J.-M.: IPCC climate models do not capture Arctic sea ice drift acceleration: Consequences in terms of projected sea ice thinning and decline, Journal of Geophysical Research: Oceans, 116, doi:https://doi.org/10.1029/2011JC007110, URL https://agupubs.onlinelibrary.wiley.com/doi/abs/10.1029/2011JC007110, 2011.

Randelhoff, A., Holding, J., Janout, M., Sejr, M. K., Babin, M., éric Tremblay, J., and Alkire, M. B.: Pan-Arctic Ocean Primary Production Constrained by Turbulent Nitrate Fluxes, Frontiers in Marine Science, 7, doi:10.3389/fmars.2020.00150, URL https://www.frontiersin.org/article/10.3389/fmars.2020.00150, 2020.

Rantanen, M., Karpechko, A. Y., Lipponen, A., Nordling, K., Hyvärinen, O., Ruosteenoja, K., Vihma, T., and Laaksonen, A.: The Arctic has warmed nearly four times faster than the globe since 1979, Communications Earth & Environment, 3, 168, doi:10.1038/s43247-022-00498-3, URL https://doi.org/10.1038/s43247-022-00498-3, 2022.

Raphael, M. N., Marshall, G. J., Turner, J., Fogt, R. L., Schneider, D., Dixon, D. A., Hosking, J. S., Jones, J. M., and Hobbs, W. R.: The Amundsen Sea Low: Variability, Change, and Impact on Antarctic Climate, Bulletin of the American Meteorological Society, 97, 111 – 121, doi:10.1175/BAMS-D-14-00018.1, URL https://journals.ametsoc.org/view/journals/bams/97/1/bams-d-14-00018.1.xml, 2016.

Rigor, I. G., Wallace, J. M., and Colony, R. L.: Response of Sea Ice to the Arctic Oscillation, Journal of Climate, 15, 2648 – 2663, doi:10.1175/1520-0442(2002)015<2648:ROSITT>2.0.CO;2, URL https://journals.ametsoc.org/view/journals/clim/15/18/1520-0442_2002_015_2648_rositt_2.0.co_2.xml, 2002.

Roach, L. A., Dean, S. M., and Renwick, J. A.: Consistent biases in Antarctic sea ice concentration simulated by climate models, Cryosphere, 12, 365–383, doi:10.5194/tc-12-365-2018, 2018.

Roach, L. A., Dörr, J., Holmes, C. R., Massonnet, F., Blockley, E. W., Notz, D., Rackow, T., Raphael, M. N., O'Farrell, S. P., Bailey, D. A., and Bitz, C. M.: Antarctic Sea Ice Area in CMIP6, Geophysical Research Letters, 47, e2019GL086 729, doi:https://doi.org/10.1029/2019GL086729, URL https://agupubs.onlinelibrary.wiley.com/doi/abs/10.1029/2019GL086729, e2019GL086729 10.1029/2019GL086729, 2020.

Roach, L. A., Eisenman, I., Wagner, T. J. W., Blanchard-Wrigglesworth, E., and Bitz, C. M.: Asymmetry in the seasonal cycle of Antarctic sea ice driven by insolation, Nature Geoscience, 15, 277–281, doi:10.1038/s41561-022-00913-6, 2022.

Roberts, C. D., Senan, R., Molteni, F., Boussetta, S., Mayer, M., and Keeley, S. P.: Climate model configurations of the ECMWF integrated forecasting system (ecmwf-ifs cycle 43r1) for HighResMIP, Geoscientific Model Development, 11, 3681–3712, doi:10.5194/gmd-11-3681-2018, 2018.

Roberts, M. J., Jackson, L. C., Roberts, C. D., Meccia, V., Docquier, D., Koenigk, T., Ortega, P., Moreno-Chamarro, E., Bellucci, A., Coward, A., Drijfhout, S., Exarchou, E., Gutjahr, O., Hewitt, H., Iovino, D., Lohmann, K., Putrasahan, D., Schiemann, R., Seddon, J., Terray, L., Xu, X., Zhang, Q., Chang, P., Yeager, S. G., Castruccio, F. S., Zhang, S., and Wu, L.: Sensitivity of the Atlantic Meridional Overturning Circulation to Model Resolution in CMIP6 HighResMIP Simulations and Implications for Future Changes, Journal of Advances in Modeling Earth Systems, 12, doi:10.1029/2019MS002014, 2020.

Robson, J., Aksenov, Y., Bracegirdle, T. J., Dimdore-Miles, O., Griffiths, P. T., Grosvenor, D. P., Hodson, D. L. R., Keeble, J., MacIntosh, C., Megann, A., Osprey, S., Povey, A. C., Schröder, D., Yang, M., Archibald, A. T., Carslaw, K. S., Gray, L., Jones, C., Kerridge, B., Knappett, D., Kuhlbrodt, T., Russo, M., Sellar, A., Siddans, R., Sinha, B., Sutton, R., Walton, J., and Wilcox, L. J.: The Evaluation of the North Atlantic Climate System in UKESM1 Historical Simulations for CMIP6, Journal of Advances in Modeling Earth Systems, 12, doi:10.1029/2020ms002126, URL https://onlinelibrary.wiley.com/doi/10.1029/2020MS002126, 2020.

Rolph, R. J., Feltham, D. L., and Schröder, D.: Changes of the Arctic marginal ice zone during the satellite era, The Cryosphere, 14, 1971–1984, doi:10.5194/tc-14-1971-2020, URL https://tc.copernicus.org/articles/14/1971/2020/, 2020.

Rousset, C., Vancoppenolle, M., Madec, G., Fichefet, T., Flavoni, S., Barthélemy, A., Benshila, R., Chanut, J., Levy, C., Masson, S., and Vivier, F.: The Louvain-La-Neuve sea ice model

LIM3.6: global and regional capabilities, Geoscientific Model Development, 8, 2991–3005, doi:10.5194/gmd-8-2991-2015, URL https://gmd.copernicus.org/articles/8/2991/2015/, 2015.

Schlosser, E., Haumann, F. A., and Raphael, M. N.: Atmospheric influences on the anomalous 2016 Antarctic sea ice decay, Cryosphere, 12, 1103–1119, doi:10.5194/tc-12-1103-2018, 2018.

Schroeter, S. and Sandery, P. A.: Large-ensemble analysis of Antarctic sea ice model sensitivity to parameter uncertainty, Ocean Modelling, 177, 102 090, doi:https://doi.org/10.1016/j.ocemod.2022.102090, URL https://www.sciencedirect.com/science/article/pii/S1463500322001093, 2022.

Schroeter, S., Hobbs, W., and Bindoff, N. L.: Interactions between Antarctic sea ice and large-scale atmospheric modes in CMIP5 models, The Cryosphere, 11, 789–803, doi:10.5194/tc-11-789-2017, URL https://tc.copernicus.org/articles/11/789/2017/, 2017.

Screen, J. A. and Simmonds, I.: The central role of diminishing sea ice in recent Arctic temperature amplification, Nature, 464, 1334–1337, doi:10.1038/nature09051, 2010.

Screen, J. A., Eade, R., Smith, D. M., Thomson, S., and Yu, H.: Net Equatorward Shift of the Jet Streams When the Contribution From Sea-Ice Loss Is Constrained by Observed Eddy Feedback, Geophysical Research Letters, 49, e2022GL100 523, doi:https://doi.org/10.1029/2022GL100523, URL https://agupubs.onlinelibrary.wiley.com/doi/abs/10.1029/2022GL100523, e2022GL100523 2022GL100523, 2022.

Senftleben, D., Lauer, A., and Karpechko, A.: Constraining Uncertainties in CMIP5 Projections of September Arctic Sea Ice Extent with Observations, Journal of Climate, 33, 1487 – 1503, doi:https://doi.org/10.1175/JCLI-D-19-0075.1, URL https://journals.ametsoc.org/view/journals/clim/33/4/jcli-d-19-0075.1.xml, 2020.

Serreze, M. C. and Meier, W. N.: The Arctic's sea ice cover: trends, variability, predictability, and comparisons to the Antarctic, Annals of the New York Academy of Sciences, 1436, 36–53, doi:10.1111/nyas.13856, 2019.

Shen, Z., Duan, A., Li, D., and Li, J.: Assessment and Ranking of Climate Models in Arctic Sea Ice Cover Simulation: From CMIP5 to CMIP6, Journal of Climate, 34, 3609 – 3627, doi:10.1175/JCLI-D-20-0294.1, URL https://journals.ametsoc.org/view/journals/clim/34/9/JCLI-D-20-0294.1.xml, 2021.

Shu, Q., Song, Z., and Qiao, F.: Assessment of sea ice simulations in the CMIP5 models, Cryosphere, 9, 399–409, doi:10.5194/tc-9-399-2015, 2015.

Shu, Q., Wang, Q., Song, Z., Qiao, F., Zhao, J., Chu, M., and Li, X.: Assessment of Sea Ice Extent in CMIP6 With Comparison to Observations and CMIP5, Geophysical Research Letters, 47, e2020GL087 965, doi:https://doi.org/10.1029/2020GL087965, URL https://agupubs.onlinelibrary.wiley.com/doi/abs/10.1029/2020GL087965, e2020GL087965 2020GL087965, 2020.

Simmonds, I.: Simmonds, I. (2015). Comparing and contrasting the behaviour of Arctic and Antarctic sea ice over the 35 year period 1979-2013. Annals of Glaciology, 56(69), 18-28.

doi:10.3189/2015AoG69A909, 2015.

Smedsrud, L. H., Ingvaldsen, R., Nilsen, J. E. Ø., and Skagseth, Ø.: Heat in the Barents Sea: transport, storage, and surface fluxes, Ocean Science, 6, 219–234, doi:10.5194/os-6-219-2010, URL https://os.copernicus.org/articles/6/219/2010/, 2010.

Smith, G. C., Allard, R., Babin, M., Bertino, L., Chevallier, M., Corlett, G., Crout, J., Davidson, F., Delille, B., Gille, S. T., Hebert, D., Hyder, P., Intrieri, J., Lagunas, J., Larnicol, G., Kaminski, T., Kater, B., Kauker, F., Marec, C., Mazloff, M., Metzger, E. J., Mordy, C., O'Carroll, A., Olsen, S. M., Phelps, M., Posey, P., Prandi, P., Rehm, E., Reid, P., Rigor, I., Sandven, S., Shupe, M., Swart, S., Smedstad, O. M., Solomon, A., Storto, A., Thibaut, P., Toole, J., Wood, K., Xie, J., Yang, Q., and the, W. P. P. P. S. G.: Polar Ocean Observations: A Critical Gap in the Observing System and Its Effect on Environmental Predictions From Hours to a Season, Frontiers in Marine Science, 6, doi:10.3389/fmars.2019.00429, 2019.

Smith, M. M., von Albedyll, L., Raphael, I. A., Lange, B. A., Matero, I., Salganik, E., Webster, M. A., Granskog, M. A., Fong, A., Lei, R., and Light, B.: Quantifying false bottoms and under-ice meltwater layers beneath Arctic summer sea ice with fine-scale observations, Elementa: Science of the Anthropocene, 10, 000 116, doi:10.1525/elementa.2021.000116, URL https://doi.org/10.1525/elementa.2021.000116, 2022.

Song, J. N., Fu, G., Xu, Y., Han, Z. Y., Sun, Q. Z., and Wang, H.: Assessment of the capability of CMIP6 global climate models to simulate Arctic cyclones, Advances in Climate Change Research, 12, 660–676, doi:10.1016/j.accre.2021.07.007, 2021.

Spreen, G., Kwok, R., and Menemenlis, D.: Trends in Arctic sea ice drift and role of wind forcing: 1992-2009, Geophysical Research Letters, 38, doi:https://doi.org/10.1029/2011GL048970, URL https://agupubs.onlinelibrary.wiley.com/doi/abs/10.1029/2011GL048970, 2011.

Stammerjohn, S. and Maksym, T.: Gaining (and losing) Antarctic sea ice: variability, trends and mechanisms, doi:https://doi.org/10.1002/9781118778371.ch10, URL https://onlinelibrary.wiley.com/doi/abs/10.1002/9781118778371.ch10, 2017.

Stammerjohn, S. E., Martinson, D. G., Smith, R. C., Yuan, X., and Rind, D.: Trends in Antarctic annual sea ice retreat and advance and their relation to El Niño-Southern Oscillation and Southern Annular Mode variability, Journal of Geophysical Research: Oceans, 113, doi:10.1029/2007jc004269, 2008.

Stern, H. L. and Laidre, K. L.: Sea-ice indicators of polar bear habitat, The Cryosphere, 10, 2027–2041, doi:10.5194/tc-10-2027-2016, URL https://tc.copernicus.org/articles/10/2027/2016/, 2016.

Stevens, B., Giorgetta, M., Esch, M., Mauritsen, T., Crueger, T., Rast, S., Salzmann, M., Schmidt, H., Bader, J., Block, K., Brokopf, R., Fast, I., Kinne, S., Kornblueh, L., Lohmann, U., Pincus, R., Reichler, T., and Roeckner, E.: Atmospheric component of the MPI-M earth system model: ECHAM6, Journal of Advances in Modeling Earth Systems, 5, 146–172, doi:10.1002/jame.20015, 2013.

Storto, A., Masina, S., and Navarra, A.: Evaluation of the CMCC eddy-permitting global ocean physical reanalysis system (C-GLORS, 1982-2012) and its assimilation components, Quarterly Journal of the Royal Meteorological Society, 142, 738–758, doi:https://doi.org/10.1002/qj.2673, URL https://rmets.onlinelibrary.wiley.com/doi/abs/10.1002/qj.2673, 2016.

Storto, A., Masina, S., Simoncelli, S., Iovino, D., Cipollone, A., Drevillon, M., Drillet, Y., Schuckman, K., Parent, L., Garric, G., Greiner, E., Desportes, C., Zuo, H., Balmaseda, M., and Peterson, K.: The added value of the multi-system spread information for ocean heat content and steric sea level investigations in the CMEMS GREP ensemble reanalysis product, Climate Dynamics, 53, doi:10.1007/s00382-018-4585-5, 2019.

Strandberg, G. and Lind, P.: The importance of horizontal model resolution on simulated precipitation in Europe - from global to regional models, Weather and Climate Dynamics, 2, 181–204, doi:10.5194/wcd-2-181-2021, URL https://wcd.copernicus.org/articles/2/181/2021/, 2021.

Stroeve, J., Barrett, A., Serreze, M., and Schweiger, A.: Using records from submarine, aircraft and satellites to evaluate climate model simulations of Arctic sea ice thickness, The Cryosphere, 8, 1839–1854, doi:10.5194/tc-8-1839-2014, URL https://tc.copernicus.org/articles/8/1839/2014/, 2014.

Stroeve, J. C., Kattsov, V., Barrett, A., Serreze, M., Pavlova, T., Holland, M., and Meier, W. N.: Trends in Arctic sea ice extent from CMIP5, CMIP3 and observations, Geophysical Research Letters, 39, doi:10.1029/2012GL052676, 2012a.

Stroeve, J. C., Serreze, M. C., Holland, M. M., Kay, J. E., Malanik, J., and Barrett, A. P.: The Arctic's rapidly shrinking sea ice cover: A research synthesis, Climatic Change, 110, 1005–1027, doi:10.1007/s10584-011-0101-1, 2012b.

Stroeve, J. C., Jenouvrier, S., Campbell, G. G., Barbraud, C., and Delord, K.: Mapping and assessing variability in the Antarctic marginal ice zone, pack ice and coastal polynyas in two sea ice algorithms with implications on breeding success of snow petrels, Cryosphere, pp. 1823–1843, doi:10.5194/tc-10-1823-2016, 2016.

Strong, C. and Rigor, I. G.: Arctic marginal ice zone trending wider in summer and narrower in winter, Geophysical Research Letters, 40, 4864–4868, doi:https://doi.org/10.1002/grl.50928, URL https://agupubs.onlinelibrary.wiley.com/doi/abs/10.1002/grl.50928, 2013.

Strong, C., Foster, D., Cherkaev, E., Eisenman, I., and Golden, K. M.: On the Definition of Marginal Ice Zone Width, Journal of Atmospheric and Oceanic Technology, 34, 1565 – 1584, doi:https://doi.org/10.1175/JTECH-D-16-0171.1, URL https://journals.ametsoc.org/view/journals/atot/34/7/jtech-d-16-0171.1.xml, 2017.

Stuecker, M. F., Bitz, C. M., and Armour, K. C.: Conditions leading to the unprecedented low Antarctic sea ice extent during the 2016 austral spring season, Geophysical Research Letters, 44, 9008–9019, doi:10.1002/2017GL074691, 2017.

Sun, S. and Eisenman, I.: Observed Antarctic sea ice expansion reproduced in a climate model after correcting biases in sea ice drift velocity, Nature Communications, 12, 1060, doi:10.1038/

s41467-021-21412-z, URL https://doi.org/10.1038/s41467-021-21412-z, 2021.

Svendsen, E., Matzler, C., and Grenfell, T.: A model for retrieving total sea ice concentration from a spaceborne dual-polarized passive microwave instrument operating near 90 GHz, International Journal of Remote Sensing, 8, 1479–1487, doi:10.1080/01431168708954790, 1987.

Tan, I., Storelvmo, T., and Zelinka, M. D.: Observational constraints on mixed-phase clouds imply higher climate sensitivity, Science, 352, 224–227, doi:10.1126/science.aad5300, URL https://www.science.org/doi/abs/10.1126/science.aad5300, 2016.

Tápias, G., Lizotte, M., Kieber, M., D. Randelhoff, A., Xue, R., Dinasquet, L., Babin, J., Rehm, M., and Levasseur, E.: DMS emissions from the Arctic marginal ice zone, Elementa: Science of the Anthropocene, 9, doi:10.1525/elementa.2020.00113, 2021.

Taylor, P. C., Boeke, R. C., Boisvert, L. N., Feldl, N., Henry, M., Huang, Y., Langen, P. L., Liu, W., Pithan, F., Sejas, S. A., and Tan, I.: Process Drivers, Inter-Model Spread, and the Path Forward: A Review of Amplified Arctic Warming, doi:10.3389/feart.2021.758361, 2022.

Tebaldi, C., Debeire, K., Eyring, V., Fischer, E., Fyfe, J., Friedlingstein, P., Knutti, R., Lowe, J., O'Neill, B., Sanderson, B., Vuuren, D. V., Riahi, K., Meinshausen, M., Nicholls, Z., Tokarska, K., Hurtt, G., Kriegler, E., Meehl, G., Moss, R., Bauer, S., Boucher, O., Brovkin, V., Yhb, Y., Dix, M., Gualdi, S., Guo, H., John, J., Kharin, S., Kim, Y. H., Koshiro, T., Ma, L., Olivié, D., Panickal, S., Qiao, F., Rong, X., Rosenbloom, N., Schupfner, M., Séférian, R., Sellar, A., Semmler, T., Shi, X., Song, Z., Steger, C., Stouffer, R., Swart, N., Tachiiri, K., Tang, Q., Tatebe, H., Voldoire, A., Volodin, E., Wyser, K., Xin, X., Yang, S., Yu, Y., and Ziehn, T.: Climate model projections from the Scenario Model Intercomparison Project (ScenarioMIP) of CMIP6, Earth System Dynamics, 12, 253–293, doi:10.5194/esd-12-253-2021, 2021.

Tetzner, D., Thomas, E., and Allen, C.: A Validation of ERA5 Reanalysis Data in the Southern Antarctic Peninsula - Ellsworth Land Region, and Its Implications for Ice Core Studies, Geosciences, 9, doi:10.3390/geosciences9070289, URL https://www.mdpi.com/2076-3263/9/7/289, 2019.

Thompson, D. W. J. and Wallace, J. M.: The Arctic oscillation signature in the wintertime geopotential height and temperature fields, Geophysical Research Letters, 25, 1297–1300, doi:https://doi.org/10.1029/98GL00950, URL https://agupubs.onlinelibrary.wiley.com/doi/abs/10.1029/98GL00950, 1998.

Tikhonov, V. V., Raev, M. D., Sharkov, E. A., Boyarskii, D. A., Repina, I. A., and Komarova, N. Y.: Satellite microwave radiometry of sea ice of polar regions: a review, Izvestiya, Atmospheric and Oceanic Physics, 52, 1012–1030, doi:10.1134/S0001433816090267, URL https://doi.org/10.1134/S0001433816090267, 2016.

Tilling, R., Ridout, A., and Shepherd, A.: Assessing the Impact of Lead and Floe Sampling on Arctic Sea Ice Thickness Estimates from Envisat and CryoSat-2, Journal of Geophysical Research: Oceans, 124, doi:10.1029/2019JC015232, 2019.

Tilling, R. L., Ridout, A., Shepherd, A., and Wingham, D. J.: Increased Arctic sea ice volume after anomalously low melting in 2013, Nature Geoscience, 8, 643–646, doi:10.1038/ngeo2489,

URL https://doi.org/10.1038/ngeo2489, 2015.

Tjiputra, J. F., Assmann, K., and Heinze, C.: Anthropogenic carbon dynamics in the changing ocean, Ocean Science, 6, 605–614, doi:10.5194/os-6-605-2010, URL https://os.copernicus.org/articles/6/605/2010/, 2010.

Turner, J., Hosking, J. S., Bracegirdle, T. J., Marshall, G. J., and Phillips, T.: Recent changes in Antarctic Sea Ice, doi:10.1098/rsta.2014.0163, 2015.

Turner, J., Phillips, T., Marshall, G. J., Hosking, J. S., Pope, J. O., Bracegirdle, T. J., and Deb, P.: Unprecedented springtime retreat of Antarctic sea ice in 2016, Geophysical Research Letters, 44, 6868–6875, doi:10.1002/2017GL073656, 2017.

Turner, J., Holmes, C., Caton Harrison, T., Phillips, T., Jena, B., Reeves-Francois, T., Fogt, R., Thomas, E. R., and Bajish, C. C.: Record Low Antarctic Sea Ice Cover in February 2022, Geophysical Research Letters, 49, e2022GL098 904, doi:https://doi.org/10.1029/2022GL098904, URL https://agupubs.onlinelibrary.wiley.com/doi/abs/10.1029/2022GL098904, e2022GL098904 2022GL098904, 2022.

Uotila, P., Iovino, D., Vancoppenolle, M., Lensu, M., and Rousset, C.: Comparing sea ice, hydrography and circulation between NEMO3.6 LIM3 and LIM2, Geoscientific Model Development, 10, 1009–1031, doi:10.5194/gmd-10-1009-2017, 2017.

Uotila, P., Goosse, H., Haines, K., Chevallier, M., Barthélemy, A., Bricaud, C., Carton, J., Fučkar, N., Garric, G., Iovino, D., Kauker, F., Korhonen, M., Lien, V. S., Marnela, M., Massonnet, F., Mignac, D., Peterson, K. A., Sadikni, R., Shi, L., Tietsche, S., Toyoda, T., Xie, J., and Zhang, Z.: An assessment of ten ocean reanalyses in the polar regions, Climate Dynamics, 52, 1613–1650, doi:10.1007/s00382-018-4242-z, URL https://doi.org/10.1007/s00382-018-4242-z, 2019.

Vichi, M.: An indicator of sea ice variability for the Antarctic marginal ice zone, The Cryosphere, 16, 4087–4106, doi:10.5194/tc-16-4087-2022, URL https://tc.copernicus.org/articles/16/4087/2022/, 2022.

Vichi, M., Eayrs, C., Alberello, A., Bekker, A., Bennetts, L., Holland, D., de Jong, E., Joubert, W., MacHutchon, K., Messori, G., Mojica, J. F., Onorato, M., Saunders, C., Skatulla, S., and Toffoli, A.: Effects of an Explosive Polar Cyclone Crossing the Antarctic Marginal Ice Zone, Geophysical Research Letters, 46, 5948–5958, doi:https://doi.org/10.1029/2019GL082457, URL https://agupubs.onlinelibrary.wiley.com/doi/abs/10.1029/2019GL082457, 2019.

Voldoire, A., Saint-Martin, D., Sénési, S., Decharme, B., Alias, A., Chevallier, M., Colin, J., Guérémy, J. F., Michou, M., Moine, M. P., Nabat, P., Roehrig, R., y Mélia, D. S., Séférian, R., Valcke, S., Beau, I., Belamari, S., Berthet, S., Cassou, C., Cattiaux, J., Deshayes, J., Douville, H., Ethé, C., Franchistéguy, L., Geoffroy, O., Lévy, C., Madec, G., Meurdesoif, Y., Msadek, R., Ribes, A., Sanchez-Gomez, E., Terray, L., and Waldman, R.: Evaluation of CMIP6 DECK Experiments With CNRM-CM6-1, Journal of Advances in Modeling Earth Systems, 11, 2177–2213, doi:10.1029/2019MS001683, 2019.

Wadhams, P.: The Seasonal Ice Zone, doi:10.1007/978-1-4899-5352-0_15, URL https://doi.org/10.1007/978-1-4899-5352-0_15, 1986.

Wadhams, P. and Deacon, G. E. R.: Sea-ice topography of the Arctic Ocean in the region 70° W to 25° E, Philosophical Transactions of the Royal Society of London. Series A, Mathematical and Physical Sciences, 302, 45–85, doi:10.1098/rsta.1981.0157, URL https://royalsocietypublishing.org/doi/abs/10.1098/rsta.1981.0157, 1981.

Wang, J., Min, C., Ricker, R., Shi, Q., Han, B., Hendricks, S., Wu, R., and Yang, Q.: A comparison between Envisat and ICESat sea ice thickness in the Southern Ocean, The Cryosphere, 16, 4473–4490, doi:10.5194/tc-16-4473-2022, URL https://tc.copernicus.org/articles/16/4473/2022/, 2022.

Wang, M. and Overland, J. E.: A sea ice free summer Arctic within 30 years: An update from CMIP5 models, Geophysical Research Letters, 39, doi:https://doi.org/10.1029/2012GL052868, URL https://agupubs.onlinelibrary.wiley.com/doi/abs/10.1029/2012GL052868, 2012.

Wang, X., Key, J., Kwok, R., and Zhang, J.: Comparison of Arctic sea ice thickness from satellites, aircraft, and PIOMAS data, Remote Sensing, 8, doi:10.3390/RS8090713, 2016.

Wang, Z., Turner, J., Wu, Y., and Liu, C.: Rapid decline of total Antarctic sea ice extent during 2014-16 controlled by wind-driven sea ice drift, Journal of Climate, 32, 5381–5395, doi:10.1175/JCLI-D-18-0635.1, 2019.

Watanabe, Y. Y., Ito, K., Kokubun, N., and Takahashi, A.: Foraging behavior links sea ice to breeding success in Antarctic penguins, Science Advances, 6, eaba4828, doi:10.1126/sciadv.aba4828, URL https://www.science.org/doi/abs/10.1126/sciadv.aba4828, 2020.

Watterson, I. G., Keane, R. J., Dix, M., Ziehn, T., Andrews, T., and Tang, Y.: Analysis of CMIP6 atmospheric moisture fluxes and the implications for projections of future change in mean and heavy rainfall, International Journal of Climatology, 41 (S1), E1417–E1434, doi:10.1002/joc.6777, URL https://onlinelibrary.wiley.com/doi/10.1002/joc.6777, 2021.

Watts, M., Maslowski, W., Lee, Y. J., Kinney, J. C., and Osinski, R.: A Spatial Evaluation of Arctic Sea Ice and Regional Limitations in CMIP6 Historical Simulations, Journal of Climate, 34, 6399–6420, doi:10.1175/JCLI-D-20-0491.1, 2021.

Williams, K. D., Copsey, D., Blockley, E. W., Bodas-Salcedo, A., Calvert, D., Comer, R., Davis, P., Graham, T., Hewitt, H. T., Hill, R., Hyder, P., Ineson, S., Johns, T. C., Keen, A. B., Lee, R. W., Megann, A., Milton, S. F., Rae, J. G. L., Roberts, M. J., Scaife, A. A., Schiemann, R., Storkey, D., Thorpe, L., Watterson, I. G., Walters, D. N., West, A., Wood, R. A., Woollings, T., and Xavier, P. K.: The Met Office Global Coupled Model 3.0 and 3.1 (GC3.0 and GC3.1) Configurations, Journal of Advances in Modeling Earth Systems, 10, 357–380, doi:https://doi.org/10.1002/2017MS001115, URL https://agupubs.onlinelibrary.wiley.com/doi/abs/10.1002/2017MS001115, 2018.

Worby, A. P., Geiger, C. A., Paget, M. J., Van Woert, M. L., Ackley, S. F., and DeLiberty, T. L.: Thickness distribution of Antarctic sea ice, Journal of Geophysical Research: Oceans, 113,

doi:https://doi.org/10.1029/2007JC004254, URL https://agupubs.onlinelibrary.wiley.com/doi/abs/10.1029/2007JC004254, 2008.

Yoshimori, M., Abe-Ouchi, A., and Laîné, A.: The role of atmospheric heat transport and regional feedbacks in the Arctic warming at equilibrium, Climate Dynamics, 49, 3457–3472, doi:10.1007/s00382-017-3523-2, 2017.

Zanowski, H., Jahn, A., and Holland, M. M.: Arctic Ocean freshwater in CMIP6 Ensembles: Declining Sea Ice, Increasing Ocean Storage and Export, Journal of Geophysical Research: Oceans, doi:10.1029/2020jc016930, URL https://onlinelibrary.wiley.com/doi/10.1029/2020JC016930, 2021.

Zelinka, M. D., Myers, T. A., McCoy, D. T., Po-Chedley, S., Caldwell, P. M., Ceppi, P., Klein, S. A., and Taylor, K. E.: Causes of Higher Climate Sensitivity in CMIP6 Models, Geophysical Research Letters, 47, e2019GL085 782, doi:https://doi.org/10.1029/2019GL085782, URL https://agupubs.onlinelibrary.wiley.com/doi/abs/10.1029/2019GL085782, 2020.

Zhang, J. and Rothrock, D. A.: Modeling Global Sea Ice with a Thickness and Enthalpy Distribution Model in Generalized Curvilinear Coordinates, Monthly Weather Review, 131, 845 – 861, doi:https://doi.org/10.1175/1520-0493(2003)131<0845:MGSIWA>2.0.CO;2, URL https://journals.ametsoc.org/view/journals/mwre/131/5/1520-0493_2003_131_0845_mgsiwa_2.0.co_2.xml, 2003.

Zhang, X.: Sensitivity of Arctic Summer Sea Ice Coverage to Global Warming Forcing: Toward Reducing Uncertainty in Arctic Climate Change Projections, Tellus A, 62, 220 – 227, doi:10.1111/j.1600-0870.2010.00441.x, 2010.

Zhu, J., Xie, A., Qin, X., Wang, Y., Xu, B., and Wang, Y.: An Assessment of ERA5 Reanalysis for Antarctic Near-Surface Air Temperature, Atmosphere, 12, doi:10.3390/atmos12020217, URL https://www.mdpi.com/2073-4433/12/2/217, 2021.

Zuo, H., Balmaseda, M. A., Tietsche, S., Mogensen, K., and Mayer, M.: The ECMWF operational ensemble reanalysis-analysis system for ocean and sea ice: a description of the system and assessment, Ocean Science, 15, 779–808, doi:10.5194/os-15-779-2019, URL https://os.copernicus.org/articles/15/779/2019/, 2019.

Zygmuntowska, M., Rampal, P., Ivanova, N., and Smedsrud, L. H.: Uncertainties in Arctic sea ice thickness and volume: New estimates and implications for trends, Cryosphere, 8, 705–720, doi:10.5194/tc-8-705-2014, 2014.